Ground Improvement of Non-cohesive Soil Using Nanoparticles, Specifically, Laponite

A Dissertation Submitted to the Faculty of Engineering,

Department of Civil Engineering

By

SHUMSUN NAHAR SIDDIQUE

In Partial Fulfillment of the Requirements for the Degree of

Doctor of Philosophy

Faculty of Graduate Studies

Lakehead University

Thunder Bay, Ontario, Canada

September 2024

Certificate of Examination

Supervisor

Dr. Eltayeb Mohamedelhassan

Co-supervisor

Dr. Jian Deng

Examining Board

Dr. Baoqiang Liao

Dr. Liang Cui

External Examiner

Dr. Sumi Siddiqua

The Dissertation by

SHUMSUN NAHAR SIDDIQUE

entitled

Ground Improvement of Non-cohesive Soil Using Nanoparticles, Specifically, Laponite

is accepted in partial fulfillment of the requirements for the degree of

Doctor of Philosophy

Date: _____

_____

Chair of the Examination Board

Abstract

Ground improvement through densification is a widely used techniques to mitigate the risk of liquefaction and significant soil deformations. Traditional site stabilization techniques have certain limitations such as insufficient field treatment, substantial disturbances, environmental pollution, and high costs. However, incorporating nanoparticles into ground improvement techniques can lessen these negative impacts, offering a more efficient and environmentally friendly alternative. This study examines the characteristics of laponite, a promising soil improvement nanoparticle, when it is mixed with non-cohesive soil under full saturated conditions. The findings revealed that laponite is both environmental-friendly and biologically inert. Even a small amount of laponite significantly reduces the generation of pore water pressure under static loadings due to its good rheological properties as a transparent gel. Additionally, the modulus of elasticity of sand-laponite specimens is nearly double that of pure sand. The swelling strain of compacted laponite increases over time and as the concentration of laponite increased in specimens. Laponite also effectively restricts the migration of contaminants and reduces soil permeability due to its repeated swelling performance. Moreover, the damping ratio of treated samples is higher compared to untreated sand samples. The damping ratio begins to reduce after reaching its peak and eventually reaches equilibrium in case of sand+ laponite samples. The coefficient of permeability is significantly reduced with the presence of small amounts of laponite in sand samples. The compressive behaviour of laponite hydrogel indicates that laponite hydrogels exhibit the nonlinear stress-strain relationships which represents typical viscoelastic characteristics. This research provides novel insights into the improvement and modification of the properties of non-cohesive soil (sand) elaborately in the presence of laponite, demonstrating its potential as an effective ground improvement material.

Keywords: Laponite, *Chlorella* sp., Chlorophyll content, Specific growth rate, Inhibition ratio, Pore water pressure, laponite, hydrogel, permeability, compression, Nanoparticles, Swelling, Reswelling, Hydrogel, swelling pressure, Piezoceramics, bender element, damping ratio, half-power bandwidth method, frequency, amplitude,

Dedication

To my beloved husband, Syed Iftekhar Ahmed

To my beloved son, Yousuf Ibn Ahmed

To my beloved daughter, Maryam Bint Ahmed

To my loving parents, Md. Abu Baker Siddique and Sheuly Siddique

Co-authorship

This dissertation has been prepared in accordance with the guidelines and regulations for a manuscript format dissertation stipulated by the Faculty of Graduate Studies at Lakehead University. The following chapter has been co-authored:

Chapter 3: Effect of laponite nanoparticles on growth characteristics and Chlorophyll Content of *Chlorella* sp.

S. Siddique, J. Khatiwada, S. Shrestha, C. Chio, X. Chen, E. Mohamedelhassan, J. Deng, W. Qin

Published in *Water, Air, & Soil Pollution, Vol. 233, article num. 308, (2022)*

Contributions:

S. Siddique: designed the experimental procedure, performed laboratory tastings, interpreted the test results, processed the testing information, and wrote the draft of the manuscript

J. Khatiwada: assisted in designing the experimental procedure, performed laboratory tastings, interpreted the test results, processed the testing information, and assisted in writing of the draft of the manuscript

S. Shrestha: participated in reviewing and editing

C. Chio: participated in reviewing and editing

X. Chen: participated in reviewing and editing

E. Mohamedelhassan: participated in reviewing, editing, and funding acquisition

J. Deng: participated in reviewing and editing

W. Qin: participated in reviewing, editing, and funding acquisition

Chapter 4: Improving the strength properties of sand using laponite, a promising nanoparticle

S. Siddique, J. Deng, and E. Mohamedelhassan

Published in *International Journal of Civil Engineering, Vol. 21, Pages:679-693(2023)*

Contributions:

S. Siddique: designed the apparatus, developed the experimental procedure, performed laboratory tastings, interpreted the test results, processed the testing information, and wrote the draft of the manuscript

J. Deng: assisted in reviewing and editing the manuscript

E. Mohamedelhassan: initiated the study, contributed advice in the design of the apparatus and the testing procedure, and assisted in the interpretation of the results and writing the manuscript

Chapter 5: Swelling Behaviour of Super-absorbent Laponite Hydrogel under One-dimensional Loading

S. Siddique, J. Deng, and E. Mohamedelhassan

Published in *Geotechnical and Geological Engineering (2024)*

Contributions:

S. Siddique: initiated the study, designed the apparatus, developed the experimental procedure, performed experiments, interpreted the test results, processed the testing information, and wrote the draft of the manuscript

J. Deng: assisted in reviewing and editing

E. Mohamedelhassan: contributed advice in the design of the apparatus, assisted in the interpretation of the results, and writing the manuscript

Chapter 6: Experimental Investigation of Damping Ratio of Sand-Laponite and Sand-Bentonite Mixtures Using One-dimensional Bender Elements

S. Siddique, J. Deng, and E. Mohamedelhassan

**Submitted for publication (under review)

Contributions:

S. Siddique: designed the apparatus, developed the experimental procedure, performed experiments, interpreted the test results, processed the testing information, and wrote the draft of the manuscript

J. Deng: assisted in reviewing and editing

E. Mohamedelhassan: initiated the study, contributed advice in the design of the apparatus, assisted in the interpretation of the results, and writing the manuscript

Chapter 7: Permeability of Sand-Laponite Mixture and Compression Properties of Laponite Hydrogel

S. Siddique, J. Deng, and E. Mohamedelhassan

Contributions:

S. Siddique: designed the apparatus, developed the experimental procedure, performed experiments, interpreted the test results, processed the testing information, and wrote the draft of the manuscript

J. Deng: assisted in reviewing and editing

E. Mohamedelhassan: initiated the study, contributed advice in the design of the apparatus, assisted in the interpretation of the results, and writing the manuscript

Acknowledgements

I would like to express my deepest gratitude to Allah Ta'ala for granting me the strength and ability to successfully complete my Ph.D. research. I extend my heartful thanks to my supervisor, Dr. Eltayeb E. Mohamedelhassan, for his unwavering support, insightful advice, and exceptional guidance throughout my research journey. It has been an immense honor to work under his mentorship, and I am profoundly grateful for his patience and encouragement during the many challenges I faced.

A special thanks to my co-supervisor, Dr. Jian Deng, for his insightful opinions and recommendations. I am also deeply thankful to Morgan Ellis, the technician in the Civil Engineering department, for his outstanding assistance in constructing various experimental setup during my study. His dedication and expertise have been invaluable. I am equally grateful to Cory Hubbard, the lab technologist, for his constant presence in the laboratories and for always being there to support me with everything I needed. I feel privileged to have worked with such an incredible team and am incredibly appreciative of the opportunity to learn from them.

Studying at Lakehead University has been a blessing, providing me with a wonderful platform to gather knowledge and experiences diverse global cultures and people. I extend my heartfelt thanks to all the staffs of the Department of Civil Engineering. My gratitude also goes to the Departments of Biology, Chemical Engineering, Electrical Engineering, and Mechanical Engineering for allowing me to utilize their various devices and research laboratories during my research. I am deeply appreciative of all the graduate students who worked alongside me in my offices and labs. Their encouraging advice and support made long hours and challenging situations in the lab bearable, creating a pleasant, supportive, and wonderful atmosphere that helped me sail through. Being a part of this amazing community fills me with immense joy. Special thanks to Raghdah Al-Chalabi, Janak Khatiwada, and Sarita Shrestha for always being there during this long research journey.

I would also like to extend my sincere thanks to the National Science and Engineering Research Council of Canada (NSERC) for the financial support and to Lakehead University for awarding me various scholarships and grants, including Ontario Graduate Scholarship (OGS).

To my sunshine, my beloved son, Yousuf Ibn Ahmed, words cannot express the depth of my gratitude for your unwavering patience and support throughout my Doctoral program. You are my purest love, my greatest inspiration, and my superhero. Your presence has been a constant source of motivation, pushing me forward even during the most challenging times. The sacrifices we have made together will be cherished, and I believe we will both enjoy the rewards. Your resilience and understanding have been extraordinary, and I am endlessly grateful for your love, understanding, and for being my steadfast companion on this journey.

To my little angel, my beloved daughter, Maryam Bint Ahmed, thank you for your cooperation and understanding as I completed this program. You are my true love, my biggest encourager, and my little fairy. Your smiles and hugs have been my solace during the toughest times. Your ability to adapt and support me, even at such a young age, has been incredibly heartwarming. I am profoundly grateful for your patience and for bringing so much joy and light into my life. Your love has been my greatest source of strength, and I am blessed beyond measure to have you as my daughter.

My sincere gratitude goes to my dearest husband, Syed Iftekhar Ahmed, for his unconditional love, constant support, admirable motivation, and unceasing patience. You are my rock and a true source of inspiration. Your unwavering belief in me has been my anchor through every high and low of this journey. The countless sacrifices you have made and your steadfast encouragement have been the pillars of my strength. Words cannot fully express how deeply grateful I am for your presence in my life. You have been my confidant, my cheerleader, my greatest love, and my guiding light. I am blessed to have you by my side, and I owe so much of my success to your endless support and love. Thank you for walking this path with me, for understanding my struggles, and for celebrating my achievements. You are my greatest blessing and my eternal partner in all endeavors.

I am also deeply grateful to my dearest parents for their unwavering love, support, sacrifices, and encouragement throughout this incredible journey. Their belief in me has been a constant source of strength and inspiration. The sacrifices you made and the countless ways you've supported me, both big and small, have been pivotal in helping me reach this milestone. I am deeply thankful for your guidance, your wisdom, and for always being my strongest supporters. Your love and support have been the foundation upon which I have built my dreams.

I am deeply grateful to my sister, who, despite living on the other side of the world, has been a constant source of support. Your unwavering engouement and the scarifies you made have been instrumental in helping me reach this important milestone. I am forever indebted to you for your love and support, which have carried me through this journey.

Last but not least, I would like to express my heartfelt admiration for the Bangladeshi-Thunder Bay community for providing a warm, homely atmosphere that made this journey more comfortable. I am also profoundly thankful to all of my cousins, friends, and well-wishers around the world for their endless assistance, support, and belief in me. Your collective encouragement has been instrumental in my success, and I feel truly blessed to have such a wonderful network of people in my life.

This journey has been a collective effort, and I am deeply fortunate to have had such incredible individuals by my side.

Table of Contents

Certificate of Examination ii
Abstract iii
Dedication iv
Co-authorship v
Acknowledgements viii
Table of Contents xi
List of Tables xvi
List of Figures xx
List of Abbreviations and Symbols xxiv
CHAPTER 1 Introduction 1
1.1 Problem Statement 1
1.2 Research Objectives 5
1.2.1 General Objective 5
1.2.2 Specific Objectives 5
1.3 Dissertation Organization 5
1.4 References 7
CHAPTER 2 Literature Review 9
2.1 Introduction 9
2.2 Liquefaction 12
2.3 Nanoparticles 15
2.4 Liquefaction Resistance Using Nanoparticles 16
2.4.1 Carbon Nanotubes 17
2.4.2 Colloidal Silica 18
2.4.3 Bentonite 23
2.4.4 Laponite - a promising nanoparticle 28
2.5 Laponite and its Characteristics 34
2.5.1 Flow Behaviour of Laponite 36
2.5.2 Time Dependent Flow Behaviour of Laponite 39
2.5.3 Viscoelasticity of Laponite 40
2.5.4 Rheology of Laponite 40
2.5.5 Modification of Laponite Suspensions 41

2.6 Conclusions 41
2.7 References 44
CHAPTER 3 Effect of Laponite Nanoparticles on Growth Characteristics and Chlorophyll Content of *Chlorella* sp. 59
3.1 Introduction 60
3.2 Materials and Methods 61
3.2.1 Microalgae Strains 61
3.2.2 Laponite 62
3.2.3 Cultivation Medium and Conditions 63
3.2.4 Parameter Analysis 63
3.2.5 Sample Preparation for SEM 64
3.2.6 Statistical Analysis 64
3.3 Results and Discussion 65
3.3.1 Effects of Laponite on Microalgae Growth 65
3.3.2 Chlorophyll Variation 71
3.3.3 Structural Characterization of Laponite and Algal Cells 73
3.4 Conclusions 77
3.5 References 77
CHAPTER 4 Improving the Strength Properties of Sand Using Laponite, a Promising Nanoparticle 82
4.1 Introduction 83
4.2 Experimental Materials 86
4.2.1 Sand 86
4.2.2 Laponite 87
4.3 Experimental Methods 89
4.3.1 Specimen Preparation 89
4.3.2 Test Procedures 90
4.3.3 Test Program 92
4.4 Results and Discussions 93
4.4.1 Pore Water Pressure Generation 93
4.4.2 Stress-Strain and Modulus of Elasticity 97
4.4.3 Friction Angle and Cohesion 99
4.4.4 Effects of Temperature on Friction Angle 101

4.4.5 Homogeneity of Sand-Laponite Mixture 102
4.5 Conclusions 106
4.6 References 107
CHAPTER 5 Swelling Behaviour of Super-absorbent Laponite Hydrogel Under One-dimensional Loading 113
5.1 Introduction 114
5.2 Experimental Materials 118
5.2.1 Laponite 118
5.2.2 Bentonite 119
5.2.3 Sand 120
5.3 Experimental Methods 120
5.3.1 Specimen Preparation 120
5.3.2 Experimental Procedures 121
5.4 Results and discussions 123
5.4.1 Determination of swelling 123
5.4.2 Reswelling tests 130
5.4.3 Bentonite Swelling 134
5.4.4 Study of Hydrogel 135
5.4.5 Uneven Swelling Surface 136
5.4.6 Swelling Pressure of Laponite 137
5.5 Conclusions 138
5.6 References 139
CHAPTER 6 Experimental Investigation of Damping Ratio of Sand-Laponite Mixtures Using One-dimensional Bender Elements 145
6.1 Introduction 146
6.2 Experimental Materials 149
6.2.1 Sand 149
6.2.2 Nanoparticles 149
6.3 Experimental Set-up 152
6.3.1 Bender Elements 152
6.3.2 Sample Preparation 157
6.3.3 Sample Set-up 157
6.3.4 Signal 158

6.3.5 Damping Determination 160
6.3.6 Matlab Scripts 162
6.4 Results and Discussions 162
6.4.1 Damping of Pure Sand 163
6.4.2 Damping of Sand-laponite Samples 165
6.4.3 Damping of Sand-Bentonite Samples 167
6.4.4 Samples After Releasing from the Set-Up 168
6.5 Conclusions 169
6.6 References 171
CHAPTER 7 Permeability of Sand-Laponite Mixture and Compression Properties of Laponite Hydrogel 176
7.1 Introduction 177
7.2 Experimental Materials 180
7.2.1 Laponite 180
7.2.2 Bentonite 181
7.2.3 Sand 182
7.3 Experimental Methods 182
7.3.1 Specimen Preparation 182
7.3.2 Experimental Procedures 183
7.4 Results and Discussions 184
7.4.1 Change of Permeability 184
7.4.2 Compressive Strength of Laponite Hydrogel 192
7.5 Conclusions 194
7.6 References 196
CHAPTER 8 Conclusions and Recommendations 199
8.1 Introduction 199
8.2 Specific Conclusions 200
8.2.1 Laponite is Environment-Friendly 200
8.2.2 Laponite Improves Shear Strength of Sand 200
8.2.3 Laponite Hydrogel Swells Significantly 201
8.2.4 Laponite Enhances Damping Ratio 201
8.2.5 Laponite Reduces Permeability and Compressive Strength of Hydrogel 201
8.3 Major Contributions 202

8.3.1 Environmentally Friendly Additive 202
8.3.2 Improvement of Soil Shear Strength and Stability 202
8.3.3 Swelling Behavior in Hydrogel Applications 202
8.3.4 Damping Properties for Vibration Control 202
8.3.5 Potential in Soft Ground Improvement 202
8.4 Limitations 203
8.5 Recommendations for Future Research 203
8.5.1 Field-Scale Testing 203
8.5.2 Passive Site Stabilization Technique 204
8.5.3 Laboratory Testing to Find Optimal Concentration of Laponite 204
8.5.4 Strengthening the Structure of Laponite Suspensions 204
8.5.5 Weaken the Structure of Laponite Suspension 204
8.5.6 Micromechanical Investigations and Studies of the Microstructure 205
8.5.7 Numerical Analyses 205
Appendix A 208
Appendix B 212
Appendix C 215

List of Tables

Figure 1-1: (a) Soil liquefaction in Christchurch: the 2011 earthquake led to the formation a layer of water and fine sand on street surface [3], (b) Sand boil (erupted of liquefied sand) during the 2010 Randolph earthquake, one of the smallest earthquakes recorded events to induce liquefaction [4]. 2
Figure 2-1: Liquefaction concept of Schofield, after Schofield [67] 14
Figure 2-2: Scale comparison of nanoparticles dimension 15
Figure 2-3: Formulation of siloxane bonds and a schematic of the colloidal silica particle, after Spencer et al. [101] 19
Figure 2-4: Unconfined compressive strength of sand-CS mixture versus the concentration of CS, after Persoff et al. [52] 20
Figure 2-5: Bentonite Powder 24
Figure 2-6: The structural formula of bentonite, after Perry [140] 24
Figure 2-7: (a) Effect of bentonite treatment in increasing cyclic resistance of sand in undrained cyclic triaxial tests, and (b) Effect of aging time (1 to 10 days) preceding shear, after El Mohtar et al., [166] 26
Figure 2-8: Laponite Powder 29
Figure 2-9: (a) Geometry of individual laponite particles, and (b) Idealized structural formula of laponite, after BYK Additives and Instruments [174] 29
Figure 2-10: (a) Relationship between cyclic stress ratio (CSR) and number of cycles to liquefaction for pure sand and laponite-sand specimens, and (b) Effect of laponite on the CSR corresponding to a given number of cycles to liquefaction, after Ochoa-Cornejo et al. [181]..... 32
Figure 2-11: Typical consistency curves for 3% laponite-RD suspensions at different ageing times, after Chen [185] 38
Figure 2-12: Thixotropic loop of laponite suspension, after Chen [185]. 39
Figure 3-1: Images of Chlorella sp. a) lower magnification (40x), and b) higher magnification (100x) using a compound microscope 62
Figure 3-2: Cell density of *Chlorella* sp. under different concentrations of laponite versus cultivation days, a) 0.1% (r^2=0.621, P<0.001), b) 0.2% (r^2=0.643, P<0.001), c) 0.3% (r^2=0.191, P<0.001), d) 0.4% (not significant), and e) 0.5% (not significant) laponite (by dry weight) in the growth medium, and f) BG-11 (r^2=0.536, P<0.001) only. The dots show the mean cell density and the error bars represent standard deviations. 66
Figure 3-3: Effect of laponite treatment at different concentrations on the cell density of *Chlorella* sp. The bars show the mean cell density and errors refer to standard deviation. The statistic was derived from a one-way ANOVA with a posthoc Tukey test. The letters above the bars signified the differences between treatments at P<0.05. 67
Figure 3-4: The specific growth rate of *Chlorella* sp. under different laponite concentrations with culture period. The bars show the mean specific growth rate and errors refer to standard deviation. The statistic was derived from a one-way ANOVA with a posthoc Tuk Tukey test. The letters above the bars signified the differences between treatments at P<0.05. 69
Figure 3-5: The Growth Inhibition Ratio (IR) of Chlorella sp. under different concentrations of laponite versus cultivation days 70

Figure 3-6: Chlorophyll content of *Chlorella* sp. under different concentrations of laponite versus cultivation days, a) 0.1% (r^2=0.650, P<0.001), b) 0.2% (r^2=0.489, P<0.001), c) 0.3% (r^2=0.497, P<0.001), d) 0.4% (r^2=0.541, P=0.05), and e) 0.5% (r^2=0.407, P<0.001) laponite (by dry weight) in the growth medium and f) BG-11 (r^2=0.625, P<0.001) only. The dots show mean chlorophyll content and error bars represent the standard deviation. 72
Figure 3-7: Effect of laponite concentrations on the chlorophyll content of *Chlorella* sp. The bars show the mean chlorophyll content and errors refer to standard deviation. The statistic derived from a one-way ANOVA with post-hoc Tukey test. The letters above the bars signified the differences between treatments at P<0.05. 73
Figure 3-8: SEM images a) a single cell of Chlorella sp. in the control medium (BG-11), b) a single cell of Chlorella sp. at 0.1% treatment, c) microalgae accumulation, and d-f) different patterns of Chlorella sp. accumulation in the control medium. 75
Figure 3-9: SEM images a-c) the cells of *Chlorella* sp. are sitting on laponite gel (0.1% treatment), d-g) the cells of *Chlorella* sp. are surrounded by laponite gel (0.2% treatment), h) the cells of *Chlorella* sp. are covered by laponite gel (0.4% treatment), and i) laponite gel formation (0.5% treatment). 76
Figure 4-1: Grain size distribution of sand 86
Figure 4-2: (a) Laponite particle in dry state, (b) Laponite dispersion in gel state, and (c) Sand-laponite..... 88
Figure 4-3: Change of viscosity with gelling time for 0.5%, 1.5%, and 3% laponite suspension at room temperature (viscosity was measured at spindle speed 100) 88
Figure 4-4: Generation of pore water pressure in pure sand and sand specimens treated with laponite at different concentrations after 72 hours of resting time. 95
Figure 4-5: Comparisons of stress-strain graphs of pure sand and sand-laponite mixtures at room temperature. 97
Figure 4-6: Friction angles and cohesion of pure sand and treated sand specimens at room temperature 99
Figure 4-7: Effect of temperature on the friction angle of pure sand and sand-laponite mixtures 101
Figure 4-8: Microstructure images by SEM of (a) pure sand under 1.00 mm magnification, (b) pure sand under 500 µm magnification, (c) sand+1.5% laponite specimen under 1.00 mm magnification, and (d) sand+1.5% laponite specimen under 500 µm magnification 103
Figure 4-9: Microstructure images by SEM of (a) sand+1.5% laponite specimen under 50 µm magnification, and (b) sand+1.5% laponite specimen under 5 µm magnification 105
Figure 5-1: Microstructure of laponite gel, SEM images at (a) 500 µm, (b) 100 µm, and (c) 10 µm magnification.....119
Figure 5-2: Particle Size Distribution (PSD) of laponite and bentonite 120
Figure 5-3: Cross-section of a one-dimensional oedometer cell..... 121
Figure 5-4: (a) Cross-section of the modified triaxial cell, and (b) modified triaxial cell for the swelling pressure tests..... 122
Figure 5-5: Swelling test using the tea bags. 123
Figure 5-6: Swelling index of laponite using the visual tube tests. 124

Figure 5-7: (a) Laponite powder, (b) laponite hydrogel inside the sample holder, and (c) laponite hydrogel after the initial swelling test. 125
Figure 5-8: Swelling tests of the fresh laponite powder. 127
Figure 5-9: Swelling strain of sand+3% laponite and sand+5% laponite specimens. 129
Figure 5-10: Laponite hydrogel after dried up at 100°C for 24 hours in a temperature-controlled oven 130
Figure 5-11: (a) Swelling strain of compacted laponite hydrogel from the swelling and reswelling tests, (b) close-up of the swelling strain of the compacted laponite hydrogel from the swelling and reswelling tests for the initial 50 hours. 132
Figure 5-12: Water Retention Ratio (%) of the swollen laponite hydrogel during the reswelling tests at room temperature (23°C) 133
Figure 5-13: Swelling strain of the compacted bentonite from the swelling and reswelling tests 134
Figure 5-14: (a) Laponite hydrogel after the initial swelling test, (b) after the reswelling test-1 (laponite only), and (c) after the reswelling test-2 (laponite only) 135
Figure 5-15: Swelling pressure of the compacted laponite hydrated with water 137
Figure 6-1: (a) Hysteretic loop, shear modulus, and damping, after Park (1998), and (b) Effect of damping in a single degree of freedom system, after Moreira (2015) 147
Figure 6-2: Particle Size Distribution (PSD) of laponite and bentonite. 150
Figure 6-3: Chemical composition of laponite and bentonite using the X-ray Diffraction Method (XDM) 151
Figure 6-4: Bender Elements manufactured by Piezo.com, Division of Mide Technology, Woburn, MA, United States. 154
Figure 6-5: (a) Parallel-connected and (b) Series-connected wired bender elements 154
Figure 6-6: Bender elements housing set-up 155
Figure 6-7: (a) Schematic diagram of experimental setup using bender elements, (b) Photo of the experimental setup 157
Figure 6-8: Electronic Devices 159
Figure 6-9: Resonant curve for the half-power bandwidth method, after Moreira, (2015) 161
Figure 6-10: Comparisons of damping ratio (%) of pure sand and sand treated with laponite at different concentrations 165
Figure 6-11: Comparisons of damping ratio (%) of pure sand and sand+bentonite at different concentrations 167
Figure 6-12: (a) Sand+3% laponite sample immediately after releasing from the experimental set-up, (b) Sand+3% laponite sample after drying, (c) Sand+1% laponite, sand+2% laponite, and sand-3% laponite samples after drying, (d) Sand+2% bentonite sample, and (e) Sand+3% laponite and sand+3% bentonite samples after drying. 169
Figure 7-1: Microstructure of laponite gel, SEM images at (a) 500 μm, (b) 100 μm, and (c) 10 μm magnification 181
Figure 7-2: Coefficient of Permeability (κ) of untreated (pure) sand and sand treated with nanoparticles (laponite, bentonite) at various concentrations 186
Figure 7-3: Coefficient of Permeability (κ) of sand treated with nanoparticles (laponite, bentonite) at different confining pressures (69, 172, and 275 kPa) 187

Figure 7-4: Relationship between the coefficients of permeability (κ) and void ratio (e) of sand-nanoparticle samples (0.5%, 1%, 2%, and 3% of dry mass of nanoparticle/dry mass of sand) . 189
Figure 7-5: Variation of Skeleton and bulk (e_{min} and e_{max}) with laponite at different concentrations, after, Ochoa-Cornejo (2015)..... 190
Figure 7-6: The stress-strain curves of laponite hydrogel at two different displacement rates. 192

List of Figures

Figure 1-1: (a) Soil liquefaction in Christchurch: the 2011 earthquake led to the formation a layer of water and fine sand on street surface [3], (b) Sand boil (erupted of liquefied sand) during the 2010 Randolph earthquake, one of the smallest earthquakes recorded events to induce liquefaction [4]. 2
Figure 2-1: Liquefaction concept of Schofield, after Schofield [67] 14
Figure 2-2: Scale comparison of nanoparticles dimension 15
Figure 2-3: Formulation of siloxane bonds and a schematic of the colloidal silica particle, after Spencer et al. [101] 19
Figure 2-4: Unconfined compressive strength of sand-CS mixture versus the concentration of CS, after Persoff et al. [52] 20
Figure 2-5: Bentonite Powder 24
Figure 2-6: The structural formula of bentonite, after Perry [140] 24
Figure 2-7: (a) Effect of bentonite treatment in increasing cyclic resistance of sand in undrained cyclic triaxial tests, and (b) Effect of aging time (1 to 10 days) preceding shear, after El Mohtar et al., [166] 26
Figure 2-8: Laponite Powder 29
Figure 2-9: (a) Geometry of individual laponite particles, and (b) Idealized structural formula of laponite, after BYK Additives and Instruments [174] 29
Figure 2-10: (a) Relationship between cyclic stress ratio (CSR) and number of cycles to liquefaction for pure sand and laponite-sand specimens, and (b) Effect of laponite on the CSR corresponding to a given number of cycles to liquefaction, after Ochoa-Cornejo et al. [181]..... 32
Figure 2-11: Typical consistency curves for 3% laponite-RD suspensions at different ageing times, after Chen [185] 38
Figure 2-12: Thixotropic loop of laponite suspension, after Chen [185]. 39
Figure 3-1: Images of Chlorella sp. a) lower magnification (40x), and b) higher magnification (100x) using a compound microscope 62
Figure 3-2: Cell density of *Chlorella* sp. under different concentrations of laponite versus cultivation days, a) 0.1% (r^2=0.621, P<0.001), b) 0.2% (r^2=0.643, P<0.001), c) 0.3% (r^2=0.191, P<0.001), d) 0.4% (not significant), and e) 0.5% (not significant) laponite (by dry weight) in the growth medium, and f) BG-11 (r^2=0.536, P<0.001) only. The dots show the mean cell density and the error bars represent standard deviations. 66
Figure 3-3: Effect of laponite treatment at different concentrations on the cell density of *Chlorella* sp. The bars show the mean cell density and errors refer to standard deviation. The statistic was derived from a one-way ANOVA with a posthoc Tukey test. The letters above the bars signified the differences between treatments at P<0.05. 67
Figure 3-4: The specific growth rate of *Chlorella* sp. under different laponite concentrations with culture period. The bars show the mean specific growth rate and errors refer to standard deviation. The statistic was derived from a one-way ANOVA with a posthoc Tuk Tukey test. The letters above the bars signified the differences between treatments at P<0.05. 69
Figure 3-5: The Growth Inhibition Ratio (IR) of Chlorella sp. under different concentrations of laponite versus cultivation days 70

Figure 3-6: Chlorophyll content of *Chlorella* sp. under different concentrations of laponite versus cultivation days, a) 0.1% (r^2=0.650, P<0.001), b) 0.2% (r^2=0.489, P<0.001), c) 0.3% (r^2=0.497, P<0.001), d) 0.4% (r^2=0.541, P=0.05), and e) 0.5% (r^2=0.407, P<0.001) laponite (by dry weight) in the growth medium and f) BG-11 (r^2=0.625, P<0.001) only. The dots show mean chlorophyll content and error bars represent the standard deviation. 72
Figure 3-7: Effect of laponite concentrations on the chlorophyll content of *Chlorella* sp. The bars show the mean chlorophyll content and errors refer to standard deviation. The statistic derived from a one-way ANOVA with post-hoc Tukey test. The letters above the bars signified the differences between treatments at P<0.05. 73
Figure 3-8: SEM images a) a single cell of Chlorella sp. in the control medium (BG-11), b) a single cell of Chlorella sp. at 0.1% treatment, c) microalgae accumulation, and d-f) different patterns of Chlorella sp. accumulation in the control medium. 75
Figure 3-9: SEM images a-c) the cells of *Chlorella* sp. are sitting on laponite gel (0.1% treatment), d-g) the cells of *Chlorella* sp. are surrounded by laponite gel (0.2% treatment), h) the cells of *Chlorella* sp. are covered by laponite gel (0.4% treatment), and i) laponite gel formation (0.5% treatment). 76
Figure 4-1: Grain size distribution of sand 86
Figure 4-2: (a) Laponite particle in dry state, (b) Laponite dispersion in gel state, and (c) Sand-laponite..... 88
Figure 4-3: Change of viscosity with gelling time for 0.5%, 1.5%, and 3% laponite suspension at room temperature (viscosity was measured at spindle speed 100) 88
Figure 4-4: Generation of pore water pressure in pure sand and sand specimens treated with laponite at different concentrations after 72 hours of resting time. 95
Figure 4-5: Comparisons of stress-strain graphs of pure sand and sand-laponite mixtures at room temperature. 97
Figure 4-6: Friction angles and cohesion of pure sand and treated sand specimens at room temperature 99
Figure 4-7: Effect of temperature on the friction angle of pure sand and sand-laponite mixtures 101
Figure 4-8: Microstructure images by SEM of (a) pure sand under 1.00 mm magnification, (b) pure sand under 500 µm magnification, (c) sand+1.5% laponite specimen under 1.00 mm magnification, and (d) sand+1.5% laponite specimen under 500 µm magnification 103
Figure 4-9: Microstructure images by SEM of (a) sand+1.5% laponite specimen under 50 µm magnification, and (b) sand+1.5% laponite specimen under 5 µm magnification 105
Figure 5-1: Microstructure of laponite gel, SEM images at (a) 500 µm, (b) 100 µm, and (c) 10 µm magnification.....119
Figure 5-2: Particle Size Distribution (PSD) of laponite and bentonite 120
Figure 5-3: Cross-section of a one-dimensional oedometer cell..... 121
Figure 5-4: (a) Cross-section of the modified triaxial cell, and (b) modified triaxial cell for the swelling pressure tests..... 122
Figure 5-5: Swelling test using the tea bags. 123
Figure 5-6: Swelling index of laponite using the visual tube tests. 124

Figure 5-7: (a) Laponite powder, (b) laponite hydrogel inside the sample holder, and (c) laponite hydrogel after the initial swelling test. 125
Figure 5-8: Swelling tests of the fresh laponite powder. 127
Figure 5-9: Swelling strain of sand+3% laponite and sand+5% laponite specimens. 129
Figure 5-10: Laponite hydrogel after dried up at 100°C for 24 hours in a temperature-controlled oven 130
Figure 5-11: (a) Swelling strain of compacted laponite hydrogel from the swelling and reswelling tests, (b) close-up of the swelling strain of the compacted laponite hydrogel from the swelling and reswelling tests for the initial 50 hours. 132
Figure 5-12: Water Retention Ratio (%) of the swollen laponite hydrogel during the reswelling tests at room temperature (23°C) 133
Figure 5-13: Swelling strain of the compacted bentonite from the swelling and reswelling tests 134
Figure 5-14: (a) Laponite hydrogel after the initial swelling test, (b) after the reswelling test-1 (laponite only), and (c) after the reswelling test-2 (laponite only) 135
Figure 5-15: Swelling pressure of the compacted laponite hydrated with water 137
Figure 6-1: (a) Hysteretic loop, shear modulus, and damping, after Park (1998), and (b) Effect of damping in a single degree of freedom system, after Moreira (2015) 147
Figure 6-2: Particle Size Distribution (PSD) of laponite and bentonite. 150
Figure 6-3: Chemical composition of laponite and bentonite using the X-ray Diffraction Method (XDM) 151
Figure 6-4: Bender Elements manufactured by Piezo.com, Division of Mide Technology, Woburn, MA, United States. 154
Figure 6-5: (a) Parallel-connected and (b) Series-connected wired bender elements 154
Figure 6-6: Bender elements housing set-up 155
Figure 6-7: (a) Schematic diagram of experimental setup using bender elements, (b) Photo of the experimental setup 157
Figure 6-8: Electronic Devices 159
Figure 6-9: Resonant curve for the half-power bandwidth method, after Moreira, (2015) 161
Figure 6-10: Comparisons of damping ratio (%) of pure sand and sand treated with laponite at different concentrations 165
Figure 6-11: Comparisons of damping ratio (%) of pure sand and sand+bentonite at different concentrations 167
Figure 6-12: (a) Sand+3% laponite sample immediately after releasing from the experimental set-up, (b) Sand+3% laponite sample after drying, (c) Sand+1% laponite, sand+2% laponite, and sand-3% laponite samples after drying, (d) Sand+2% bentonite sample, and (e) Sand+3% laponite and sand+3% bentonite samples after drying. 169
Figure 7-1: Microstructure of laponite gel, SEM images at (a) 500 μm, (b) 100 μm, and (c) 10 μm magnification 181
Figure 7-2: Coefficient of Permeability (κ) of untreated (pure) sand and sand treated with nanoparticles (laponite, bentonite) at various concentrations 186
Figure 7-3: Coefficient of Permeability (κ) of sand treated with nanoparticles (laponite, bentonite) at different confining pressures (69, 172, and 275 kPa) 187

Figure 7-4: Relationship between the coefficients of permeability (κ) and void ratio (e) of sand-nanoparticle samples (0.5%, 1%, 2%, and 3% of dry mass of nanoparticle/dry mass of sand) . 189
Figure 7-5: Variation of Skeleton and bulk (e_{min} and e_{max}) with laponite at different concentrations, after, Ochoa-Cornejo (2015)..... 190
Figure 7-6: The stress-strain curves of laponite hydrogel at two different displacement rates. 192

List of Abbreviations and Symbols

SGR:	Specific growth rate
IR:	Growth inhibition ratio
CD_0:	Cell density values of the control group
CD:	Cell density values of the experimental group
CD_1:	Cell density values at the Nth day
CD_2:	Cell density values at the (N+1)th day
T_1:	The cultivation time of Nth day
T_2:	The cultivation time of (N+1)th day
nZVI:	Nano-zerovalent-iron
BG-11:	Control growth medium
SEM:	Scanning Electron Microscope
E:	Modulus of Elasticity
C:	Cohesion
HA-PDMS:	Hyaluronate-Poly dimethylsiloxane-diglycidyl
GMZ:	Gaomiaozi -bentonite
d_{50}:	Median diameter
d_{90}:	Particle size below which 90% of all particles are found
e_{max}:	Maximum void ratio
e_{min}:	Minimum void ratio
PPT	Pore pressure transducer
S:	Swelling capacity
W_s:	The measured weights of hydrogel at the swelling state
W_d:	The measured weights of hydrogel at the dry state
SI:	Swelling index
h:	Height of the sample to the nearest hundredth of millimeter
h_{min}:	The minimal height of laponite displaying maximum compression for a given set of samples.
ξ:	Damping ratio
FFT:	Fast Fourier Transform

DFT:	Discrete Fourier Transform
CEC:	Cation Exchange Capacity [meq/100g]
XFM:	X-ray Fluorescence Method
XDM:	X-ray Diffraction Method
HDPE:	High-density polyethylene
HPBM:	Half-Power Bandwidth Method
κ:	Coefficient of permebaility
F-x:	Load-displacement
σ-ε:	Stress-strain
G_s:	Specific Gravity
$e_{skeleton}$:	Skeleton void ratio
e_{bulk}:	Bulk void ratio
$e_{min\ bulk}$:	The minimum Bulk void ratio
$e_{max\ bulk}$:	The maximum bulk void ratio
$e_{min\ skeleton}$:	The minimum skeleton void ratio
$e_{max\ skeleton}$:	The maximum skeleton void ratio
e:	Overall void ratio
f_c:	The percentage of the mass of particles smaller than 5 mm in the total particle mass and can be also expressed as $P_{<5}$
B:	The percentage of the mass of the fine particles that serve as skeletons to the mass of all fine particles

CHAPTER 1 Introduction

1.1 Problem Statement

In general, there are two primary types of ground responses that can damage civil engineering structures: soil liquefaction and soil amplification of ground motion [1]. Earthquakes induce rapid ground shaking, leading to undrained cyclic shearing in loose, saturated granular deposits. This process generates excess pore pressure since the water within the pores cannot escape quickly enough. The phenomenon of liquefaction, along with the associated catastrophic damage, was first extensively documented during the 1964 Alaska Earthquake and the Niigata Earthquake, both of which had magnitudes exceeding M=9 [2]. To effectively address liquefaction, it is essential to comprehend the mechanisms governing the development of excess pore pressure under undrained conditions. Effective stresses, strains, and technical features like stiffness and compressibility are all influenced by the excess pore pressures. Liquefaction occurs in saturated loose granular soils when cyclic shearing causes movement in sand particles, leading to excessive pore water pressures during earthquakes. This prevents the sand particles from becoming denser and reduces effective stress with each loading cycle. When the effective stress eventually reaches zero, liquefaction occurs, resulting in significant ground deformations, and eventually catastrophic failure of structures on sand deposits. As shown in **Figure *1-1***, liquefaction was notably observed during the 2011 earthquake in Christchurch and the 2010 Randolph earthquake (M=4.5), the latter being one of the smallest recorded earthquakes to induce liquefaction. These events highlight the critical need for assessing liquefaction potential even in relatively minor seismic activities. Such assessments are crucial for ensuring the safety of structures, as earthquake can trigger liquefaction in susceptible soils, leading to unexpected and severe impacts. Research has focused on developing effective methods to strengthen the liquefaction resistance of susceptible soil deposits. Understanding the fundamental processes governing excess pore water pressure development is essential for mitigating the risks associated with soil liquefaction.

(a) (b)

Figure 1-1: (a) Soil liquefaction in Christchurch: the 2011 earthquake led to the formation a layer of water and fine sand on street surface [3], (b) Sand boil (erupted of liquefied sand) during the 2010 Randolph earthquake, one of the smallest earthquakes recorded events to induce liquefaction [4].

Densification is one of the most common soil improvement techniques aimed at increasing liquefaction resistance and limiting sand deformation. Traditional densification techniques are generally classified into two main categories: (a) in-situ or active site densification techniques; and (b) grouting or passive site densification techniques. These techniques can effectively enhance the bearing capacity of soil; however, they can also cause significant environmental and residential disturbance and potentially compromise structural stability through dynamic compaction and vibration. These limitations make in-situ densification techniques more suitable for undeveloped areas, posing challenges for application in developed sites. The grouting (underpinning) are the most practical methods in constrained and developed sites [5]. Underpinning involves extending the foundation in-depth or breadth, allowing it to eventually rest on a more supportive soil layers and distribute its load over a wider region. This approach significantly increases the stress states of existing structural components to prevent liquefaction, focusing on specific structures rather than the entire ground. Cement slurry, sodium silicate ($Na_2O.nSiO_2$), and chemical grouts (such as acrylate and epoxy) are commonly used grouting materials. However, the chemical compounds are often hazardous and can pollute local subterranean water, as well as provide a significant threat of damage to nearby structures if mishandled [6]. Alternative methods and materials for reducing the liquefaction risks should be explored as a result of progress in urbanization and technological advancement.

Researchers are increasingly utilizing nanoscale modifications to enhance the properties of geotechnical materials for specific applications. Due to the rapid growth of nanotechnology, nanoparticles are now being investigated for their potential to improve the soil strength. Nanoparticles are small particles with at least one dimension smaller than 100 nanometers, characterized by their unique structure, large specific surface area, and high surface activity [7]. According to the US National Research Council [8], studies of clay-sized particles in geotechnical engineering are in the early stages of nanotechnology application. The well-known nanoparticles, carbon nanotubes, colloidal silica, bentonite, and laponite, have the potential to enhance soil strength and stability. Yonekura and Kaga [9], Persoff et al. [10], and Gallagher [11] suggested using nanoparticles, particularly colloidal silica, for passive site rehabilitation to lessen the liquefaction risk. Various methodologies, including laboratory experiments, model testing, and full-scale field tests, have demonstrated how colloidal silica increases liquefaction resistance. El Mohtar et al. [12,13] and Rugg et al. [14] examined the effects of bentonite on the initiation of excess pore pressure at small strains, the development of pore water pressure at large strains under monotonic loading, and the rate of pore pressure generation during cyclic loading. These investigations provide critical insights into the mechanisms by which bentonite can enhance the liquefaction resistance of susceptible soils.

Huang and Wang [15] and Ochoa-Cornejo et al. [16] investigated the impact of small percentages of laponite (1% to 3%) on the liquefaction resistance of sand. These percentages of the nanoparticles are below the threshold values for liquefaction resistance and are on the lower end of values tested by other researchers, such as Youd et al. [17]. Laponite can increase the liquefaction resistance of sand, offering better material properties and conductivity than nano bentonite [13], while also being more cost-effective in terms of price/performance ratio [15]. Its small size and favorable rheological features which form a transparent gel, make laponite simpler to use than other existing nanoparticles. Howayek et al. [18] used direct imaging to reveal the structure of sand–laponite suspension systems, highlighting their elongated cellular structure, which influences their macro-scale geotechnical properties. The applications of nanotechnology in geotechnical engineering are relatively new and remains in the research and development phase. Nanoparticles are being used to control the movement of liquids, including various types of contaminants within soil layers. However, there are growing concerns about the environmental and human health impacts of nanoparticle in aquatic ecosystems. For example, carbon nanotubes

have been suggested to potentially affect the immune system and cause serious human diseases such cancer, lung disorders, and skin disorders [19]. Therefore, it is important to determine whether laponite is environmentally safe before injecting it into the ground. Currently, no published studies address the effects of laponite on aquatic ecosystems.

Limited research [15,16] provides some insight into the microstructural characteristics and rheological properties of laponite suspensions, but there is no comprehensive literature explaining how laponite alters or enhances the characteristics of sand under static loading conditions. The swelling of laponite has received little attention, despite its advantages over natural clays, such as smaller particle size, lower structural polydispersity (dimensions, surface charge), and superior water stability compared to montmorillonite [20]. However, the foundation and superstructure of any engineering structure risk catastrophic collapse if the treated ground beneath it swells significantly. Therefore, understanding this phenomenon is essential before using laponite suspensions to improve ground performance in seismic zones. Comprehensive investigation onto the swelling capacity and repetitive drying-wetting behaviour of laponite are necessary. Understanding the dynamic characteristics of soil is vital for assessing the potential for catastrophes during seismic events. In geotechnical engineering, the damping ratio is commonly used to measure energy dissipation at the grain-to-grain contact level due to friction interactions [21]. During primary consolidation, the dynamic shear modulus of remolded kaolinite and Ca-montmorillonite increased by 10% and 40%, respectively [22]. Though, the effect of clay mineralogy on the damping ratio remains unclear. Ochoa-Cornejo [16] reported that higher damping values for sand-laponite specimens reflect a viscous damping contribution from the presence of laponite at the sand-grain contacts. Nonetheless, the damping ratio (ξ) of treated sand has not been thoroughly examined. Further research is needed to fully understand the environmental impact and mechanical behavior of laponite, including its swelling properties and damping ratio, before it can be safely and effectively used to improve soil performance in seismic zones.

This study presents a novel approach by addressing critical gaps in the existing literature regarding the effects of laponite on non-cohesive soils, particularly under static loading conditions. While previous research has explored the microstructural and rheological properties of laponite suspensions, this research is pioneering in its comprehensive investigation into the mechanical

behavior of sand treated with laponite, including its swelling properties and damping ratio. The study also uniquely explores the potential toxic effects of laponite on freshwater algae, providing valuable insights into both its environmental impact and engineering applications. Furthermore, by focusing on the influence of laponite on soil permeability and compressive behavior, this research opens new avenues for improving soil performance in geotechnical applications, particularly in seismic zones.

1.2 Research Objectives

1.2.1 General Objective

The main objective of this research is to experimentally investigate the effects of laponite on the strength properties and indices of non-cohesive soil. This study aims to provide a comprehensive and high-quality database, as well as a conceptual framework, detailing the changes in sand properties when treated with laponite.

1.2.2 Specific Objectives

1. Examine the potential toxic effects of laponite on the growth characteristics of freshwater green algae *Chlorella* sp.
2. Investigate the efficacy of laponite in increasing the effective stress and subsequently the shear strength of sand by reducing the excess pore water generation under static loading.
3. Investigate the swelling properties of laponite hydrogel and sand treated with laponite at different concentrations.
4. Examine the damping ratio of sand specimens mixed with laponite using a one-dimensional bender elements setup.
5. Assess the coefficient of permeability of sand treated with laponite at different concentrations and investigate the compressive behaviour of laponite hydrogel.

1.3 Dissertation Organization

In addition to this chapter, the dissertation comprises seven more chapters, each addressing various aspects of the research work.

Chapter 2 presents a comprehensive literature review on nanoparticles, liquefaction, ground improvement using nanoparticle, the current understanding of nanoparticles' effects on liquefactions, and potential field applications.

Chapter 3 examines the potential toxic effects of laponite on aquatic system. This chapters investigates the growth rate (cell density, specific growth rate) and total chlorophyll content of the freshwater green algae *Chlorella* sp. isolated from northern Ontario.

Chapter 4 analyses the efficacy of laponite in improving the strength properties of sand under static loading. It includes a series of triaxial tests to determine the effects of laponite concentration and resting time on sand strength, along with shear box tests to assess the temperature effects on laponite-treated sand samples. Scanning Electron Microscope (SEM) imaging is presented to understand the possible reasons for the non-homogenous mixture of sand-laponite.

Chapter 5 contains various experimental setups to study the swelling properties of laponite hydrogel and sand-laponite mixtures in a controlled laboratory environment. It includes a one-dimensional oedometer setup to examine the effects of repeated drying and wetting processes on laponite hydrogel and a one-dimensional in-built experimental setup to assess the swelling pressure. Additionally, the SEM imaging is used to analyse the microstructure of the swollen laponite, proving the detailed insights into its behavior and characteristics.

Chapter 6 presents findings on the damping ratio of sand specimens mixed with laponite using a one-dimensional bender elements setup. It also includes comparative results from similar experiments conducted with pure sand and sand treated with bentonite. Detailed step-by-step instructions for the construction and operation of the bender elements setup are provided, ensuring reproducibility and clarity in experimental methodology.

Chapter 7 demonstrates the coefficient of permeability (κ) of sand treated with different concentrations of laponite and the compressive behaviour of laponite hydrogel. Permeability of sand-laponite is assessed using both a standard compaction mold permeameter and a triaxial cell. A uniaxial universal tester is used for compression testing of laponite hydrogel, providing comprehensive insights into its mechanical properties.

Chapter 8 summarizes the research, highlights the main findings, and provides conclusions. Recommendations for future research are also suggested to further enhance the understanding and application of laponite in geotechnical engineering.

Appendices

- **Appendix A**
- **Appendix B**: MATLAB Code
- **Appendix C**: License agreement for the published journal papers.

1.4 References

[1] Dobry R and Iai S (2000) Recent developments in the understanding of earthquake site response and associated seismic code implementation, *Proceedings of GeoEngg Conference*, Melbourne (Australia).

[2] Youd L (1978) Major cause of earthquake damage is ground failure, *Civil Engineering-ASCE*, 48(4):47-51.

[3]https://en.wikipedia.org/wiki/Soil_liquefaction#/media/File:Liquefaction_in_Peterborough_St.JPG (last accessed on June 2024)

[4] https://geology.utah.gov/hazards/earthquakes/liquefaction/ (last accessed on June 2024)

[5] Gallagher P, Pamuk A and Abdoun T (2007) Stabilization of liquefiable soils using colloidal silica grout. *J Mater Civ Eng* 19:33–40.

[6] Vik E, Sverdrup L, Kelley L, Storhaug R, Beitnes A, Boge K, Grepstad G and Tveiten V (2000) Experiences from environmental risk management of chemical grouting agents used during construction of the romeriksporten tunnel. *Tunnelling and Underground Space Technol* 15(4):369–378.

[7] Cao W (2004) Nanostructures and nanomaterials-synthesis, properties and applications. Imperial College Press, London.

[8] National Research Council (2006). Geological and geotechnical engineering in the new Millennium: opportunities for research and technological innovation. *National Academies Press*, Washington.

[9] Yonekura R and Kaga M (1992) Current chemical grout engineering in Japan, *Proc Grouting Soil Improvement and Geosynthetics*, ASCE, New York.

[10] Persoff P, Apps J, Moridis G and Whang J (1999) Effect of dilution and contaminants on sand grouted with colloidal silica. *J of Geotechnical and Geoenvironmental Engineering* 125:461–469.

[11] Gallagher P (2000) Passive site remediation for mitigation of liquefaction risk (PhD Dissertation). Virginia Polytechnic Institute and State University, Virginia, United States.

[12] El Mohtar C, Bobet A, Santagata M, Drnevich V and Johnston C (2013) Liquefaction mitigation using bentonite suspensions. ASCE *J Geotechnical and Geoenvironmental Engineering* 139:1369–1380.

[13] El Mohtar C, Bobet A, Santagata M, Drnevich V and Johnston C (2008) Cyclic response of sand with thixotropic pore fluid, Geotech earthquake eng and soil dyn IV (eds D. Zeng, M. T. Manzari and D. R. Hiltunen). *Geotech Special Pub* 181 (CD-ROM). Reston, VA, USA: ASCE.
[14] Rugg D, Yoon J, Hwang H and El Mohtar CS (2011) Undrained shearing properties of sand permeated with a bentonite suspension for static liquefaction mitigation. Geo-frontiers 2011 *Adv Geotech Eng Geotech Special Publication* 211, 677686 (CD-ROM).
[15] Huang Y and Wang L (2016) Laboratory investigation of liquefaction mitigation in silty sand using nanoparticles. *Eng Geol* 204, 23–32.
[16] Ochoa-Cornejo F, Bobet A, Johnston C, Santagata M and Sinfield J (2016) Cyclic behavior and pore pressure generation in sands with laponite, a super-plastic nanoparticle. *Soil Dyn Earthq Eng* 88:265–279.
[17] Youd T, Idriss I, Andrus R, Arango I, Castro G and Christian J (2001) Liquefaction resistance of soils: summary report from the 1996 NCEER and 1998 NCEER/NSF workshops on evaluation of liquefaction resistance of soils. *J Geotechnical and Geoenvironmental Engineering* 127:817–33.
[18] Howayek A, Bobet A, Johnston C, Santagat M and Sinfield J (2014) Microstructure of sand laponite water systems using cryo-sem. Presented at *the Geo-Congress 2014 Technical Papers*, ASCE, pp. 693-702.
[19] Dhawan V, Dhoat S, Williams A, Dimarco A, Pal S, Forbes A, Tobías A, Martinez-Martin P, and Chaudhuri K (2006) The range and nature of sleep dysfunction in untreated Parkinson's disease (PD). A comparative controlled clinical study using the Parkinson's disease sleep scale and selective polysomnography. *J Neurol Sci* 25:158–62.
[20] Valencia GA, Djabourov M, Carn F and Sobral PJA (2018) Novel insights on swelling and dehydration of laponite. *Colloid and Interface Science Communications* 23:1-5.
[21] Ram AK and Mohanty S (2023) Laboratory investigation on damping characteristics of homogeneous and stratified soil-ash system. *J of Rock Mech Geotech Eng* 15: 2757-2777.
[22] Marcuson WF and Wahls HE (1972) Time effects on dynamic shear modulus of clays. *J Soil Mech Found Div* 98(12):1359-1373.

CHAPTER 2 Literature Review

2.1 Introduction

In geotechnical engineering, the development and intensification of excess pore water pressure in saturated or partially saturated sand are critical to understanding and predicting liquefaction, as it ultimately affects the shear strength and stress-strain behavior of sand under static and cyclic loading [1]. The generation of excess pore pressure can lead to loss of strength and ultimately liquefaction, causing considerable deformation in sand and, in certain situations, catastrophic destruction of structures on the loose to medium granular deposits [2-5]. Published studies illustrate a strong correlation between the normalized excess pore water pressure ratio and the ratio of the number of loading cycles to the total cycles required for liquefaction (e.g., [6-8]). Lee and Albaisa [7] showed a continuous increase in excess pore water pressure as cyclic loading advanced in undrained cyclic loading tests on the Sacramento River and Monterey sands. The authors proposed that the excess pore pressure for given sand falls within a narrow band, which is unaffected by the initial density and consolidation stress of sand. De Alba et al. [6] obtained similar results with Monterey sand. Dobry et al. [9] and Dobry [10] investigated the pore pressure development as a function of shear strain during strain-controlled, undrained cyclic loading at different relative densities. Interestingly, it has been mentioned that the developed excess pore pressure lay within a restricted narrow band, which did not show until a threshold shear strain was reached. Dobry [10] referred to it as the threshold shear strain. Hsu and Vucetic [11] and Hazirbaba and Rathje [12] also found the same threshold strain in their studies. The response of clean sand has been the focus of substantial research on the cyclic behavior and pore pressure development in the granular soil layers (e.g., [13-15]). Natural sand deposits can contain varying proportions of fine particles and cementation, necessitating research into the effect of variation on the cyclic behavior of sand [16-19].

** A version of this chapter has been published in Soil Mechanics and Foundation Engineering, Vol. 60, Pages:149-157 (2023) and Soil Mechanics and Foundation Engineering, Vol. 60, Pages:244-252 (2023).*

Several laboratory experiments on the impact of non-plastic fines focusing on the cyclic response and pore pressure development in the sand during undrained loading have been studied (e.g., [17, 20-27]). The presence of plastic particles as well as cementation is widely acknowledged for increasing the cyclic resilience of sand by both field observations and laboratory experiments [28-32]. These investigations reveal a complex behavior of fines in sand response, where the quantity and types of both plastic and non-plastic fines are critical. Georgiannou et al. [33], Yamamuro and Lade [34], Murthy et al. [35], and Bobei et al. [36] proved that under static loading, the existence of fines also influences the undrained response. Sand with fines has been demonstrated to have a reverse pattern of pore pressure development with enhanced instability at lower pre-shear effective stresses [34]. Polito [37] found that the curves of normalized excess pore pressure against the normalized number of cycles for up to 17% kaolinite in Yatesville sand fall within the band formed by the data for sand with no fines and are within the range found in the earlier studies for clean sand. Furthermore, these findings show that fines with higher plasticity generate pore water pressure at a faster rate during the initial half of the test. Few researchers have explored the effect of fines on pore pressure generation [12]. According to Hsu and Vucetic [11], increasing the plasticity of the fines (such as cohesive soils) could lead to an increase in the threshold shear strain. The goal of the research presented in their study was to gain a better understanding of the mechanisms that cause excess pore pressure to develop in the sand with highly plastic fines. Liquefaction is a common issue of damaging engineered structures during natural and artificial ground-shaking events, such as explosions, blasting, earthquakes [38-40]. Bird and Bommer [41] examined fifty destructive earthquakes worldwide and found that liquefaction occurred in 62% of those earthquakes, causing 15%–30% of the earthquake damage. As a result, the geotechnical community continues to be interested in finding better solutions to reduce liquefaction, particularly near existing structures, where traditional treatment methods relying on soil densification are not always feasible.

Densification is a widely used soil improvement techniques aimed at increasing liquefaction resistance and minimizing sand deformation. Traditional liquefaction mitigation techniques are generally classified into two main categories: (a) in-situ densification techniques; and (b) grouting. In-situ densification techniques include methods such as deep mixing, dynamic compaction, Vibro-compaction, explosive compaction, and granular piles [42-45]. These methods can successfully increase the liquefaction resistance and bearing capacity of soil. However, they often

cause significant environmental and residential disturbance and undermine structural stability due to vibration and dynamic impacts. These drawbacks limit their applicability in developed sites, where such techniques may be less feasible. In contrast, these methods are more suitable in undeveloped areas. Grouting and underpinning are practical alternatives for constrained and developed locations [46]. Underpinning involves extending the foundation in depth or breadth to rest on a more supportive soil layer, thus distributing the load across a larger area and enhancing the stress states of existing structural components to prevent liquefaction. This approach focuses on individual structures rather than treating the entire ground. Common grouting materials include cement slurry, sodium silicate ($Na_2O.nSiO_2$), and chemical grouts (such as acrylate and epoxy). Cement grouts are typically injected under high pressure due to the high initial viscosity and are used to create grout columns rather than penetrating the entire area beneath the infrastructure. This cement grouts are generally suitable for fine to medium sand. However, chemical grouts can be hazardous, potentially contaminating local subterranean water and posing risks to nearby structures if not handled properly [47]. Given the challenges posed by urbanization and technological advancements, alternative methods and materials for reducing liquefaction risks should be explored [48].

Nanoparticle materials are increasingly being utilize to improve soil strength due to their unique properties, including a large specific surface area, and high surface activity [49]**.** Defined as small particles with at least one dimension under 100 nanometers, nanoparticles present significant potential in various applications within geotechnical engineering. Soil, a widely abundant and cost-effective natural building material, serves as an ideal candidate for nanotechnology interventions. The US National Research Council noted that the initial explorations into nanotechnology in this field involved studies of clay-sized particles [50]. Researchers have employed nanoscale modifications to geotechnical materials, improving their suitability for specific applications. This study examines the major advances and developments in nano-science research and applications for soil improvement applications, with a particular focus on mitigating the liquefaction risk. Key studies have demonstrated the effectiveness of nanoparticles in enhancing soil properties. Yonekura and Kaga [51], Persoff et al. [52], and Gallagher [53] proposed a passive site rehabilitation using nanoparticles, namely colloidal silica, with laboratory experiments, model testing, and full-scale field tests illustrating improved liquefaction resistance. Further research by El Mohtar et al. [54-55] and Rugg et al. [56] investigated the use of bentonite suspensions for

treating liquefiable soils. These studies examined the impact of bentonite on the initiation of excess pore pressure at small strains, pore pressure developed at large strains under monotonic loading, and the rate of pore pressure generation during cyclic loading to liquefaction. Additionally, Ochoa-Cornejo et al. [57] and Huang and Wang [58] explored the influence of small percentages of laponite nanoparticles on the liquefaction resistance of sand, using nanoparticles-clay particles percentages ranging from 1% to 3%. This is lower than the values tested by other researchers, such as Youd et al. [59] and below the liquefaction resistance threshold values. The collective work of these studies aims to develop methods for improving the liquefaction resistance of granular soils using nanoparticles, showcasing significant potential for enhancing soil stability and resilience.

The present paper primarily reviews the characteristics of various nanoparticles in mitigating soil liquefaction. This study is structured into three main sections: Section 2.2 explains the fundamental concepts of soil liquefaction; Section 2.3 presents detailed information on nanoparticles; Section 2.4 discusses the four types of nanoparticles used in soil improvement, examining their potential and mechanisms for enhancing soil strength and reinforcement, and Section 2.5 describes the specific characterises of laponite suspension/hydrogel.

2.2 Liquefaction

Liquefaction is a well-known phenomenon in which soil strength and stiffness are significantly eliminated or reduced due to cyclic loading. It usually occurs in loosely packed, water-logged sediments at or near the ground surface, which lose their strength and stiffness from strong ground vibrations. In essence, soil liquefaction occurs when the effective stress of the soil is reduced to zero or close to zero. This reduction can be initiated by either monotonic or cyclic loading. Monotonic loading is a single, sudden change in stress, such as the sudden loss of toe support, while cyclic loading involves repeated changes in stress conditions, such as those caused by earthquake, explosions, waves, and wind shaking. Fully or partially saturated loose sand is particularly prone to liquefaction under both loading circumstances, as it can generate substantial pore pressure when the load changes. In shared and loose soils, a considerable amount of excess pore water pressure is generated as the load is transmitted from the soil skeleton to the neighboring pore water during undrained loading. As pore water pressure rises, effective stress decreases, leading to a gradual loss of soil strength. Liquefaction generally occurs in sandy or non-plastic silty soils, but it can also affect clayey soils such as quick clay [60-61].

During earthquakes, liquefaction beneath engineering structures has caused extensive damage to properties and infrastructure, along with loss of life. The excess pore water pressure generated during earthquakes exerts force on the soil particles, influencing how firmly the particles are packed together. Before an earthquake, the pore water pressure is relatively low but increases drastically due to shaking or construction-related activities such as blasting. For example, the 1964 Niigata earthquake in Japan caused significant liquefaction, destroying many buildings. Similarly, the 1989 Loma Prieta earthquake in California led to considerable subsidence, fracturing, and horizontal spreading due to the liquefaction of soil and debris used to fill a lagoon [62]. Liquefaction places extreme pressure on structures, causing them to tilt or slide, potentially leading to settlement and destruction. Increased pore water pressure can potentially result in landslides and structure collapses. If soil strength decreases below the stress required to maintain slope of a structure, *flow failure* might occur, potentially resulting in sudden and catastrophic consequences from monotonic or cyclic loading. The Aberfan disaster is a historical example of such an occurrence. Despite being in a condition of zero effective stress, this phenomenon is called flow liquefaction [63]. The state of soil where high shear strains accumulate in response to cyclic loading is known as cyclic liquefaction. A 5% double amplitude shear strain is commonly used as a reference for the approximate occurrence of zero effective stress, typically determined using cyclic triaxial, cyclic direct simple shear, or cyclic torsional shear apparatus [3, 28]. These tests determine liquefaction resistance by counting the number of loading cycles at a specific shear stress amplitude required to cause failure. The mechanism of effective stress reduction due to cyclic loading is referred to as cyclic mobility [14]. This can happen in any type of soil, including dense soils, which tend to dilate and regain strength once they reach a state of zero effective stress, resulting in lower shear strains compared to actual soil liquefaction.

Florin and Ivanov [64] described liquefaction as a mechanical breakdown of sand structure, defining the *degree of liquefaction* as the *degree of breakdown* of sand structure, which can be expressed as a percentage of contact breakdown. This study stated two requirements for liquefaction to occur: structural collapse with the possibility of sand consolidation, and partial or complete sand saturation with water. In contrast, Casagrande [65,66], Castro and Poulos [14], and Schofield [67] defined liquefaction as a class of instability (e.g., channeling, piping, boiling, fluidizing) observed in soil that is denser than the critical states near zero effective stress in the

presence of a high hydraulic gradient. Schofield [67] hypothesized that three conditions must be met for liquefaction (Figure 2-1):

- A source of water i.e., high hydraulic gradient from below to the point of inspection,
- Shearing of the soil or a mechanism of mixing to open up cracks or fissures,
- Effective stress is close to zero.

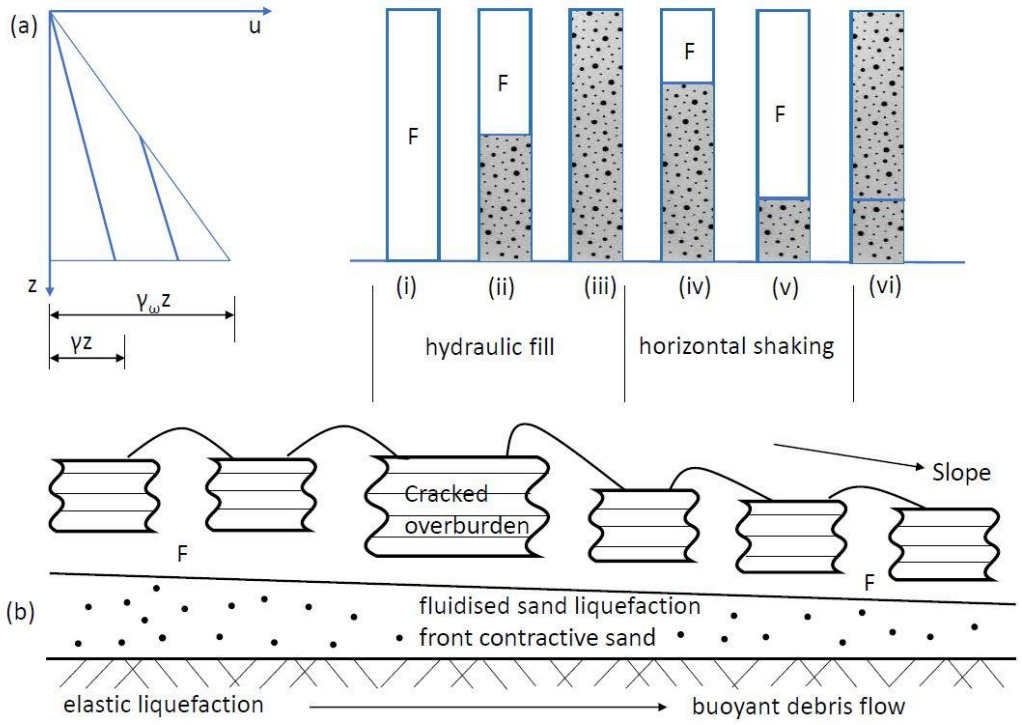

Figure 2-1: Liquefaction concept of Schofield, after Schofield [67]

According to Muhunthan and Schofield [68], a 100% rise in pore pressure is necessary for liquefaction, but it may not be a sufficient condition on its own. Another critical requirement is the creation of openings and the existence of a high hydraulic gradient, which causes the soil continuum to disintegrate into elastic blocks. True liquefaction is identified by a complete loss of shear strength and bearing capacity. Therefore, it is essential in engineering practice to evaluate the potential for soil liquefaction through both laboratory and field testing. Laboratory testing primarily focuses on assessing the grain-size distribution of the soil. In contrast, field testing includes the Standard Penetration Test (SPT), Cone Penetration Test (CPT), and shear wave velocity measurements in soil deposits. Tsuchiya [69] presented grain size distribution boundary curves to identify soils not vulnerable to liquefaction in the Port and Harbour Research Institute

1970 (in Japanese which is translated into English and obtained from the National Research Council) [70]. Various empirical relationships exist between earthquake intensity, SPT or CPT value of soil, and the cyclic stress ratio required for liquefaction. These predictions are based on extensive field performance data from the previous earthquakes. Seed et al. [71] developed a current version of this type of correlation using data from magnitude 7.5 earthquake in the United States, Japan, and China. Most case histories of pile foundations reported in the literature provide information on the SPT-N value of the soil versus depth, helping engineers to better understand the liquefaction potential at different soil depths.

2.3 Nanoparticles

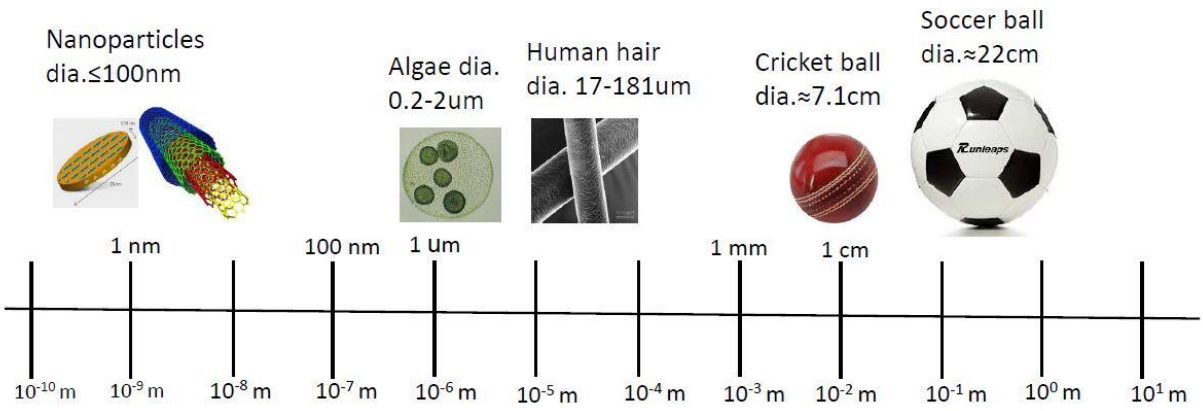

Figure 2-2: Scale comparison of nanoparticles dimension

There have been numerous revolutionary developments in the field of nanotechnology since Nobel laureate Richard P. Feynman introduced the term in his well-known 1959 lecture *There's Plenty of Room at the Bottom* [72]. At the nanoscale level, nanotechnology has led to the creation of a wide variety of materials. According to the European Commission's definition, nanoparticles are particles with at least one dimension of 100 nm or less. Figure 2-2 shows a scale comparison of nanoparticle dimensions, which typically comprise only a few hundred atoms. Despite being invisible to the naked eye, nanoparticles can exhibit radically different physical and chemical properties compared to their bigger counterparts. These materials can be categorized as zero, one, two and three-dimensional based on their overall shape [73]. The significance of these materials became evident when researchers discovered that size could significantly influence a substance's physicochemical properties, such as its optical capabilities. For instance, nanoparticles can display

distinct colors and features based on their size and shape, making them valuable in fields like bioimaging applications [74]. Variation in aspect ratio, nano-shell thickness, and concentration affect nanoparticles' absorption capabilities, resulting in different absorption colors. Nanoparticles typically consist of three layers:

- Surface layer: functionalized with various small molecules, metal ions, surfactants, and polymers;
- Shell layer: chemically and physically distinct from the core,
- Core: the central component, which is the nanoparticles itself [75].

Nanotechnology is thus considered an *enabling technology*, extending existing science and technology by making the improbable feasible and the imperfect flawless [76]. It transcends traditional disciplinary boundaries, impacting a wide range of fields, including medicine, environment, energy, information and communication, and heavy industry [77-79].

2.4 Liquefaction Resistance Using Nanoparticles

In recent years, nanotechnology has been increasingly applied in civil and construction engineering projects to improve material properties, reduce environmental impact, and lower energy consumption. This also increases safety and reduces infrastructure expenditures [80-82]. Common applications of nanotechnology include:

(a) Improving Steel Surface Roughness: using copper nanoparticles to improve weldability and make steel surface corrosion-resistant [83].

(b) Boosting Concrete's Self-Cleaning Capabilities: Using catalyst ingredients, as demonstrated in the Dives in Misericordia church, Rome [84].

(c) Strengthening Concrete: Filling the pores of self-compacting in concrete with silicon dioxide nanoparticles to reduce segregation, making the concrete stronger, more durable, and more sustainable [85].

(d) Monitoring Structural Health: Using nano-sensors to monitor the structural health of concrete during the construction phase [86-87].

Ground and structural strengthening, along with environmental sustainability, are important and challenging issues that traditional soil stabilization methods face due to industrialization and urbanization. Traditional materials like cement and chemical grouts (e.g., sodium silicate, acrylate, epoxy) are used in active and passive site stabilization techniques to improve soil reinforcement.

However, these approaches are often limited in their ability to treat entire field, cause significant disruption, and are expensive. Consequently, there is a need to explore novel materials that can overcome these limitations and mitigate negative impacts. With the rapid growth of nanotechnology, researchers are now investigating the use of nanoparticles to enhance soil strength properties. Although applications of nanotechnology in geotechnical engineering are still in an exploratory stage, four nanoparticles- carbon nanotubes, colloidal silica, bentonite, and laponite- have shown potential in enhancing soil strength and stability.

2.4.1 Carbon Nanotubes

Carbon Nanotubes (CNTs) are recognized as the world's strongest known substance. These cylinder-shaped molecules consist of rolled-up sheets of single-layer carbon atoms. A super-thin layer of carbon atoms organized in a hexagonal honeycomb pattern is known as graphene. When graphene is rolled into a tube, it forms a CNT, which is 100 times stronger than a single layer of graphene and six times lighter than steel [88]. There are two types of CNTs: Single-Walled Carbon Nanotubes (SWCNTs) and Multi-Walled Carbon Nanotubes (MWCNTs). SWCNTs have diameters of less than 1 nm, while MWCNTs have diameters greater than 100 nm and are composed of multiple concentric nanotubes. The lengths of CNTs can range from a few micrometers to several millimeters. CNTs are chemically bonded with sp^2 bonds, an incredibly strong form of molecular contact. This property, combined with the natural tendency of CNTs to rope together due to van der Waals forces, allows for the development of ultra-high-strength, low-weight materials with highly conductive electrical and thermal properties [89]. This makes them highly appealing for a wide range of applications. CNTs are used as reinforcement fillers in metals to improve material strength due to their extraordinarily high elastic characteristics and high aspect ratios [90]. Additionally, CNTs can be distributed on a considerably finer scale than traditional fibers, resulting in more efficient fracture bridging at the very early stages of crack propagation in composites. However, the characteristics and dimensions of CNTs are greatly influenced by deposition parameters and the synthesis method used, such as arc discharge, laser ablation, or chemical vapor deposition [91-93]. CNTs can act as a filler within cement grains, increasing the density of composites [94]. Hence, CNT reinforcements can yield significantly stronger and tougher composites compared to traditional typical reinforcing fibers.

Arabania et al. [95] investigated the impact of CNTs on the mechanical properties of clayey sand, including shear and compressive strength. The findings show that CNTs reduce the friction angle while increasing cohesiveness and increasing compressive strength in very small amounts. This study blended clayey sand with 0.05%–3% CNTs by weight of the soil to enhance soil improvement. Compared to the original clayey soil, the compressive strength of soil containing 3% CNTs increased by roughly 120%. Morsy et al. [96] investigated the performance of hybrid CNTs/nano-clay cement mortar composites in terms of microstructure, physical qualities, and mechanical properties. The study used nano-kaolin as the nano-clay, which was thermally activated at 750°C for 2 hours. The clay platelets were exfoliated with the help of organic ammonium chloride. The ordinary Portland cement, carbon nanotubes, and exfoliated nano metakaolin were used to create a blended cement. The ordinary Portland Cement was substituted with 6% nano metakaolin and the ratios of added CNT were 0.005%, 0.02%, 0.05%, and 0.1% of the cement. The blended cement mortar was made using a water-to-cement ratio of 0.5%. The fresh mortar pastes were initially cured at 100% relative humidity for 24 hours and then in water for 28 days. After curing, the compressive strength, phase composition, and microstructure of the bender cement were evaluated. The results revealed that replacing ordinary Portland cement with 6% nano metakaolin enhanced the compressive strength of the blended mortar by 18% compared to the control mix. Combining 6% nano metakaolin with 0.02% CNTs raised the compressive strength by 29% compared to the control mix [96], showing that adding only 0.02% CNTs to the nano metakaolin cement mortar increased the compressive strength by 11% [96]. Despite the benefits, there is a growing concern that CNTs may have unforeseen detrimental effects on organisms and the environment. Studies suggest that CNTs have the potential to cause significant human diseases such as cancer, lung diseases, skin diseases, and to affect the immune system [97]. Though, CNTs are also used in the adsorption of contaminants from groundwater due to their plentiful nanoscale void structure and large specific surface area [98]. Tong et al. [99] and Johansen et al. [100] stated that CNTs have little or no effect on soil microbes. Hence, the validity and feasibility of using CNTs as soil reinforcing material remain under consideration.

2.4.2 Colloidal Silica

Colloidal Silica (CS) is a suspension of fine amorphous, nonporous, and generally spherical silica particles in a liquid phase. Siloxane linkages (*Si-O-Si*) and silanol groups (*Si-OH*) cover the surface

of CS in contact with water. As a result, CS is extremely hydrophilic and may generate a lot of hydrogen bonds. Figure 2-3 shows the formulation of siloxane bonds and a schematic of CS particles [101]. CS is a water-based dispersion of microscope silica particles made from saturated solutions of silica acid and in the range in size from 7 to 22 nm. CS is harmless, physiologically and chemically inert, and has excellent durability characteristics [102]. Chapa-Gonzalez et al. [103] stated that CS is typically made in a multi-step process that involves partially neutralizing an alkali-silicate solution and forming silica nuclei. CS particles have subunits that are typically 1 to 5 nm in size. The conditions of polymerization determine whether these subunits are linked together or not. Initial acidification of water glass (sodium silicate) solution yields $Si(OH)_4$. The units tend to fuse in chains if *pH* is dropped below 7 or if salt is added, which is often named silica gel. The subunits stay separated and eventually increase if *pH* is kept slightly on the alkaline side of neutral. These are often entitled precipitated silica or silica sols. In the aqueous solution, hydrogen ions from the surface of CS tend to dissociate, resulting in a strong negative charge. The negative colloidal charge is known to rise when some of the Si-atoms are replaced by Al, especially when measured at *pH* below the neutral point. The surface area of CS is quite high due to its microscopic size. *pH* adjustment stabilizes the colloidal suspension, which is then concentrated by evaporation and the possible maximum concentration is determined by particle size.

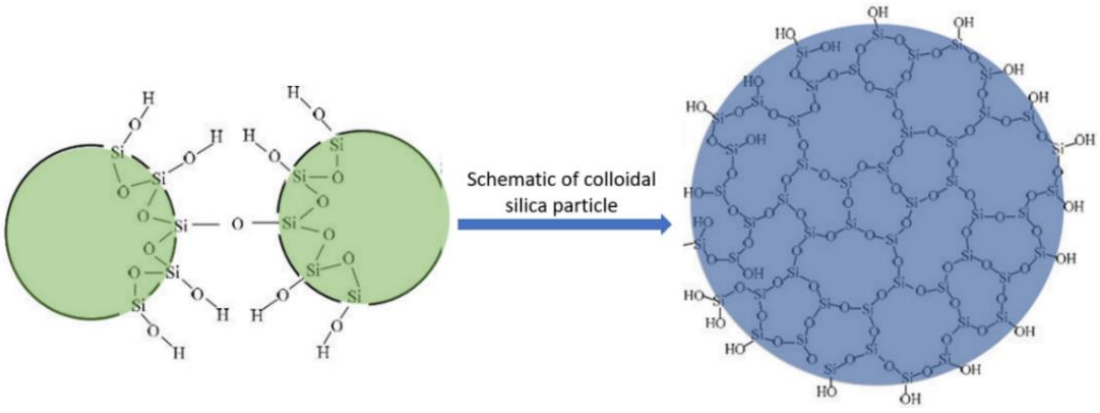

Figure 2-3: Formulation of siloxane bonds and a schematic of the colloidal silica particle, after Spencer et al. [101]

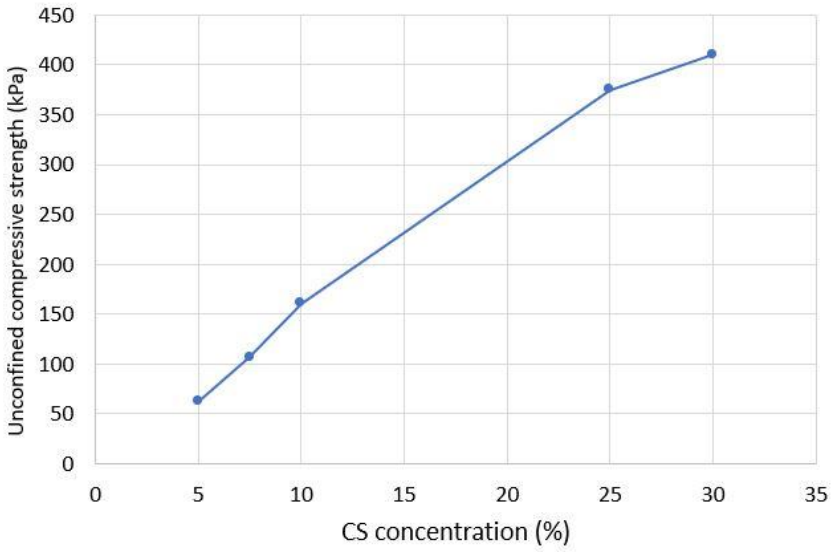

Figure 2-4: Unconfined compressive strength of sand-CS mixture versus the concentration of CS, after Persoff et al. [52]

Gelation is the transformation of CS solution into gel-like solid, induced by lowering the repulsive forces between particles [104]. During gelation, CS particles aggregate into chain-like structures, eventually forming uniform three-dimensional networks until the gelling process is finished. The gel time of CS is defined as the duration between mixing and the formation of a firm gel. This time is determined by the rate of particle interaction, which is affected by several factors, including the concentration of silica in the solution, the size of the silica particles, and the ionic strength, *pH*, and temperature of the solution [105,106]. Research has demonstrated that CS effectively improves the compressive strength of sand. The unconfined compressive strength of sand grouted with CS improves linearly with the percentage of CS [107], as illustrated in Figure 2-4. This improvement in compressive strength underscores the potential of a CS as a valuable material in soil stabilization and geotechnical engineering applications.

2.4.2.1 **Liquefaction Mitigation by Colloidal Silica**

Colloidal Silica (CS) was proposed by Yonekura and Kaga [51] as an alternative to sodium silicate, the most extensively used chemical grout. Persoff et al. [52] investigated the effects of CS concentration on the strength properties and hydraulic conductivity of CS-treated sand. Sand specimens stabilized with 10% and 20% CS (by weight) exhibited unconfined compressive strengths of 158 and 317 kPa, respectively, illustrating a direct correlation between strength gain

and CS concentration. Gallagher [53] proposed the use of CS for passive site remediation to reduce liquefaction risk and enhance the liquefaction resistance, a theory proven by laboratory experiments, model tests, and full-scale field tests. This method involves enriching the pore fluid of a liquefiable soil with CS, an environmentally safe, nontoxic dispersion of silica nanoparticles in water. Implementing this ground improvement technique in practice requires stringent quality control and assurance procedures. Gallagher and Mitchell [108] found that unconfined compressive strength of samples treated with 5%–20% CS varied from 32 to 222 kPa.

Gallagher et al. [109] investigated the efficacy of CS treatment in enhancing liquefaction resistance and reducing deformation in loose sands using centrifuge modeling. Gallagher and Koch [110] reported on box model experiments where CS was delivered to lose sands via low-head injection wells. The effects of CS treatment on liquefaction and deformation properties of loose, liquefiable sands during centrifuge in-flight shaking are investigated using centrifuge modeling. A loose and fine Nevada sand (pass sieve no. 120) was saturated with a 6% CS stabilizer and subjected to earthquake motions with peak accelerations of 0.20 and 0.25 g. The treated sand layer did not liquefy, and the treated centrifuge models exhibited significantly lower strains (0.5%-1.0%) compared to untreated soil models (3%-6%) in Taboada [111]. The use of box modeling to analyze the distribution of dilute CS stabilizers through loose sand deposits under small gradients induced by injection and extraction wells was also described. The study aimed to identify key parameters influencing CS delivery in a box model experiment. This pore fluid alteration can be achieved by injecting CS solution at low pressure into the foundation soil via groundwater flow controlled by injection and extraction wells on either side of the structure. Low-pressure injection is effective due to the slightly higher viscosity of CS solution compared to water at the preliminary stage. Liao et al. [112] investigated the liquefaction resistance of sand stabilized with CS. Kodaka et al. [113] observed a significant improvement in cyclic shear strength post-CS treatment. Treated soil specimens remained intact with minimal strain during cyclic loading, while untreated specimens collapsed within a few loading cycles [113,114]. To validate the strength and deformation properties of the nano-sand composite under cyclic loading in model tests, the relationship between gel density, viscosity, and gel duration was investigated, and the CS grouting process was simulated [46]. Full-scale field testing was conducted to evaluate the practical validity of CS grouting for mitigating liquefaction risks [115].

Research has shown that after a controllable time, the viscosity of CS rises quickly, and the enriched pore fluid hardens into a stiff gel, reducing the risk of excessive strain accumulation due to liquefaction [113-119]. Agapoulaki and Papadimitriou [120] stated a set of viscosity measurements of a variety of CS solutions, corroborating previous findings and identifying temperature as a new governing parameter. The extensive number of measurements allows for credible statistical analysis, leading to the development of charts and equations for estimating the time-increasing viscosity of CS solutions. This information is crucial for the in-situ injection process, as evidenced by one-dimensional injection studies of CS in sand columns. Low-pressure or low-flow gradient grouting does not directly disturb the sand skeleton, thus avoiding erosion as seen with jet grouting, and achieving soil improvement by altering pore fluid features, such as substituting water with nanoparticles [121,122]. One-dimensional sand column injection tests were performed by Gallagher and Lin [123,124], Lin [125], and Lin and Gallagher [126], along with multidimensional injection tests [112,115,127-130]. These studies emphasized the importance of controlling the viscosity versus time curve of CS solution, dimensions of the stabilization area, properties (density and hydraulic conductivity) of the liquefiable material, and applied flow gradient for effective injection.

Gallagher [53] and Gallagher and Mitchell [108] conducted comprehensive studies on the rheology of CS, focusing on viscosity measurements for three types of CS with varying particle sizes under different *pH* values and salt concentrations. Their research highlighted that these parameters significantly impact the gelation process. These viscosity measurements contribute to the extensive existing literature on CS rheology (e.g., [46,53,108-110,115,123,124,127]) by incorporating temperature as a key control parameter. The identical tests performed were instrumental in developing an approximation for evaluating the viscosity-versus-time curve of CS solutions based on rheometric parameters. The importance of this methodology was validated through one-dimensional vertical injection tests in sand columns, which obviate the need for case-specific measurements. According to these viscosity tests and recent observations [125,128,129,131], all tested CS solutions exhibited qualitatively similar viscosity-versus-time curves. The current state of the art assumes that as the percentage by weight of silica particles and the concentration of cations (e.g., salt) in the solution increases, the gelation time for any given CS form decreases monotonically. Additionally, research data revealed a non-univocal relationship between *pH* and

gelation time [132]. Temperature also plays a significant role in determining the gelation time of CS solution [133]. These studies recommend performing case-specific viscosity measurements prior to in-situ injection of CS into the ground, which required measurements necessitate specialized equipment and expertise. Consequently, having a reliable methodology to estimate the viscosity-versus-time curve of CS solutions- taking into account factors such as silica type, CS and cation concentration, *pH*, and temperature-would be extremely beneficial.

2.4.3 Bentonite

Bentonite is a water-absorbent swelling clay primarily composed of montmorillonite, an aluminum phyllosilicate mineral. This processed clay mineral forms when volcanic ash undergoes weathering in seawater, converting the volcanic glass in the ash into clay minerals [134-136]. Freshly exposed bentonite beds appear white or pale blue or green, but as they age and weather, they transition to a cream tint and eventually to yellow, red, or brown (**Figure 2-5**) [137]. Nano bentonite, which is more purified form of natural clay, exhibits enhanced moisture absorption and swelling properties [138]. When submerged in water, nano bentonite disperses to form gelatinous or suspended solutions characterized by high viscosity, thixotropy, and lubricity [139]. As a swelling clay, bentonite can absorb substantial amounts of water, increasing its volume by up to eight times [137]. The clay's small platy grains of montmorillonite provide a large total surface area, making it an effective adsorbent. When moistened, these plates adhere together, making it an excellent binder and a suitable additive for increasing the flexibility of kaolinite clay [135]. This swelling property benefits applications such as drilling mud and groundwater sealants. The aluminum phyllosilicate mineral montmorillonite in bentonite has a low-charge TOT crystal structure. A montmorillonite crystal comprises layers, each consisting of two T-sheets connected to either side of an O-sheet. The T-sheets derive their name from the tetrahedral arrangement of four oxygen ions around each aluminum or silicon ion. The O-sheets are named for the octahedral arrangement of six oxygen or hydroxyl ions around each aluminum ion. The entire TOT layer has a weak negative electrical charge, which is neutralized by calcium or sodium cations that bind neighboring layers together, leaving approximately 1 nm gaps between layers. Due to the weak negative charge, only a small percentage of the available cation sites on the surface of a TOT layer contain calcium or sodium. These gaps allow water molecules to easily pass through and fill the empty spaces [135]. **Figure 2-6** illustrates the structural formula of bentonite [140].

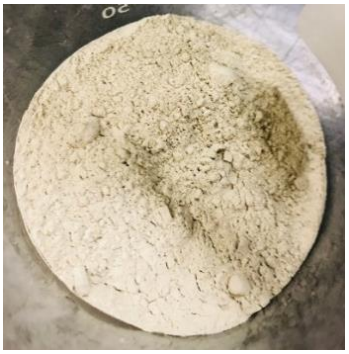

Figure 2-5: Bentonite Powder

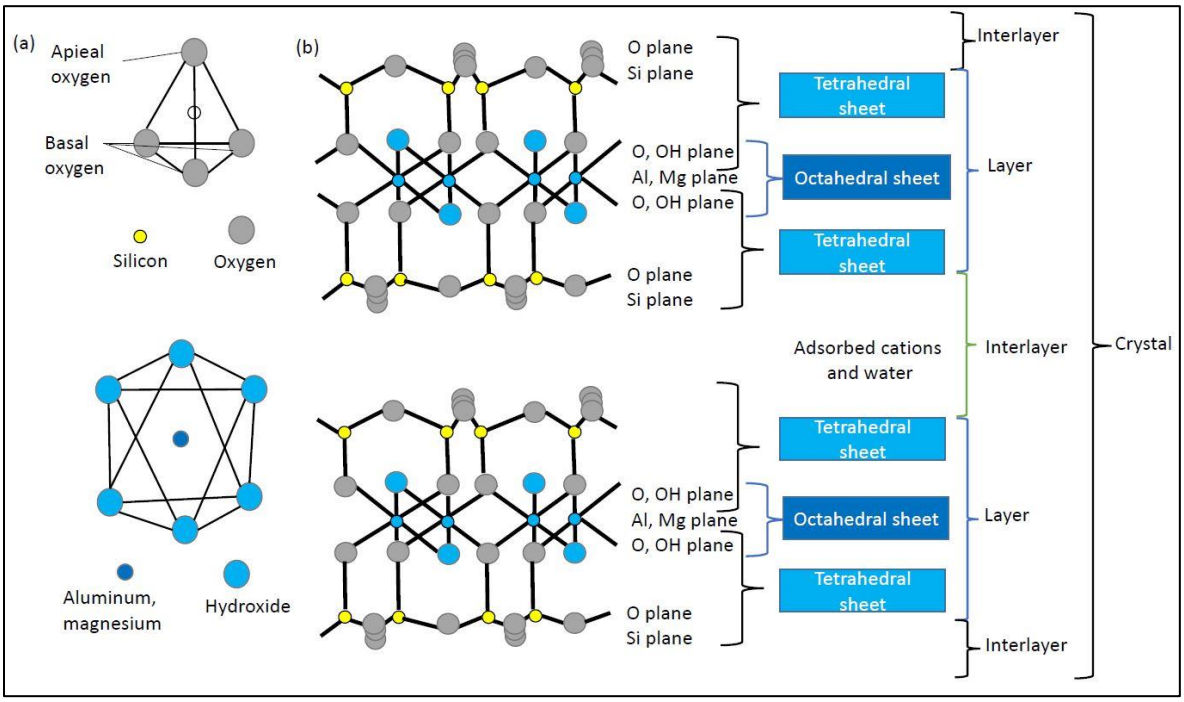

Figure 2-6: The structural formula of bentonite, after Perry [140]

The various types of bentonites are categorized based on the dominant cation present [141]. The two most commonly used types in various industries are sodium bentonite and calcium bentonite, with calcium bentonite being more prevalent and sodium bentonite being more valuable [142].

- ***Sodium bentonite***: Sodium bentonite swells significantly and absorbs several times its dry mass in water when wet. Its exceptional colloidal properties make it highly suitable for use in drilling mud for oil and gas wells, as well as boreholes for geotechnical investigations [143]. Additionally, sodium bentonite serves as an effective sealant, forming a self-sealing, low permeability barrier, and is utilized as backfill material in waste containment projects [144]. In

geoenvironmental applications, surface modifications to sodium bentonite, such as the addition of polymers, can enhance certain rheological and sealing behaviors [145]. Sodium bentonite is also used in fertilizer prills mixed with sulfur, which allows for slower sulfur oxidation to sulfate, an essential plant nutrient. This helps maintain sulfate levels in rainfall-leached soil longer than pure powdered sulfur or gypsum [146]. Sulfur/bentonite pads combined with organic fertilizers are also utilized in organic farming [147].

- ***Calcium bentonite***: Calcium bentonite is an effective adsorbent of ions in solution and is a key component of fuller's earth, one of the earliest industrial cleaning agents [148]. Through an ion-exchange technique, calcium bentonite can be converted into sodium bentonite (a process known as sodium activation). This typically involves adding 5%–10% of a soluble sodium salt, such as sodium carbonate, to wet bentonite, mixing thoroughly, and allowing time for ion exchange and water to remove the exchanged calcium [149,150]. However, some properties of sodium-beneficiated calcium bentonite, such as viscosity and fluid loss of suspensions, may not match those of natural sodium bentonite [151].
- ***Potassium bentonite***: Potassium bentonite, also known as potash bentonite or K-bentonite, is a potassium-rich illicit clay formed through the alteration of smectic clay [152]. Illite, high-charge TOT clay mineral, has sheets strongly bound by potassium ions, making it a non-swelling clay with limited industrial applications [135].

2.4.3.1 **Mitigate Liquefaction by Bentonite**

Bentonite dispersions are widely used as drilling fluids for excavation support, grouting, and impermeable barriers. The effectiveness of these applications heavily depends on controlling the rheological characteristics of the bentonite dispersions. Several features, including clay concentration, *pH*, water ionic strength, and type of cation and anion, influence the rheology of bentonite dispersions [153-160]. These factors can cause bentonite to exist in various states such as repulsive gel, attractive gel, and sediment [161-163]. Regarding the impact of plastic fines, there is a general consensus that their presence enhances liquefaction resistance. This has been corroborated by field observations (e.g., [3,28,31]) and laboratory data (e.g., [29,164]). Gratchev et al. [165] utilized a ring-shear apparatus to study the liquefaction of clayey soils using bentonite–sand mixtures and natural clayey soils collected from the sliding surfaces of earthquake-induced landslides. Their findings indicated that a small amount of bentonite (7%) causes quick liquefaction, whereas an increased bentonite content (11%) significantly enhances soil resistance

to liquefaction. The study demonstrated that bentonite–sand mixtures are substantially more resistant to liquefaction compared to kaolin– and illite–sand mixtures. This underscores the significant role of plasticity in liquefaction resistance. Further investigation using a scanning electron microscope revealed that the liquefaction potential of soil was highly correlated with specific particle configurations. In soils susceptible to liquefaction, clay aggregations often accumulated at the contact points of sand particles, forming low-strength *clay bridges* that easily broken during cyclic loading. Conversely, in soils resistant to liquefaction, the microfabric appeared more compact, with clay providing a matrix that prohibited the sand grains from liquefying.

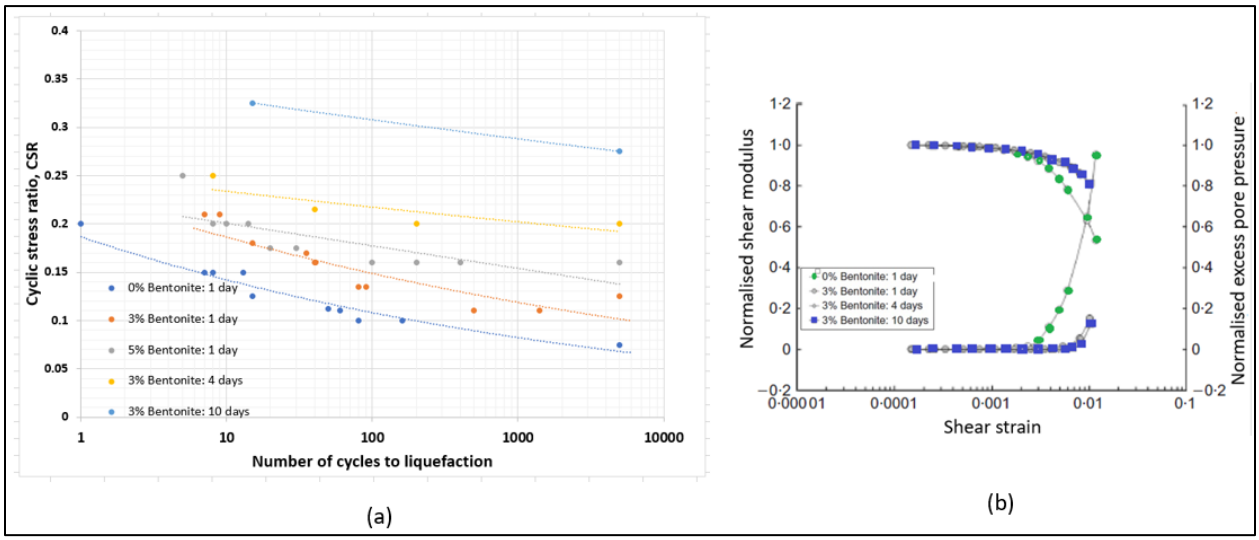

Figure 2-7: (a) Effect of bentonite treatment in increasing cyclic resistance of sand in undrained cyclic triaxial tests, and (b) Effect of aging time (1 to 10 days) preceding shear, after El Mohtar et al., [166]

El Mohtar et al. [55] and Clarke [167] conducted comprehensive experimental research into these properties and effectiveness of bentonite treatment for soil improvement. The research aimed to (i) assess the qualities of bentonite slurry, and (ii) investigate the efficacy of bentonite treatment in preventing liquefaction. Clarke [167] focuses on the rheological properties of bentonite slurry, addressing issues such as the feasibility of permeation through the soil matrix and the time required for pore fluid gelation. El Mohtar et al. [55] examined the mechanical properties of bentonite-treated sand and evaluated the efficiency of treatment in mitigating liquefaction. They found that bentonite treatment increased the number of loading cycles that a sand sample could withstand

before liquefaction under undrained cyclic triaxial conditions. The bentonite gel acts as an "elastic restraint to particle movement," limiting the accumulation of plastic shear deformation and slowing the generation of excess pore pressure that leads to liquefaction. The research indicated that incorporating only 3%–5% of bentonite significantly enhanced cyclic resistance compared to clean sand at the same skeleton relative density. Moreover, a longer pre-shear aging period amplified the number of cycles required to liquefy the soil at a given cyclic stress ratio. **Figure 2-7**(a) shows the effect of bentonite treatment in increasing the cyclic resistance of sand specimens in undrained cyclic triaxial tests. El Mohtar et al. [54,55] also investigated the application of bentonite for treating sand deposits susceptible to earthquake-induced liquefaction, which occurs in saturated loose-medium granular deposits due to increased pore pressure and subsequent effective stress loss triggered by rapid loading. Their findings demonstrated that delivering roughly 3% bentonite by dry mass of sand into the sand pore space considerably increased liquefaction resistance, with a 10-fold increase in cyclic resistance compared to pure sand specimens [54]. This effect is attributed to the gel-like pore fluid formed in the presence of bentonite within the sand pores, which effectively inhibits sand grain mobility and decreases pore pressure generation. The study by El Mohtar et al. [55], based on resonant column, static triaxial, and cyclic triaxial tests on samples prepared by dry-mixing Ottawa sand and bentonite at a 35% skeleton relative density, identified two key factors: the proportion of bentonite and the aging time (1 to 10 days) preceding shear (**Figure 2-7**(b)). In resonant column tests, the presence of bentonite increased the shear strain required to initiate the generation of excess pore pressures, lowered the mean pore pressure generated per loading cycle, and allowed the sample to sustain a greater loss of effective stress before liquefaction began. These effects are further amplified with prolonged pre-shear aging, resulting in more stable sand behavior under static conditions. The observed effects cannot be solely attributed to the increased bulk density of bentonite specimens but rather to the presence of a concentrated clay gel pore fluid with solid-like qualities. This pore fluid raises the threshold shear strain of sand, which is linked to the strength of the sand.

Bentonite dispersions, characterized by their gel-like structure and rheological features, are typically unable to permeate porous media at certain concentrations. As a result, the rheology of the dispersion must be modified. This modification needs to be reversible so that the bentonite dispersion can regain its gel structure and qualities, ensuring its efficiency in liquefaction mitigation within the sand [122]. Santagata et al. [169] discussed the use of sodium pyrophosphate

(SPP) decahydrate to modify concentrated bentonite dispersions for treating liquefiable soils. Previous research (e.g., [159,162,169-171]) has demonstrated that the adsorption of SPP reduces the yield stress of clay dispersions by neutralizing the positively charged sites on the clay particles, sometimes achieving Newtonian behavior. Furthermore, adding pyrophosphate to laponite, a smectite clay similar to montmorillonite, can delay the gelation process [106,172]. Clarke [167] discovered that this effect also occurs in bentonite at much lower dosages. These conclusions are based on rheological tests examining the at-rest and flow properties of concentrated (10% clay by total mass) bentonite dispersions mixed with varying amounts of SPP (0 to 2% by mass of bentonite). These experiments were conducted from the moment of mixing and continued until the dispersions aged for approximately two years. Rheological data obtained from these tests, performed using a rheometer, directly relate to the performance of the bentonite dispersion. Additionally, Witthoeft et al. [173] validated the efficacy of bentonite suspensions for liquefaction mitigation and control at the field scale using the finite difference method (FLAC) and further delineated the scope of reinforcement.

2.4.4 Laponite - a promising nanoparticle

In 1962, UK scientist Barbara Neumann obtained a patent for laponite, a synthetic layered silicate that improves the performance of a wide range of industrial and consumer products, making them more valuable to their users. Laponite is manufactured from naturally occurring inorganic mineral sources and, in its dry state, is a fine white powder (**Figure 2-8**). It is significantly smaller than bentonite, with a thickness of 1 nm and a width of 25 nm. **Figure 2-9**(a) illustrates the geometry of individual laponite particles [174]. Laponite consists of synthetic silicate nanoparticles with a structure comprising two tetrahedral and one octahedral layer, similar to natural montmorillonite [175]. **Figure 2-9**(b) represents the idealized structural formula of laponite, which has a chemical composition of 65.82% SiO_2, 30.15% MgO, 3.20% Na_2O, and 0.83% Li_2O. The corresponds to the general formula: $Na^{+0.7}[Si_8Mg_{5.5}Li_{0.3}H_4O_{24}]^{-0.7}$ [176,177]. Laponite disperses rapidly in water into disc-shaped grain structures, resulting in a colorless and transparent suspension. Due to the substitution of some bivalent magnesium ions with lithium ions on the particle surface, the surface discharges a significant number of negative charges. Hydroxides on the edge, such as *Mg-OH* and *S-OH,* acquire a small amount of positive charge through protonation. While laponite is insoluble in water, some of the suspended material eventually

settles, leading to a loss pf liquidity over time [178]. Laponite is used to improve the value of various industrial and consumer items by improving their performance and characteristics.

Figure 2-8: Laponite Powder

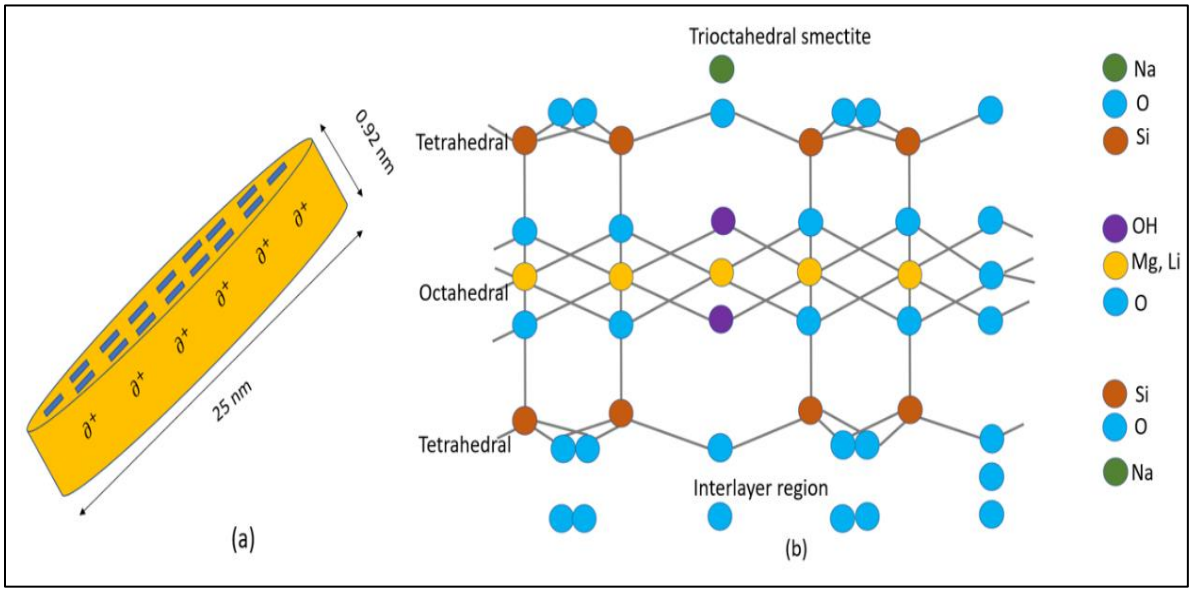

Figure 2-9: (a) Geometry of individual laponite particles, and (b) Idealized structural formula of laponite, after BYK Additives and Instruments [174]

Laponite has two primary functional applications [174]:

- Rheology modifier: Laponite can be used in the formulation of a wide range of water-borne goods, including surface coatings, household cleansers, and personal care products. It increases stability and syneresis control by imparting thixotropic, shear-sensitive viscosity.
- Film former: Laponite serves as a film-forming agent used to produce electrically conductive, antistatic, and barrier coatings.

There are two types of laponite products:

- Gel-forming Grades: These grades dissolve quickly in water with agitation to produce clear, colorless dispersions. The viscosity of these dispersions depends on the solids content and electrolyte content of the water used. Highly thixotropic gels develop at 2% in tap water, while low viscosity soils form at the same concentration in deionized water. Laponite interacts with the soluble components in a formulation to develop viscosity.
- Sol-forming Grades: These grades also disperse rapidly in water when agitated but contain dispersing agents that delay the formation of a thixotropic gel structure. Low viscosity liquid sols can be made at solids concentrations of up to 30%. In hard water, sol-forming grades are effective as the dispersants used are effective sequestrants for Ca^{+} and Mg^{+} ions.

BYK Additives and Instruments offers two types of soil-forming products:

- Temporary Sol-grades*:* These have a short stability period at low viscosity. The stability times of dispersions with higher solid concentration will be shorter.
- Permanent Sol-grades: These are modified with patented dispersing agents to be more stable. Sols that are stable for up to one year can be prepared at solid concentrations up to 30%.

According to Tanaka et al. [179], electrostatic repulsion between particles occurs when the ionic strength is small, resulting in a commonly exclusive glassy state. At high ionic strength, the electric double layer on the particle surface is compressed, reducing the distance of electrostatic interaction, and the distance between particles, generating a physically cross-linked gel. Laponite can improve the liquefaction resistance of liquefiable sand and has better material characteristics and conductivity than nano bentonite due to its excellent rheological properties and small size scale [55]. Howayek et al. [180] used direct imaging to demonstrate the structure of sand–laponite suspension systems, highlighting their elongated cellular structure, which impacts their macro-scale geotechnical properties.

2.4.4.1 **Liquefaction Resistance by Laponite**

Recent research studies by Ochoa-Cornejo et al. [57] and Huang and Wang [58] has provided innovative insights into using laponite to mitigate liquefaction risk. These studies explored the impact of high plastic fines on the cyclic response of sands and the extreme effects of fine plasticity, suggesting that laponite could effectively mitigate liquefaction. Ochoa-Cornejo et al.

[57] investigated the effect of 1%–5% laponite by dry mass of sand, with a plasticity index greater than 1000%, on the cyclic response of sand with a relative density of 15%–25%. This research, based on cyclic triaxial tests performed on specimens prepared by dry pluviation and then saturated with water, demonstrated that even 1% laponite increases cyclic resistance throughout all stages of testing. More significant benefits were observed with a longer pre-shear aging times or higher laponite dosages (3%–5%). The improved behavior is attributed to two mechanisms: (a) bonding/bridging at the particle contacts due to charged laponite fines attracted to the sand grains, and (b) the production of a pore fluid with solid-like properties. The former governs behavior at 1% laponite, while the latter is responsible for higher laponite doses.

This study compared the response of laponite-treated specimens to that of clean sand specimens, focusing on excess pore pressure response from initial loading to large strain development. Adding only 1% laponite significantly influenced the cyclic response of the granular medium. These findings provide insights into the extreme effects of fines plasticity, with various laponite levels compared to existing data on sand-bentonite specimens [54,166]. Multiple mechanisms may account for the increased cyclic strength depending on particle nature and content, suggesting that sand-laponite mixtures could be a viable alternative to bentonite for liquefaction treatment. Bentonite, while effective, faces several challenges, including the need for chemical treatment with sodium pyrophosphate to regulate short-term viscosity [122], inherent variability leading to unreliable results, and permeation issues with fine deposits. Laponite, with its smaller size and delayed gelation properties, could overcome these difficulties. Huang and Wang [58] also proposed using laponite with liquefiable silty sand to resist liquefaction. They studied mixing methods, analyzing the cyclic behavior and liquefaction resistance of laponite-sand specimens through dynamic triaxial tests. This research validated laponite's efficacy in liquefaction mitigation by examining pore pressure buildup and deformation parameters of untreated and laponite-treated sand. Rheological properties of laponite suspensions were measured, and the microstructure of laponite–silty sand mixtures was investigated using a scanning electron microscope (SEM).

Both studies agree that laponite mitigates liquefaction potential through pore fluid solidification, soil grain cementation, and delayed pore pressure development. Laponite's rheological properties enhance liquefaction resistance, although thinning behavior can weaken resistance under amplified cyclic loading. During sample preparation, dry-mixing laponite and sand resulted in residual cavities beyond those created by the laponite gel and soil grains, affecting pore pressure

measurements in dynamic cyclic tests. Huang and Wang [58] also examined the influence of laponite content and curing duration on liquefaction resistance, finding that higher laponite concentration or longer curing time improved resistance. Notably, the influence of laponite concentration is stronger during the initial cycles, while the effect of curing time becomes more significant after more cycles

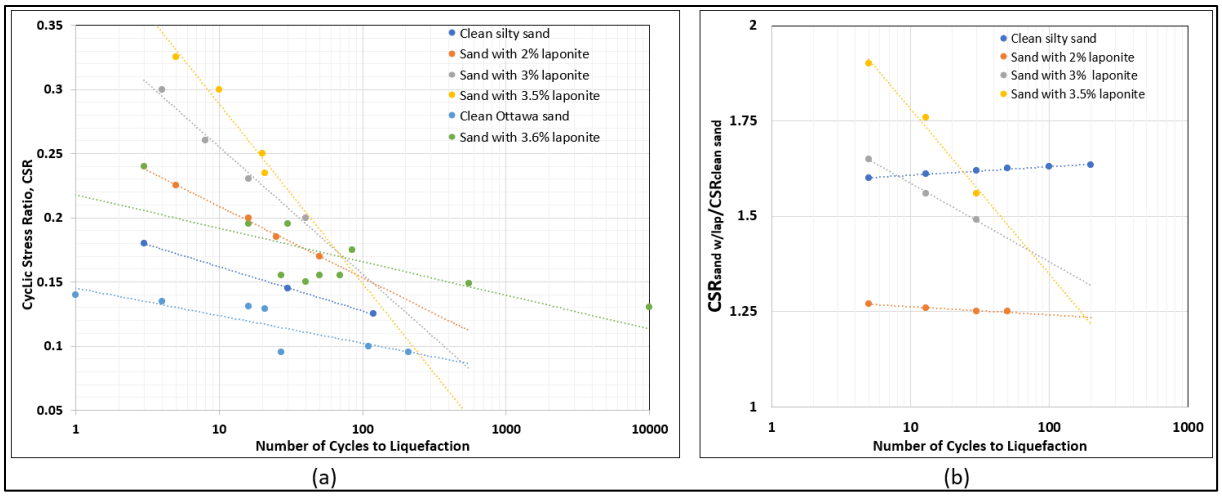

Figure 2-10: (a) Relationship between cyclic stress ratio (CSR) and number of cycles to liquefaction for pure sand and laponite-sand specimens, and (b) Effect of laponite on the CSR corresponding to a given number of cycles to liquefaction, after Ochoa-Cornejo et al. [181]

Given the similarities in the approaches of Ochoa-Cornejo et al. [57] and Huang and Wang [58], it is possible to compare their findings on the processes by which laponite modifies the behaviour of sands under cyclic loadings. These studies represent the only published work on this topic and provide a coherent picture of the effects of small percentages of laponite on liquefaction resistance. Huang and Wang [58] investigated laponite concentrations of 0, 2%, 2.5%, 3%, and 3.5% in specimens. Their findings demonstrate improvements in cyclic resistance, as assessed by the number of cycles to liquefaction at a given cyclic stress ratio. Increased laponite content and longer curing times further enhanced the reaction. These findings align with the cyclic triaxial data presented by Ochoa-Cornejo et al. [57,182]. It is noteworthy that water was supplied before compaction of the material in a rigid mold in Huang and Wang [58], whereas Ochoa-Cornejo et al. [57,182] flushed water through the specimen generated by dry pluviation after setup in the triaxial setup. Despite some variances between the two studies, **Figure 2-10**(a) shows the number of cycles to liquefaction versus the applied cyclic stress ratio, combining data from both studies. The

findings acquired by Ochoa-Cornejo et al. [57] are at the lower end of the range compared to Huang and Wang's results. The differences in sand characteristics and relative density serve as a benchmark against which the impacts of adding laponite can be assessed. **Figure 2-10**(b) plots the cyclic stress ratio corresponding to a specific number of cycles to liquefaction, normalized by the CSR applicable to pure sand. Both studies show that the enhancement, as measured by the rise in CSR for a given number of loading cycles, approaches 50% for laponite concentrations of 3%–3.6%. The data presented by Ochoa-Cornejo et al. [57] show a constant $CSR_{sandw/lap}/CSR_{cleansand}$ ratio of up to 200 cycles, while Huang and Wang's [58] results reveal a decline in this ratio as the number of cycles increases. This deviation may be due to fabric variations caused by different specimen preparation procedures. This deviation may be due to fabric variations caused by different specimen preparation procedures, which play a crucial role in the mixing of sand-laponite and the physical mechanisms of particle-particle and particle-pore water interactions during cyclic loading [181].

Ochoa-Cornejo et al. [181] explained the effects of 1%–3% laponite on Ottawa sand based on undrained resonant column tests. The effect of laponite is determined by consolidation time, confining stress, and laponite concentration. Laponite increases small-strain damping, extends the linear strain threshold, and delays the development of excess pore pressure, shear modulus degradation, and enhancement of damping. Resonant column experiments revealed behavioral tendencies due to differences in the fabric of sand-laponite and particle-to-particle interactions. The thickness of laponite present at the contact point and how much pore space is occupied by hydrated laponite determine the reaction to small strains. A thin laponite layer provides bonding/bridging at sand grain contacts, responsible for a higher initial shear modulus and reduced sensitivity of the shear modulus. Increases in layer thickness with laponite concentration explain trends in the damping ratio and sensitivity to aging. The formation of laponite hydrogel and its occupancy of pore space account for behavior in the non-linear region, impacting the linear threshold, modulus deterioration, and rate of excess pore pressure development. Huang et al. [183] investigated the application of laponite in high-performance water-based drilling fluids by assessing its shale inhibition, plugging, and lubricating properties. The linear swelling test and shale recovery test were used to assess shale inhibition performance. Nitrogen adsorption experiments and scanning electron microscope observations were used to assess plugging performance. The lubricating property was assessed using an extreme pressure lubricity test.

Experiments have shown that laponite has better shale inhibition properties than commonly used inhibitors like polyamine and KCl. Shale pores can be successfully blocked by laponite, significantly reducing surface area and pore volume. Additionally, it can minimize shale porosity and generate a smooth nanofilm, according to scanning electron microscope data. By improving the smoothness of the drill pipes/wellbore interface and isolating direct contact between the wellbore and drill string, laponite enhances the lubricating properties of drilling fluid. The disk-like nanostructure and charged surfaces are primarily responsible for laponite's superior performance.

2.5 Laponite and its Characteristics

There are at least ten types of laponite products available in the market, with some of the commonly used varieties including Laponite-RD/RDS, Laponite-XLS/XLG, Laponite-D/DF/DS, and Laponite-S/JS. Laponite-RD is particularly notable for its application as a rheology additive. This synthetic phyllosilicate is designed to enhance the rheological properties of aqueous system, particularly in low shear range. As a rheology modifier, Laponite-RD is widely used in the formulation of several waterborne products, including surface coatings, household cleaners, and personal care products. It imparts shear-sensitive viscosity and improves stability. Additionally, laponite functions effectively as a film former, used in the production of electrically conductive, antistatic, and barrier coatings. Table 2-1 Presents a summary of the applications, properties, and benefits of laponite, as outlined in the BYK technical report [174].

Table 2-1: Summary of application, properties, and benefits of laponite (modified from BYK Technical Report [174])

Applications	***Properties***	***Benefits***	***Laponite Grades***
Personal Care	Manufactured under carefully controlled conditions from selected inorganic chemicals	○ Product does not contain crystalline silica ○ Very low heavy and transition metal content ○ Table to UV ○ Not susceptible to microbial attack ○ Suitable for sterilization by gamma irradiation or ethylene oxide ○ Colorless in formulations	Laponite XLG Laponite XLS Laponite XL21

	Unequalled degree of shear thinning	○ Gives a light, clean texture to creams and lotions ○ Reduces oily feel of emulsions ○ Gels and pastes readily dispensed	
	High gel strength	○ Improves stability of o/w, w/o and HIPES emulsions ○ 'Emulsifier-free' systems can be stabilized ○ Improves stability of suspended abrasives and solid actives ○ Suitable for making non tacky gels with high yield values	
	Thixotropic viscosity	○ Allows controlled rate of restructure after shear	
Surface Coatings	High viscosity at low shear	○ Excellent pigment suspension to give good in-can appearance and syneresis control	Laponite RD Laponite RDS Laponite S482 Laponite SL25
	Highly shear thinning	○ Readily formulated for brush, roller or spray application	
	Progressive restructuring after shear	○ Allows good flow and levelling ○ Prevents sag ○ Excellent flip-flop in metallic and pearlescent spray coatings ○ Interaction with polymeric thickeners	
	Performance benefits when used with polymeric co-thickeners	○ Unique synergistic increases in viscosity when combined many other types of thickener ○ Precise rheological profiles may be engineered	
Household products	High viscosity at low shear rates	○ Formulate gelled products for easy spray and cling to vertical surfaces	Laponite RD Laponite RDS
	High chemical purity and inorganic nature	○ Compatible with non-ionic, anionic and some amphoteric surfactants	
	Colorless	○ Does not affect the color of products	
Film forming agent	Small size particles and high SSA	○ Used as a barrier forming substance	Laponite S Laponite JS
	Disc-shaped crystals with anionic nature	○ Increase moisture resistance ○ Conductive/antistatic ○ Prevent migration of molecular particles between two layers	

Paper and polymer films		○ Static dissipative (antistatic) coatings ○ Electrographic paper and film ○ Inert barrier films ○ Anti-blocking coatings ○ Microparticle for retention and drainage systems ○ Paper coating colors and sizing ○ Ink jet coatings	
Building products		○ Plasters and fillers ○ Setting retardants ○ Wood treatment suspensions ○ Wood and tile adhesives	
Agricultural		○ Seed germination gels ○ Plant rooting gels ○ Agrochemical flowable-herbicides, pesticides ○ Essential element suspensions	
General Industrial		○ Mold release suspensions ○ Children's toys ○ Processing aids ○ Oil drilling fluids ○ Ceramic body formulations and glazes ○ Rubber latex ○ Foundry coatings ○ Electrorheological fluids	

2.5.1 Flow Behaviour of Laponite

Understanding the flow behavior of clay suspensions is critical in various applications, such as in drilling fluids in the petroleum industry, ceramics, and pharmaceuticals. In practical applications, rheometers are used to measure the shear stress and shear rate, allowing the determination of the flow behavior and viscosity of materials. This information is crucial for designing processes and equipment that involve fluid flow. The flow behavior of clay suspensions is described by the relationship between shear stress (τ) and shear rate (γ). Shear rate is defined as the change in shear strain per unit time, while shear stress is the tangential force applied per unit area. The ratio of shear stress to shear rate is known as viscosity (η), which measures a fluid's resistance to shear flow, similar to how the elastic modulus measures a material's resistance to deformation. The plot of shear stress versus shear rate is called the consistency curve. There are four primary types of flow behavior: Newtonian, pseudoplastic, Bingham plastic, and dilatant. In Newtonian fluids,

shear stress is proportional to shear rate, resulting in constant viscosity. Common examples of Newtonian fluids include water, mineral oil, and honey. Non-Newtonian fluids have viscosities that change with shear rate. Clay suspensions often exhibit non-Newtonian behavior due to the interaction between clay particles. The type of non-Newtonian behavior can depend on factors such as the concentration of clay particles, the nature of the clay, and the presence of other substances (e.g., electrolytes). Aqueous clay suspensions with relatively high particle concentrations are traditionally described by Bingham's theory of plastic flow [184]. This model suggests that the initiation of flow occurs upon the application of a finite stress and at greater stress the flow will be Newtonian. Therefore, the resistance to flow in these suspensions has two components: a Newtonian part, where shear stress is proportional to shear rate, and a non-Newtonian part, where shear stress remains constant regardless of shear rate. In contrast, very dilute clay suspensions or drilling fluids containing polymers exhibit pseudoplastic behavior, characterized by shear thinning. This means that the viscosity decreases as the shear rate increases, indicating a continuous breakdown of the material's internal structure due to increased shearing. This behavior is often caused by the breakdown of flocs in colloidal systems. Dilatant flow, on the other hand, is characterized by shear thickening behavior, where the viscosity increases as the shear rate increases. This indicates a continuous buildup of the material's internal structure due to increased shearing. Since most fluid-like materials exhibit Newtonian or pseudoplastic behavior (e.g., laponite suspensions show pseudoplastic behavior), dilatant flow and thickening behavior will not be discussed further in this thesis. Both the Herschel-Bulkley and Casson models are used to describe the consistency curves of non-dilute clay suspensions. These suspensions exhibit an initial yield stress at low shear stress levels and show pseudoplastic or shear-thinning behavior when the shear stress exceeds the yield stress.

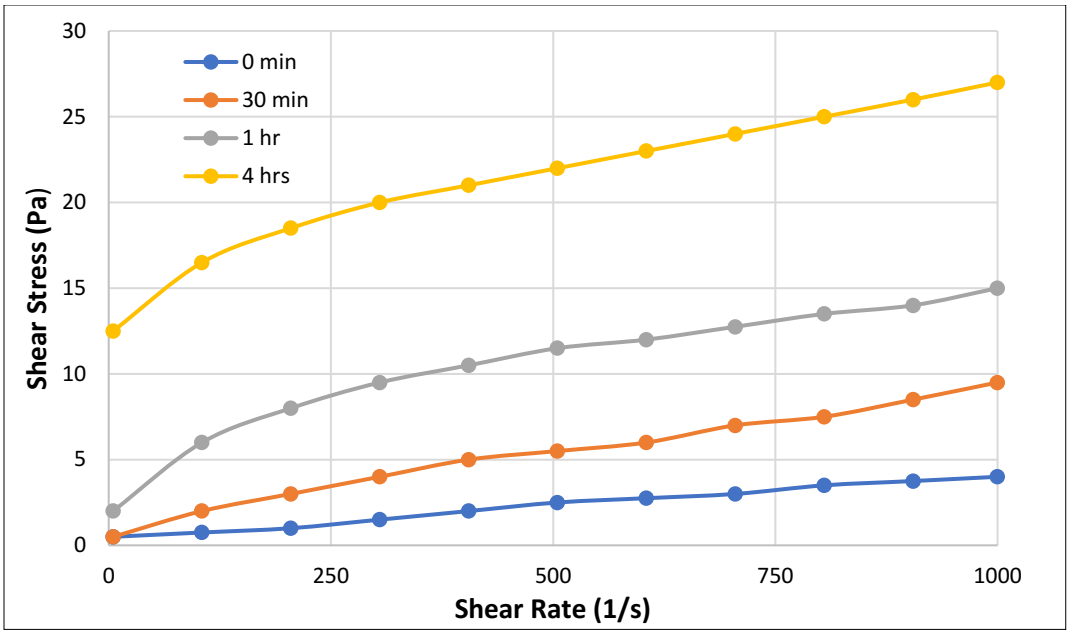

Figure 2-11: Typical consistency curves for 3% laponite-RD suspensions at different ageing times, after Chen [185]

Figure 2-11 presents the consistency curves for a 3% laponite-RD suspension at different times: 0 minutes, 30 minutes, 1 hour, and 4 hours. At 0 minutes, the laponite suspension behaves as a Newtonian fluid, with shear stress proportional to shear rate. As time progresses, the suspension's rheological behavior changes. It transitions from a Newtonian fluid at 0 minutes to a pseudoplastic fluid between 30 minutes and 1 hour, and finally to a cross-model gel. The consistency curve of laponite suspensions can be divided into three regions:

a) *Low Shear Rates*: At exceptionally low shear rates, the viscosity of the suspension remains constant and relatively high. In this region, the suspensions behave as flocculated systems with a linear viscoelastic response, exhibiting a high constant viscosity.

b) *Shear Thinning Region*: Between the low and high shear rate regions lies the shear thinning region, where the viscosity continuously decreases as the shear rate increases. This occurs because the flocculated structures within the suspension break down once the shear stress exceeds the yield stress.

c) *High Shear Rates*: At exceptionally high shear rates, the viscosity levels off and becomes constant again, but at a much lower value. This indicates that the internal structure of the material has been completely destroyed.

This behavior can be described by the Cross model:

$$\tau = \frac{\gamma(\eta_0 - \eta_\infty)}{1 + \gamma^{(1-n)}} + \gamma\eta_0$$

where γ is shear rate, η_0 is the viscosity at infinitely low shear rates, and η_∞ is the viscosity at infinitely high shear rates.

2.5.2 Time Dependent Flow Behaviour of Laponite

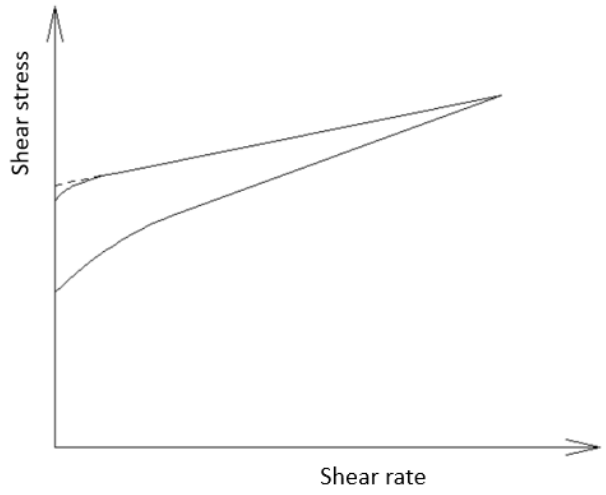

Figure 2-12: Thixotropic loop of laponite suspension, after Chen [185].

Laponite suspensions often exhibit time-dependent flow behavior known as thixotropy [186]. After mixing, the yield stress and plastic viscosity decrease but gradually recover over time when the suspension is left undisturbed. This recovery occurs because the colloidal system rebuilds its internal structure once the shear is reduced or completely removed. To investigate thixotropy, "step" experiments are commonly conducted, where the shear stress response to an applied shear rate or the shear rate response to an applied shear stress is monitored. These experiments are widely used to determine the time required to apply shear rates or stress to achieve a steady-state response. Chen [2014] reported a Curve (**Figure *2-12***) which demonstrates the response of laponite suspensions to shear stress when the shear rate is ramped up and then immediately ramped down. At a specific shear rate, the corresponding shear stress recorded in the ramped-down region is lower than in the ramped-up region, creating a hysteresis loop. This suggests that the fragment of the network broken under shear requires substantial recovery time to be linked back into a network.

2.5.3 Viscoelasticity of Laponite

An alternative method for examining the stability and flocculation of laponite and other colloidal dispersions involves conducting viscoelastic measurements. Viscoelasticity refers to the time-dependent property of a material, demonstrating both viscous and elastic behaviors. In elastic materials, the stress response is directly proportional to the strain for a constant applied strain, and once the strain is removed, the material promptly returns to its original state. Conversely, in viscous materials, the stress response to a constant applied strain immediately relaxes to zero. Viscoelastic materials exhibit a stress response that decreases to an asymptotic value, while viscoelastic liquids gradually reduce stress towards zero over time. The oscillatory test is used to assess the viscoelastic properties of a substance involves conducting. This method examines how materials respond to small amplitude oscillatory shear During such tests, a small amplitude sinusoidal oscillation (either in strain or stress) is applied to the sample at a constant frequency. Although sinusoidal strains are more commonly used, the corresponding stress or shear rate is tracked relative to the applied strain over time. In a viscoelastic suspension, the stress oscillates at the same frequency as the strain but exhibits a phase difference.

In a perfectly elastic system, stress aligns exactly with strain ($\delta=0°$ and $\phi=90°$), whereas in a purely viscous liquid, it opposes the strain completely ($\delta=90°$ and $\phi=0°$). For viscoelastic systems, the phase angle shift falls between these two extremes, and the sinusoidal stress measurement splits into elastic (τ') and viscous (τ'') components. Thus, phase angles derived from sinusoidal stress measurements range from $0° < \phi' \leq 45°$ for materials showing elastic-like behavior, and $45° < \phi' \leq 90°$ for those displaying viscous-like behavior.

2.5.4 Rheology of Laponite

A dilute dispersion of laponite in deionized water can maintain low viscosity over a prolonged period. However, as the laponite concentration increases, the viscosity of the suspension rises, impeding its flow through the soil unless sufficient pressure is applied. Numerous studies have examined various factors influencing the rheological properties of laponite suspensions, including laponite concentration, ionic strength, *pH* of the solution, and temperature [18,178,180-182]. Laponite concentration, in particular, plays a critical role in the rheological behavior of these suspensions. As the concentration increases, laponite crystals come into closer contact, leading to an earlier viscosity increase.

2.5.5 Modification of Laponite Suspensions

Laponite suspensions and other clay minerals have drawn a lot of attention because to their potential to modify target materials' rheological behaviour to suit specific needs for paints, varnishes, cosmetics, and other applications. Changes in laponite concentration, ionic strength, temperature, and *pH* can all affect the rheological behaviour of laponite suspensions. Several mechanisms can be used to modify clay minerals such as adsorption, ion exchange with inorganic and organic cations, binding of inorganic and organic anions, grafting of organic compounds, reaction with acids, pillaring by different types of poly cations, intraparticle and interparticle polymerization, dihydroxylation and calcination, delamination and reaggregation od smectites, and lyophilisation, ultra sound and plasma (187). These mechanisms can be broadly categorized into two groups: weakening the initial gel structure and strengthening the overall structure of laponite suspension.

It is possible to alter laponite to weaken its original structure by adding specific compounds, such as condensed Phosphate and polymers. The addition of condensed Phosphate is one of the common procedures of reducing the aggregation rate of laponite suspension. Sodium Pyrophosphate (*SPP*) and Tetrasodium Pyrophosphate (*TSPP*) are two options (174). The use of polymers is another method to alter the original microstructure of laponite suspensions. The effects of water-soluble polymers on laponite dispersions depend on the type of polymer, concentration, and molecular weight of polymer chains (188). To strengthen/enhance the structure of laponite suspensions, chemical additives such as electrolytes (simple salts), acids, surface active agents, and polymers include in laponite suspensions, which interact with laponite particles and change the rheological properties. The addition of simple salts or electrolyte is one of the common methods of altering the initial microstructure of laponite suspensions (189).

2.6 Conclusions

Soil densification is a prevalent method used to mitigate liquefaction risks and control potential deformations in sandy soils. However, traditional densification techniques have significant drawbacks, including limitations in full-field treatment, significant disturbance, environmental pollution, and high cost. Consequently, there is a pressing need to explore alternative materials to address these issues. Recent research has highlighted the significant potential of nanoparticles to enhance soil strength. Experimental studies have demonstrated the effectiveness of various

nanoparticles, including carbon nanotubes, colloidal silica, bentonite, and laponite, in improving soil properties. Key factors contributing to soil strength enhancement include the size, microstructure, surface functional groups, binding strength, and rheology of nanoparticle suspensions.

This study reviews the potential of four prominent nanoparticles for mitigating liquefaction risks under cyclic loadings by enhancing soil compressive strength:

- Carbon Nanotubes**:** Composed of graphene, carbon nanotubes are renowned for their exceptional strength. However, they may present environmental toxicity risks.
- Colloidal Silica (CS)**:** Colloidal silica has been proven effective in preventing liquefaction. The concentration of CS and curing time are crucial factors for ground improvement. Challenges such as controlling gelation time, achieving high injection success rates, and ensuring minimal deposition need to be addressed. Once these challengers are overcome, CS is expected to become widely used in anti-seismic applications.
- Bentonite**:** Bentonite is characterized by its high viscosity, thixotropy, and lubricity, forming gelatinous or suspended solutions in aqueous media. Research indicates that a 10% concentration of bentonite can create a thixotropic gel to reduce liquefaction risks. However, penetrating bentonite suspensions into sandy soils presents a challenge. Some studies suggest adding 0.5%-2% sodium pyrophosphate to reduce the early yield stress and viscosity of bentonite suspensions, improving their effectiveness. Addressing this challenge could make bentonite a more viable option for mitigating liquefaction risks.
- Laponite: Experimental studies have demonstrated that adding a small amount of laponite to sand can significantly reduce excess pore pressure development during static and cyclic loadings. Compared to clean sand under identical loading conditions, liquefaction initiation is delayed in laponite-treated sand due to the slower generation of pore pressure. Laponite not only enhances liquefaction resistance but also exhibits superior material characteristics and conductivity compared to nano-bentonite, owing to its transparent gel rheology and small particle size.

To advance the application of nanomaterials in soil improvement, comprehensive research methodologies that integrate nanomaterial science with geotechnical engineering approaches should be developed. Future studies should focus on:

- Maintaining the homogeneity of soil-nanoparticle mixtures in the target area.
- Ensuring that nanoparticles can travel the necessary distance without premature gel formation.
- Keeping nanoparticle-water suspensions in a liquid state until they reach the desired location.
- Investigating the formation time of nanoparticle hydrogels under various hydrological and geological conditions.
- Examining the effects of temperature on the gelling properties of nanoparticles.
- Characterizing nanoparticles, including their chemical composition, microstructure, and interaction with soil mediums, to assess their performance and practical applications.
- Analyzing the material properties of nanoparticles that enhance soil attributes.
- Investigating nanoparticle toxicity to address environmental and health risks, given its significant economic and societal implications.

The existing body of research provides a foundational understanding of laponite's microstructural and rheological properties, yet several significant gaps remain. One of the key gaps is the lack of comprehensive studies that explore how laponite alters or enhances the mechanical characteristics of sand, particularly under static loading conditions. While limited research has touched upon its potential for improving soil performance, critical aspects such as the long-term swelling behavior of laponite-treated soils and its repetitive drying-wetting cycles have received minimal attention. This is particularly important given the risks associated with excessive swelling, which could jeopardize the stability of engineering structures. Additionally, the environmental impact of laponite, including its potential toxicity to aquatic ecosystems, has not been thoroughly investigated, leaving uncertainties about its broader applicability in geotechnical projects.

Challenges in this field include the limited availability of advanced testing equipment, such as shaking tables and centrifuges, which hinders the ability to conduct dynamic tests necessary for understanding the behavior of laponite-treated soils under seismic conditions. Furthermore, boundary conditions in laboratory settings do not fully replicate complex field environments, posing difficulties in translating experimental results to real-world applications. Despite these challenges, there are significant opportunities for future research. Investigating the damping ratio and dynamic properties of laponite-treated soils could provide valuable insights for improving soil

performance in earthquake-prone regions. Similarly, further studies on the environmental impact of laponite, coupled with in-depth examinations of its swelling behavior, can open new avenues for its safe and effective use in soil stabilization and infrastructure development projects. This research offers a promising starting point for addressing these gaps and advancing the understanding of laponite's potential in both environmental and geotechnical applications.

2.7 References

[1] C.R. Yao, B. Wang, Z.-Q. Liu, H. Fan, F.-H. Sun and X.-H. Chang, "Evaluation of liquefaction potential in saturated sand under different drainage boundary conditions-an energy approach", *J Mar. Sci. Eng*. 7, 411 (2019).

[2] P. De Alba, C. Chan and H. Seed, "Determination of soil liquefaction characteristics by large-scale laboratory tests (No. Report No. EERC75-14)", Berkeley, CA (1975).

[3] K. Seed, "Rankine Lecture: Liquefaction and flow failure during earthquakes", *Geotechnique* 43, 351–415 (1993).

[4] S. Poulos, G. Castro and J. France, "Liquefaction evaluation procedure", *J Geotech. Eng*. 111, 772–92 (1985).

[5] R. Verdugo and J. Gonzalez, "Liquefaction-induced ground damages during the 2010 Chile earthquake", *Soil Dyn. Earthq. Eng*. 79, 280–95 (2015).

[6] P. De Alba, H. Seed and C. Chan, "Sand liquefaction in large-scale simple shear tests", *J Soil Mech. Found.* Div. ASCE 102, 909–927 (1976).

[7] K. Lee and A. Albaisa, "Earthquake-induced settlements in saturated sands", *J Geotech. Engng. Div*. ASCE 100, 387–406 (1974).

[8] H. Seed, P. Martin and J. Lysmer, "Pore-water pressure changes during soil liquefaction", *J Geotech. Engng. Div*. ASCE 102, 323–346 (1976).

[9] R. Dobry, R. Ladd, F. Yokel, R. Chung and D. Powell, "Prediction of pore water pressure buildup and liquefaction of sands during earthquakes by the cyclic strain method", District of Columbia: U.S. Dept. of Commerce, National Bureau of Standards; National Technical Information Service, (1982).

[10] R. Dobry, "Liquefaction of soils during earthquakes, National Research Council, Committee on Earthquake Engineering (Report No. CETS-EE-001)", National Academy Press, Washington, DC, USA (1985).

[11] C. Hsu and M. Vucetic, “Volumetric threshold shear strain for cyclic settlement”, *J Geotech. Geoenviron. Eng*. ASCE 130, 58–70 (2004).
[12] K. Hazirbab and E. Rathje, “Pore pressure generation of silty sands due to induced cyclic shear strains”, *J Geotech. Geoenviron. Engng*. ASCE 135, 1892–1905 (2009).
[13] A. Alarcon-Guzman, G. Leonards and J Chameau, “Undrained monotonic and cyclic strength of sands”, *J Geotech. Eng.* 114, 1089–109 (1988).
[14] G. Castro and S. Poulos, “Factors affecting liquefaction and cyclic mobility”, *J Geotech. Eng. Div.* 103, 501–516 (1977).
[15] R. Verdugo and K. Ishihara, “The steady state of sandy soils”, *Soils Found*. 36, 81–91 (1996).
[16] G. Clough, J. Iwabuchi, N. Rad and T. Kuppusamy, “Influence of cementation on liquefaction of sands”, *J Geotech. Eng*. 115, 1102–1117 (1989).
[17] J. Troncoso and R. Verdugo, “Silt content and dynamic behavior of tailings sands”, Idriss IM, editor. XI. Presented at the *Int. Conf. on Soil Mechanics Found. Engineering*., San Francisco: Balkema, pp. 1311–1314 (1985).
[18] Y. Vaid and S. Sivathayalan, “Static and cyclic liquefaction potential of Fraser Delta sand in simple shear and triaxial tests”, *Can. Geotech. J* 2, 281–289 (1996).
[19] M. Vucetic and R. Dobry, “Effect of soil plasticity on cyclic response”, *J Geotech. Eng*. 117, 89–107 (1991).
[20] J. Carraro, P. Bandini and R. Salgado, “Liquefaction resistance of clean and nonplastic silty sands based on cone penetration resistance”, *J Geotech. Geoenviron. Engng*. 129, 965–976 (2003).
[21] N. Chang, S. Yeh and L. Kaufman, “Liquefaction potential of clean and silty sands”, In *Pro of the 3rd Int Earthquake Microzonation Conference*. Seattle, WA, USA, pp. 1017–1032 (1982).
[22] W. Finn, R. Ledbetter and G. Wu, “Liquefaction in silty soils: design and analysis”, Ground failures under seismic conditions (eds S Prakash and P Dakoulas). *Geotech. Spec. Publ.* NY USA ASCE 44, 51–76 (1994).
[23] J. Koester, “The influence of fine type and content on cyclic strength”, Ground failures under seismic conditions (eds S Prakash and P Dakoulas). *Geotech. Spec. Publ*. NY USA ASCE 44, 17–33 (1994).

[24] K. Law and Y Ling, “Liquefaction of granular soils with non-cohesive and cohesive fines”, Presented at *the Proceedings of the 10th world conference on earthquake engineering*, Rotterdam, the Netherlands, pp. 1491–1496 (1992).
[25] C. Polito and J Martin, “A reconciliation of the effects of non-plastic fine on the liquefaction resistance of sands reported in the literature”, *Earthq. Spectra* 19, 635–651 (2003).
[26] S. Thevanayagam, T. Shenthan, S. Mohan and J. Liang, “Undrained fragility of clean sands, silty sands, and sandy silts”, *J Geotech. Geoenviron. Engng*. 128, 849–859 (2002).
[27] V. Vaid, “Liquefaction of silty soils”, In Ground failures under seismic conditions (eds S Prakash and P Dakoulas). *Geotech. Spec. Publ.* NY USA ASCE 44, 1–16 (1994).
[28] K. Ishihara, “Soil behaviour in earthquake Geotechnics”, Oxford Science Publication, Clarendon Press, Oxford, UK (1996).
[29] K. Ishihara and J. Koseki, “Discussion of cyclic shear strength of fines-containing sands”, Presented at the *Proceedings of the 12th international conference on soil mechanics and foundation engineering*, Rio de Janeiro, Brazil, p. 101-106 (1989).
[30] S. Saxena, K. Reddy and A. Avramidis, “Liquefaction resistance of artificially cemented sand”, *J Geotech. Eng*. 114, 1395–413 (1988).
[31] K. Tokimatsu and Y. Yoshimi, “Criteria of soil liquefaction with SPT and fines content”, Presented at the *8th World conf on earthquake eng*, San Francisco, CA: Prentice Hall (1984).
[32] G. Wang and J. Kuwano, “Modeling of strain dependency of shear modulus and damping of clayey sand”, *Soil Dyn. Earthq. Eng*. 18, 463–71 (1999).
[33] V. Georgiannou, D. Hight and J. Burland, “Behaviour of clayey sands under undrained cyclic triaxial loading”, *Geotechnique* 41, 383–393 (1991).
[34] J. Yamamuro and P. Lade, “Steady-state concepts and static liquefaction of silty sands,” *J Geotech. Geoenviron. Engng.* ASCE 124, 868–877 (1998).
[35] T. Murthy, D. Loukidis, J. Carraro, M. Prezzi and R. Salgado, “Undrained monotonic response of clean and silty sands”, *Geotechnique* 57, 273–288 (2007).
[36] D. Bobei, S. Lo, D. Wanatowski, C. Gnanendran and M. Rahman, “Modified state parameter for characterizing static liquefaction of sand and fines”, *Can. Geotech. J* 46, 281–295 (2009).
[37] C. Polito, “The effects of non-plastic and plastic fines on the liquefaction of sandy soils”, (Ph.D. thesis). Virginia Polytechnic Institute and State University, Blacksburg, VA, USA (1999).

[38] J. Bray, M. Cubrinovski, J. Zupan and M. Taylor, “Liquefaction Effects on Buildings in the Central Business District of Christchurch”, *Earthq. Spectra* 30, 85–109 (2004).
[39] J. Bray and J. Frost, “Geo-engineering Reconnaissance of the 2010 Maule, Chile, Earthquake”, (a Report of the NSF- Sponsored GEER Association Team, primary authors: Arduino et al.) (2010).
[40] M. Cubrinovski, J. Bray, M. Taylor, S. Giorgini, B. Bradley, L. “Wotherspoon and J. Zupan, Soil liquefaction effects in the central business district during the February 2011 Christchurch earthquake”, *Seism. Res. Lett*. 82, 893–904 (2011).
[41] J. Bird and J. Bommer, “Earthquake losses due to ground failure”, *Eng. Geol*. 75, 147–179 (2004).
[42] A. Krishna, “Mitigation of liquefaction hazard using granular piles”, *J Geotech. Earthq. Eng.* 2, 44–66 (2011).
[43] A. Porbaha, K. Zen and M. Kobayashi, “Deep mixing technology for liquefaction mitigation”, *J Infrastruct. Syst*. 5, 21–34 (1999).
[44] T. Shenthan, R. Nashed, S. Thevanayagam and G. Martin, “Liquefaction mitigation in silty soils using composite stone columns and dynamic compaction”, *Earthq. Eng. Vib*. 3, 39–50 (2004).
[45] S. Yasrobi and M. Biglari, “The use of dynamic compaction in liquefaction hazards mitigation at reclaimed lands in Assalouyeh petro-chemical complex—Iran”, *Soft Soil Eng.* 587–593 (2007).
[46] P. Gallagher, A. Pamuk and T. Abdoun, “Stabilization of liquefiable soils using colloidal silica grout”, *J Mater. Civ. Eng*. 19, 33–40 (2007).
[47] E. Vik, L. Sverdrup, L. Kelley, R. Storhaug, A. Beitnes, K. Boge, G. Grepstad and V. Tveiten, “Experiences from environmental risk management of chemical grouting agents used during construction of the romeriksporten tunnel”, *Tunn. Undergr*. *Space Technol.* 15,4, 369–378 (2000).
[48] Y. Huang and Z. Wen, “Recent developments of soil improvement methods for seismic liquefaction mitigation”, *Nat. Hazards* 76, 927–1938 (2015).
[49] W. Cao, “Nanostructures and nanomaterials-synthesis, properties and applications”, *Imperial College Press,* London (2004).

[50] National Research Council, 2006. “Geological and geotechnical engineering in the new Millennium: opportunities for research and technological innovation”, *National Academies Press,* Washington (2006).
[51] R. Yonekura and M. Kaga, “Current chemical grout engineering in Japan, Proc., Grouting”, *Soil Improvement and Geosynthetics*, ASCE, New York (1992).
[52] P. Persoff, J. Apps, G. Moridis and J. Whang, “Effect of dilution and contaminants on sand grouted with colloidal silica”, *J Geotechn. Geoenviron. Eng*. 125, 461–469 (1999).
[53] P. Gallagher, “Passive site remediation for mitigation of liquefaction risk”, Ph.D. Dissertation, Virginia Polytechnic Institute and State University, Virginia (2000).
[54] C. El Mohtar, A. Bobet, M. Santagata, V. Drnevich and C Johnston, “Liquefaction mitigation using bentonite suspensions”, ASCE *J Geotech. Geoenviron. Engng*. 139, 1369–1380 (2013).
[55] C. El Mohtar, A. Bobet, M. Santagata, V. Drnevich and C. Johnston, “Cyclic response of sand with thixotropic pore fluid”, *Geotechnical earthquake eng. and soil dyn*. IV (eds D. Zeng, M. T. Manzari and D. R. Hiltunen). Geotechnical Special Publication 181 (CD-ROM). Reston, VA, USA: ASCE (2008).
[56] D. Rugg, J. Yoon, H. Hwang and C. El Mohtar, “Undrained shearing properties of sand permeated with a bentonite suspension for static liquefaction mitigation”, *Geofrontiers* 2011 Adv. Geotech. Eng. Geotechnical Special Publication 211, 677686 (CD-ROM) (2011).
[57] F. Ochoa-Cornejo, A. Bobet, C. Johnston, M. Santagata and J. Sinfield, “Cyclic behavior and pore pressure generation in sands with laponite, a super-plastic nanoparticle”, *Soil Dyn. Earthq. Eng*. 88, 265–279 (2016).
[58] Y. Huang and L. Wang, “Laboratory investigation of liquefaction mitigation in silty sand using nanoparticles”, *Eng. Geol*. 204, 23–32 (2016).
[59] T. Youd, I. Idriss, R. Andrus, I. Arango, G. Castro and J. Christian, “Liquefaction resistance of soils”, summary report from the 1996 NCEER and 1998 NCEER/NSF workshops on evaluation of liquefaction resistance of soils. *J Gecotech. Geoenviron. Eng.* 127, 817–33 (2001).
[60] B.M. Das and G. Ramana, “Principles of Soil Dynamics”, 2nd edition, Stamford, Printed in the United States of America (2011).
[61] M. Jefferies and K. Been, “Soil Liquefaction: A Critical State Approach”, 2nd edition, Taylor and Francis Group (2015).

[62] P. Loma, M 6.9- Loma Prieta, “California Earthquake, Advanced National Seismic System” (Comprehensive Catalog, US Geological Survey) (1989).
[63] A. Casagrande, “Liquefaction and cyclic deformation of sands: A critical review”, *Harv. Soil Mech*. Ser. No 88 (1976).
[64] V. Florin and P. Ivanov, “Liquefaction of saturated sandy soils”, in: Proceedings of the 5th *International Conference on Soil Mechanics and Foundation Engineering* (ICSMFE), Paris. pp. 107–111 (1976).
[65] A. Casagrande, “On liquefaction phenomenon”, *Geotechnique* 21, 197–202 (1969).
[66] A. Casagrande, “Characteristics of cohesionless soils affecting the stability of slopes and earth fills”, *J. Boston Soc. Civ. Eng.* (1936).
[67] A. Schofield, “Dynamic and Earthquake Geotechnical Centrifuge Modelling”, in: Proceedings of the *International Conference Recent Advances in Geotechnical Earthquake Engineering and Soil Dynamics*. pp. 1081–1100 (1981).
[68] B. Muhunthan and A. Schofield, “Liquefaction and Dam failure” (This is a technical report of the University of Cambridge, CUED/D/SOILS/TR 310 (October 1999).), Proceedings of ASC Conference, GeoDenver 2000 (2000).
[69] H. Tsuchida, “Prediction and Countermeans Against the Liquefaction in Sand Deposits”, Abstract of the Seminar in the Port and Harbor Research Institute, Yokohama, Japan, 3.1-3.33 (1970).
[70] National Research Council, “Liquefaction of Soils During Earthquakes”, Report No. CETS-EE-001, Committee on Earthquake Eng., National Academy Press, Washington, D.C. (1985).
[71] H. Seed, K. Tokimatsu, L. Harder and R. Chung, “Influence of SPT Procedures in Soil Liquefaction Evaluations”, *J. Geotech. Eng*. 3, 1425–1445 (1985).
[72] R. Feynman, “There’s plenty of room at the bottom”, *Eng. Sci*. 22, 22–36 (1960).
[73] J. Tiwari, R. Tiwari and K. Kim, “Zero-dimensional, one-dimensional, two-dimensional and three-dimensional nanostructured materials for advanced electrochemical energy devices”, *Prog. Mater. Sci*. 57, 724–803 (2012).
[74] E. Dreaden, A. Alkilany, X. Huang, C. Murphy and M. El-Sayed, “The golden age: gold nanoparticles for biomedicine”, *Chem. Soc. Rev*. 41, 2740–2779 (2012).

[75] W. Shin, J. Cho, A. Kannan, Y. Lee and D. Kim, “Cross-linked composite gel polymer electrolyte using mesoporous methacrylate-functionalized SiO_2 nanoparticles for lithium-ion polymer batteries”, *Sci. Rep*. 6, 26332 (2016).
[76] M. Cacciatore, D. Scheufele and E. Corley, “From enabling technology to applications: the evolution of risk perceptions about nanotechnology”, *Public Underst. Sci*. 20, 385–404 (2009).
[77] G. Finch, H. Havel, M. Analoui, R. Barton, A. Diwan and M. Hennessy, “Nano-medicine drug development: a scientific symposium entitled Charting a Roadmap to Commercialization”, *AAPS J* 16, 698–704 (2014).
[78] H. Hyung, J. Fortune, J. Hughes and J. Kim, “Natural organic matter stabilizes carbon nanotubes in the aqueous phase”, *Environ. Sci. Technol*. 41, 179–184 (2007).
[79] K. Peng and S. Lee, “Silicon nanowire for photovoltaic solar energy conversion”, *Adv. Mater.* 23, 198–215 (2011).
[80] F. Halicioglu, “The potential benefits of nanotechnology for innovative solutions in the construction sector”, Nanotechnol. Constr. 3 Springer Heidelb. 209–214 (2009).
[81] M. Hanus and A. Harris, “Nanotechnology innovations for the construction industry”, *Prog. Mater. Sci.* 58, 1056–1102 (2013).
[82] O. Ugwu, J. Arop, C. Nwoji and N. Osadebe, “Nanotechnology as a preventive engineering solution to highway infrastructure failure”, *J Constr. Eng. Manag*. 139, 987–993 (2013).
[83] Z. Ge and Z. Gao, “Applications of nanotechnology and nano-materials in construction”, in: *1st International Conference on Construction in Developing Countries*. pp. 235–240 (2008).
[84] F. Pacheco-Torgal and S. Jalali, “Nanotechnology: advantages and drawbacks in the field of construction and building materials”, *Constr. Build. Mater*. 25, 582–590 (2011).
[85] P. Balaguru and K. Chong, “Nanotechnology and concrete research opportunities”, In: *Proceedings of ACI Session on Nanotechnology of Concrete: Recent Developments and Future Perspectives*. Denver, pp. 15–28 (2006).
[86] A. Qureshi, W. Kang, J. Davidson and Y. Gurbuz, “Review on carbon-derived, solid-state, micro and nano sensors for electro-chemical sensing applications”, *Diam. Relat. Mater*. 18, 1401–1420 (2009).
[87] F. Sanchez and K. Sobolev, “Nanotechnology in concrete: a review”, *Constr. Build Mater*. 24, 2060–2071 (2010).

[88] K. Chong, “Nano science and engineering in mechanics and materials”, *Rev. Adv. Mater*. 5, 110–116 (2003).
[89] M. Berger, “Nanotechnology; the future is tiny”, Royal Society of Chemistry, 1st edition (2016).
[90] S. Sathurusinghe, W. Herath, H. Subhashini and K Herath, “Stress concentrations in single walled carbon nanotube reinforced metal and polymer composites under uniaxial loading”, *J Adv. Struct. Geotechn. Eng*. 1, 58–60 (2012).
[91] Y. Ando, “The preparation of carbon nanotubes”, *Fuel Sci. Technol*. 2, 173–80 (1994).
[92] W. Maser, A. Benito and M. Martinez, “Production of carbon nanotubes the light approach”, *Carbon* 40, 1685–95 (2002).
[93] C. Oncel and Y. Yurum, “Carbon nanotube synthesis via the catalytic CVD method, a review on the effect of reaction parameters, Fullerene, Nanotubes”, *Carbon Nanostruct.* 14, 17–37 (2006).
[94] B. Fakhim, A. Hassani, A Rashidi and P. Ghodousi, “Predicting the impact of multiwalled carbon nanotubes on the cement hydration products and durability of cementitious matrix using artificial neural network modeling technique”, *Sci. World J*. ID 103713 (2013).
[95] M. Arabania, A. Haghib and Y. Moradic, “Evaluation of mechanical properties improvement of clayey sand by using carbon nanotubes”, In: *Proceedings of the 4th International Conference on Nanostructures* (ICNS4). Kish Island, I.R. Iran, pp. 1567–1569 (2012).
[96] M. Morsy, S. Alsayed and M. Aqel, “Hybrid effect of carbon nanotube and nano-clay on physicomechanical properties of cement mortar”, *Constr. Build. Mater.* 25, 145–149 (2011).
[97] V. Dhawan, S. Dhoat, A. Williams, A. Dimarco, S. Pal, A. Forbes, A. Tobías, P. Martinez-Martin and K. Chaudhuri, “The range and nature of sleep dysfunction in untreated Parkinson’s disease (PD). A comparative controlled clinical study using the Parkinson’s disease sleep scale and selective polysomnography”, *J Neurol. Sci*. 25, 158–62 (2006).
[98] S. Li, T. Anderson, M. Green, J. Maul and J. Canas-Carrell, “Polyaromatic hydrocarbons (PAHs) sorption behavior unaffected by the presence of multi-walled carbon nanotubes (MWNTs) in a natural soil system”, *Environ. Sci. Process. Impacts* 15, 1130–1136 (2013).
[99] Z. Tong, M. Bischoff and L. Nies, “Impact of fullerene (C_{60}) on a soil microbial community”, *Env. Sci. Technol*. 41, 2985–2991 (2007).

[100] A. Johansen, A. Pedersen and K. Jensen, "Effects of C_{60} fullerene nanoparticles on soil bacteria and protozoans", *Env. Toxicol. Chem*. 27, 1895–1903 (2008).
[101] L. Spencer, G. Rix and P. Gallagher, "Colloidal silica gel and sand mixture dynamic properties", *Geotech. Earthq. Eng. Soil Dyn. Congr*. IV PP1-10 ASCE Rest. VA USA (2008).
[102] S. Chang, L. Liu and S. Asher, "Preparation and properties of tailored morphology, monodisperse colloidal silica cadmium sulfide nanocomposites", *J Am. Chem. Soc*. 116, 6739–6744 (1994).
[103] C. Chapa-Gonzalez, A. Pinon-Urbina and P. Garcia-Casillas, "Synthesis of controlled-size silica nanoparticles from sodium metasilicate and the effect of the addition of PEG in the size distribution", *Mater. Basel* 11, 510 (2018).
[104] G. Dietler, C. Aubert and D. Cannell, "Gelation of colloidal silica", *Phys. Rev. Lett*. 57, 3117 (1986).
[105] Y. Liu, C. Hsu and W. Wei, "Preparation and thermal properties of epoxy-silica nanocomposites from nanoscale colloidal silica", *Polymer* 44, 5159–5167 (2003).
[106] J. Martin, J. Wilcoxon and D. Schaefer, "Fast aggregation of colloidal silica", *Phys. Rev*. 41, 4379 (1990).
[107] R. Yonekura and M. Miwa, "Fundamental properties of sodium silicate-based grout", Presented at the *11th Southeast Asia Geotech Conference*, Singapore, pp. 439–444 (1993).
[108] P. Gallagher and J. Mitchell, "Influence of colloidal silica grout on liquefaction potential and cyclic undrained behavior of loose sand", *Soil Dyn. Earthq. Eng*. 22, 1017–1026 (2002).
[109] P. Gallagher, A. Pamuk, A. Koch and T. Abdoun, "Centrifuge Modeling of Passive Site Remediation", in: Proc., 7th *United States National Conf. on Earthquake Engineering* (7NCEE): Urban Earthquake Risk. Presented at the Earthquake Eng Research Inst, Oakland, Calif. (2002).
[110] P. Gallagher and A. Koch, "Model testing of passive site stabilization: A new grouting technique, Grouting and Ground Treatment", in: *Proc., 3rd Int. Conf., ASCE*, Reston, Va. pp. 1478–1489 (2003).
[111] V. Taboada, "Centrifuge modeling of earthquake-induced lateral spreading in sand using a laminar box", (Ph.D. Dissertation), Rensselaer Polytechnic Institute, Troy, NY (1995).
[112] H. Liao, C. Huang and B. Chao, "Liquefaction resistance of a colloid silica grouted sand, Grouting and ground treatment", in: *Proc. 3rd Int. Conf., ASCE*. Reston, Va., pp. 1305–1313 (2003).

[113] T. Kodaka, F. Oka, Y. Ohno, T. Takyu and N. Yamasaki, “Modelling of cyclic deformation and strength characteristics of silica treated sand”, in: *Proc., 1st Japan–US Workshop on Testing, Modelling, and Simulation* (GSP 143) 205–216. Reston, VA: ASCE (2005).
[114] J. Diaz-Rodriguez, V. Antonio-Izarraras, P. Bandini and J. Lopez-Molina, “Cyclic strength of a natural liquefiable sand stabilized with colloidal silica grout”, *Can. Geotech. J* 45, 1345–1355 (2008).
[115] P. Gallagher, C. Conlee and K. Rollins, “Full-scale field testing of colloidal silica grouting for mitigation of liquefaction risk”, *J Geotech. Geoenviron. Eng*. 133, 186–196 (2007).
[116] K. Andrianopoulos, G. Agapoulaki and A. Papadimitriou, “Simulation of seismic response of passively stabilized sand”, *Geotech. Res.* 3, 40-53 (2016).
[117] I. Towhata, “Geotechnical earthquake engineering, Geomechanics and geoengineering”, edited by W Wu and RI Borja, 697. Berlin: Springer (2008).
[118] D. Porcino, V. Marciano and R. Granata, “Static and dynamic properties of a lightly cemented silicate-grouted sand”, *Can. Geotech. J* 49, 1117–1133 (2012).
[119] A. Vranna and T. Tika, “The mechanical behavior of a clean sand stabilized with colloidal silica”, In *Proc., 16th European Conf on Soil Mechanics and Geotech Eng*. ICE Publishing. London (2015).
[120] G. Agapoulaki and A. Papadimitriou, “Rheological Properties of Colloidal Silica Grout for Passive Stabilization Against Liquefaction”, *J Mater. Civ. Eng*. 30, 04018251 (2018).
[121] S. Shen, Z. Wang, J. Yang and C. Ho, “Generalized approach for prediction of jet grout column diameter”, *J Geotech. Geoenviron. Eng*. 139, 2060–2069 (2013).
[122] M. Santagata, A. Bobet, A. El-howayek, F. Ochoa-Carnejo and J. Sinfield, “Building a nanostructure in the pore fluid of granular soils”, London, Taylor, and Francis (2015).
[123] P. Gallagher and Y. Lin, “Colloidal silica transport through liquefiable porous media”, *J Geotech. Geoenviron. Eng*. 135, 1702–1712 (2009).
[124] p. Gallagher and Y. Lin, “Column testing to determine colloidal silica transport mechanisms”, *Geo-Frontiers Congress 2005: Innovations in Grouting and Soil Improvement*, Reston, VA: ASCE, (2005).
[125] Y. Lin, “Colloidal silica transport mechanisms for passive site stabilization of liquefiable soils”, Ph.D. Dissertation, Drexel Univ., Philadelphia, United States (2006).

[126] Y. Lin and P. Gallagher, “Three-meter column testing of colloidal silica transport through porous media”, in: *Ground Modification and Seismic Mitigation* (GSP 152), 417-424. Reston, VA: ASCE. Presented at the GeoShanghai International Conference 2006 (2006).
[127] P. Gallagher and S. Finsterle, “Physical and numerical model of colloidal silica injection for passive site stabilization”, *Vadose Zone J* 3, 917–925 (2004).
[128] M. Hamderi and P. Gallagher, “Pilot-scale modeling of colloidal silica delivery to liquefiable sands”, *Soils Found*. 55, 143–153 (2015).
[129] A. Koch, “Model testing of passive site stabilization”, Ph.D. Dissertation, Drexel Univ., Philadelphia, United States (2002).
[130] M. Noll, D. Epps, C. Bartlett and P. Chen, “Pilot field application of a colloidal silica gel technology for in situ hot spot stabilization and horizontal grouting”, in: *7th National Outdoor Action Conf., National Groundwater Asso*., 207219. Westerville, OH: Water Well Journal Publishing Com. (1993).
[131] C. Conlee, “Dynamic properties of colloidal silica soils using centrifuge model tests and a full-scale field test”, Ph.D. Dissertation, Drexel Univ., Philadelphia, United States (2010).
[132] DuPont, “Ludox colloidal silica: properties, uses, storage and handling”, Product Information, 19, Wilmington, DE: DuPont (1997).
[133] P. Greenwood and J. Otterstedt, “Some Important, fairly new uses of colloidal silica/silica sol, Fundamentals and Applications, Chapter; 57”, 1st ed. Publisher: Taylor and Francis, Editors: Bergna, HE and Roberts, WO (2005).
[134] Z. Darvishi and A. Morsali, “Synthesis and characterization of nano bentonite by sonochemical method”, Ultrason. Sonochem. 18, 238–242 (2011).
[135] W. Nesse, “Introduction to mineralogy”, New York: Oxford University Press (2000).
[136] W. Sutherland, “Wyoming Bentonite”, Wyoming State Geological Sur. Retrieved 12 Jan 2021 (2014).
[137] J. Jackson, “Bentonite, Glossary of geology”, 4th ed. American Geological Institute, Alexandria, Virginia (1997).
[138] M. Abdou, A. Al-sabagh and M. Dardir, “Evaluation of Egyptian bentonite and nano-bentonite as drilling mud”, *Egypt J Pet*. 22, 53–59 (2013).
[139] A. Teplitskiy, R. Gee and R. Kourmaev, “Application of physical-chemical properties of bentonite utilized in construction”, as viewed through the TRIZ Prism (2005).

[140] A. Perry, “Why bentonite clays are safe to ingest”, Bentonite clay info.com website (last access on June 16, 2021) (2019).
[141] D. Anderson and P. Hoekstra, “Migration of Interlamellar Water During Freezing and Thawing of Wyoming Bentonite”, *Soil Sci. Soc. Am. J.* 29, 498–503 (1965).
[142] T. Brown, N. Idoine, E. Raycraft, R. Shaw, S. Hobbs, P. Everett, E. Deady and T. Bide, “World Mineral Production 2012-16”, British Geological Survey, Nottingham, England (2016).
[143] J. Hosterman and S. Patterson, “Bentonite and fuller’s earth resources of the United States”, U.S. Geological Survey Professional Paper. 1522, United States Government Printing office, Washington, DC, USA (1992).
[144] B. Butcher, “The Advantages of a Salt/Bentonite Backfill for Waste Isolation Pilot Plant Disposal Rooms”, *MRS Proceedings*, 333, 911 (1993).
[145] B. Theng, “Formation and Properties of Clay Polymer Complexes”, *Developments in Soil Science* 9. Elsevier, Amsterdam (1979).
[146] C. Boswell, B. Swanney and W. Owers, “Sulfur/sodium bentonite prills as sulfur fertilizers. Effect of sulfur-sodium bentonite ratios on the availability of sulfur to pasture plants in the field”, *Fertil. Res*. 15, 33–45 (1988).
[147] A. Muscolo, T. Papalia, G. Settineri, C. Mallamaci and M. Panuccio, “Sulfur bentonite organic based fertilizers as tool for improving bio-compounds with antioxidant activities in red onion”, *Sci. Food Agric*. 100, 785–793 (2020).
[148] R. Robertson, “Fuller’s Earth. A History of calcium montmorillonite”, 1st ed. Volturna Press, U.K. (1986).
[149] G. Christidis, A. Blum and D. Eberl, “Influence of layer charge and charge distribution of smectites on the flow behaviour and swelling of bentonites”, *Appl. Clay Sci*. 34, 125–138 (2006).
[150] D. Eisenhour and R. Brown, “Bentonite and Its Impact on Modern Life”, *Elements* 5, 83–88 (2009).
[151] I. Odom, “Smectite clay Minerals: Properties and Uses”, *Philos. Trans. R. Soc. Math. Phys. Eng. Sci*. 311, 391–409 (1984).
[152] D. McCarty, B. Sakharov and V. Drits, “New insights into smectite illitization: A zoned K-bentonite revisited”, *Am. Mineral*. 94, 1653–1671 (2009).
[153] K. Bekkour, M. Leyama, A. Benchabane and O. Scrivener, “Time-dependent rheological behavior of bentonite dispersions: an experimental study”, *J Rheol.* 49, 1329–1345 (2005).

[154] J. Durn, M. Ramos-Tejada, F. Arroyo and F. Gonzlez-Caballero, “Rheological and electrokinetic properties of sodium montmorillonite suspensions: I. Rheological properties and interparticle energy of interaction”, *J Colloid Interf. Sci*. 229, 107–117 (2000).
[155] C. Harvey and G. Lagaly, “Industrial applications”, In: Bergaya, F., Lagaly, G. (Eds.), Handbook of Clay Science, 5B, 2nd ed. Elsevier (2013).
[156] V. Kelessidis, C. Tsamantaki and P. Dalamarinis, “Effect of pH and electrolyte on the rheology of aqueous Wyoming bentonite dispersions”, *Appl. Clay Sci*. 38, 86–96 (2007).
[157] S. Laribi, J. Fleureau, J. Grossiord and N. Kbir-Ariguib, “Effect of pH on the rheological behavior of pure and interstratified smectite clays”, *Clay Min*. 54, 29–37 (2006).
[158] C. Malfoy, A. Pantet, P. Monnet and D. Righi, “Effects of the nature of the exchangeable cation and clay concentration on the rheological properties of smectite suspensions”, *Clay Miner.* 51, 656–663 (2003).
[159] D. Penner and G. Lagaly, “Influence of anions on the rheological properties of clay mineral dispersions’, *Appl. Clay Sci*. 19, 131–142 (2001).
[160] E. Tombacz and M. Szekeres, “Colloidal behavior of aqueous montmorillonite suspensions: the specific role of pH in the presence of indifferent electrolytes”, *Appl. Clay Sci.* 27, 75–94 (2004).
[161] S. Abend and G. Lagaly, “Solgel transitions of sodium montmorillonite dispersions”, *Appl. Clay Sci.* 16, 201–227 (2000).
[162] G. Lagaly and I. Dekany, “Chapter 8: Colloid Clay Science in Handbook of Clay Science. Part A: Fundamentals”, In: Bergaya F, Lagaly G (Eds.), Elsevier, Amsterdam (2013).
[163] L. Michot, I. Bihannic, K. Porsch, S. Maddi, C. Baravian, J. Mougel and P. Levitz, “Phase diagrams of Wyoming Na-montmorillonite clay. Influence of particle anisotropy”, *Langmuir* 20, 10829-10837 (2004).
[164] S. Yasuda, K. Wakamatsu and H. Nagase, “Liquefaction of artificially filled silty sands”, In *Ground failures under seismic conditions* (eds S. Prakash and P. Dakoulas), New York, NY, USA: ASCE. Geotech. Spec. Publ. 44, 91–104 (1994).
[165] I. Gratchev, K. Sassa, V Osipov and V. Sokolov, “The liquefaction of clayey soils under cyclic loading”, *Eng. Geol*. 86, 70–84 (2006).

[166] C. El Mohtar, A. Bobet, V. Drnevich, C. Johnston and M. Santagata, “Pore pressure generation in sands with bentonite: from small strains to liquefaction”, *Geotechnique* 64, 108–117 (2014).
[167] J. Clarke, “Investigation of Time-Dependent Rheological Behavior of Sodium Pyrophosphate Bentonite Suspensions”, MSc thesis, Purdue University, West Lafayette, Indiana (2008).
[168] M. Santagata, J. Clarke, A. Bobet, V. Drnevich, C. El Mohtar, P. Huang and C. Johnston, “Rheology of concentrated bentonite dispersions treated with sodium pyrophosphate for application in mitigating earthquake-induced liquefaction”, *Appl. Clay Sci*. 99, 24–34 (2014).
[169] R. Goh, Y. Leong and B. Lehane, “Bentonite slurries-zeta potential, yield stress, adsorbed additive and time-dependent behaviour”, *Rheol. Acta*. 50, 29–38 (2011).
[170] G. Lagaly, “Principles of flow of kaolin and bentonite dispersions”, *Appl. Clay Sci*. 4, 105–123 (1989).
[171] P. Shankar, J. Teo, Y. Leong, A. Fourie and M. Fahey, “Adsorbed phosphate additives for interrogating the nature of interparticle forces in kaolin clay slurries via rheological yield stress”, *Adv. Powder Technol*. 21, 380–385 (2010).
[172] P. Mongondry, T. Nicolai and J. Tassin, “Influence of pyrophosphate or polyethylene oxide on the aggregation and gelation of aqueous laponite dispersions”, *J Colloid Interf. Sci*. 275, 191–196 (2004).
[173] A. Witthoeft, M. Santagata and A. Bobet, “Numerical study of the effectiveness of bentonite treatment for liquefaction mitigation”, Presented at the Geotechnical special publication, Conference: GeoCongress 2012 (2012).
[174] BYK, “Technical Information B-RI 21: Laponite performance”, BYK Additives and Instruments, Wesel, Germany (2014).
[175] M. Kroon, G. Vos and G. Wegdem, “Structure and formation of a gel of colloidal disks”, *Phys. Rev. E*. 57, 1962–1970 (1998).
[176] A. El-Howayek, “Characterization, rheology and microstructure of laponite suspensions”, MSc thesis, Purdue University, West Lafayette, USA (2011).
[177] F. Paula, G. da Silva, R. Aquino, J. Depeyrot, J. Fossum, K. Knudsen, G. Helgesen and F. Tourinho, “Gravitational and magnetic separation in self-assembled clay ferrofluid nanocomposites”, *Braz. J Phys*. 39, 163–170 (2009).

[178] P. Levitz, E. Lecolier and A. Mourhid, “Liquid-solid transition of laponite suspensions at very low ionic strength: long-range electrostatic stabilization of anisotropic colloids”, *Eur. Lett*. 49, 676–677 (2000).
[179] H. Tanaka, J. Meunier and D. Bonn, “Nonergodic states of charged colloidal suspensions: repulsive and attractive glasses and gels”, *Phys. Rev. E*. 69, 031404-1-6 (2004).
[180] A. Howayek, A. Bobet, C. Johnston, M. Santagat and J. Sinfield, “Microstructure of sand laponite water systems using cryo-sem”, Presented at the *Geo-Congress 2014 Technical Papers, ASCE*, pp. 693-702 (2014).
[181] F. Ochoa-Cornejo, A. Bobet, A. El-Howayek, C. Johnston, M. Santagata and J. Sinfield, “Discussion On: Laboratory investigation of liquefaction mitigation in silty sand using nanoparticles [Eng.Geol.204:23-32]”, *Eng. Geol*. 216, 161–164 (2017).
[182] F. Ochoa-Cornejo, “Cyclic behaviour of sands with superplastic fines”, a dissertation submitted for the degree of Doctor of Philosophy, Purdue University, West Lafayette, Indiana (2015).
[183] X.B. Huang, J.S. Sun, Y. Huang, B.C. Yan, X.D. Dong, F. Liu and R. Wang, “Laponite: a promising nanomaterial to formulate high-performance water-based drilling fluids”, *Pet. Sci*. 18, 579–590 (2021).
[184] E.C. Bingham, Fluidity and plasticity. McGraw-Hill (1922).
[185] M. Shen, Rheological properties of laponite and chemically modified laponite suspensions, Master of Science in Civil Engineering, Purdue University, West Lafayette, Indiana, USA (2014).
[186] H. Olphen, Internal mutual flocculation in clay suspensions*, J of Colloid Science* 19(4): 313-322 (1964).
[187] F. Bergaya, M. Jaber, J.F. Lambert, Rubber-Clay Nanocomposites: Science, Technology and Applications, Chapter 1: Clays and Clay Minerals, Editor: M Galimberti, Print ISBN:9780470562109, John Wiley & Sons, Inc. (2011).
[188] P. Mongondry, T Nicolai, J. F. Tassin, Influence of pyrophosphate or polyethylene oxide on the aggregation and gelation of aqueous laponite dispersions, *J of Colloid and Interface Science* 275(1): 191-196 (2004).
[189] P. Mongondry, J. F. Tassin, T Nicolai, Revised state diagram of laponite dispersions. *J of Colloid and Interface* Science 283(2): 397-405 (2004).

CHAPTER 3 Effect of Laponite Nanoparticles on Growth Characteristics and Chlorophyll Content of *Chlorella* sp.

Abstract

Laponite nanoparticles have been proposed for soil densification to reduce the negative impacts of seismic hazards. However, the effects of laponite on the aquatic ecosystem are lacking. In this study, different concentrations (0.1%, 0.2%, 0.3%, 0.4%, and 0.5%) of laponite were used to investigate the growth and total chlorophyll content of microalgae: *Chlorella* sp. This study examined the potential toxic effects of laponite on the growth characteristics of freshwater green algae *Chlorella* sp. isolated from northern Ontario. The experiments were carried out in a 500 ml glass flask with 300 ml working volume and placed under white fluorescent lights for 16 hr: 8 hr day-night cultivation cycle in a constant orbital shaker. The results revealed that the lower concentration of laponite can enhance microalgae growth, while the higher laponite concentration had a growth inhibitory effect. The total chlorophyll content increased by 33% at 0.1% treatment group than that of the control group. Based on the SEM images, aggregation of microalgae was significantly noticeable at the lower concentration of laponite (0.1% treatment) whereas, in the higher laponite concentration (0.4% and 0.5 % treatment), algal cells were embedded in laponite gel and also noticed some physical impairment.

Keywords: Laponite, *Chlorella* sp., Chlorophyll content, Specific growth rate, Inhibition ratio

**A version of this chapter has been published in Water, Air, and Soil Pollution 233:308 (2022).*

3.1 Introduction

Laponite is a very promising nanoparticle that has been proposed for soil treatment to mitigate liquefaction risk due to the rapid growth of civilization [1,2]. Nanoparticles are ultrafine particles with at least one spatial dimension measured in nanometers. It has a unique structure, a huge specific surface area, and strong activity on the surface [3]. The gel-like solid nanoparticles can increase soil strength by firming the soil skeleton and amending pore water. Researchers proposed to use nanoscale alterations in the geotechnical materials to make them more effective [4-8]. Due to the good rheological property of transparent gel along with small-size scale, nanoparticles (for instance carbon nanotube, colloidal silica, bentonite, and laponite) can improve the liquefaction resistance of soil [9-11]. These nanoparticles are used in order to curb the uncontrolled movement of liquid including various types of contaminants in the soil layers. However, there is a growing concern about using nanoparticles in aquatic ecosystems due to the raising of serious environmental as well as human health concerns. For instance, carbon nanotubes have the potential to induce major human diseases (such as cancer, lung diseases, skin diseases) and to affect the immune system [12].

Microalgae are widely used as model organisms to identify the detrimental impacts of microplastics [13], antibiotics, nanoparticles [14] and other harmful chemicals [15,16] on the ecosystem. They are capable to biodegrade polycyclic aromatic hydrocarbons [15], phenols [16], and nanoparticles [17]. Microalgae are the principal source of food in the aquatic ecosystem. Hence, any type of impairment to algal flora could lead to disturbance in the entire food chain, and eventually to the aquatic ecosystem [18]. Subsequently, algae are the ideal model organisms for studying the effects of nanoparticles on the environment [19,20]. Based on the literature, the prime factors imparting toxicity of microalgae were dissolution and aggregation [21,22], reactive oxygen generation production [23], reduction in photosynthetic pigment [24], algal growth inhibition [25] and lipid peroxidation [26]. Interestingly, some nanoparticles are emerging as an effective tool to stimulate microalgae cultivation, harvesting, and pre-treatment [27-29]. The physical properties of nanoparticles affect the growth and biochemical composition of microalgae. In the previous research, various types of nanoparticles have been shown to have distinct impacts on different microalgae. For instance, Saxena and Harish [30] found that nano-form of ZnO was more toxic than bulk-form to freshwater algal. ZnO-nanoparticle concentration between 0.06 and 100 $mg.L^{-1}$

was reported to be responsible to create toxic effects on most algae [22,31-34]. According to Kadar et al. [27], a 100 $mg.L^{-1}$ dosage of nZVI increased biomass concentration by 18.75% and lipid accumulation by 3.57% in *Isochrsis galbana*. At the same dose of nZVI, an approximately 40% reduction in biomass and 41.90% increase in lipid accumulation was in *Tetraselmis suecica*. Demir et al. [35] found that alpha-iron-oxide (α-Fe_2O_3) and gamma-iron-oxide (γ-Fe_2O_3) nanoparticles possessed varying levels of toxicity on *Nannochloropsis* sp. and *Isochrysis* sp. In addition, carbon nanotubes, iron-oxide nanoparticles, and MgO-nanoparticles showed cell growth inhibition to *Scenedesmus oblicuus* at concentrations of 10, 40, and 0.8 $mg.L^{-1}$ respectively [36]. However, low doses ($\leq$5 $mg.L^{-1}$) of carbon nanotubes and iron-oxide nanoparticles resulted in a considerable increase in lipid accumulation, whereas the higher dosages resulted in a decline in lipid productivity. Alpha-iron-oxide has been found to be less toxic to microalgae compared to other forms of iron-nanoparticles (such as nZVI and Fe_2O_3) [25]. For a particular type of microalgae, namely *C. vulgaris*, TiO_2-nanoparticles showed negative effects, whereas Cu, Pb, Mg, and Zn-nanoparticles showed a rise in biomass by 8.82, 21.55, 13.95, and 20%, respectively [37,38]. There is no available published work on the effects of laponite on the aquatic ecosystem. Therefore, locally isolated microalgae species: *Chlorella* sp. was used as a model organism and investigated the effects of laponite, a very promising nanoparticle, on the growth characteristics and total chlorophyll content of microalgae and observe the interaction between them.

3.2 Materials and Methods

3.2.1 Microalgae Strains

To evaluate the effects of laponite on the typical freshwater microalgae was chosen as target microalgae strains (**Figure *3-1***). The water samples were collected from Lake Superior, Thunder Bay, Ontario, Canada. The samples were distributed on the BG-11 agar plates using sterile disposable spreaders and incubated for two to three weeks at room temperature under continuous lighting. The microalgae were identified as *Chlorella* sp. using the guidebook [39].

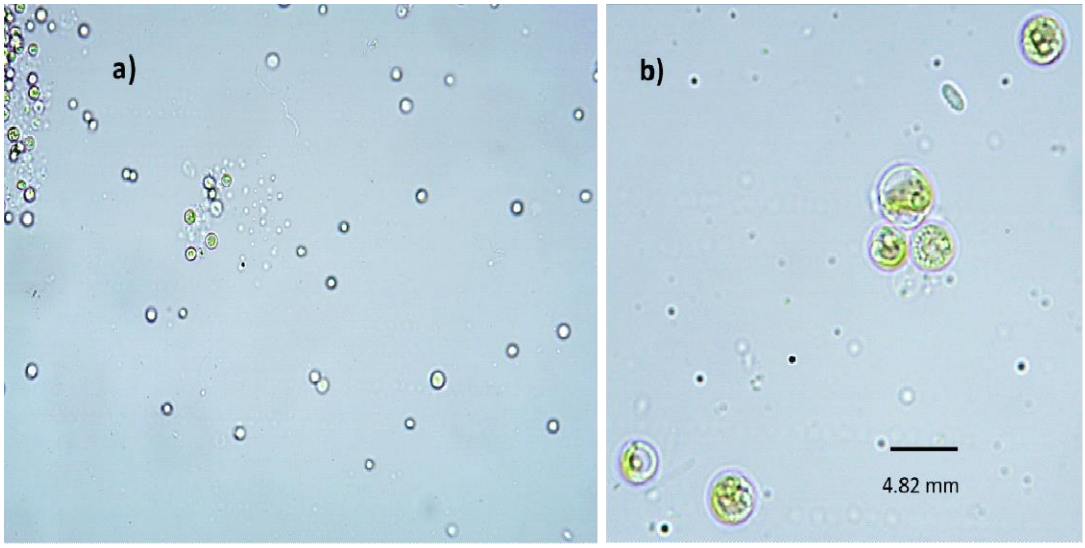

Figure 3-1: Images of *Chlorella* sp. a) lower magnification (40x), and b) higher magnification (100x) using a compound microscope

3.2.2 Laponite

Laponite is a multilayer silicate made from inorganic mineral materials found in nature. Laponite is layered synthetic hectorite clay, made up of disk-shaped nanoparticles with two tetrahedral layers and one octahedral layer [40]. The structure of laponite is identical to that of natural montmorillonite. The chemical composition formula is $Na^{+0.7}[(Si_8Mg_{5.5}Li_{0.3})O_{20}(OH_4)]^{-0.7}$. This has a negative charge of 0.70 per unit cell, which is neutralized during production by sodium ions adsorbed onto the crystal surfaces. The crystals form stacks that are kept together electrostatically by the sodium ions shared between adjacent crystals in the interlayer area. In the dry state, laponite appears to be a fine white powder with a diameter of around 25 nm, a thickness of 1 nm, and a specific gravity of 2.57 [41]. It hydrates, swells, and forms a colourless, clear monodisperse suspension that resembles a highly thixotropic gel when dispersed in water. When the ionic strength is strong, the electric double layer on the surface of particles is compressed, the electrostatic interaction distance reduces, and the distance between particles shortens, resulting in the formation of a physically cross-linked gel. Because of its small particle size and affinity for water, laponite has a plasticity index of about 1000%, which is significantly higher than that of natural clays [42]. A general-purpose grade Laponite-RD is used in this research which is manufactured by BYK Additive and Instruments, USA.

3.2.3 Cultivation Medium and Conditions

Microalga was cultivated into the BG-11 medium at room temperature (22±1° C). The *pH* of the BG-11 medium was adjected to 7.1 (Stanier et al., 1971). To show the effects of laponite on microalgae growth, different concentrations (0.1%, 0.2%, 0.3%, 0.4%, and 0.5%) of laponite were added into the BG-11 medium. Laponite has been fully dissolved and made a uniformly distributed solution using a magnetic stirrer. 500 ml Erlenmeyer glass flasks were used to cultivate microalgae with 300 ml working volume and placed under white fluorescent lights for 16 hr-8 hr day-night cultivation cycle in a constant orbital shaker (125 rpm). The experiment was carried out in a controlled growth room with a constant temperature. The growth of microalgae was examined by the cell count and chlorophyll contents measurement in the interval of every 3 days. Three parallel samples were set in each group of concentrated laponite and control samples to study the interaction mechanism between laponite and microalgae during the culture period. Table 3-1 shows the *pH* variations of the growth medium.

Table 3-1. *pH* variation on growth medium

Laponite concentrations (by dry weight)	***pH* variation of growth medium**	
	Day 1	**Day 21**
0.1%	9.27	9.41
0.2%	9.45	9.51
0.3%	9.63	9.59
0.4%	9.71	9.71
0.5%	9.78	9.73

3.2.4 Parameter Analysis

The total algal cell counts were determined by a microscopic cell count method (0.1 mm Tiefe deep Neubauer Improved Haemocytometer, Hamburg, Germany) with the use of a compound microscope (Olympus, Japan). The Specific Growth Rate (SGR) and growth Inhibition Ratio (IR) can be calculated as follows [13,43]:

$$SGR\ (d^{-1}) = \frac{CD_2 - CD_1}{T_2 - T_I} \qquad 3\text{-}1$$

$$IR(\%) = \frac{CD_0 - CD_1}{CD_0} \qquad 3\text{-}2$$

where, CD_1 (cell/ml) and CD_2 (cell/ml) are cell density values at the Nth and (N+1)th day. T_1 (day) and T_2 (day) are the cultivation time of Nth and (N+1)th day. CD_0 (cell/ml) and CD (cell/ml) are the cell density values of the control and experimental groups, respectively.

The chlorophyll content was measured following the method of Song et al. [13,43]. In detail, 2 mL algal solution was harvested by centrifugation at 5000 rpm for 10 min to obtain the algal cells. The supernatant was discarded and the pellet was resuspended in 1 mL of 90% methanol, incubated at 60-70°C for 10 min, kept it in dark for 15 min, and then centrifuged again for 10 min. The absorbance of the supernatant was recorded at 652 nm and 665 nm via the visible spectrophotometer (BioTek Epoch Microplate Spectrophotometer, Vermont, USA). The following equations were used to compute the total chlorophyll content [43]:

$$Chlorophyll\ \alpha\ \left(\frac{mg}{L}\right) = 16.82A_{665} - 9.28A_{652} \qquad 3\text{-}3$$

$$Chlorophyll\ \beta = 36.92A_{652} - 16.54A_{665} \qquad 3\text{-}4$$

$$Total\ Chlorophyll\ Content = Chlorophyll\ \alpha + Chlorophyll\ \beta \qquad 3\text{-}5$$

3.2.5 Sample Preparation for SEM

To study the microstructure of microalgae and laponite in the growth medium, two drops of each treatment solution were put on carbon adhesive tape attached to aluminum mountain pins. Placed it in a freeze at -80°C for 6 hours. After that, the samples were placed in the freeze drier for 24 hours to completely dry. Finally, sputtered coat the samples with gold to get better Scanning Electrons Microscope (SEM) images. SEM samples were pretreated and prepared according to the method of Xu et al. [44] and Zhao et al. [45].

3.2.6 Statistical Analysis

All the numerical variables were checked for normality before conducting the parametric test. Linear regression analysis was carried out to explore the relationship between the algal cell density and total chlorophyll content versus the number of culture days. One-way analysis of variance (ANOVA) was carried out to analyze the mean difference of the cell count and total chlorophyll content of the treatments, followed by Tukey's HSD posthoc test for pairwise differences. Differences between treatments were evaluated at $P<0.05$. All the experiments were performed in

triplicates, and the results are expressed as means with standard deviation. All statistical analyses were carried out in R v. 3.6.1 software (R Development Core Team, 2019).

3.3 Results and Discussion

3.3.1 Effects of Laponite on Microalgae Growth

3.3.1.1 Cell density

The cell density of *Chlorella* sp. significantly increased with the number of the cultivation days increased under different concentrations of laponite in the experimental and control groups (Figure 3-2). From the initial stage of the culture period until day 15, the growth of *Chlorella* sp. at 0.1% laponite concentration was higher than that of the control group (Figure 3-2a and f). There was a significant positive growth trend of microalgae at 0.1%, 0.2%, and 0.3% treatment conditions. However, in the case of 0.4% and 0.5% treatment conditions, the growth of microalgae was not significant. The polynomial regression analysis relevels that 0.1% and 0.2% of laponite treatments have higher cell density in comparison to BG-11. Similar types of observations were reported in the literature on the effects of nanoparticles on different kinds of microalgae. Kadar et al. (2012) observed that 18.75% enhancement in biomass concentration for *Isochrisis galbana* with 100 $mg \cdot L^{-1}$ nano-zerovalent-iron (nZVI) and the same dose showed 14%–40% inhibition in growth of *Pavlova lutheri* and *Tetraselmis suecica*. Similarly, Padrova et al. (2015) stated that 5.1 $mg.L^{-1}$ nZVI concentration increased the growth of various microalgae species by 15-92%. Moreover, Rana et al. (2020) reported the highest biomass concentration (2.4 $g.L^{-1}$) for *C. pyrenoidosa* at 20 $mg.L^{-1}$, which is higher than that of the control group (1.60 $g.L^{-1}$). In the current study, the cell density of 0.1% and 0.2% treatments gradually increased with the culture period. However, 0.3% concentration of laponite explained significantly lower (Figure 3-2b-e). Similar results have been reported at Rana et al. (2020) in the case of higher concentrated treatments. Hence, the higher concentrated laponite may have some negative impacts on the growth of *Chlorella* sp. A comparable decrease in *Chlorella* sp. has also been observed during the cultivation in Cu, Pb, Mg, and Zn-nanoparticles supplemented media [38].

The average cell density of each treatment group and control group is represented in Figure 3-3. One-way ANOVA revealed that there was a significant difference in the mean cell density among the treatments ($F=38.82$, $P<0.001$). The maximum average cell density of the control group was 27.67 $cell.ml^{-1}$. Furthermore, the multiple comparison tests explained that the maximum average cell density was 34.94 $cell.ml^{-1}$ at 0.1% laponite concentration after 21 days of the culture period,

followed by 0.2% treatment. However, there is no significant difference in the average cell density among 0.3, 0.4, and 0.5% treatments (Figure 3-3).

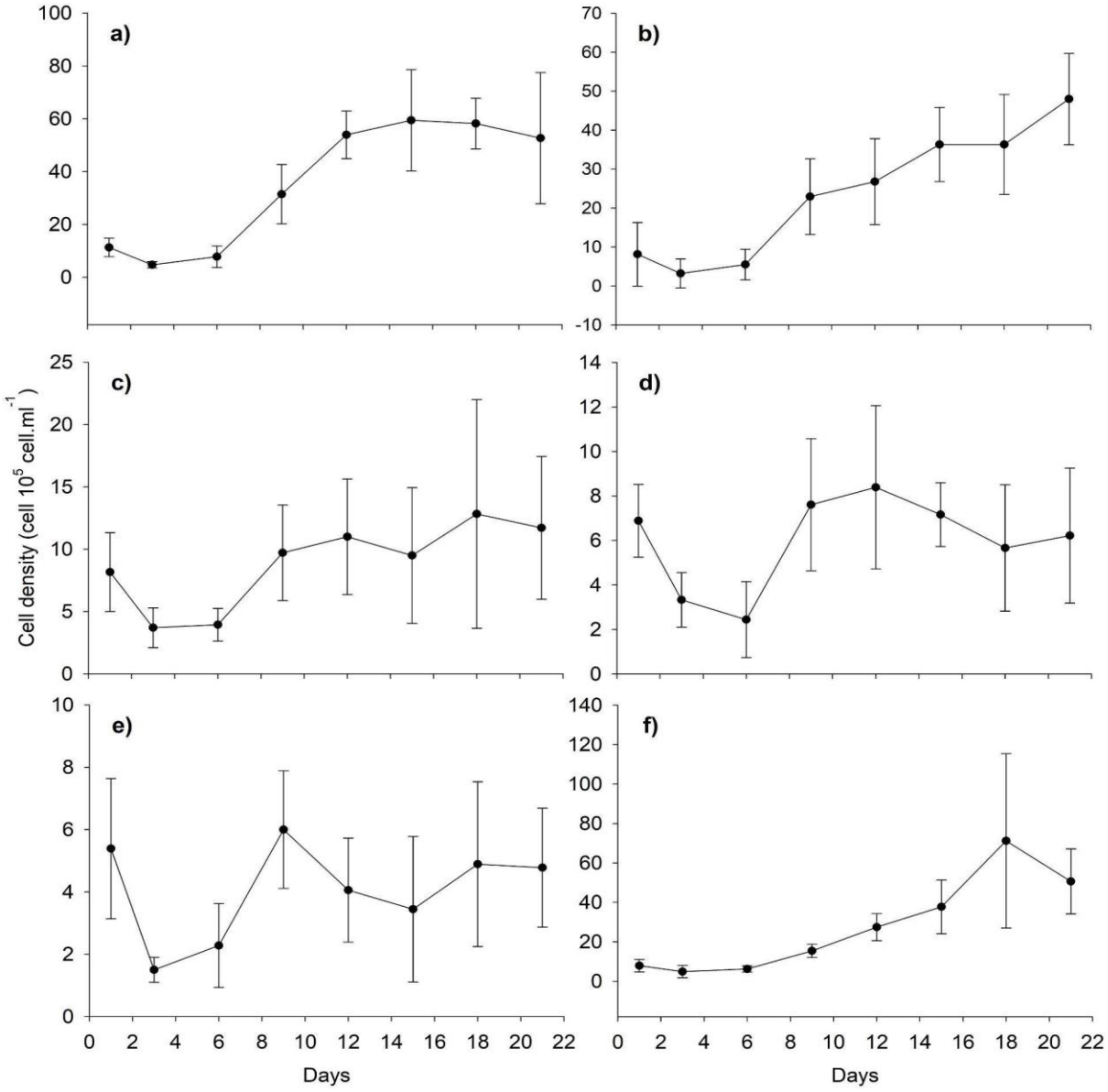

Figure 3-2: Cell density of *Chlorella* sp. under different concentrations of laponite versus cultivation days, a) 0.1% (r^2=0.621, P<0.001), b) 0.2% (r^2=0.643, P<0.001), c) 0.3% (r^2=0.191, P<0.001), d) 0.4% (not significant), and e) 0.5% (not significant) laponite (by dry weight) in the growth medium, and f) BG-11 (r^2=0.536, P<0.001) only. The dots show the mean cell density and the error bars represent standard deviations.

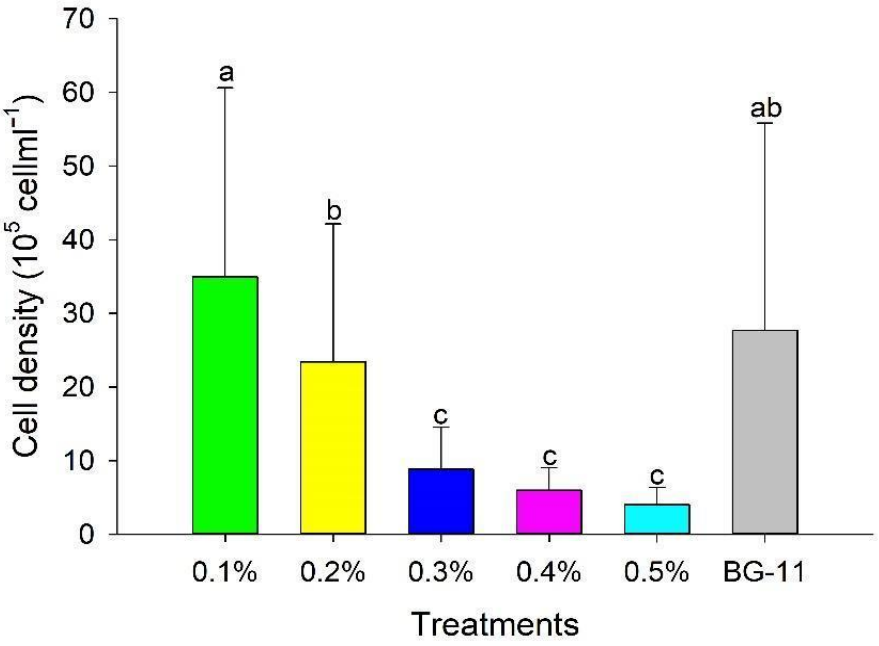

Figure 3-3: Effect of laponite treatment at different concentrations on the cell density of *Chlorella* sp. The bars show the mean cell density and errors refer to standard deviation. The statistic was derived from a one-way ANOVA with a posthoc Tukey test. The letters above the bars signified the differences between treatments at $P<0.05$.

3.3.1.2 Specific Growth Rate

There was a variable trend in the Specific Growth Rate (SGR) of microalgae with the culture period increased (Figure 3-4). It could be seen that the SGR of *Chlorella* sp. was negative in all the experimental and control groups until the 3rd day. On the third day, the minimum SGR reached -3.28 d^{-1} at 0.1% laponite concentration, which gradually reduced as the concentration increased and reached -1.94 d^{-1} at 0.5% laponite concentration. The SGR of BG-11 was -1.51 d^{-1} on the 3rd day. In this case, the presence of laponite could negatively stimulate microalgae growth as illustrated in **Figure 3-4**. The SGR on the 6th day was positive for most of the treatments. The SGR of 0.1% and 0.2% treatment was 125% and 66% higher, respectively than that of the control group. Hence, the presence of laponite could positively stimulate microalgae growth from this particular day. The possible explanation might be that the addition of laponite to the growth medium placed the microalgae in an unfavorable state at the earlier stages. However, over time, microalgae overcame the initial shock and adjusted/adapted to the new environment created by the inclusion

of laponite. Song et al. [13] observed a similar behavior of the SGR of *Phaeodactylum tricornutum* MASCC-0025 in the presence of microplastics. The highest SGR were 7.89, 6.19, 2.57, 1.98, and 1.24 d^{-1} for the laponite concentrations of 0.1%, 0.2%, 0.3%, 0.4%, and 0.5%, respectively. In the case of BG-11, the SGR on the 9^{th} day was 3.06 d^{-1} and kept increasing as the culture period increased. Based on the one-way ANOVA results, there was a significant difference in the SGR among the treatments on the 9^{th} day ($F=7.56$, $P<0.001$). The mean SGR was highest in 0.1% of treatment compared to the control group. On the twelfth day, the SGR of 0.1% laponite concentration and control groups showed a significant positive growth rate. However, the other treatments have a negative growth rate. Among all treatments, the SGR of 0.1% treatment was highest (7.57 d^{-1}) on the 12^{th} day. The SGR of 0.1% laponite concentration gradually decreased and reached negative values (-2.52 d^{-1}) on the 18^{th} day. Contradictorily, the control group reached the highest SGR (11.17 d^{-1}) on the 18^{th} day. The associated with cultivation, the SGR would gradually decrease after reaching the peak of the cultivation. This might be explained by the fact that the nutrient was consumed gradually during the culture period [13]. It should be noted that all the experimental groups reached the peak SGR on the 9^{th} day and then dropped down, while the control group reached the peak on the 18^{th} day (ten days after the experimental groups).

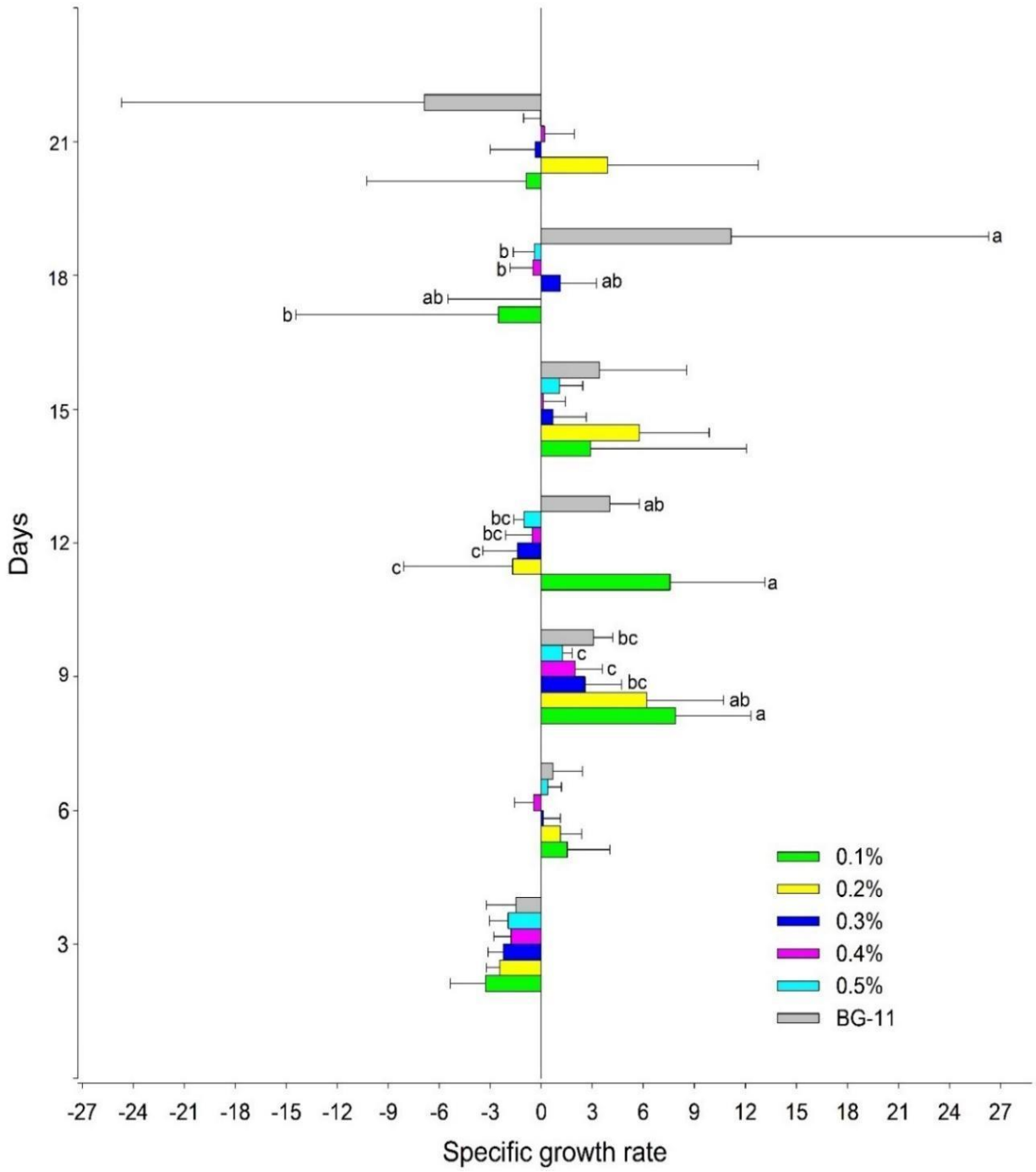

Figure 3-4: The specific growth rate of *Chlorella* sp. under different laponite concentrations with culture period. The bars show the mean specific growth rate and errors refer to standard deviation. The statistic was derived from a one-way ANOVA with a posthoc Tuk Tukey test. The letters above the bars signified the differences between treatments at $P<0.05$.

3.3.1.3 Growth Inhibition Ratio

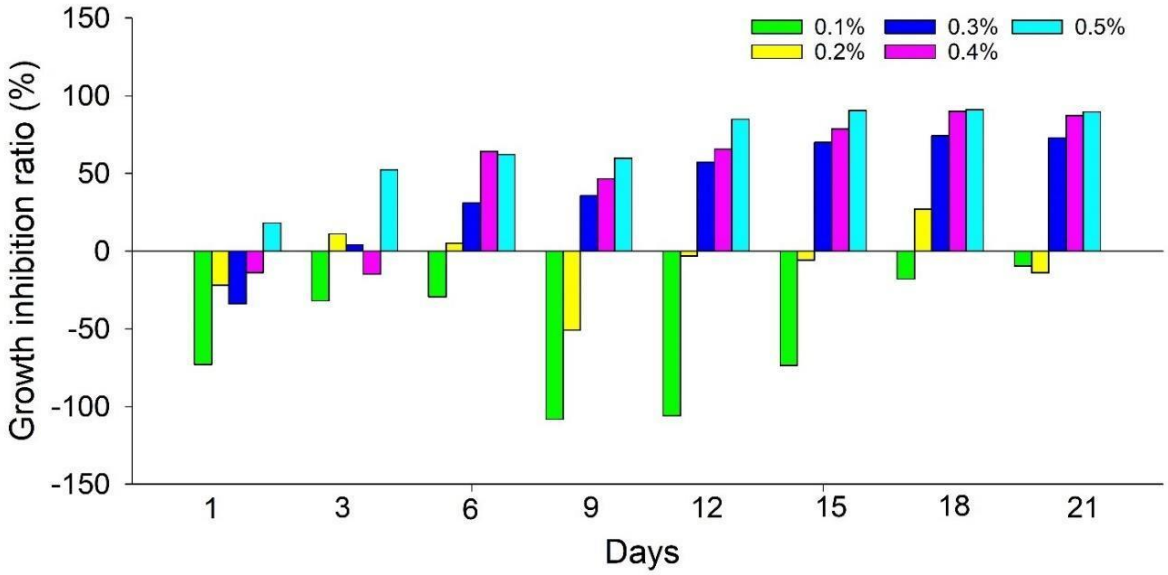

Figure 3-5: The Growth Inhibition Ratio (IR) of *Chlorella* sp. under different concentrations of laponite versus cultivation days

Figure *3-5* shows the Inhibition Ratio (IR) of *Chlorella* sp. at all laponite concentrations of the culture period. A treatment of 0.1% laponite concentration showed negative IR throughout the culture period (1-21 days) signified that the promoting effect (negative value) of microalgae reached the maximum (108%) on the 9th day and then gradually decreased. A similar promoting effect was observed by Song et al. (2020a) on *Chlorella* sp. in the presence of three types of microplastics. By contrast, the higher concentrated laponite groups presented an obvious inhibition effect. Throughout the culture period, 0.5% treatment showed an inhibition effect and reached the highest IR (91%) on the 18th day. The inhibition effect of microplastic on marine microalgae was increased with the increase of culture time [13]. For all the treatments, except 0.5% laponite, the promoting effect activated on the 1st day, and then the inhibition effects gradually increased with the increase of the culture period and reached the highest values on the 18th day. The peak IR of 0.2%, 0.3%, and 0.4% laponite concentrations was 27%, 74%, and 90%, respectively. Song et al. (2020b) found that florfenicol had an inhibitory effect on two types of microalgae (*Chlorella* sp. *UTEX1602* and *L38*) and the inhibition effect became more obvious as the concentration increased. A higher concentration of ethinylestradiol could inhibit microalgae growth due to its negative

impacts on the photosynthetic activity of microalgae cells [46]. This could be because the pharmaceutical compound with microalgal cells interfered with the energy transfer between mitochondria and chloroplast, preventing microalgae growth [47].

3.3.2 Chlorophyll Variation

In order to further investigate the effect of laponite on microalgae growth, the total chlorophyll content of microalgae treated with laponite at different concentrations during the cultivation days was determined, as illustrated in Figure 3-6. The total chlorophyll content gradually increases from day 1 to day 21 in all the treatment concentrations including the control group. In the case of 0.1% treatment, the chlorophyll content was higher than the control group throughout the culture period. The total chlorophyll content at 0.1% laponite (r^2 =0.650, P<0.001) was around 4 $mg.L^{-1}$ at 21 days, while the control group has the chlorophyll content (r^2 =0.625, P<0.001) around 2.4 $mg.L^{-1}$ at 21 days. In other words, the chlorophyll content increased by 33% after adding 0.1% laponite in the growth medium than that of the control group. There was a significant difference in the total chlorophyll content of each experimental group and control group (r^2=3.62, P=0.004). The highest average chlorophyll content (2.02 $mg.L^{-1}$) appeared at 0.1% laponite treatment followed by the control group (1.61 $mg.L^{-1}$) after the 21 days culture period in comparison to that of other treatments. In addition, there were no significant differences among 0.2%, 0.3%, 0.4%, and 0.5% laponite treatment groups as shown in Figure 3-7. The chlorophyll content increased when 0.1% laponite concentration was added in the growth medium and decreased when the higher concentrated laponite was added. Interestingly, the total chlorophyll content exhibits a steady increase at all treatment and control groups.

Similar observations for the effect of nanoparticles on different microalgae have been stated in the literature [14,36]. Rana et al. [14] stated that after treating the medium with 20 $mg.L^{-1}$ iron-oxide nanoparticles, the chlorophyll content was 17.54 $\mu g.mL^{-1}$ which is significantly higher than that of the control medium (12.82 $\mu g.mL^{-1}$). Similarly, He et al. [36] observed about 17% higher growth of *Scenedesmus Obliquus* at 20 $mg.L^{-1}$ dose of iron-oxide nanoparticles in comparison to that of the respective control group. Contrastingly, Saxena and Harish [30] found radically different findings, while their microalgae were treated with ZnO nanoparticles. It is reported that the total chlorophyll content dropped at 11.32 and 5.11 $\mu g.mL^{-1}$ after ZnO nanoparticles treatment of 0.1 and 0.5 $mg.L^{-1}$ concentrations, respectively, while the total chlorophyll content of the control was

13.34 µg.mL^{-1} [30]. The study concluded that significant reductions in the chlorophyll content were found after the exposure of ZnO nanoparticles at the higher concentrations (0.5 mg.L^{-1}) and no significant changes were recorded at the lowest concentration (0.1 mg.L^{-1}).

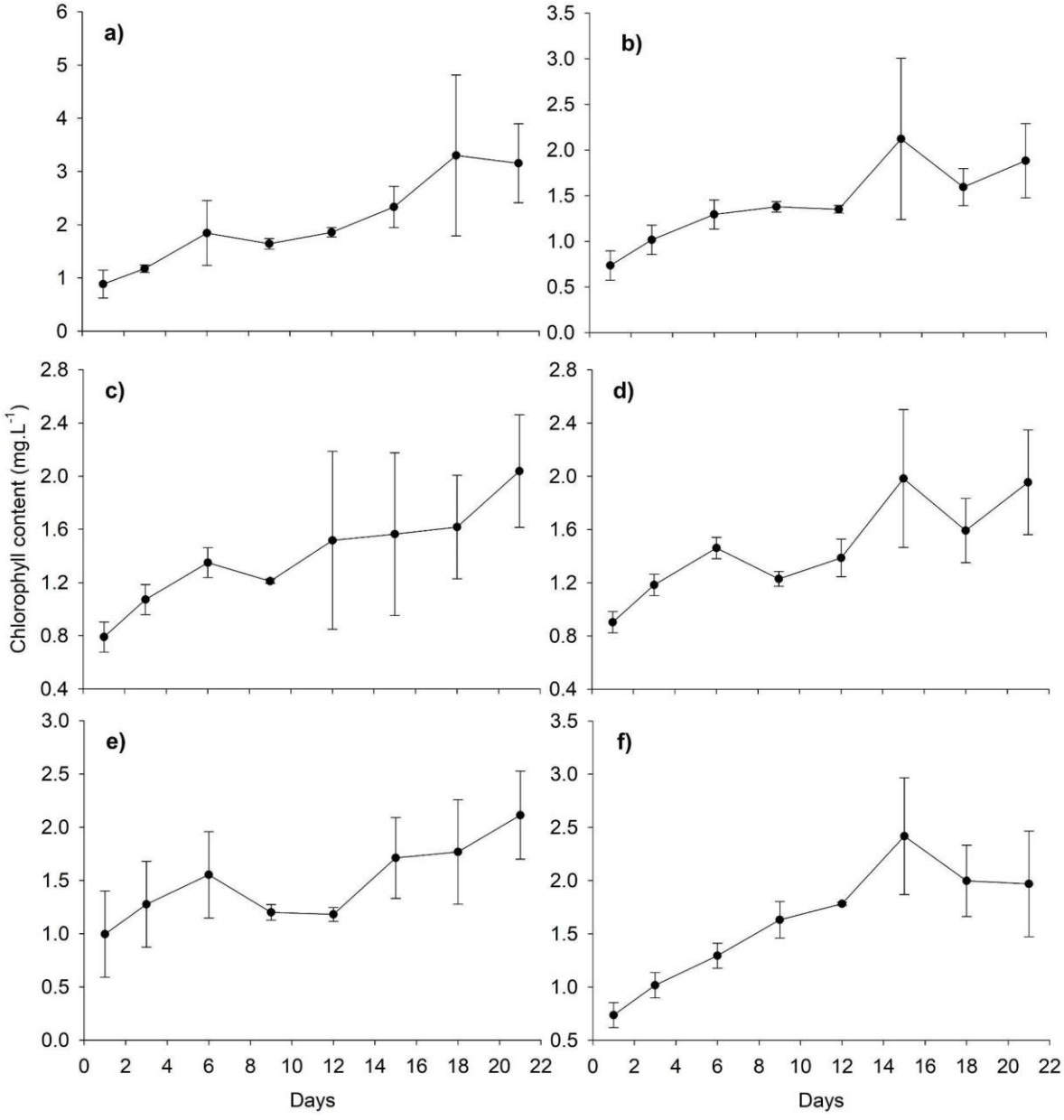

Figure 3-6: Chlorophyll content of *Chlorella* sp. under different concentrations of laponite versus cultivation days, a) 0.1% (r^2=0.650, P<0.001), b) 0.2% (r^2=0.489, P<0.001), c) 0.3% (r^2=0.497, P<0.001), d) 0.4% (r^2=0.541, P=0.05), and e) 0.5% (r^2=0.407, P<0.001) laponite (by dry weight)

in the growth medium and f) BG-11 (r^2=0.625, P<0.001) only. The dots show mean chlorophyll content and error bars represent the standard deviation.

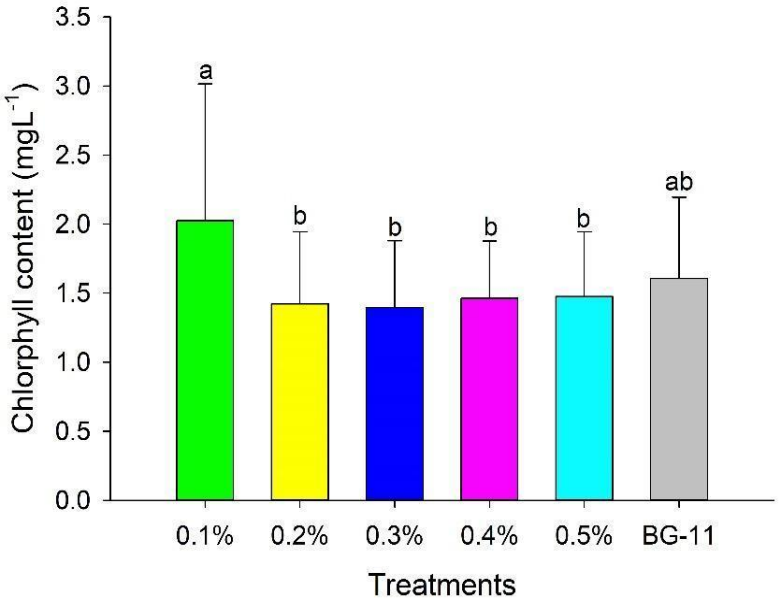

Figure 3-7: Effect of laponite concentrations on the chlorophyll content of *Chlorella* sp. The bars show the mean chlorophyll content and errors refer to standard deviation. The statistic derived from a one-way ANOVA with post-hoc Tukey test. The letters above the bars signified the differences between treatments at P<0.05.

3.3.3 Structural Characterization of Laponite and Algal Cells

In order to further investigate the interactions of *Chlorella* sp. with laponite at different concentrations, the morphological properties were studied by SEM imaging. As shown in **Figure *3-8***a, a single cell of *Chlorella* sp. has a regular globular shape with a smooth surface. Similar structural properties of *Chlorella* sp. were observed by Song et al. [13]. After laponite treatment, the surface of *Chlorella* sp. cell became irregular. This might be due to the coating of laponite gel on the microalgae surface, which further signified that laponite gel did not noticeably destroy or damage the cells of microalgae (**Figure *3-8***b). Laponite disperses into water easily and forms a transparent gel within 72 hours due to its good rheological properties [1,2]. In addition, the cell wall of *Chlorella* sp. generally consists of three layers, making the external and internal structures

difficult to destroy [13]. The accumulation of algae cells can be observed as shown in **Figure *3-8***(c-f). These microalgae cells typically seek to cluster together to maintain a stable condition.

The interaction between laponite and *Chlorella* sp. cells is shown in Figure 3-9, which revealed that microalgae may absorb laponite on the cell's surface, wrapping them up in the surface caveolae despite the existence of microalgae cell walls. Wang et al. [48] also found similar interaction between microplastic and diatoms. The present observations indicate a higher aggregation of microalgae at 0.1% laponite concentration (Figure 3-9a-c). As laponite concentration increased, *Chlorella* sp. was embedded in laponite gel and caused the physical impairment, exerting a negative influence on the growth of microalgae. This could be due to the increase of laponite concentration which eventually reduces the photosynthesis of microalgae. A higher concentration of nanoparticles can block microalgae cells to absorb nutrients and light [14,49]. Rana et al. [14] and He et al. [36] also reported iron-oxide nanoparticles aggregation on microalgae surfaces and subsequently declined growth of *Chlorella* sp. as the concentration of iron-oxide nanoparticles increased. However, iron-oxide nanoparticles supplementation showed encouraging results in terms of growth for *C. pyrenoidosa* [14]. Navarro et al. [50] reported another possible reason to lessen the cell growth, which is the shading effect of iron-oxide nanoparticles aggregation during microalgae cultivation. In the current study, *Chlorella* sp. aggregation was significantly noticeable at the lower concentrations of laponite (Figure 3-9).

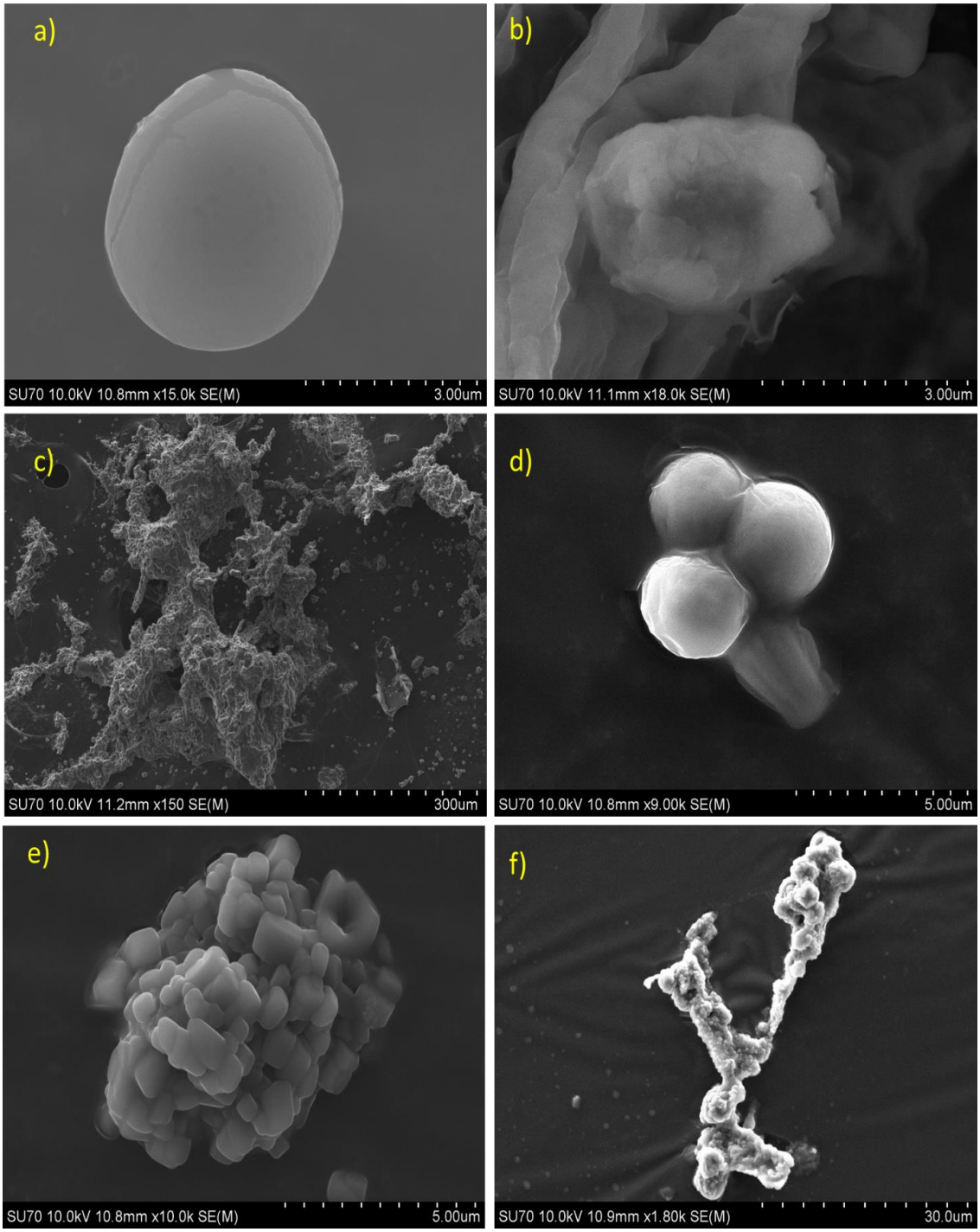

Figure 3-8: SEM images a) a single cell of *Chlorella* sp. in the control medium (BG-11), b) a single cell of *Chlorella* sp. at 0.1% treatment, c) microalgae accumulation, and d-f) different patterns of *Chlorella* sp. accumulation in the control medium.

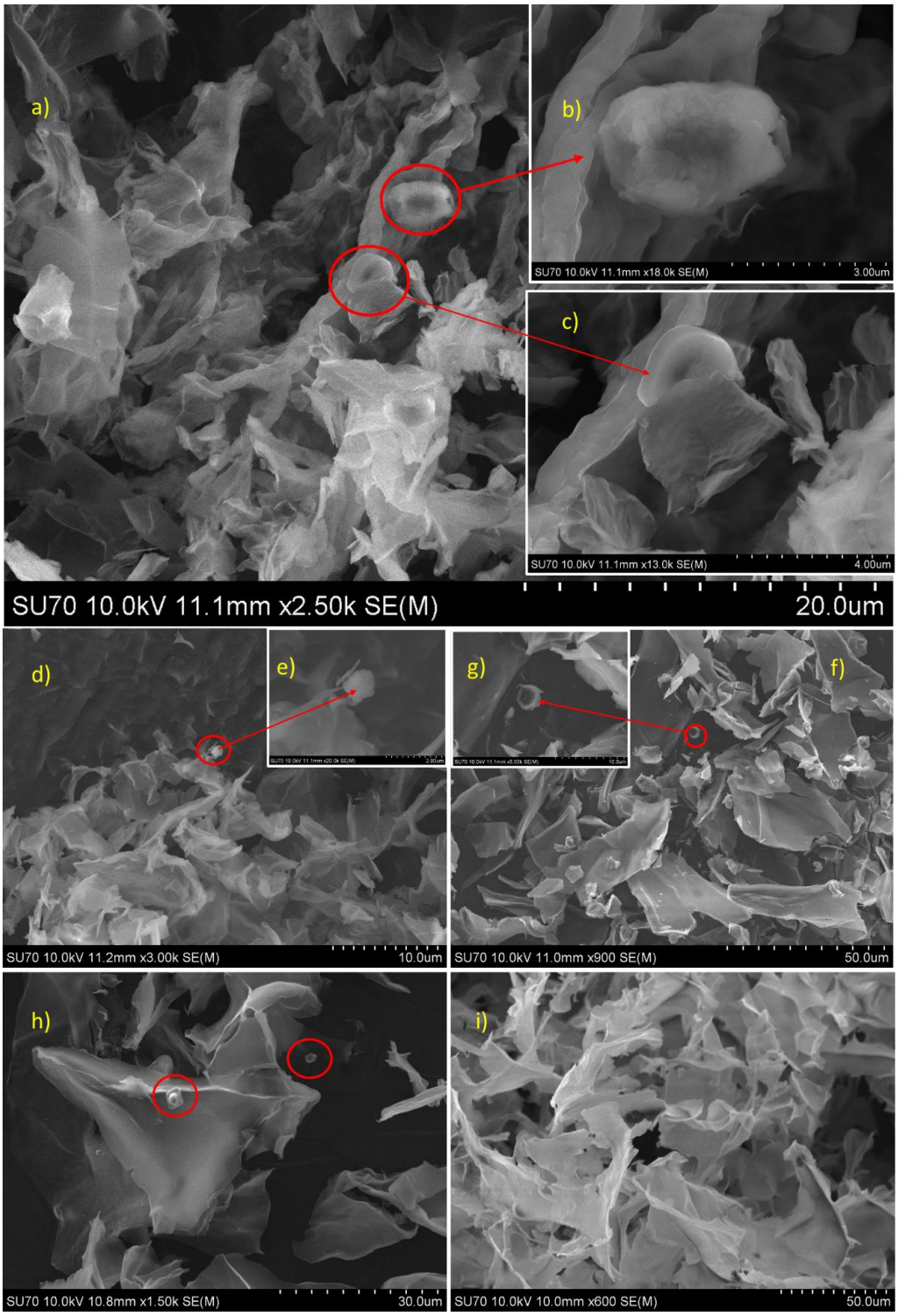

Figure 3-9: SEM images a-c) the cells of *Chlorella* sp. are sitting on laponite gel (0.1% treatment), d-g) the cells of *Chlorella* sp. are surrounded by laponite gel (0.2% treatment), h) the cells of

Chlorella sp. are covered by laponite gel (0.4% treatment), and i) laponite gel formation (0.5% treatment).

3.4 Conclusions

The current study reveals the effects of laponite on the growth characteristics and total chlorophyll content of *Chlorella* sp. A treatment of 0.1% laponite has positive impacts on microalgae growth in the growth medium. With the increase in laponite concertation (0.4% and 0.5%), the inhibitory effect was amplified. According to the specific growth rate, all the experimental groups reached the peak values 10 days earlier than that of the control group. The total chlorophyll content at 0.1% treatment group was higher (4 $mg.L^{-1}$ at 21 days) compared to the control group (2.4 $mg.L^{-1}$), indicating a 33% increase in total chlorophyll content. SEM images showed that microalgae can absorb laponite on the surface of cells, enveloping them in the surface caveolae. Low concentrated laponite was possibly integrated within microalgae. However, when the laponite concentration increased, the aggregation capability of microalgae gets reduced due to physical impairment and inhibitory effects. It is found that microalgae were lodged in laponite gel as laponite concentration increased. The effects of laponite on microalgae aggregation are directly proportional to laponite concentrations used in the growth medium. Hence, laponite is safe for the aquatic ecosystem at low concentrations. More research is needed to develop a better understanding of the nature of microalgae growth in relation to media and exposure period in presence of laponite.

3.5 References

[1] Huang, Y., & Wang, L. (2016). Laboratory investigation of liquefaction mitigation in silty sand using nanoparticles. *Eng. Geol. 204*, 23–32.

[2] Ochao-Cornejo, F., Bobet, A., Johnston, C., Santagata, M., & Sinfield, J. (2016). Cyclic behavior and pore pressure generation in sands with laponite, a super-plastic nanoparticle. *Soil Dyn. Earthq. Eng. 88*, 265–279.

[3] Cao, W. (2004). Nanostructures and nanomaterials-synthesis, properties and applications. Imperial College Press, London.

[4] El Mohtar, C., Bobet, A., Santagata, M., Drnevich, V., & Johnston, C. (2013). Liquefaction mitigation using bentonite suspensions. *ASCE J. Geotech. Geoenviron. Engng. 139*, 1369–1380.

[5] Gallagher, P. (2000). Passive site remediation for mitigation of liquefaction risk (Ph.D. Dissertation). Virginia Polytechnic Institute and State University, Virginia.

[6] Persoff, P., Apps, J., Moridis, G., & Whang, J. (1999). Effect of dilution and contaminants on sand grouted with colloidal silica. *J. Geotechn. Geoenviron. Eng. 125*, 461–469.
[7] Rugg, D., Yoon, J., Hwang, H., & El Mohtar CS, C. (2011). Undrained shearing properties of sand permeated with a bentonite suspension for static liquefaction mitigation. Geofrontiers 2011 *Adv. Geotech. Eng. Geotechnical Special Publication 211*, 677686 (CD-ROM).
[8] Yonekura, R., & Kaga, M. (1992). Current chemical grout engineering in Japan, *Proc., Grouting. Soil Improvement and Geosynthetics*, ASCE, New York.
[9] Agapoulaki, G., & Papadimitriou, A. (2018). Rheological Properties of Colloidal Silica Grout for Passive Stabilization Against Liquefaction. *J. Mater. Civ. Eng. 30*, 04018251.
[10] Ochoa-Cornejo, F. (2017). Dynamic Behavior of Sand with NanoParticles, in: Proceedings of the 19th International Conference. Presented at the *Soil Mech and Geotech Eng*, Seoul.
[11] Ochoa-Cornejo, F. (2015). Cyclic behaviour of sands with superplastic fines (a dissertation submitted for the degree of Doctor of Philosophy). Purdue University, West Lafayette, Indiana.
[12] Dhawan, V., Dhoat, S., Williams, A., Dimarco, A., Pal, S., Forbes, A., Tobías, A., Martinez-Martin, P., & Chaudhuri, K. (2006). The range and nature of sleep dysfunction in untreated Parkinson's disease (PD). A comparative controlled clinical study using the Parkinson's disease sleep scale and selective polysomnography. *J Neurol. Sci. 25*, 158–62.
[13] Song, C., Liu, Z., Wang, C., Li, S., & Kitamura, Y. (2020). Different interaction performance between microplastics and microalgae: the bio-elimination potential of *Chlorella* sp. L38 and Phaeodactylum tricornutum MASCC-0025. *Sci. Total Environ. 723*, 138–146.
[14] Rana, M., Bhushan, S., Sudhakar, D., & Prajapati, S. (2020). Effect of iron oxide nanoparticles on growth and biofuel potential of *Chlorella* spp. *Algal Res. 49*, 101942.
[15] El-Sheekh, M., Abomohra, A., & Hanelt, D. (2013). Optimization of biomass and fatty acid productivity of Scenedesmus obliquus as a promising microalga for biodiesel production. *World J Microbiol Biotechnol 29*, 915–922.
[16] Nazos, T., Mavroudakis, L., & Pergantis, S. (2020). Biodegradation of phenol by Chlamydomonas reinhardtii. *Photosynth Res. 144*, 383–395.
[17] da Silva Rodrigues, D., da Cunha, C., Freitas, M., de Barros, A., Castro, P., Pereira, A., de Queiroz Silva, S., da Fonseca Santiago, A., & de Cássia Franco Afonso, R. (2020). Biodegradation of sulfamethoxazole by microalgae-bacteria consortium in wastewater treatment plant effluents. *Sci. Total Environ. 749*.

[18] Nowack, B., & Bucheli, T. (2007). Occurrence, behaviour and effects of nanoparticles in the environment. *Env. Pollut 150*, 5–22.
[19] Cattaneo, A. (2018). Nanotoxicological evaluation in marine water ecosystem: a detailed review, in: Environment Toxicity of Nanomaterials. Press-Francis & Taylor Group, pp. 61–90.
[20] Espinasse, B., Geitzer, N., Schierz, A., Therezien, M., Richardson, C., Lowry, G., Ferguson, L., & Wiesne, M. (2018). Comparative persistence of engineered nanoparticles in a complex aquatic ecosystem. *Environ. Sci. Technol. 52*, 4072–4078.
[21] Chen, P., Powell, B., Mortimer, M., & Ke, P. (2012). Adaptive interactions between zinc oxide nanoparticles and *Chlorella* sp. *Env. Sci. Technol. 16*, 12178–12185.
[22] Ma, H., Williams, P., & Diamond, S. (2013). Ecotoxicity of manufactured ZnO nanoparticles-a review. *Env. Pollut. 172*, 76–85.
[23] Klaine, S., Alvarez, P., Batley, G., Fernandes, T., Handy, R., Lyon, D., Mahendra, S., McLaughlin, M., & Lead, R. (2008). Nanomaterials in the environment: behavior, fate, bioavailability, and effects. *Env. Toxicol. Chem. 27*, 1825–1851.
[24] Hazeem, L., Bououdina, M., Rashdan, S., Brunet, L., Slomianny, C., & Boukherroub, R. (2016). Cumulative effect of zinc oxide and titanium oxide nanoparticles on growth and chlorophyll content of *Picochlorum* sp. *Env. Sci Pollut. Res 23*, 2821–2830.
[25] Lei, C., Zhang, L., Yang, K., Zhu, L., & Lin, D. (2016). Toxicity of iron-based nanoparticles to green algae: effects of particle size, crystal phase, oxidation state and environmental aging. *Env. Pollut. 218*, 505–512.
[26] Ji, J., Long, Z., & Lin, D. (2011). Toxicity of oxide nanoparticles to the green algae *Chlorella* sp. *Chem. Eng. J. 170*, 525–530.
[27] Kadar, E., Rooks, P., Lakey, C., & White, D. (2012). The effect of engineered iron nanoparticles on growth and metabolic status of marine microalgae cultures. *Sci. Total. Env. 439*, 8–17.
[28] Seo, J., Lee, K., Praveenkumar, R., Kim, B., Lee, S., Oh, Y., & Park, S. (2015). Tri-functionality of Fe3O4-embedded carbon microparticles in microalgae harvesting. *Chem. Eng. J. 280*, 206–214.
[29] Yoo, C., Jun, S., Lee, J., Ahn, C. & Oh, H. (2010). Selection of microalgae for lipid production under high levels carbon dioxide. *Bioresour. Technol. 101*, S71–S74.

[30] Saxena, P., & Harish (2019). Toxicity assessment of ZnO nanoparticles to freshwater microalgae *Coelastrella terrestris*. *Env. Sci. Pollut. Res. 26*, 26991–27001.
[31] Bhuvaneshwari, M., Iswarya, V., Vishnu, S., Chandrasekaran, N., & Mukherjee, A. (2018). Dietary transfer of zinc oxide particles from algae (*Scenedesmus obliquus*) to daphnia (*Ceriodaphnia dubia*). *Env. Res. 164*, 395–404.
[32] Franklin, N., Rogers, N., Apte, S., Batley, G., Gadd, G., & Casey, P. (2007). Comparative toxicity of nanoparticulate ZnO, bulk ZnO, and ZnCl2 to a freshwater microalga (*Pseudokirchneriella subcapitata*): the importance of particle solubility. *Env. Sci Technol. 41*, 8484–8490.
[33] Li, J., Schiavo, S., Rametta, G., Miglietta, M., La Ferrara, V., Wu, C., & Manzo, S. (2017). Comparative toxicity of nano ZnO and bulk ZnO towards marine algae T*etraselmis suecica* and *Phaeodactylum tricornutum*. *Env. Sci Pollut. Res.* 24, 6543–6553.
[34] Miao, A., Zhang, X., Luo, Z., Chen, C., Chin, W., Santschi, P., & Quigg, A. (2010). Zinc oxide-engineered nanoparticles: dissolution and toxicity to marine phytoplankton. *Env. Toxicol Chem. 29*, 2814–2822.
[35] Demir, V., Ates, M., Arslan, Z., Camas, M., Celik, F., Bogatu, C., & Can, S. (2015). Influence of Alpha and Gamma-Iron Oxide Nanoparticles on Marine Microalgae Species. *Bull. Env. Contam. Toxic. 95*, 752–757.
[36] He, M., Yan, Y., Pei, F., Wu, M., Gebreluel, T., Zou, S., & Wang, C. (2017). Improvement on lipid production by *Senedesmus obliquus* triggered by low dose exposure to nanoparticles. *Sci. Rep. 7*, 15526.
[37] Cardinale, B., Bier, R., & Kwan, C. (2012). Effects of TiO2 nanoparticles on the growth and metabolism of three species of freshwater algae. *J. Nanopart. Res. 14*, 913.
[38] Sibi, G., Kumar, A., Gopal, T., Harinath, K., Banupriya, S., & Chiatra, S. (2017). Metal nanoparticle triggered growth and lipid production in *Chlorella vulgaris*. *Int. J. Sci. Res. Env. Sci Toxicol 1–8*.
[39] Bellinger, E., & Sigee, D. (2015). Freshwater algae: identification, enumeration and use as bioindicators. Akademiai Kiado, John Wiley & Sons Ltd., West Sussex, UK.
[40] BYK (2014). Technical Information B-RI 21: Laponite performance. BYK Additive and Instruments, USA.

[41] Kroon, M., Vos, G., & Wegdem, G. (1998). Structure and formation of a gel of colloidal disks. *Phys. Rev. E 57*, 1962–1970.
[42] El-Howayek, A. (2011). Characterization, rheology and microstructure of laponite suspensions (MSc thesis). Purdue University, West Lafayette, USA.
[43] Song, C., Wei, Y., Sun, J., Song, Y., Li, S., & Kitamura, Y. (2020). Biodegradation and metabolic fate of thiamphenicol via *Chlorella* sp. UTEX1602 and L38. *Bioresour. Technol. 296*, 122320.
[44] Xu, X., Wang, S., Gao, F., Li, J., Zheng, L., Sun, C., He, C., Wang, Z., & Qu, L. (2019). Marine microplastic-associated bacterial community succession in response to geography, exposure time, and plastic type in China's coastal seawaters. *Mar. Pollut. Bull. 145*, 278–286.
[45] Zhao, T., Tan, L., Huang, W., & Wang, J. (2019). The interactions between micro polyvinyl chloride (mPVC) and marine dinoflagellate *Karenia mikimotoi*: the inhibition of growth, chlorophyll and photosynthetic efficiency. *Env. Pollut 247*, 883–889.
[46] Cheng, J., Ye, Q., Li, K., Liu, J., & Zhou, J. (2017). Removing ethinylestradiol from wastewater by microalgae mutant *Chlorella* PY-ZU1 with CO2 fixation. *Bioresour. Technol. 249*, 284–289.
[47] Vannini, C., Domingo, G., Marsoni, M., Mattia, F., Labra, M., Castiglioni, S., & Bracale, M. (2011). Effects of a complex mixture of therapeutic drugs on unicellular algae *Pseudokirchneriella subcapitata*. *Aquat. Toxicol. 101*, 459–465.
[48] Wang, S., Wang, Y., Liang, Y., Cao, W., Sun, C., Ju, P., & Zheng, L. (2020). The interaction between microplastic polyvinyl chloride and marine diatoms: physiological, morphological, and growth effects. *Ecotoxicol. Environ. Saf. 203*, 111000.
[49] Aruja, V., Pokhrel, S., Sihtmae, M., M. Mortimer, M., Madler, L., & Kahru, A. (2015). Toxicity of 12 metal-based nanoparticles to algae, bacteria and protozoa. *Env. Sci. Nano. 2*, 630–644.
[50] Navarro, E., Baun, A., Behra, R., Hatmann, N., Filser, J., Miao, A., Quigg, A., Santschi, P., & Sigg, L. (2008). Environmental behaviour and ecotoxicity of engineered nanoparticles to algae, plants and fungi. *Ecotoxicology 17*, 372–386.

CHAPTER 4 Improving the Strength Properties of Sand Using Laponite, a Promising Nanoparticle

Abstract

Soil treatment to mitigate liquefaction risks can be considered as an alternative possibility to reduce structural damages during earthquakes. While the traditional site stabilization techniques have some limitations, nanoparticles can be used to lessen negative issues. In this paper, laponite has been studied to evaluate its properties with sand in fully saturated conditions to reduce the development of pore water pressure. This paper also investigated the effect of laponite concentration and resting time in a series of triaxial tests. The results show that even a little amount of laponite can significantly decrease the pore water pressure generation due to the good rheological property of transparent gel. It can be stated that the modulus of elasticity of sand-laponite specimens is almost double than that of pure sand. In addition, changes in friction angle and cohesion with different laponite concentrations are also examined using direct shear box tests considering three different temperatures. Microstructural imaging with Scanning Electron Microscope (SEM) is assessed in conjunction with the pore pressure generation mechanism. Finally, this study provides an elaborate explanation of the non-homogeneity of the sand-laponite mixture. The study provides novel insight into the improvement and modification of sand strength properties elaborately in the presence of laponite under static loading.

Keywords: Pore pressure, Modulus of Elasticity, Viscosity, Laponite

**A version of this chapter has been published in International Journal of Civil Engineering 21:679-693(2023).*

4.1 Introduction

Earthquakes cannot be accurately predicted and are impossible to prevent. However, understanding the behavior of soil-structure interaction under such events allows engineers to design earthquake-resistant structures. A collapse of pile foundation, which is a specific type of deep foundation for heavily loaded structures such as high-rise buildings, bridges, ports, and flyovers, in liquefiable soil is commonly observed after earthquakes despite the fact of including the factor of safety in design [1-6]. Several studies, e.g., [7-12], proved that slender pile requires lateral support from the surrounding soil to avoid instability. During an earthquake, fully or partially saturated sand loses its effective confining stress and becomes liquefiable. This liquefiable sand cannot provide enough support to pile foundations. Hence, the pile may buckle sideways in the direction of the least elastic bending stiffness and eventually fail under the increased bending moment and shear force. In the literature, scale-down one- and two-dimensional laboratory experiments have been conducted to evaluate the soil-pile interaction in liquefaction [7,8,13]. The utmost challenging fact is to understand the dynamic properties of soil, which are fundamental for application in more advanced geotechnical models, as well as the possible phenomena that stimulate these properties are more complex. An accurate prediction of soil behavior and resulting structural displacements is only possible with sophisticated laboratory tests with high-quality specimens or with carefully performed in-situ tests. The most critical part of a design assessment is estimating the solid representative values for the required soil properties, which is extremely difficult due to the strong dependence on many parameters. Hardin and Drnevich [14] stated that the dynamic properties of soil might alter by a factor of 10 in a soil deposit. Apart from the modification of the current design code for pile foundations, the treatment of soil in order to resist the liquefaction effects can be considered as an alternative possibility to eliminate and reduce structural damages during and after earthquakes. Soil improvement by densification is one of the most common techniques to mitigate the liquefaction risk and limit potential deformations of soil. Primarily, there are two types of densification techniques available and widely applicable, namely active and passive site stabilization techniques. The former is only applicable in undeveloped sites, whereas the latter can be implemented in both developed and undeveloped sites. Traditional materials such as cement and chemical grouts are used in the soil strength improvement. The use of the traditional techniques has limitations of full-field treatment,

cause intensive disturbance, create environmental pollution, and are costly to use. Therefore, it is necessary to explore other materials that can reduce these adverse issues.

The development of nanotechnology has triggered the proposed use of nanoparticles to treat soils to improve the strength properties and minimize the susceptibility to liquefaction [15-25]. Nanoparticles are ultrafine particles with at least one dimension below 100 nm and a special structure with a large volume-specific surface area ranging from > 20 m^2/m^3 to > 60 m^2/m^3 [26]. As the pore water pressure has a remarkable impact on soil strength triggering the liquefaction, nanoparticles can enhance soil strength by reinforcing the soil skeleton and amending pore fluid. It has been shown in research that due to good rheological properties of transparent gel along with small-size scale, nanoparticles such as carbon nanoparticles, colloidal silica, bentonite, and laponite can improve the liquefaction resistance of soil [17,20,24-27,29-36]. The effectiveness of colloidal silica for the liquefaction resistance of soils was verified using a centrifugal model and full-scale field tests [27-29]. Laboratory tests and fieldwork have shown that the colloidal silica can mobilize in aquifers, which supports the evidence of colloidal silica mobility in the liquefiable soil layers [17]. El Mohtar et al. [30] proved that bentonite suspension forms a thixotropic gel and improves the liquefaction resistance by reducing excess pore fluid between the sand grains. In specimens prepared with sand and bentonite (only 3% of dry mass of sand), the number of cycles required to trigger liquefaction of sand increased by over an order of magnitude, which can also be boosted with continuous curing of specimens [30]. The effectiveness of bentonite suspension in mitigating the liquefaction risk at the field scale has been verified using the finite difference method [19]. Another nanoparticle is laponite, which is smaller than bentonite and can form a transparent gel-like solid. Ochoa-Cornejo et al. [23] and Huang et al. [24,37] showed that laponite gel has outstanding abilities to mitigate the liquefaction risks under cyclic loadings. Only limited published research [38] provides in-detailed information on the microstructural characteristics of laponite and the rheological properties of laponite suspension. There is no comprehensive literature that explains how laponite alters or enhances the characteristics of sand under static loading conditions. Laponite, a nanoparticle material with a promising property for geotechnical applications, was chosen for this study to evaluate the improvement of sand properties since it is environmentally safe, and less expensive in terms of price/performance ratio than existing admixtures. Also, laponite is easier to utilize than other available nanoparticles. **Table *4-1*** represents the comparisons among the performance of the existing admixtures and nanoparticles

in the case of the site stabilization technique. However, using laponite in geotechnical engineering is a completely new concept.

Table 4-1: Compare the performance of the existing admixtures and nanoparticles for the site stabilization technique

Type of Materials			Environment pollution	Disturbance	Price/performance ratio	Difficulties to use
Traditional grouts	Cement		High[a]	Intense[c]	Less[e]	-only applicable in undeveloped sites
	Chemical solutions	Sodium Silicate	High[b]	Less[c]	Medium[e]	
		Epoxy	High[b]	Less[c]	High[e]	
Nanoparticles	Colloidal Silica		Low[c]	Less[c]	Less(c)	-coverage will not be uniformed[f] -controlling gel time is challenging[g]
	Bentonite		Low[c]	Less[c]	Less-Medium[c]	-permeation of bentonite suspensions might not be possible in sands with fines[h]
	Laponite		Low[d]	Less[c]	Medium[c]	-no known issue

[a] van Oss and Padovani 2003; Shafigh et al. 2014
[b] Vik et al. 2000
[c] Huang and Wang, 2016
[d] BYK, 2014
[e] Gallagher, 2000
[f] Gallagher et al. 2007
[g] Greenwood and Otterstedt, 2005
[h] El Mohtar et al. 2008, 2013

The current study is aimed to investigate the efficacy of laponite in improving the strength properties of sand, particularly in terms of reducing the excess pore water generation under static loading. Therefore, the results of the experimental analysis of sand-laponite specimens at different concentrations were demonstrated. The modifications of pore water pressure generation in the fully

saturated soil layers with respect to various concentrations of laponite mixing with sand and different resting time were evaluated in a controlled laboratory environment. Similar tests using pure sand were carried out as a control for comparison. The study also presents the effects of temperature on laponite in a series of shear box tests. The shear box was selected since it is the most commonly used apparatus for determining friction angle of sand. Finally, the Scanning Electron Microscope images were used to describe the likely reasons for non-homogenous mixture of sand-laponite. In this study, the experimental materials are detailed in Section 4.2, followed by a comprehensive presentation of the experimental methodologies and procedures in Section 4.3. In Section 4.4, the experiment findings were compared and discussed. The paper concludes with a summary and final remarks in Section 4.5.

4.2 Experimental Materials

4.2.1 Sand

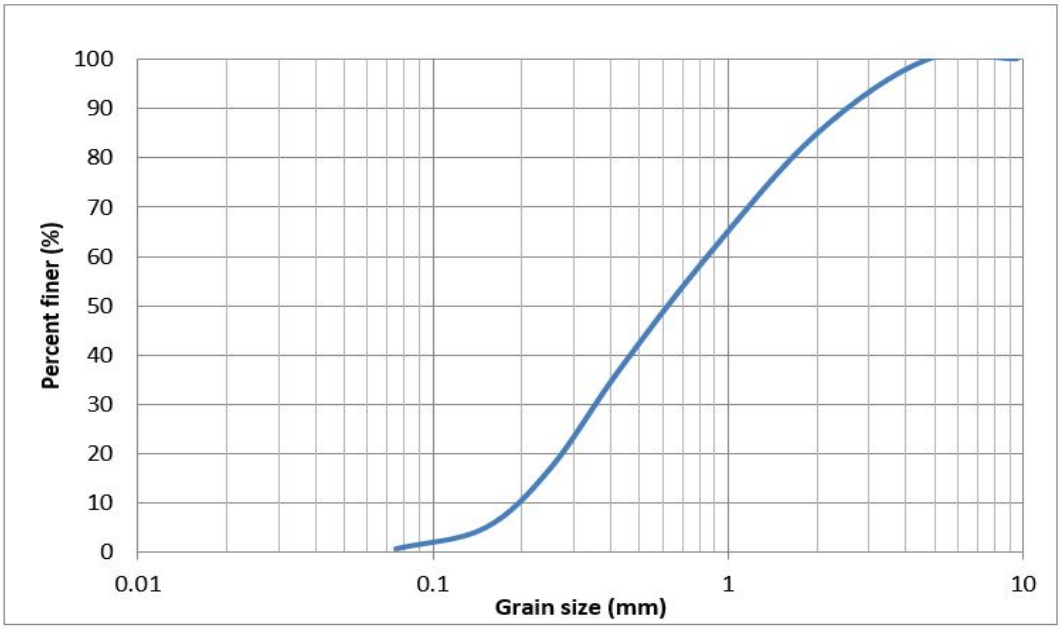

Figure 4-1: Grain size distribution of sand

This study uses sand from the Pioneer Construction, Thunder Bay, ON, Canada, in all the experiments. The grain size distribution analysis of the sand, shown in **Figure *4-1***, was carried out according to the ASTM D6913 [39]. The analysis showed that the uniformity coefficient (C_u) and the coefficients of curvature (C_c) of the sand were 4.40 and 0.74, respectively. The median diameter (d_{50}) of the sand is 0.62 mm, and the fine is less than 5%. According to the Unified Soil Classification System, the group symbol of the sand is *SP*, and the group name is poorly graded

sand. The natural water content, by the ASTM D2216-19 [40], and relative density of the sand, obtained in accordance with the ASTM C128-15 [41], were 1.60% and 2.60, respectively.

4.2.2 Laponite

4.2.2.1 **Chemical Composition**

Laponite is a synthetic hectorite clay nanoparticle that is commonly used as a rheology modifier in various industries, including cosmetics, inks, paint, surface coatings, and glazes [42]. Laponite structure is made from a synthetic sheet of silicate nanoparticles with layered structures of two tetrahedral layers and one octahedral layer [43]. Laponite has a neutral charge with six divalent magnesium ions in the octahedral layer, giving a positive charge of twelve. However, the monovalent lithium ions may substitute some magnesium ions, and some positions are empty to provide a chemical composition formula as: $Na^{+0.7}[(Si_8Mg_{5.5}Li_{0.3})O_{20}(OH)_4]^{-0.7}$. This formula has a negative charge of 0.70 per unit cell, which becomes neutralized during manufacture as sodium ions are adsorbed onto the surfaces of the crystals. The crystals become arranged into stacks, which are held together electro-statically by sharing the sodium ions in the interlayer region between adjacent crystals. The disk-like laponite particle has a diameter of approximately 25 nm, a thickness of 1 nm, and a specific gravity of 2.57 [44]. Laponite looks like a fine white power in dry form. When dispersed in water, laponite hydrates, swells, and forms a colorless transparent monodisperse suspension which looks like a highly thixotropic gel. **Figure *4-2*** shows laponite in the dry state, gel state, and sand-laponite mixture. When the ionic strength is high, the electric double layer on the surface of particles is compressed, electrostatic interaction distance decreases, and the distance between particles is shortened, forming a physically cross-linked gel [45].

(a) (b) (c)

Figure 4-2: (a) Laponite particle in dry state, (b) Laponite dispersion in gel state, and (c) Sand-laponite

4.2.2.2 **Viscosity of Laponite**

Table 4-2: Viscosity variations of 0.5% and 1.5% laponite solutions

Solution	Resting period	Spindle speed, RPM	Viscosity, mPa.s	Torque, %
0.5% laponite	3 months	100	193.8-194.4	63-64
1.5% laponite	3 weeks	100	447.5-448.7	37.3-37.4

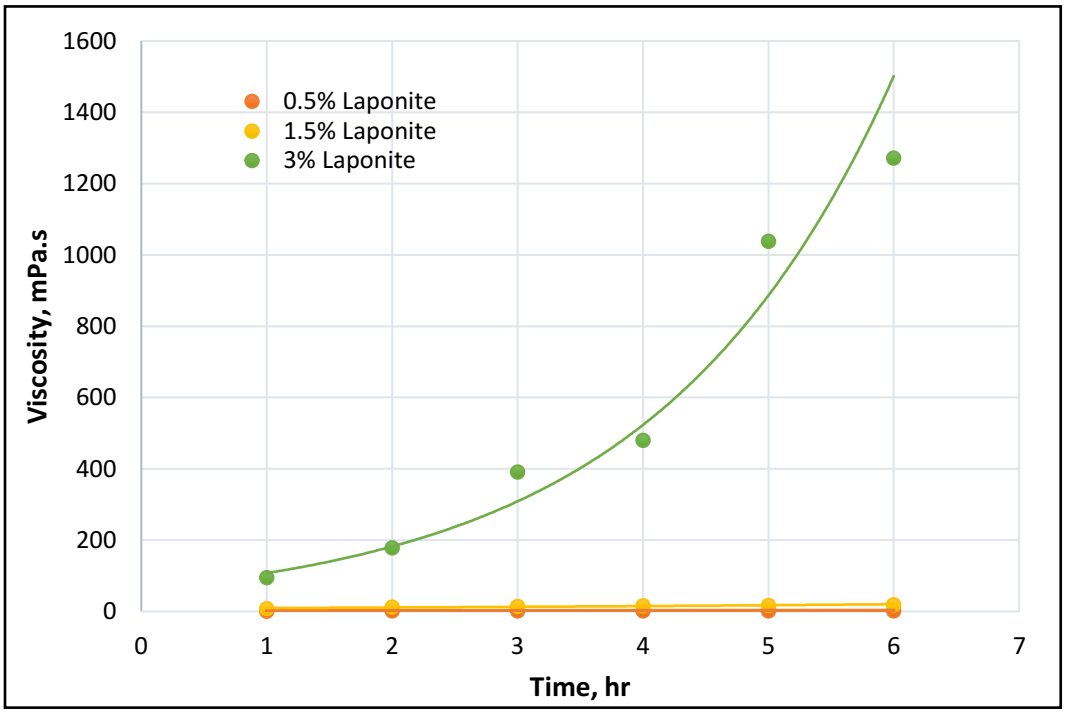

Figure 4-3: Change of viscosity with gelling time for 0.5%, 1.5%, and 3% laponite suspension at room temperature (viscosity was measured at spindle speed 100)

When laponite is added to deaired distilled water and stirred for 30 seconds continuously, it forms a transparent low-viscous uniform suspension. The viscosity of laponite suspension depends on the amount of laponite added to water. In this particular section, the viscosity of various concentrated laponite solutions is studied by the Brookfield Viscometer *DV-II+Pro* of the Green

Process Research Center at Lakehead University, Thunder Bay, Ontario, Canada. The spindle speed has been selected as 100 rpm in all the viscosity tests. Trials with spindles ranging in size from LV1 to LV4 was used to determine the correct viscosity until stable data was obtained. The measured viscosity of 0.5% laponite solution (2.1 mPa.s) was minimal after the first 6 hours when compared to that of 1.5% laponite solution (19.2 mPa.s) at room temperature (23^{o}C). For further analysis, both solutions have been kept in the laboratory environment without any disturbance. After three months of the resting period, 0.5% laponite solution showed a viscosity of 194.4 mPa.s viscosity, which was noticeably high compared to the measured viscosity at the earlier hours (Table 4-2). On the other hand, 1.5% laponite solution has a viscosity of about 448.7 mPa.s after three weeks of resting time. As the resting time increases, the viscosity of both laponite solutions increases significantly. When laponite solution transfers into a gel-like solid, it rapidly gains elastic properties that improve the strength of solutions [23]. **Figure *4-3*** shows the change of viscosity with gelling time for 3% laponite suspension. It is clearly seen that within the first hour, the viscosity of 3% laponite solution reaches around 100 mPa.s, which gradually rises to around 1275 mPa.s after 6 hours. After 24 hours, the viscosity of 3% laponite was too high, even the LV4 spindle displayed '*out-of-range*' in the viscometer. These findings contrasted sharply with the viscosity graph of Huang and Wang [24]. Huang and Wang [24] found that the apparent viscosity of 3% laponite solution was less than 20 mPa.s after the first 4 hours, which reached 100 mPa.s after about 13 hours (800 mins), and eventually close to 500 mPa.s after 48 hours. These findings demonstrated that the soil-gel transition for 3% laponite suspensions in the current study differs significantly from Huang et al. The possible reason can be the types of laponite used in these two studies. Huang and Wang [24] did not provide any information about the laponite manufacturing company used in their research. According to the technical information published by the BYK Additives and instruments (BYK, 2014), multiple grades of laponites are available with a variety of features. In the current study, Laponite-RD (rheology additive) was used, which has high efficiency in water-based systems.

4.3 Experimental Methods

4.3.1 Specimen Preparation

Laponite was stored in an airtight container in a dry chamber at room temperature to avoid moisture absorption. Pure sand and sand-laponite specimens were prepared by dry pluviation. Dry sand and laponite were mixed manually in an airtight container for 20 minutes. After that, deaired distilled

water was added to sand-laponite mixture to achieve a full saturation condition. To investigate the effects of laponite concentration on the pore water pressure generation, different laponite concentrations (0.5%, 1%, 1.5%, and 2% dry mass of laponite by dry mass of sand) were prepared. The sand-laponite mixture was compacted in a triaxial mold. Porous stones and filter papers were placed on both the top and bottom of the specimen mold, and finally, a latex membrane was used to enclose the whole system. The cylindrical specimens were 53 mm in diameter and 68 mm in height. The same procedure was applied to prepare the pure (untreated) sand specimens. For the direct shear box tests, the sand-laponite samples with 1%, 2%, and 5% laponite (by dry mass of sand) were prepared using the same procedure. These samples were tested at room temperature, as well as at elevated and cold temperatures.

4.3.2 Test Procedures

4.3.2.1 **Consolidated Undrained Tests**

A series of triaxial tests were done on the pure sand (i.e., control test) and sand-laponite mixture specimens with different laponite contents using the ELE International Tri-flex 2 and associated data acquisition system. All specimens for the triaxial tests were back-pressure saturated, then isotopically consolidated to desired effective confining stress of 30 kPa representing shallow in-situ condition. The consolidation process occurred in less than 10 seconds, as validated by Ochoa-Cornejo et al. [33], in the tests with the pure sand and sand-laponite mixtures. Both the pure sand and sand-laponite specimens were kept in a sealed container for a minimum of 72 hours before the tests were conducted. Within this resting/curing time, the rheological properties of laponite should be generated [23,24]. Consolidated-Undrained (CU) conditions were chosen during the triaxial shear tests at the end of resting time.

4.3.2.2 **Direct Shear Box**

Direct shear box tests were conducted on the pure sand and sand-laponite specimens using the ELE Direct Shear Apparatus EL28-007 series and associated data acquisition system. All the specimens of the direct shear box tests were fully saturated and rested for 72 hours. The chosen shear box is (60 mm x 60 mm) in size and the surrounding space was filled with water throughout the testing period. Unconsolidated-Undrained (UU) conditions were utilized during the direct shear box tests.

Temperature is a vital constraint that should be considered in the investigation of the behavior of sand-laponite specimens. The temperature, along with ionic strength and *pH* can significantly affect the thickness of double layers in electrostatically stabilized systems and can transfer the equilibrium between the ionized groups and medium. Bensen [46] proved that the thermal energy of particles increases as temperature increases in a bimolecular reaction. Apart from these, change in temperature significantly stimulates hydraulic characteristics, i.e., permeability, water retention, and saturation time. The mechanical response such as consolidation ratio, plasticity, swelling time/pressure, thermal dilation and contraction, yielding, and compressibility, is also influenced by the temperature change. Hence, the temperature may have various contradictory effects, which may, in turn, be reversible, such as stiffening/softening, swelling/retraction, and decrease of elastic domain/over-consolidation. In addition, the temperature has a great influence on the stress-strain behavior of any polymer such as laponite. Brittle failure is detected as a break at a low strain rate at a very low temperature which is fairly below the *glass transition temperature*. If the temperature increases, the behavior of polymer changes its mechanical behavior from brittle to ductile, which is known as the *brittle-ductile transition temperature* [47]. The polymer behavior mostly depends on cross-linkage and entanglement density. Lightly cross-linked polymer undertakes bulky elastic deformation before rupture, while uncross-linked polymer shows viscoelastic behavior [46]. Temperature varies from season to season and zone to zone throughout the year. In the arid and semi-arid zones, such as the United Arab Emirates, the temperature may reach more than 48^{o}C in the summer [48], while the temperature in regions with cold winters, such as Canada, may drop below -40^{o}C [49]. Even the same country, such as Canada, has a wide range of temperature fluctuations during the summer and winter seasons. Zhang et al. [50] found a definite trend of temperature across Canada for the period 1950-1998, showing warming in the south-west, and cooling in the north-east; these trends were most evident in the winter and spring. In general, temperature varies more dramatically in the soil zones above 5-6 m, which is highly dependent on the air temperature. In the cold regions, the optimal soil temperature is not below 5^{o}C beneath the 5-6 m depth into the soil (not considering the permafrost region). While in the arid and semiarid zones, the optimal soil temperature can be achieved at a maximum of 30^{o}C at 6 m depth with negligible temperature variations throughout the year [48]. Therefore, to analyze the behavior of laponite bonding with sand at various temperatures, two representative temperatures have been selected apart from the room temperature (23^{o}C): (a) elevated temperature (30^{o}C) and (b) cold

temperature (5°C). To conduct this set of experiments, the direct shear box and specimens were shifted and stored in a temperature-controlled room. The temperature has been continuously monitored to keep it at the exact temperature throughout the experiments, storage, and resting time.

4.3.3 Test Program

The testing program includes nineteen tests in pure sand and sand-laponite specimens. Table 4-3 summarizes the testing materials, laponite content, saturation conditions, and duration of resting time of each test. All the experiments were conducted at room temperature in the laboratory environments.

Table ***4-4*** represents the summary of the direct shear box tests including the information on materials, saturation conditions, and resting period. All these experiments were conducted at room temperature (23°C), elevated temperature (30°C), and cold temperature (5°C).

Table 4-3: Summary of the triaxial tests including information on materials, saturation conditions, and duration of resting time

Test No	Materials	Saturation condition	Resting period	Remarks
Test- 1A	Pure sand	Yes	72 hours	-
Test- 1B	Pure sand	Yes	72 hours	-
Test- 1C	Pure sand	Yes	24 hours	PPT did not work properly
Test- 1D	Pure sand	Yes	1 hour	DT did not work properly
Test- 1E	Pure sand	Yes	168 hours	-
Test- 2A	Sand+1% laponite	Yes	72 hours	-
Test- 2B	Sand+1% laponite	Yes	72 hours	-
Test- 2C	Sand+1% laponite	Yes	72 hours	-
Test- 3A	Sand+1.5% laponite	Yes	72 hours	-
Test- 3B	Sand+1.5% laponite	Yes	72 hours	-
Test- 3C	Sand+1.5% laponite	Yes	72 hours	Deaired tank vent was opened
Test- 3D	Sand+1.5% laponite	Yes	72 hours	-
Test- 4A	Sand+0.5% laponite	Yes	72 hours	-

Test- 4B	Sand+0.5% laponite	Yes	72 hours	-
Test- 4C	Sand+0.5% laponite	Yes	72 hours	-
Test- 5A	Sand+0.5% laponite	Yes	168 hours	-
Test- 5B	Sand+0.5% laponite	Yes	168 hours	-
Test- 6A	Sand+1.5% laponite	Yes	168 hours	-
Test- 6B	Sand+1.5% laponite	Yes	168 hours	-
Test- 7A	Sand+2% laponite	Yes	72 hours	-
Test- 7B	Sand+2% laponite	Yes	72 hours	-
Test- 7C	Sand+2% laponite	Yes	168 hours	-

*PPT=Pore Pressure Transducer, *DT=Displacement Transducer

Table 4-4: Summary of the direct shear box tests including information on materials, saturation conditions, and duration of resting time

Test No	Materials	Sample's weight, g	Saturation condition	Resting period
Test- 1	Pure sand	140.8	Yes	1 hour
Test- 2	Pure sand	120.6	Yes	72 hours
Test- 3	Sand+2% laponite	122.6	Yes	72 hours
Test- 4	Sand+2% laponite	120.6	Yes	72 hours
Test- 5	Sand+1% laponite	122.5	Yes	72 hours
Test- 6	Sand+1% laponite	120	Yes	72 hours
Test- 7	Sand+5% laponite	120.1	Yes	72 hours
Test- 8	Sand+5% laponite	123	Yes	72 hours
Test- 9	Sand+5% laponite	122	Yes	72 hours

4.4 Results and Discussions

4.4.1 Pore Water Pressure Generation

The main factor for liquefaction is the excess pore water pressure generated in sand during dynamic loading [51-53]. Fully saturated loose sand can produce a substantial magnitude of excess pore water pressure on a change in load and subsequently is the most prone to liquefy. When

shearing, loose soil compresses, a considerable amount of excess pore water pressure is developed, as the load is transmitted from the soil skeleton to neighboring pores during undrained loading. As the pore water pressure rises excessively, the effective stress decreases, causing a steady loss of soil strength. Liquefaction is to be expected to occur in sandy or non-plastic silty soils, but it can also happen in clayey soils such as quick clay [54,55]. Ochoa-Cornejo et al. [23] and Huang and Wang [24] found that the generation of excess pore water pressure is reduced in sand treated with laponite. The current work seeks to understand the behaviour of pore water pressure generation under static loading condition. This study enhances the understanding of sand-laponite interaction in detail as the development of excess pore water pressure can vigorously distort any civil engineering infrastructure. To study the effect of laponite on the pore water pressure generation of sand-laponite specimens, static triaxial tests on pure sand and sand treated with laponite at different concentrations (0.5%, 1%, 1.5%, and 2% by dry mass of sand) were conducted at room temperature. The aforementioned concentrations of laponite are at the low end compared to similar experiments by researchers [20,31]. These concentrations are smaller than the threshold values that are thought to impact the liquefaction resistance, as reported by Youd et al. [56]. The curve with the fine contents of less than 5% is referred to as the *clean sand base curve* [56]. In the current study, all of these specimens (both pure and treated sand specimens) are allowed to rest for 72 hours, before beginning the tests. Ochoa-Cornejo et al. [23] mentioned that the rheological properties of laponite pore fluid expected to develop in the pore space were identical to those of bentonite based on rheological test results at 72 hours. Huang and Wang [24] recommended a minimum of 48 hours resting time for sand-laponite specimens based on their rheological test results.

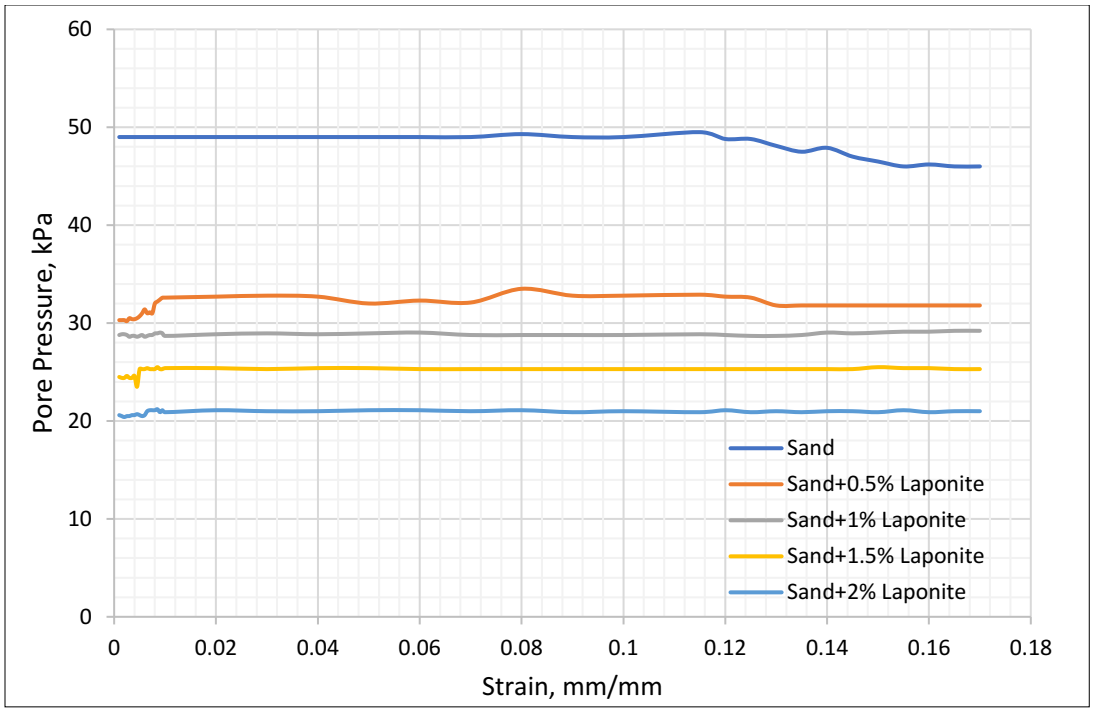

Figure 4-4: Generation of pore water pressure in pure sand and sand specimens treated with laponite at different concentrations after 72 hours of resting time.

It is seen from **Figure *4-4*** that the development of excess pore water pressure reduces noticeably after treating sand with laponite. As the concentration of laponite increases, the generation of pore water pressure decreases. This indicates that the resistance of excess pore water pressure generation improves, and the gelation process of laponite becomes stronger as laponite content increases. This is also true under the cyclic loading as examined in Ochoa-Cornejo et al. [23] and Huang and Wang [24]. **Figure *4-4*** shows that by adding only 0.5% of laponite to sand, the pore water pressure generation is reduced by about 17 kPa, representing a decrease of 37% compared with the control (i.e., sand). The decrease in pore water pressure generation among specimens with consecutively higher laponite content (e.g., 0.5%, 1%, 1.5%, and 2%) was around 17, 22.5, 25, and 27 kPa, respectively. The possible explanation can be the liquid solidification procedure by laponite around the surface of sand and between grain pores. While adding water into the dry mixture of sand-laponite specimens to represent a fully saturated condition, laponite powder undergoes a liquid-state to a soft gel-state due to hydration process. This soft gel becomes gel-like solid with time as the viscosity of laponite suspension increases with time. The pore water is gradually converted into a gel-like solid, which has shear resistance capability and significantly

improves sand strength. The cementation of sand grains becomes stronger with the presence of laponite gel with time and mitigates the liquefaction risk. Improvement of sand reinforcement can be expressed in terms of load magnitude the sand specimens can withstand. The pure sand specimens can withstand a load up to 1223 N, while sand specimens treated with only 0.5% laponite can withstand around 3140 N. Hence, the presence of a small amount of laponite in sand specimens enhances the grain reinforcement more than 2.6 times to that of pure sand specimens. The treated sand specimens with 1% and 1.5% of laponite can withstand approximately 29385 N and 38090 N load, respectively, before appearing cracks in the samples. These results ultimately prove that the presence of laponite improves the internal strength of the sand skeleton and eventually resists the excess pore water pressure generation under static loading. In other words, laponite gel enhances the shear strength of sand grains, and eventually, the whole sand-water-air system acts as a gel-like solid, which can eliminate the excess pore water pressure generation during loading. Due to laponite thixotropy, pore water pressure may still be observed; however, it appears far slower compared to that in pure sand [24]. The results clearly indicate that a small amount of laponite is required to effectively resist the pore pressure generation, which is also true under cyclic loading. Adding only 1% of laponite significantly extends the number of cycles to reach liquefaction compared to pure sand [23].

The generation of pore water pressure is considerably reduced after treating sand specimens with a small amount of laponite (0.5% of laponite/dry mass of sand). However, a little drop in the pore pressure has been observed at a strain of 0.12 mm/mm. **Figure *4-4*** also shows that at strain around 0.12 mm/mm, the pore pressure (kPa) of pure sand and sand+0.5% laponite specimen begins to decrease. It's likely that this small amount of laponite is insufficient to fill voids around and between sand grains. Huang and Wang (2016a) stated that laponite could not enter some voids based on their SEM imaging. However, there is no discernible decline in pore pressure vs. strain graphs with higher concentrations (1%, 1.5%, and 2%) of laponite-sand specimens. The resting time after preparing sand-laponite specimens has a great influence on the pore water pressure generation features. **Table *4-2*** shows the effect of curing time on the pore water pressure of sand-laponite mixtures. For this analysis, 1.5% laponite-sand specimens were prepared and conducted experiments at the triaxial machine after 72 and 168 hours of resting times. The pore water pressure generation reduces as the resting time increases for sand-laponite specimens, as expected. The generated pore water pressure is 18-20 kPa after three days (≈72 hours) of resting time which is

around 24 kPa after seven days (≈168 hours) of resting time for 1.5% laponite-sand specimens. A similar type of trend has been observed by Huang and Wang [24]; however, laponite used in their study is not the same as in the current study. As time increases, the viscosity of laponite suspension increases, which resists the excess pore water pressure generation under static loading. In this study, a section is discussed earlier on the change of viscosity of laponite with time for better understanding.

4.4.2 Stress-Strain and Modulus of Elasticity

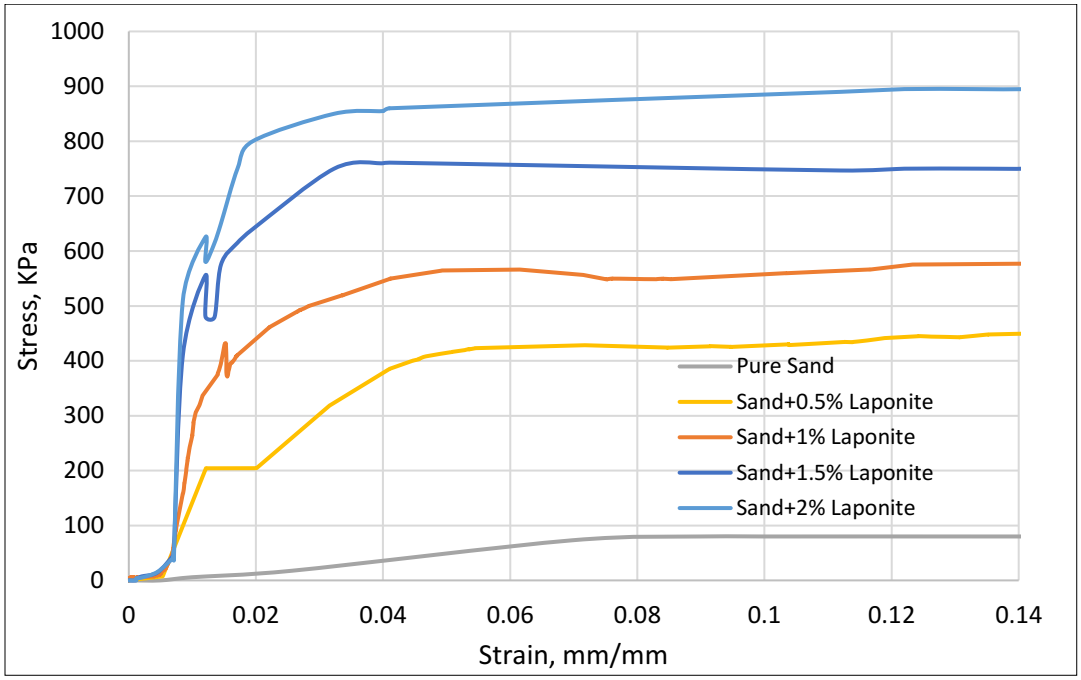

Figure 4-5: Comparisons of stress-strain graphs of pure sand and sand-laponite mixtures at room temperature.

The modulus of elasticity (E) measures the resistance of a particular material to being deformed when stress is applied. Alternatively stated, E indicates the level of stiffness or flexibility of a material. To describe the resistance of pore water pressure generation under gradually increased loading conditions, the stiffness of sand-laponite specimens has been studied. The static triaxial test results show that E of pure sand (i.e., the control) is 14000 kPa indicating *loose sand* [57]. After mixing laponite with sand, E becomes 25000-30000 kPa which represents the soil type as *medium clay* according to the USACE EM 1110-1-1904 report. This indicates that sand specimens with 0.5%-1.5% laponite exhibit E almost double than that measured on pure sand. **Figure *4-5***

shows the comparisons of the stress-strain graphs of pure sand and sand-laponite specimens. Zaragoza et al. [58] also found an enhancement in the elastic modulus after adding silica nanoparticles to the specimens. Ochoa-Cornejo et al. [35] found that sand specimens with only 1% of laponite generate about 10%-20% higher shear modulus than that of pure sand. The reason behind this may be explained with a hypothesis. As laponite interferes with the contacts between sand grains, the amount of laponite trapped at the contacts controls the effect on the small-strain shear modulus. When the layer of laponite is appropriately small, the modulus is increased, suggesting that laponite offers bonding/bridging at particle contacts [35].

In the case of pure sand, the stress increases gradually from the beginning of loading and then plateau at stress and strain of 80 kPa and 0.09 mm/mm. On the other hand, the stress of sand-laponite specimens was almost zero at the beginning of loading and then started to increase rapidly following the pattern of ductile material. A peak stress of 895 kPa at strain of 0.037 mm/mm was reported in sand+2% laponite followed that the test with sand+1.5% laponite (761 kPa at 0.04 mm/mm strain), sand+1% laponite (564 kPa at 0.049 mm/mm strain) and sand+0.5% laponite (428 kPa at 0.071 mm/mm strain). According to the stress-strain behaviour of polymers [59,60], laponite gel shows the behaviour of *hard and tough plastic* after having 72 hours of resting time. Laponite shows a characteristic yield point followed by a drop in strength at the lower stress. At this point, the gel starts to experience *plastic deformation*. Usually, the materials with high plasticity show strong necking and, in some cases, cold drawing. Beyond the yield point, the cross-section in the necking region will gradually reduce until it breaks abruptly. Strong elongating with a stressed minimum and breaking at higher stress is observed for some polymers. This phenomenon is known as strain-hardening and stress-induced crystallization. It is caused by the arrangement of polymer chains in the load direction, which raises the strength and stiffness of plastic in the stretch direction and explains the observed increase in stress. In some cases, the physically aged amorphous polymers show the true strain-softening, which is the opposite of strain-hardening. In this case, the deformation process progressively removes the effect of aging, which leads to a decline in stress when the specimen is dragged at a constant strain rate. Miehe et al. [59] suggested that the true strain softening is the result of localized shear band formation. In addition, laponite gel increases load-carrying capacity significantly as the stiffness of the specimens is increased after adding laponite. From the stress-strain diagram of **Figure *4-5***, the stress of pure sand reaches the equilibrium condition pretty quickly, while the sand specimens with a little amount of laponite did

not reach the equilibrium condition. For the same amount of strain (mm/mm), the required stress of sand+0.5% laponite specimen is around four times that of pure sand specimen in a controlled laboratory environment.

4.4.3 Friction Angle and Cohesion

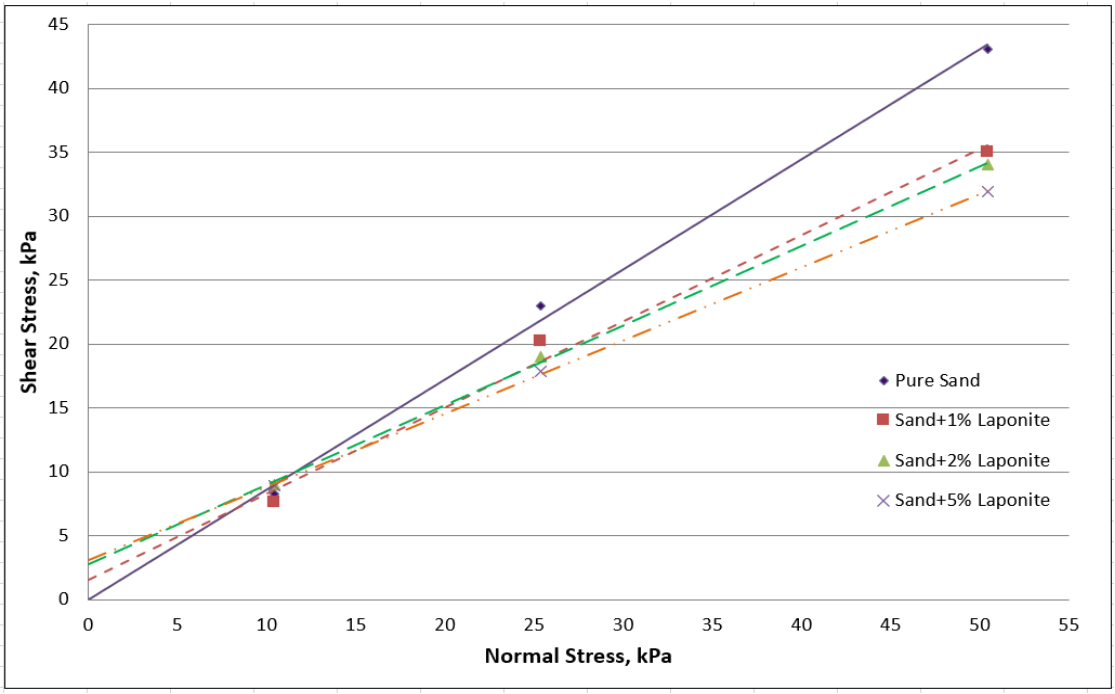

Figure 4-6: Friction angles and cohesion of pure sand and treated sand specimens at room temperature

Friction angle and cohesion are two important physical properties of soil, which help to govern the angle of rupture, shear strength, bearing capacity, and stability. To study the behavior of laponite (which is also known as nano-clay) and sand mixture, a series of experiments have been conducted using the direct shear box at room temperature, as listed in **Table *4-4***. Cohesion (C) is the attachment of elements to each other. It offers a measure of the strength of a particular material that is not directly governed by the friction law. Hence, sand does not have any cohesion property; however, soil containing fine particles shows cohesion. It can be measured by the Mohr-Coulomb Equation. The cohesion of soil alters due to the variation in the existence of cementing materials that combine soil grains inflexibly. The natural bonding of soil gains is influenced by the presence of lubricating agents, such as water. Cohesive soil does not smash and can be excavated with

vertical side slopes. Commonly, the cohesive soil is difficult to break up in dry conditions and becomes plastic in wet conditions. Moreover, it shows significant cohesion when waterlogged.

The friction angle of a specific soil is the angle on the Mohr's Circle of shear stress and normal effective stresses at which shear failure occurs. According to the Unified Soil Classification System [57], the friction angle varies from 40^{o} to 33^{o} for well-graded gravel to silt and goes below if soil contains fine particles such as clay and elastic-plastic particles. Friction angles also vary depending on the saturation conditions (dry, fully saturated, and partially saturated) of the soil. From the results of the direct shear box tests at room temperature, it can be clearly stated that the friction angle of the available sand is 40^{o}, which indicates the soil is gravel type (fine to coarse gravel). Hence it does not have any cohesion. After adding a little amount of laponite, the friction angle reduces. The evaluated friction angles are 34^{o}, 32^{o}, and 29^{o} after mixing 1%, 2%, and 5% laponite with sand under fully saturated conditions, respectively (**Figure *4-6***). Moreover, the cohesion also appears due to the presence of laponite in the sand, even in a small quantity. The cohesion of the specimens increases as the amount of laponite increases in the specimens. **Figure *4-6*** also shows that the estimated cohesions are approximately 4.1, 6.9, and 8.4 kPa for 1%, 2%, and 5% laponite-sand specimens, respectively. As the number of small particles increases, the bonding between sand grains also increases significantly. This is the exact equivalent norm which is usually seen in the existence of clay particles in soil grains.

4.4.4 Effects of Temperature on Friction Angle

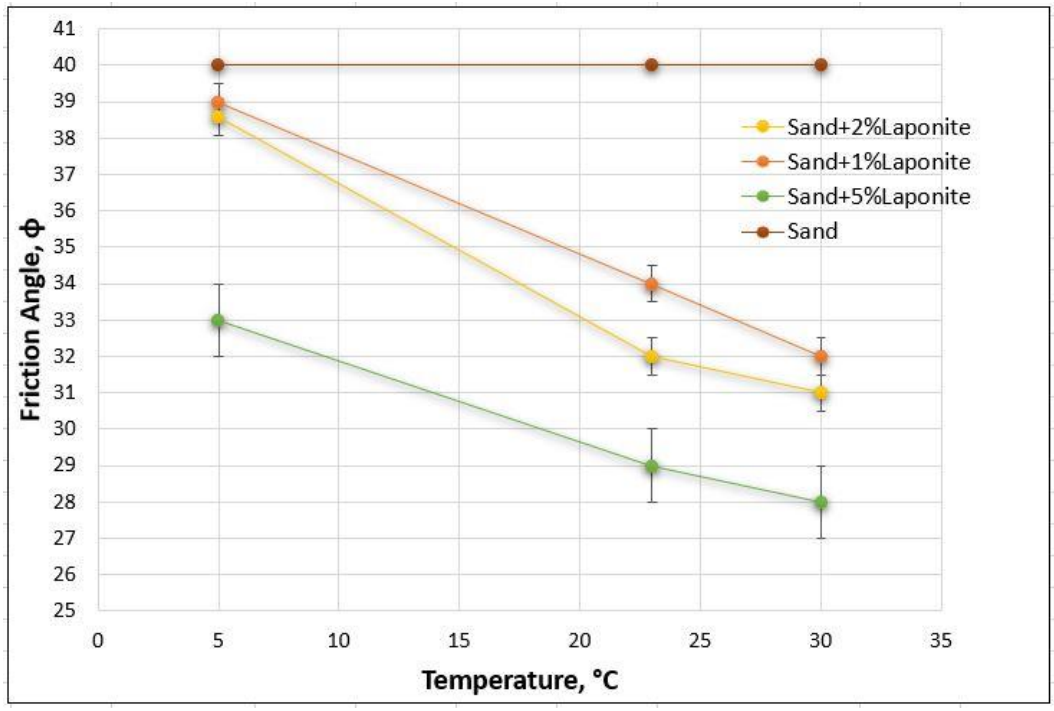

Figure 4-7: Effect of temperature on the friction angle of pure sand and sand-laponite mixtures

Figure *4-7* represents the change of friction angles of pure sand and sand-laponite specimens with different laponite concentrations (1%, 2%, and 5% by dry mass) at three different temperatures. It is clearly seen that the friction angle of pure sand is 40° at all the selected temperatures after 72 hours of resting time. That means the temperature variation has no significant effect on pure sand specimens as expected. At the cold temperature, the friction angle of sand+1% laponite and sand+2% laponite is 39° and 38.5°, respectively. Sand specimens containing a lesser amount of laponite content behave almost the same as pure sand at the cold temperature. Hence, at the cold temperature, the behavior of laponite does not significantly show up, which is due to the gelation process being noticeably delayed even after having 72 hours of resting time at a low temperature.

At the elevated temperature, the friction angle of sand+1% laponite and sand+2% laponite specimens is 32° and 31°, respectively, which are quite below the values of the friction angles at room temperature. So, it can be said that the gelation process with a very low laponite content accelerates significantly at a higher temperature. It can be stated that temperature is a strong feature influencing the characteristics of produced laponite hydrogel similar to HA-PDMS (Hyaluronate-Poly dimethylsiloxane-diglycidyl ether terminated) synthesis hydrogel [61]. A similar type of trend

has been shown by the highly concentrated (5% of dry mass of sand) laponite specimens at elevated and cold temperatures. The friction angle of sand+5% laponite at 5ºC and 30ºC is 33º and 28º, respectively. The difference between the friction angles of 1%, 2%, and 5% laponite-sand samples are 7º, 7.5º, and 5º, respectively, at elevated and cold temperatures (**Figure *4-7***). Note that the temperature effects are more prominent at lower laponite content specimens than the higher laponite content specimens.

4.4.5 Homogeneity of Sand-Laponite Mixture

The methods of mixing laponite to sand directly influence the homogeneity of sand-laponite specimens. It may be possible to prepare a highly homogeneous mixture to conduct necessary experiments in laboratory. However, having a homogeneous mixture inside the ground is impossible in the actual case scenario. The microstructure of sand-laponite mixture has been discussed in this particular section. In this study, all the specimens have been prepared by adding laponite into sand in dry condition and then shaking it manually for 20 minutes continuously in an air-tight container. After that, the deaired distilled water was added and kept in a fully saturated condition for 72 hours. The available Scanning Electron Microscope (SEM) in the Instrumentation Laboratory of Lakehead University can only take images of dry samples. As a result, after the resting time, sand-laponite specimens were dried completely in an oven at 100ºC for 24 hours in order to analyze the microstructure of sand-laponite samples using the SEM images. The dry sand-laponite samples were placed on carbon stickers as desired on top of aluminum mountain pins and then coated with gold. These samples must be completely dry for at least 48 hours before using into the SEM. The pure sand samples were prepared following the same procedure as sand-laponite specimens to compare the images between pure and treated samples. Two pure sand and two sand+1.5% laponite specimens were prepared for the SEM imaging.

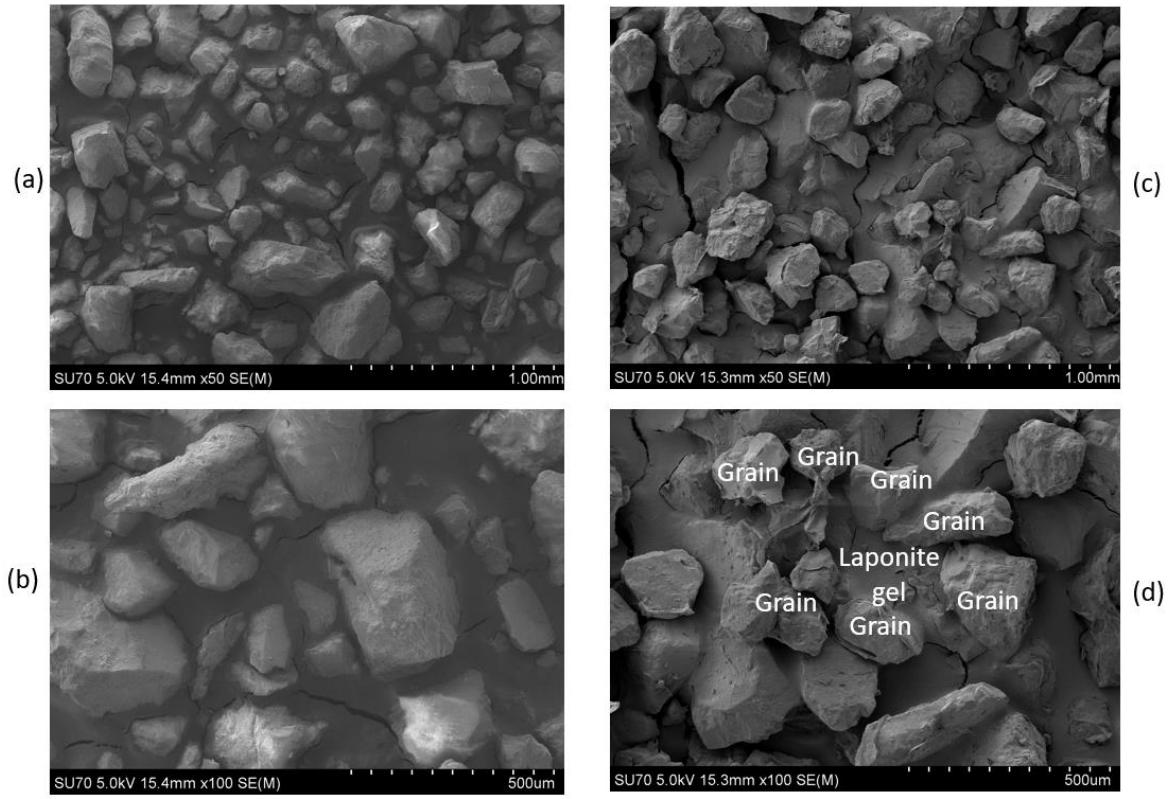

Figure 4-8: Microstructure images by SEM of (a) pure sand under 1.00 mm magnification, (b) pure sand under 500 µm magnification, (c) sand+1.5% laponite specimen under 1.00 mm magnification, and (d) sand+1.5% laponite specimen under 500 µm magnification

Figure *4-8*(a, b) show the SEM images of pure sand at 1.00 mm and 500 µm magnification factors, respectively and **Figure *4-8***(c, d) show the images of sand+1.5% laponite under 1.00 mm and 500 µm magnification factors, respectively. It is clearly seen that particles are more crowded in the presence of laponite compared to pure sand. That means laponite creates a strong bonding between sand grains. However, the actual adhesion into the fully saturated condition cannot be observed because the specimens have dried up. Besides, the SEM images of sand-laponite specimens are sharper and brighter than the images of pure sand due to the reflection of more electrons from the surface of sand-laponite specimens. As more laponite particles are accumulated into the pores of sand grains, electrons can easily bounce back from the surface of specimens rather than being absorbed by carbon. To check for the existence of laponite, distinct elements of laponite were searched at several points of the prepared samples during SEM Imaging. It is worth noting that laponite cannot be found everywhere. It can be stated that laponite cannot uniformly fill the pores

between sand grains. At some points, it fills in the spaces between sand grains, while there are no elements of laponite in other points. Hence, the mixture of sand-laponite is not uniform. There may be four possible reasons behind this non-homogeneity.

- *First:* This may occur when laponite is mixed with sand in dry condition before adding any deaired distilled water. Though the dry mixture of laponite and sand is done by continuously shaking for 20 minutes, all laponite cannot be evenly distributed into the pores of sand particles. There is a high probability that some laponite may be trapped at sand contacts. Hence, there is still free pore water inside the specimens in the fully saturated condition even after the completion of resting time, which can be attributed to the measurement of pore water pressure generation in triaxial tests. EI Mohtar et al. (2013) showed that the preparation of bentonite specimen greatly influences the microstructure of mixtures, which may also be a dominant factor in the case of sand-laponite specimens.
- *Second:* Another possible reason can be the amount of laponite used in specimens' preparation. In this specific case, the mass of laponite used in the specimens is only 1.5% of dry mass of pure sand. The added amount of laponite may be insufficient to cover the available pores of sand grains. The accessible pores in sand may be huge in number, which requires more laponite to give a complete and homogeneous coverage around and between the grains. Huang and Wang (2016a) showed a few SEM images of sand+3% laponite, and stated that there were certain voids remained where laponite could not enter. However, Huang and Wang [24] used double the amount of laponite in the specimens compared to the current study.
- *Third:* Another potential reason that may contribute to the non-homogeneity of sand-laponite mixture can be the resting time, which is related to laponite content. The viscosity analysis clearly stated that if the amount of laponite content is minimal, allowing the specimen to rest for extended periods of time eventually increases the viscosity of laponite solution. An illustration is given in the previous section on the change of viscosity with time. As the amount of laponite is only 1.5% of dry mass of soil, which may not provide a homogeneous coverage after 72 hours, the increment of the resting time may improve the homogeneity of the mixture. As the viscosity of laponite solution increases with the increment of time, the cementation by laponite gel may improve around and between the pores of sand grains to achieve the desired homogeneity.

- *Fourth:* An important potential reason can be drying sand-laponite mixture before preparing the samples for the SEM imaging. Laponite can transform into a gel in saturated conditions. However, the sand-laponite mixture must be oven dried for 24 hours as the samples must be completely dry before being used in the SEM. When the sand-laponite mixture is getting dry, the cementation of laponite with sand grains may be severely disturbed. In the dry state, most of laponite particles are segregated from the surfaces of sand grains. Even with naked eyes, it is clearly seen that the bonding of sand-laponite is fragile in dry state, and particles are isolated from one another, whereas sand-laponite bonding is quite resilient in the presence of water.

The SEM observations provide insight into the changes in the fabric and interparticle interaction that control the response of soil in the presence of laponite, a highly plastic fine. Laponite (like other clay minerals) forms a percolated network around cells occupied by water, and the pore space progressively shrinks, leaving limited space surrounding and between the grains. The image (**Figure *4-8***(d)) illustrates that fluid with a networked structure is occupying the pore space between sand particles, similar to what El Howayek [62] observed in images of laponite clay gel alone. **Figure *4-8***(d) provides proof of evidence that laponite treatment can limit particle movements during loading, which will improve the liquefaction resistance of sand, a hypothesis that was suggested by El Mohtar et al. [31].

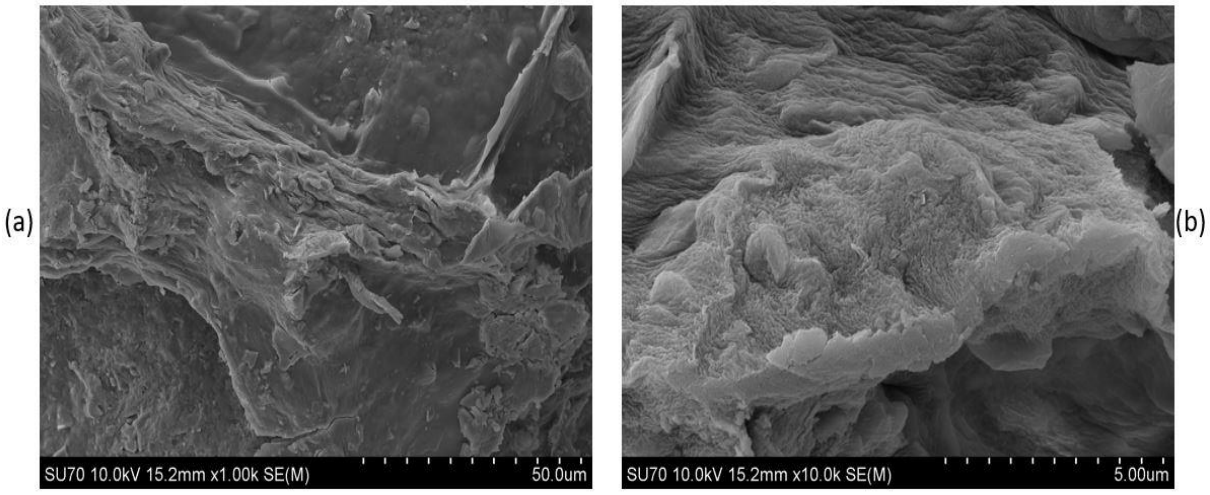

Figure 4-9: Microstructure images by SEM of (a) sand+1.5% laponite specimen under 50 µm magnification, and (b) sand+1.5% laponite specimen under 5 µm magnification

Figure *4-9* (a, b) show the images of the cementation by laponite gel on a single sand particle at 50 and 5 µm magnification factors, respectively. Some flocculent structures can be observed on the individual grain surface. These images at the higher magnification remarkably indicate that laponite suspension has a sheet-like microstructure with a consistent pattern as the untreated (pure) sand used in this study does not contain any other fine particles. This sheet-like laponite gel overwhelms the volumetric straining during loading and reduces the soil liquefaction phenomena by resisting pore water pressure generation significantly. Micrographs of El Howayek [62] revealed that the elongated laponite cells were grouped in a similar configuration.

4.5 Conclusions

There are few publications on the effects of laponite to mitigate liquefaction caused by cyclic loading. However, no published research on the improvement of sand strength properties in presence of laponite by decreasing the pore water pressure under static loading has been reported. As a result, the current study examined the efficacy of using laponite to improve the sand strength and compared the results to those of pure sand as well as data from prior sand-montmorillonite studies. The findings of this study contribute to a new understanding of how sand properties change in the presence of laponite at various concentrations.

The triaxial test results show that the pore water pressure generation mechanism is significantly reduced after treating sand specimens with laponite. Hence, nano-clay laponite can noticeably mitigate the liquefaction potential by solidification of pore fluid by cementation among sand grains, which eventually postpones the pore water pressure generation during loadings. The test results show that specimens with a very little amount (0.5% by dry mass of sand) of laponite show a reduction of around 17 kPa in pore water pressure generation than that of pure sand in the identical condition. The rheological properties of a sol-gel transition in a laponite suspension resist the pore water pressure generation. This pore water pressure generation can be evaluated by measuring the stiffness of sand-laponite specimens in the laboratory environment at room temperature. From the results of the triaxial tests, it can be clearly stated that the gelation process of laponite can improve the modulus of elasticity (E) of treated specimens, almost double than that of pure specimens. The required stress of sand-laponite specimens is approximately four times higher than pure sand for an equal amount of strain. In addition, the gel-like laponite shows the behaviour of hard and tough plastic after the resting time. As the laponite content and resting time

increase in sand-laponite specimens, the resistance of the pore water pressure generation improves accordingly. The pore water pressure generation process in the treated specimens is delayed, and the deformation is smaller compared with that of the untreated specimens. The changing of viscosity with time in various concentrations of laponite solution enlightens interesting behaviour of the gelation process of laponite content. By studying the friction angles and cohesions using the direct shear box, it can be stated that after mixing only 1% of laponite with sand, the friction angle reduces significantly, and cohesion appears due to the specimen's fluctuation in the existence of nano-clay laponite to tie the sand gains inflexibly at room temperature.

Temperature plays an important role in the behaviour of the treated specimens due to the significant influence on the thickness of the double layer in electrostatically stabilized systems as well as mechanical responses. In the case of sand-laponite specimens, the elevated temperature accelerates gelation process even with the presence of a little amount of laponite, while the cold temperature delays the gelation process remarkably. At the higher concentration (5% of dry mass of sand) of laponite in the specimens, the effects of temperature are less dominant than that of the lower concentration laponite-sand specimens. The gel-like laponite has a consistent sheet-like microstructure that adhesives individual sand grains. However, the dry-mixing of sand and laponite during the specimen preparation stage may not be capable of preparing a homogeneous mixture. In other words, laponite can partially fill up pores into the grains, not entirely. This may lead to residual cavities beyond those formed by laponite and sand grains. A possible reason may be using less amount of laponite in specimen preparation in comparison to the higher number of pores in and around the sand grains. Another probable cause may be the drying up of the mixture before preparing the samples for the SEM images. This may isolate the laponite particles from the surface of sand grains in the absence of water.

4.6 References

1. Takata T, Tada Y, Toshida I and Kuribayashi E (1965) Damage to bridges in Niigata earthquake, in. Public Works Research Institute (in Japanese).
2. Hamada M (1992) Large ground deformations and their effects on lifelines: 1964 Niigata earthquake, in. Buffalo, New York, USA. Available at: https://ci.nii.ac.jp/naid/10006542527#cit (Accessed: 10 November 2021).
3. Ishihara K (1997) Terzaghi oration: Geotechnical aspects of the 1995 Kobe earthquake, in.

Proceedings of ICSMFE, Hamburg. Available at: https://www.issmge.org/publications/publication/terzaghi-oration-geotechnical-aspects-of-the-1995-kobe-earthquake (Accessed: 10 November 2021).

4. Soga K (1997) Chapter 8: Geotechnical aspects of Kobe earthquake. EEFIT report, UK. Available at: https://www.issmge.org/uploads/publications/1/31/1997_04_0002.pdf (Accessed: 10 November 2021).
5. Berrill J, Christensent SA, Keenan RP, Okada W and Pettinga JR (2001) Case Studies of Lateral Spreading Forces on a Piled Foundation. *Geotechnique*, 51(6):01–517.
6. Madabhushi S, Patel D and Haigh S (2001) Draft version of "EEFIT report on observations of the 26th Jan 2001 Bhuj earthquake in India. Institution of Structural Engineers, UK. Available at: https://www.istructe.org/resources/report/eefit-mission-report-bhuj,-india/ (Accessed: 10 April 2022).
7. Bhattacharya S (2003) Pile instability during earthquake liquefaction. Doctoral thesis. University of Cambridge, UK.
8. Bhattacharya S and Bolton M (2004) Errors in design leading to pile failures during seismic liquefaction. *in. fifth inter conf. on Case histories in Geotech Eng*. April 13-17, New York.
9. Bhattacharya S, Bolton M and Madabhushi S (2005) A reconsideration of the safety of the piled bridge foundations in liquefiable soils. *Soils and Foundations*, 45(4):13–26.
10. Bhattacharya S, Madabhushi S and Bolton M (2004) An alternative mechanism of pile failure in liquefiable deposits during earthquakes. *Geotechnique*, 54(3):203–213.
11. Dash S, Bhattacharya S and Blakeborough A (2010) Bending-buckling interaction as a failure mechanism of piles in liquefiable soils. *Soil dynamics and Earthquake Eng*, 30:32–39.
12. Knappett, J. and Madabhushi, S. (2005) Modelling of liquefaction-induced instability in pile groups. In: Boulanger RW, Tokimatsu K, editors. Seismic performance and simulation of pile foundations in liquefied and laterally spreading ground (geotechnical special publication (GSP) no. 145). Reston, VA, USA: *American Society of Civil Engineers*, pp. 225–67.
13. Madabhushi G, Knappett J and Haigh S (2010) Design of pile foundations in liquefiable soils. Imperial College Press, London, UK.
14. Hardin B and Drnevich V (1972) Shear modulus and damping in soils: measurement and parameter effects (Terzaghi lecture*). J of soil mechanics and found division* (98):603–624.
15. Polito C and Martin J (2003) A reconciliation of the effects of non-plastic fine on the

liquefaction resistance of sands reported in the literature. *Earthquake Spectra* 19(3):635–651.
16. Gallagher P and Finsterle S (2004) Physical and numerical model of colloidal silica injection for passive site stabilization. *Vadose Zone J* 3(3):917–925.
17. Gallagher P and Lin Y (2009) Colloidal silica transport through liquefiable porous media. *J Geotech Geoenviron Eng,* 135(11):1702–1712.
18. Conlee C (2010) Dynamic properties of colloidal silica soils using centrifuge model tests and a full-scale field test. Ph.D. Dissertation. Drexel Univ., United States.
19. Witthoeft A, Santagata M and Bobet A (2012) Numerical study of the effectiveness of bentonite treatment for liquefaction mitigation, in*. Geotechnical special publication*, Conference: Geo-Congress 2012.
20. El Mohtar C, Bobet A, Drnevich VP, Johnston CT and Santagata MC (2014) Pore pressure generation in sands with bentonite: from small strains to liquefaction. *Geotechnique*, 64:108–117.
21. Hamderi M and Gallagher P (2015) Pilot-scale modeling of colloidal silica delivery to liquefiable sands. *Soils Found,* 55(1):143–153.
22. Ochoa-Cornejo F (2015a) Cyclic Behavior of Sands with Superplastic Fines, Ph.D. Dissertation. School of Civil Eng., Purdue University, United States.
23. Ochoa-Cornejo F, Bobet A, Johnston CT, Santagata M and Sinfield JV (2016) Cyclic behavior and pore pressure generation in sands with laponite, a super-plastic nanoparticle. *Soil Dy Earthquake Eng*, 88:265–279.
24. Huang Y and Wang L (2016a) Laboratory investigation of liquefaction mitigation in silty sand using nanoparticles. *Eng Geology*, 204:23–32.
25. Agapoulaki G and Papadimitriou A (2018) Rheological properties of colloidal silica grout for passive stabilization against liquefaction. *J of Mater Civil Eng.* 30(10): 04018251 -(1-11).
26. Cao W (2004) Nanostructures and nanomaterials-synthesis, properties and applications. London: Imperial College Press. Available at: https://doi.org/10.1021/ja0409457.
27. Gallagher P and Mitchell J (2002) Influence of colloidal silica grout on liquefaction potential and cyclic undrained behavior of loose sand. *Soil Dyn Earthq Eng*, 22(9–12):1017–1026.
28. Gallagher P, Conlee C and Rollins K (2007a) Full-scale field testing of colloidal silica grouting for mitigation of liquefaction risk. *J Geotech Geoenviron Eng*, 133(2):186–196.
29. Gallagher P, Pamuk A and Abdoun T (2007b) Stabilization of liquefiable soils using colloidal

silica grout. *J Mater Civ Eng*, 19(1):33–40.
30. El Mohtar C, Clarke J, Bobet A and Santagata M (2008) Cyclic response of sand with thixotropic pore fluid. *Geotech earthquake eng and soil dyn* IV (eds D Zeng, MT Manzari and DR Hiltunen). Geotech Special Pub 181 (CD-ROM). Reston, VA, USA: ASCE.
31. El Mohtar C, Bobet A, Santagata MC and Drnevich VP (2013) Liquefaction mitigation using bentonite suspensions. ASCE *J Geotech Geoenviron Eng*, 139(8):1369–1380.
32. Huang Y and Wang L (2016b) Experimental studies on nanomaterials for soil improvement: a review. *Environmental Earth Sciences*, 75:497.
33. Ochoa-Cornejo F (2015b) Cyclic behaviour of sands with superplastic fines. a dissertation submitted for the degree of Doctor of Philosophy. Purdue University, United States.
34. Ochoa-Cornejo F (2017) Dynamic Behavior of Sand with NanoParticles, in *Pro of the 19th Int Conference, Soil Mechanics and Geotech Eng*, Seoul.
35. Ochoa-Cornejo F, Bobet A, Johnston C and Santagata M (2020) Dynamic properties of a sand-nanoclay composite. *Geotechnique* 70(3):210-225.
36. Santagata M, Clarke JP, Bobet A, Drnevich VP, El Mohtar CS, Huang PT and Johnston CT (2014) Rheology of concentrated bentonite dispersions treated with sodium pyrophosphate for application in mitigating earthquake-induced liquefaction. *Applied Clay Sci.*, 99:24–34.
37. Huang Y and Wang L (2019) Centrifuge testing of liquefaction mitigation effectiveness on sand foundations treated with nanoparticles. *Engineering Geology*, 249:249-256.
38. El Howayek A, Bobet A, Johnston CT and Santagata M (2014) Microstructure of sand laponite water systems using cryo-sem, *in. Geo-Congress 2014 Technical Papers*, ASCE, pp. 693702.
39. ASTM-D6913 (2017) Standard Test Methods for Particle-Size Distribution (Gradation) of Soils Using Sieve Analysis. West Conshohocken, PA: ASTM International.
40. ASTM-D2216-19 (2019) Standard Test Methods for Laboratory Determination of Water (Moisture) Content of Soil and Rock by Mass. West Conshohocken, PA: ASTM Int.
41. ASTM-C128-15 (2015) Standard Test Method for Relative Density (Specific Gravity) and Absorption of Fine Aggregate. West Conshohocken, PA: ASTM International.
42. Huang X, Sun J-S, Huang Y and Yan B-C (2021) Laponite: a promising nanomaterial to formulate high-performance water-based drilling fluids. *Petroleum Science* 18:579-590.
43. BYK (2014) Technical Information B-RI 21: Laponite performance. a member of Altana,

Germany.
44. Kroon M, Vos G and Wegdem G (1998) Structure and formation of a gel of colloidal disks. *Physical Review E*, 57:1962–1970.
45. Tanaka H, Meunier J and Bonn D (2004) Nonergodic states of charged colloidal suspensions: repulsive and attractive glasses and gels. *Phys Rev E*, 69:031404-1-6.
46. Benson S (1976) Thermochemical Kinetics: Methods for the Estimation of Thermochemical Data and Rate Parameters. John Wiley & Sons, Inc., New York.
47. Villar M and Lloret A (2004) Influence of temperature on the hydro-mechanical behaviour of a compacted bentonite. *Applied Clay Science*, 26:337–350.
48. Ghaith F, Al Shakhshir FS, Nour MI and Al Lagtah NMA (2017) Thermal Performance of an integrated Earth-air tunnel system with building's External Wall in UAE. *Int J of Eng Research and Tech,* 6(07):206–218.
49. Qian B, Gregorich EG, Gameda S, Hopkins DW and Wang XL (2011) Observed soil temperature trends associated with climate change in Canada. *J of Geophysical Research, 116(D02106):1–16*.
50. Zhang X, Vincent LA, Hogg WD and Niitsoo A (2000) Temperature and precipitation trends in Canada during the 20th century. *Atmos Ocean*, 38:395–429.
51. Finn W, Ledbetter R and Wu G (1994) Liquefaction in silty soils: design and analysis, Ground failures under seismic conditions (eds S Prakash and P Dakoulas), *Geotech Special Publication*, New York, USA: ASCE, 44, pp. 51–76.
52. Poulos S, Castro G and France J (1985) Liquefaction evaluation procedure. *J Geotech Eng*, 111:772–92.
53. Vaid Y and Sivathayalan S (1996) Static and cyclic liquefaction potential of Fraser Delta sand in simple shear and triaxial tests. *Can Geotech J*, 2:281–289.
54. Das B and Ramana G (2011) Principles of Soil Dynamics. 2nd edn. Stamford, Printed in the United States of America.
55. Jeeries M and Been K (2015) Soil Liquefaction: A Critical State Approach. 2nd edition. Taylor and Francis.
56. Youd T, Idriss IM, Andrus RD et al. (2001) Liquefaction resistance of soils: summary report from the 1996 NCEER and 1998 NCEER/NSF workshops on evaluation of liquefaction resistance of soils. *J Gecotech and Geoenviron Eng*, 127:817–33.

57. ASTM D2487 (2022) Standard Practice for Classification of Soils for Engineering Purposes (Unified Soil Classification System). ASTM International.
58. Zaragoza J, Fukuoka S, Kraus M, Thomin J and Asuri P (2018) Exploring the role of nanoparticles in enhancing mechanical properties of hydrogel nanocomposites. *Nanomaterials*, 8(882):1–10.
59. Miehe C, Goktepe S and Diez J (2009) Finite viscoplasticity of amorphous glassy polymers in the logarithmic strain space. *Int J of Solids and Structures*, 46(1):181–202.
60. Wu S (1992) Secondary relaxation, brittle-ductile transition temperature and chain structure, *J of applied Poly Science*, 46:619–624.
61. Khaleghi M, Ahmadi E, Shahraki MK, Aliakbari F and Morshedi D (2020) Temperature-dependent formulation of a hydrogel based on Hyaluronic acid-polydimethylsiloxane for biomedical applications. *Heliyon*, 6(e03494):1–13.
62. El Howayek A (2011) Characterization, rheology and microstructure of laponite suspensions. MSc thesis. Purdue University, United States.

CHAPTER 5 Swelling Behaviour of Super-absorbent Laponite Hydrogel Under One-dimensional Loading

Abstract

Because of the inherent rheological property of transparent gel, laponite has been proposed for soil densification to withstand seismic events. One of the most critical research topics is the swelling capacity of nanoparticles, specifically laponite, as the swelling process could affect the soil-nanoparticle structure. Hence, the objective of this study is to investigate the swelling properties of pure laponite and sand treated with different contents of laponite. The swelling characteristics of compacted laponite were investigated in a one-dimensional consolidation test. Results showed that the swelling strain of compacted laponite increased with time and as the concentration of laponite increased in specimens. The initial swelling of fresh laponite took around 4 weeks to attain equilibrium, while in the reswelling tests, laponite reached equilibrium within 60 hours. The reswelling height of laponite was found to be higher than the initial swelling of fresh laponite, with distinct reswelling behavior as compared with other clay minerals. This swelling behavior of laponite is found to be consistent with other clay minerals in which the swelling strain is caused by interlayer and double-layer forces. The swelling height of sand-laponite mixture with 3% laponite reached equilibrium after 40 hours, whereas the swelling height of sand-laponite with 5% laponite specimen did not reach equilibrium even after 50 hours. Scanning Electron Microscope images revealed that the structures of swollen laponite are continuous sheet-like irregular structures with pore size. In this study, the water retention ratio and changes in laponite hydrogel characteristics due to repeated drying and wetting processes are also investigated. Additionally, the swelling pressure of compacted laponite is also measured, which varies in a range of 5.6-8.6 kPa throughout the experiment.

Keywords: Nanoparticles, Swelling, Reswelling, Hydrogel, Swelling pressure

**A version of this chapter has been published in Geotechnical and Geological Engineering (2024), https://doi.org/10.1007/s10706-024-02796-3.*

5.1 Introduction

The construction of heavily loaded structures has become necessary to meet the growing demands of rapid industrialization. Even after considering adequate factors of safety in engineering design, foundations can fail owing to seismic activities [1-3]. Engineering infrastructures can be affected by various sorts of arbitrary loading conditions, which can be imposed by human activities or by natural phenomena. The pore water pressure in partially or totally saturated sand deposits suddenly rises during seismic activity and cyclic loadings, causing the sand to lose its effective confining stress, liquefy, and lose its shear strength and ability support foundations [4,5]. Soil permeability greatly increases as a result of the easier water flow paths created by liquefaction which allows the excess pore water pressure to quickly dissipate causing abrupt settlement of soil. Therefore, liquefaction is frequently accompanied by significant lateral and vertical ground deformations, which cause significant damage to buildings and other structures [4,5].

In-situ densification and grouting stabilization procedures are frequently used to modify the soil beneath superstructures so that it can withstand the seismic shocks. Although it is relatively simple to determine the level of ground treatment of these methods, they certainly produce considerable levels of noise and vibration, and are undesirable for treating the ground beneath existing structures. Recent rapid advancements in nanotechnology have led to the investigation and recommendation of nanoparticles for the treatment of soft and liquefiable soils. Nanoparticles decrease the permeability of soil which leads to significant reduction in the sudden excess pore water pressure during seismic events and reduces the potential for liquefaction. Additionally, because of their favorable rheological characteristics, early Newtonian behavior, delayed gelation process and ability to fill spaces with nanoscale material, nanoparticles can strengthen soil by firming up its skeleton [6-11]. Strong specific charges, electrically active surfaces, and a strong water affinity are all characteristics of nano-clay particles.

Recently, laponite, a new nanoparticle from a synthetic sheet of silicate nanoparticles with structure similar to montmorillonite, shows strong properties of resisting the liquefaction risk in a few published studies [12-14]. Ochoa-Cornejo et al. [12] investigated the influence of 1%–5% laponite (by dry mass of sand) on the cyclic response of sand with a relative density in 15%–25% range. The cyclic response has been demonstrated to be significantly influenced by adding only 1% of laponite with sand. Huang and Wang [14] also recommended laponite to be used with

liquefiable silty sand to resist liquefaction. Dynamic triaxial tests were analyzed to examine the cyclic behaviour and liquefaction resistance of laponite-sand specimens. Huang and Wang [14] also discussed the effect of two main parameters on the liquefaction resistance of treated specimens: (a) laponite content, and (b) resting/curing time (laponite requires minimum 48 hours to form gel in a constant temperature). When laponite concentration and resting time of specimens increases, the liquefaction resistance improves. The research by Huang and Wang [14] agreed with Ochoa-Cornejo et al. [12] that laponite reduces the possibility for liquefaction by cementing soil grains, solidifying pore fluids, and delaying the formation of pore pressure. The liquefaction resistance of a sol-gel transition in a laponite suspension is enhanced by its rheological features, but it is weakened under the amplified cyclic loading due to its thinning behavior.

The volume of nano-clay particles expands when wet and shrinks when dry. Nano-clay particles can interact electrostatically with ions in aqueous solutions, attracting them with oppose charges and anchoring some of them close to their surfaces, as well as exchanging ions within the aqueous solution [15]. Nano-clay hydrogels is a cross-linked networks that can absorb up to 1000 times its dry weight in water while maintaining its structural integrity [16,17]. Two factors affect the time-dependent volume change behaviour of nano-clay: (a) compressibility, which refers to changes in volume due to changes in a stress state, and (b) ability to conduct pore fluid [18]. In general, the swelling performance (enlargement of particles as a result of an accumulation of fluid) of a compacted nano-clay, such as montmorillonite, can be divided into three phases, i.e., before, during, and after water absorption.

- *Phase I*: Before absorbing water, voids into the nano-clay mixture are engaged by air and free water (if any). For example, if montmorillonite is in fully dry condition, voids are occupied with air only.
- *Phase II*: During water uptake, the nano-clay absorbs water into the interlayers occupying voids. Eventually, the volume of the nano-clay increases and the swelling pressure develops. In montmorillonite, the interlayer and double-layer forces are responsible for the swelling behaviour.
- *Phase III*: After absorbing water, the volume of the nano-clay cannot rise as there are no more empty voids; however, the swelling pressure will develop because there is no escape route available.

Madsen and Muller-Vonmoos [19] stated that two mechanisms, namely (a) crystalline swelling and (b) osmotic swelling, occur within the voids of clay during the swelling phenomena. These mechanisms are dependent on the degree of hydration and cations in the interlayers. Both mechanisms are influenced by the breakup of the nano-clay particles and the de-mixing of cations [20-22]. Increased pore fluid concentration causes electrochemical repulsion forces to decrease, resulting in corresponding osmotic consolidation [18]. Conversely, the specimen originally saturated with high-concentration solution has a bigger osmotic suction and, as a result, a lower matric suction at a given total suction [23]. For example, when montmorillonite absorbs water, the crystalline swelling occurs; which increases the distance between the unit layers of montmorillonite. During the swelling state, hydration is responsible for the attraction between the water molecules and polar surface groups as well as to the charge sites and interchangeable cations, while the van der Waals interaction contributes to the energy of attraction [21]. The exchangeable cations located between the layers can be found either on the surface of layers or in the hexagonal holes of the tetrahedral sheets. The second mechanism is the osmotic swelling, which continuously enlarges the distance between the layers of a nano-clay. The osmotic swelling is related to the variation of ions concentration between the pore fluid and near the surface of the layers of nano-clay. This mechanism is mainly formed due to the interactions of the diffuse double layers and van der Waals attraction [21]. Yong [24] indicated that the difference between the crystalline and osmotic swellings activities is due to the hydration structure of water.

Some expansive soils may experience a significant volume rise as a result of the fluctuations in moisture content. The mechanical characteristics of soils are affected by changes in moisture content, particularly on the clay soils, as a result of seasonal weather variations and man-made influences. The degree of swelling depends on the activity of the mineral of clay soils (Saberi et al. 2018). In case of the soil swelling, the change in moisture content can change the volume of soil, which can cause damage to buildings, railroads, and pavement. For instance, the annual damage from the soil swelling in America is around $7 billion, nearly twice as much as the annual damage from floods, storms, and earthquakes [25]. Studies found that bentonite (consists primarily of montmorillonite minerals) swells when placed in water, whereas no appreciable increase in volume or absorption of solution when placed in the saturated sodium chloride [26]. He et al. [26] stated that Gaomiaozi (GMZ)-bentonite has a high swelling capacity and good adsorption properties. The study found that the swelling strain of the compacted GMZ-bentonite under one-

dimensional configuration decreases as the concentration of *NaCl* solution increases. Chen et al. [27] claimed that if the contact time of the GMZ-bentonite with synthetic Portland cement solution increases, the swelling pressure would decrease. In the compacted bentonite with a dual-pore structure (macro-pores and micro-pores), the volume changes of samples in the process of wetting and drying cycles are primarily caused by the interaction between macro- and micro-pores [28,29]. The swelling behaviour of bentonite-sand mixtures may also be influenced by the amount of sand content in the specimens [30]. The void ratio increases as the amount of bentonite content increases in the bentonite-sand mixtures, which has a great impact on the overall swelling behaviour [31]. Xiang and Ye [32] determined the effect of alkaline conditions on the swelling of bentonite mixed with sand. There is many research have been conducted on the swelling behaviour of bentonite and bentonite-sand mixtures in the literature.

The swelling of laponite has received little attention until yet, although having advantages over natural clays such as smaller particle size, lower structural polydispersity (dimensions, surface charge), and superior water stability, such as when compared to montmorillonite [33]. Comprehensive investigation on the swelling capacity and repetitive drying-wetting behaviour of laponite should be properly conducted, as research has proposed injecting laponite into ground treatment to mitigate liquefaction. The foundation and superstructure of any engineering structure, however, risk catastrophic collapse if the treated ground beneath it swells significantly. This phenomenon should be clearly understood before injecting laponite suspension into ground supporting engineering structures in order to improve the ground performance in seismic zones.

The objective of this study is to investigate the swelling properties of pure laponite and sand treated with different contents of laponite in a controlled laboratory environment. Various experimental set-ups were used to examine the swelling behaviour of both pure laponite and sand-laponite mixtures. Additionally, the effects of repeated drying and wetting processes were investigated using a one-dimensional oedometer set-up. The swelling pressure of pure laponite has been assessed by a one-dimensional in-built experimental set-up. The experimental findings were discussed and compared with those of bentonite and other published results. The study also assessed the water retention ratio and the changes in laponite hydrogel characteristics due to repeated drying and wetting processes. Finally, Scanning Electron Microscope (SEM) images were analyzed to understand the microstructure of swollen laponite.

5.2 Experimental Materials

5.2.1 Laponite

Laponite is a unique nanoparticles additive that is utilised as a rheology modifier in various applications including surface coatings, household cleaners, and personal care products [34]. When it is dry, laponite is a fine white power and has a disk-like shape with a diameter of around 25 nm, a thickness of 1 nm [35], and a specific gravity between 2.10 [34] and 2.57 [14]. The chemical composition formula of laponite is $Na^{+0.7}[(Si_8Mg_{5.5}Li_{0.3})O_{20}(OH)_4]^{-0.7}$ which is a 2:1 clay formed by a magnesium octahedral sheet sandwiched between two silica tetrahedral sheets. Isomorphic substitution of magnesium by lithium atoms generates negative charges on both faces, which are counterbalanced by interlayer cations, generally sodium. The edges have weaker *pH*-dependent positive charge. Estimates of the face and edge charges of laponite prepared in deionized water by *pH* and conductivity measurements revealed that the positive charge on the crystal edges (4-5 mmol/100 g) is about 10% of the total negative charge on the crystal faces (50-55 mmol/100 g) [34,36]. When dispersed in water, it hydrates, swells, and forms a colourless transparent monodisperse suspension that resembles a highly thixotropic gel. It can potentially be used as a high-performance water-based drilling fluid [13]. Laponite-RD (rheology additive) was used in the current study, which has high efficiency in water-based systems and is manufactured by the BYK Additives and Instruments, Germany. In recent research by the authors [37], laponite is shown to be environment friendly and biologically inert.

Microstructure of Laponite: The microstructure of laponite hydrogel was examined by the SEM. After allowing laponite to swell for 28 days, a couple of drops of laponite gel were placed on a carbon tap and allowed to dry entirely for 24 hours using a freeze drier. The freeze-dried method on a hydrogel sample is considered the most effective method to observe pore morphology or inter-polymer network of the hydrogel [38]. Prior to the scanning process, the dried hydrogel samples were gold sputter-coated to achieve good images. **Figure *5-1*** shows the SEM images of the laponite hydrogel morphology at 500, 100, and 10 µm magnifications. The images revealed that the structures of swollen laponite are continuous sheet-like irregular structures with pore size similar as mentioned in the case of Carrageenan hydrogel in the articles of Yacob and Hashim [38].

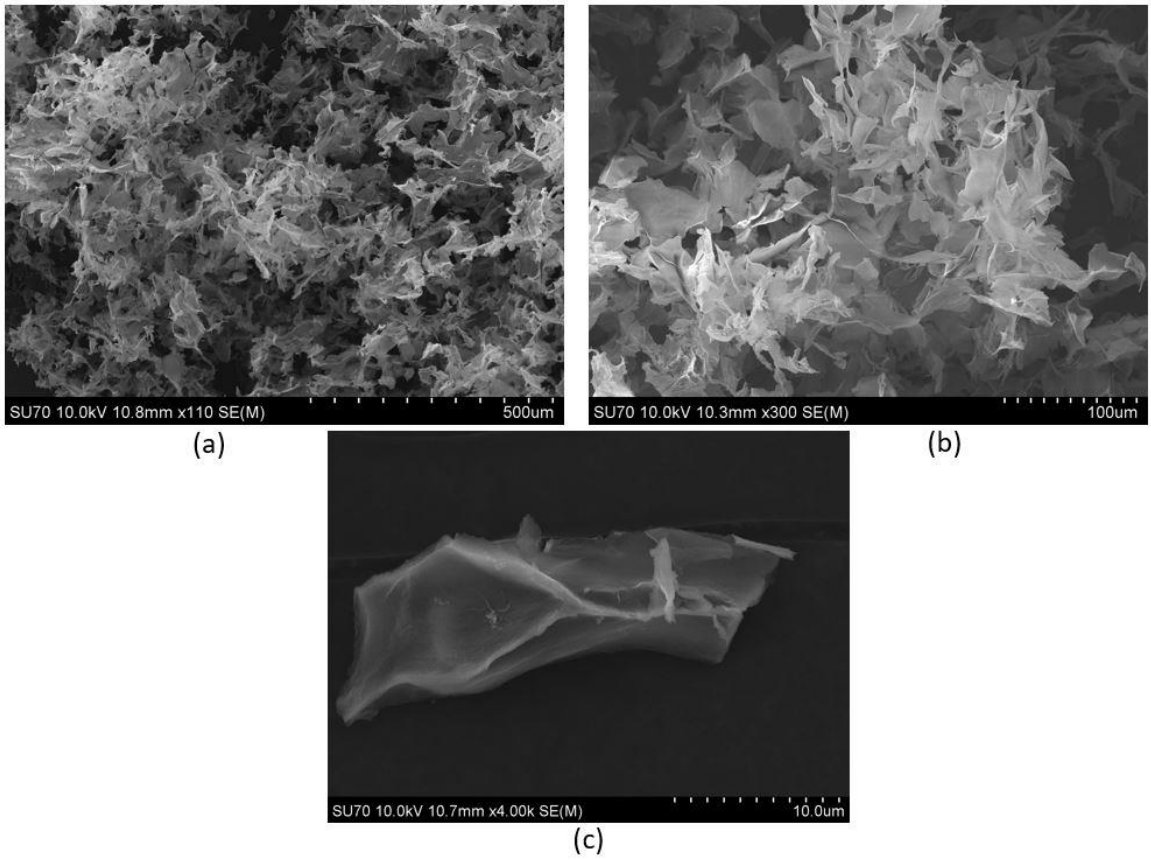

Figure 5-1: Microstructure of laponite gel, SEM images at (a) 500 µm, (b) 100 µm, and (c) 10 µm magnification

5.2.2 Bentonite

Bentonite, an absorbent aluminium phyllosilicate clay which can either be Na-montmorillonite or Ca-montmorillonite, makes up the majority of montmorillonite. The swelling capacity of Na-montmorillonite is significantly higher than that of Ca-montmorillonite. Bentonite usually forms as a result of volcanic ash being subjected to seawater weathering, which converts the volcanic glass found in the ash into clay minerals [39,40]. Bentonite particles also have a fundamental thickness of 1 nm, but the diameter is substantially larger than laponite (200-1000 nm). Fresh exposures of bentonite beds are white, pale blue, or green. As the exposure is weathered further, it changes to a cream hue, then to yellow, red, or brown [41]. Goldcorp Canada LTD supplied the bentonite, which was used in this study. **Figure *5-2*** represents the particle size distribution of laponite and bentonite conducted by Malvern Mastersizer 2000E in Lakehead University

Instrumental Laboratory, Thunder Bay, Ontario, Canada. Laponite has particle size with d_{50}=10.63 µm and d_{90}=21.45 µm, while bentonite has particle size with d_{50}=5.32 µm and d_{90}=48.40 µm.

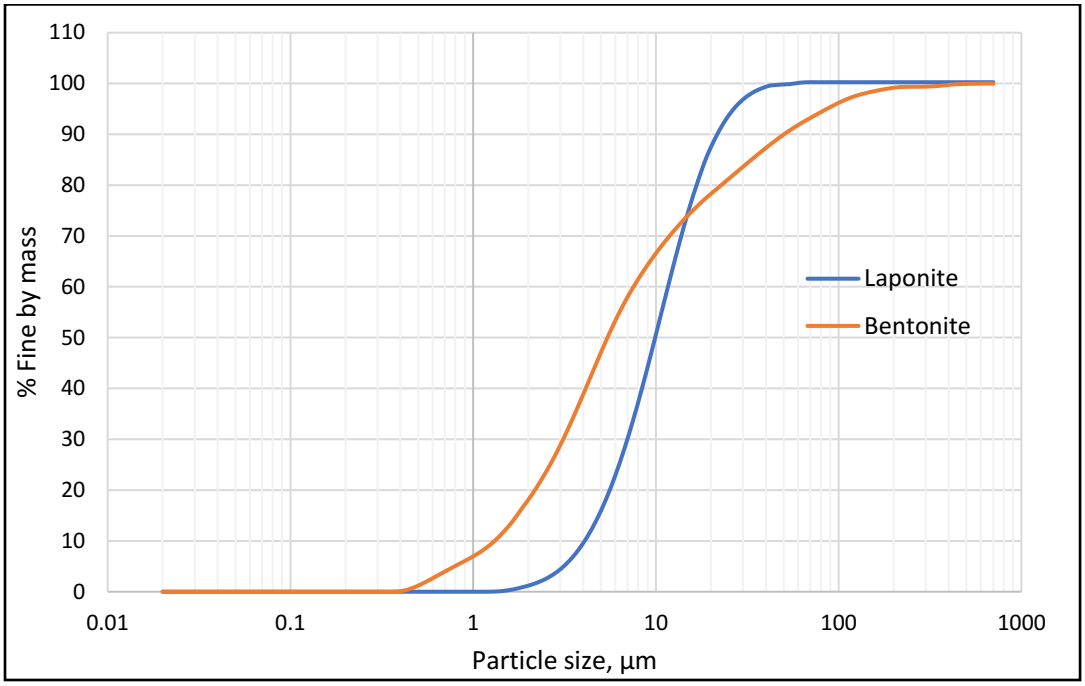

Figure 5-2: Particle Size Distribution (PSD) of laponite and bentonite

5.2.3 Sand

Sand used in this research was supplied by Pioneer Construction, Thunder Bay, Ontario, Canada. The grain size distribution analysis of sand was carried out according to ASTM D6913 [42]. The analysis showed that the uniformity and coefficients of curvature of sand were 4.40 and 0.74, respectively. The median diameter (d_{50}) of sand is 0.62 mm and the fines content is less than 5%. According to the Unified Soil Classification System, the group symbol of sand is *SP* and the group name is poorly graded sand. The moisture content, by ASTM D2216-19 [43], and specific gravity of sand, obtained in accordance with ASTM C128-15 [44], were 9.50% and 2.60, respectively. The maximum and minimum voild ratios are e_{max}= 0.30 and e_{min}=0.75.

5.3 Experimental Methods

5.3.1 Specimen Preparation

Laponite was stored in an airtight container in a dry room to avoid moisture absorption. The swelling, reswelling, and swelling pressure tests were conducted using dry fresh laponite. For the sand-laponite mixture, the specimens were prepared by dry pluviation. The desired amount of

laponite was dry mixed with sand in an airtight container and then shaken manually for 20 minutes. To investigate the expansion of sand-laponite mixtures of 3% and 5% laponite (dry mass of sand) were prepared. Same procedure has been followed to prepare the sand-bentonite samples.

5.3.2 Experimental Procedures

5.3.2.1 **One-dimensional Oedometer**

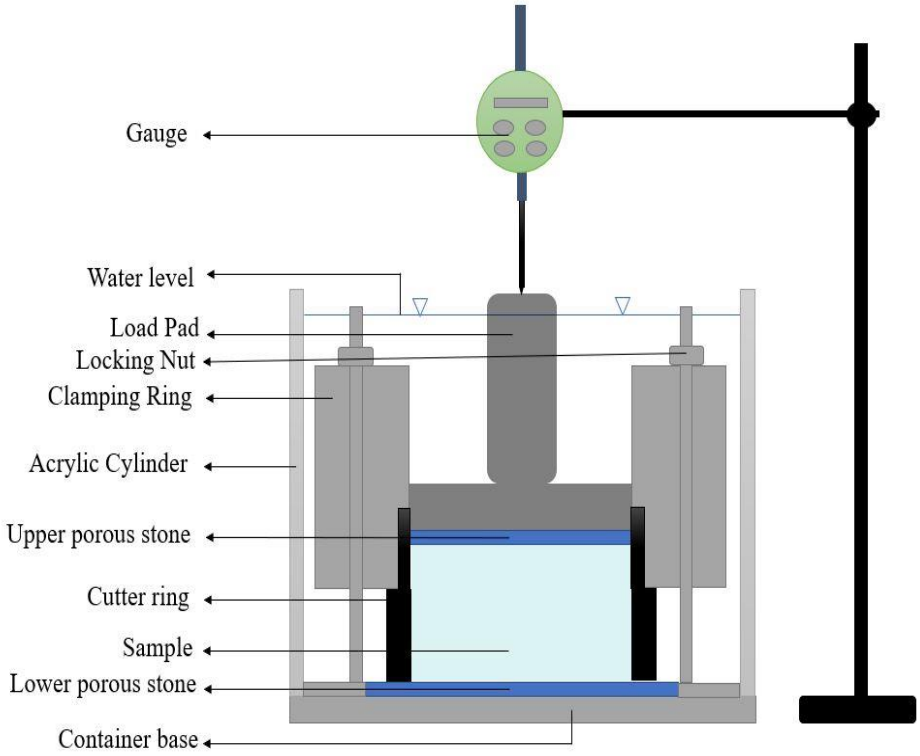

Figure 5-3: Cross-section of a one-dimensional oedometer cell

The swelling strain test is used to investigate the effect of voids on swelling pressure. It is essential in this test to keep a consistent pressure throughout the experiment in order to allow the sample to swell freely. A lower matric suction corresponds to higher water content, resulting in a higher degree of hydration for soil and corresponding osmotically induced consolidation [26]. Based on these physicochemical processes, the experimental setup for swelling and reswelling tests has been designed. The one-dimensional oedometer fixed ring consolidation cell consists of a base, load pad, cutter ring, clamping ring, cap, acrylic cylinder (surrounding wall), and two porous stones (**Figure *5-3***). This cell is manufactured by Humboldt Mfg. Co. USA. The circular sample holder ring is 50.80 mm in diameter and 19 mm in height. The samples are compacted using an initial

vertical load in the cutter ring. Finally, compacted laponite with a dry density 2.5 g/cm^3 was obtained. During the swelling tests, the cell is fully filled with distilled water**.** The sample can be freely swollen in the axial direction. Finally, the swelling strains can be measured using a strain gauge with a precision of 0.001 mm [45,46]. When the vertical displacement measurement stabilized, the wetting test was terminated. This saturation procedure took about 25 to 30 days to complete. The height of water is maintained constant throughout the testing time to prevent evaporation which causes changes in the sample concentration.

5.3.2.2 **Modified Triaxial Machine**

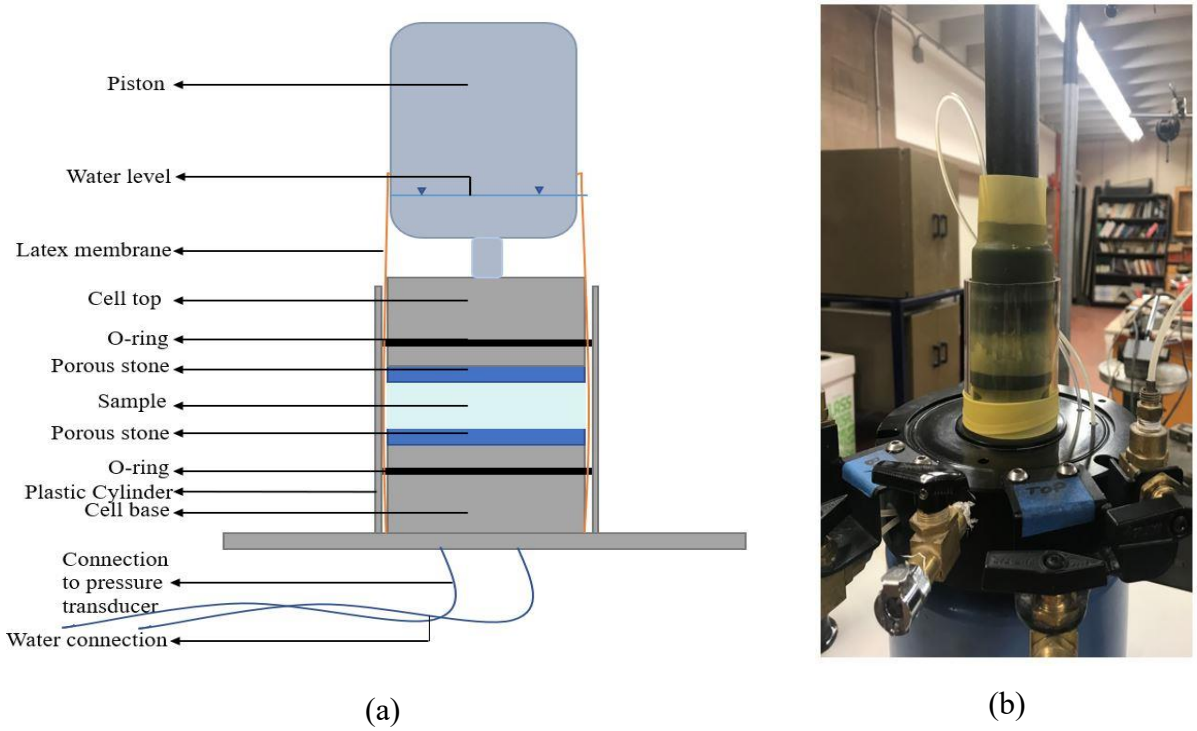

(a) (b)

Figure 5-4: (a) Cross-section of the modified triaxial cell, and (b) modified triaxial cell for the swelling pressure tests.

To carryout the swelling pressure tests, known as the constant-volume test, a triaxial machine frame and master panel were used. The most vital feature of this test is keeping a constant volume. This cell consists of a cell top, a plastic cylinder, a latex membrane, O-rings, two porous stones, a fixed piston, and a connection to water supply and another connection to a pore pressure transducer (PPT), as shown in **Figure *5-4***. The diameter and height of the cell are 50 mm and 38 mm, respectively. First, the dry laponite sample was placed into the cell. The sample was subjected to initial vertical pressure before the distilled water was supplied from the bottom. During conducting

the experiments, the whole cell was filled with water as well to represent the fully saturated condition. After submerging the sample, the swelling pressure can be measured by PPT. During the test procedure, the volume change is considered to be negligible [45-47].

5.4 Results and discussions

The results of three distinct methods to investigate the swelling height of pure laponite and sand-laponite mixtures are presented in Section 5.4.1. The reswelling behaviour (repeated drying-wetting processes) and water retention ratio of pure laponite are presented in Section 5.4.2. Section 5.4.3 compares the findings of laponite with the published data of bentonite. Section 5.4.4 shows the changes of the hydrogels after repeated swelling tests, whereas 5.4.5 presents possible causes of the uneven swelling surface of laponite. Section 5.4.6 compares the findings of laponite with the swelling behaviour of bentonite, which has been conducted on the same experimental set-up in this study.

5.4.1 Determination of swelling

The swelling of laponite was investigated by three different methods, namely, the tea bag, the visual tube, and the Oedometer cell tests. The elaboration of each method with results and discussions has been given below.

5.4.1.1 **Tea Bag Tests**

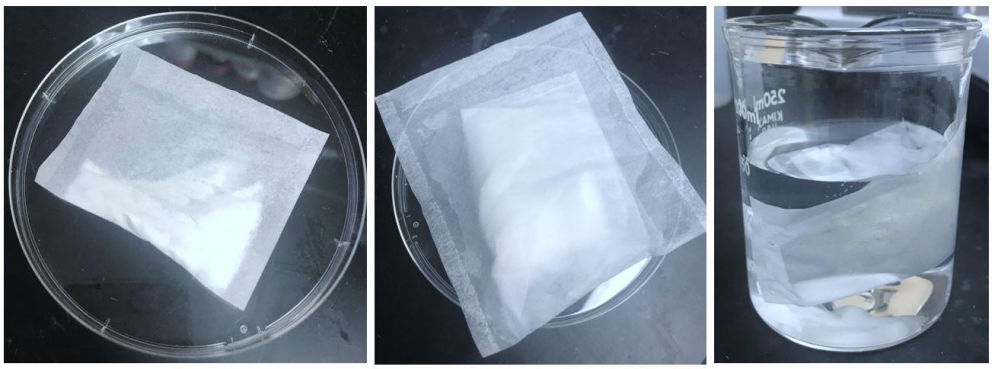

Figure 5-5: Swelling test using the tea bags.

The tea bag test (acrylic/polyester gauze with fine meshes) is the most conventional and well-known method for estimating the swelling of hydrogel. The required sample weight is usually within the range of 0.1 g to 0.3 g. The desired amount of dry sample is placed into a tea bag and

sealed. After that, the bag is immersed in an excessive amount of water. After a certain period of time depending on the type of hydrogel, the tea bag is removed from water and gently wiped-out excessive water. The swelling capacity (*S)* of hydrogel is then calculated using equation (5-1).

$$S = \frac{W_s - W_d}{W_d} \qquad 5\text{-}1$$

where W_s and W_d are the measured weights of hydrogel at the swelling state and dry state, respectively. The same procedure was followed to perform the tea bag tests with laponite in this study. According to the rheological tests, laponite should be into the water bath for at least 48 hours in order to complete its gelation process. However, after placing laponite filled tea bag into water, within two minutes all laponite seeped out through the pores of the tea bag. Due to the extremely small size of the laponite grains, they may quickly escape through the tea bag's pores before they can even swell from water. In the subsequent attempts, laponite powder was placed into double and then triple layers of the tea bags, as shown in **Figure 5-5**(b). However, again laponite escaped through the pores of the tea bag indicating that this test method is not suitable for laponite.

5.4.1.2 **Visual Tube test**

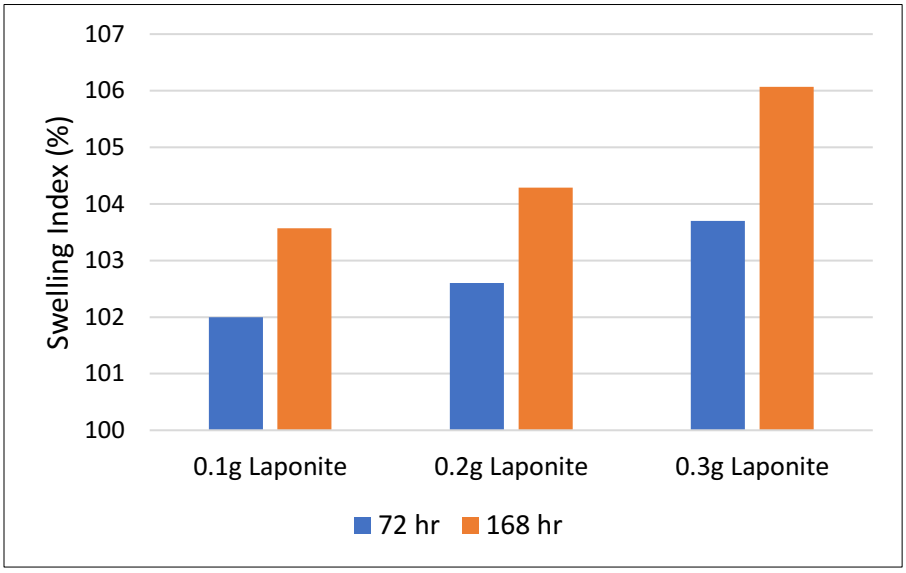

Figure 5-6: Swelling index of laponite using the visual tube tests.

The visual tube test method of montmorillonite was adapted from the American Society for Testing and Materials (ASTM) D5890-11 protocol (17)1 [48]. In three glass vials, 0.1, 0.2, and 0.3 g of fresh dry laponite was dispersed into deaired distilled water to obtain 5 g of the total weight mixture. After that, the vials were sealed, and height of the samples was precisely measured using

a caliber and recorded. The vials were then placed in the laboratory at room temperature (23°C). Ochoa-Cornejo [10] stated that based on the results of rheological tests, at 72 hours the rheological properties of laponite pore fluid expected to develop in the pore space were similar to those of the bentonite dispersions examined in El Mohtar et al. [49]. Huang et al. [12] also mentioned that laponite gel formation at room temperature of 23°C requires a curing time of more than 48 hours based on rheological tests. Hence, the swelling height of the samples using the visual test method was recorded at 72 hours (≈ 3 days) and 168 hours (≈ 7 days) in this study. The Swelling Index (*SI*) was calculated from the magnitude of the swelling height given by the formula:

$$SI = \frac{h}{h_{min}} \qquad 5\text{-}2$$

where h is the height of the sample to the nearest hundredth of millimetre and h_{min} is the minimal height of laponite displaying maximum compression for a given set of samples. **Figure *5-6*** shows the results of the swelling height of laponite by the visual tube test method. It is seen that the swelling of laponite is substantial. Thus, after 72 hours of resting time, the *SI* of laponite is 1.02, 1.026, and 1.037 (i.e., 2%, 2.6%, and 3.7% swelling) at only 0.1, 0.2, and 0.3 g laponite. The swelling of laponite hydrogel increases with resting time and concentration. After 168 hours, the swelling of laponite was 3.6%, 4.3%, and 6.1% (*SI* of 1.036, 1.043, and 1.061) for 0.1, 0.2, and 0.3 g laponite, respectively, which is significantly more than the swelling after 72 hours of resting time.

5.4.1.3 **Swelling Tests**

5.4.1.3.1 Swelling tests of pure laponite

Figure 5-7: (a) Laponite powder, (b) laponite hydrogel inside the sample holder, and (c) laponite hydrogel after the initial swelling test.

The evaluation of the vertical swelling strain with time for compacted laponite powder hydrated with deaired distilled water was conducted using a one-dimensional oedometer cell. **Figure *5-7*** shows the dry laponite powder and laponite hydrogel after the swelling test. Several trials were conducted to precisely determine the mass of laponite used in the cell. It was determined that 8 g of fresh dry laponite powder is adequate for accurate estimate of the swelling height from an oedometer test set-up. Eight grams of dry laponite was placed into the sample holder, and a vertical compacted load of 50 kg (≈ 24.7 kPa) was applied for an hour through a piston above the sample. Before wetting of the sample, a vertical load of 4 kg (≈ 2 kPa) was applied to ensure proper contact between the sample and test apparatus. The applied vertical force was significantly less than the compacted load the sample experienced, resulting in the sample remaining highly over-consolidated. The wetting process was then initiated by infiltrating the deaired distilled water from the bottom of the sample to fill the entire cell without turbulence. The sample immediately swelled after being moistened. A strain gauge with a precision of 0.001 mm was used to measure the vertical displacement of the sample. Throughout the testing time, the water level in the cell was maintained at the same level. The swelling test was terminated when the vertical displacement became steady. This saturation procedure took about four (4) weeks to complete. The described procedure is similar to the procedure by He at al. [26] to study the swelling behaviour of compacted bentonite.

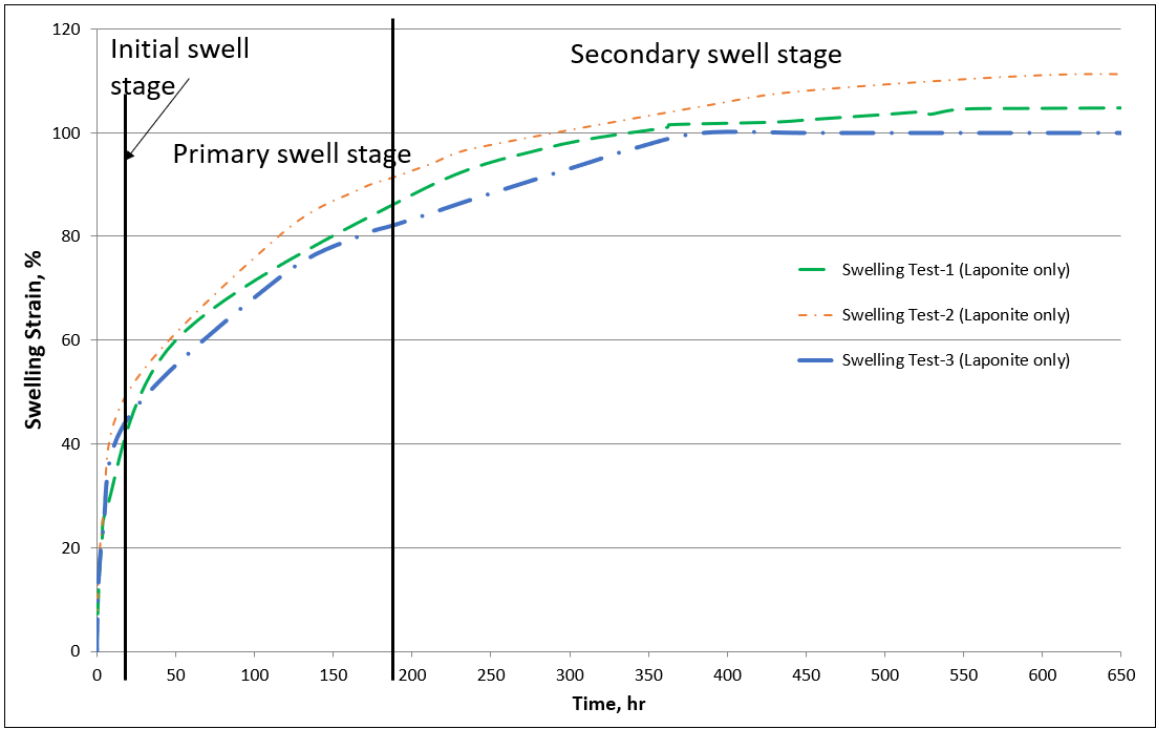

Figure 5-8: Swelling tests of the fresh laponite powder.

Figure *5-8* shows the swelling strains for three identical tests for 8 g of fresh laponite powder. Each experiment took about four (4) weeks to complete the saturation process and to reach the equilibrium condition. **Figure *5-8*** illustrates that the swelling strain of compacted laponite increases with time in the presence of deaired distilled water. After 650 hours, the maximum swelling strain is 1.12 mm/mm (i.e., an increase of 112%) and the equilibrium state is reached. There is very limited experimental data on the swelling behaviour of laponite in the literature [8,33]. Therefore, the findings of the current study are compared to the swelling behaviour of bentonite reported in the literature. The observed results are consistent with the results reported by He et al. [26] and Zhu et al. (2013). Based on the Scanning Electron Microscope images (i.e., **Figure *5-1***), it can be stated that the hydrogel network appears to be denser, resulting in a shrunken state. The pore structure inside the laponite hydrogel can operate as a storage space for water molecules because it is made up of polymer tough branches. When the hydrogel absorbs water, these polymer branches effectively distribute stress, ensuring the stability of the network structure. Furthermore, there are several hydrophilic groups on the polymer chains, which might boost hydrophilicity and hence considerably increase water molecules penetration [27]. The reasons behind the swelling can be also explained as: when the exchangeable cations absorb water, they

arrange themselves on a plane halfway between clay layers [19]. It is not verified, but it is assumed that initially the clay surface is entirely covered by layers of water molecules. The second molecular layer will be distributed after that. To summarise, the water molecules are spread out layer by layer. The water molecules are dispersed in four strata (from zero to four) in the case of solidum montmorillonite. It is a distinct procedure because interlayers cannot have a fractional number of layers of water molecules [22]. The negative dipoles of water molecules are directed towards the cation during water intake, reducing electrostatic interaction between the layers and interlayers cations. The outcome is an increase in layer distance, higher hydration energy than the bond between the clay layers and increased montmorillonite volume. As a result, the swelling pressure develops. Because of the forces described, the swelling process might thoroughly explore the separation of layers [19]. The following mechanisms can explain this phenomenon: during the saturation phase, the matrix suction dissipates causing the compacted laponite to expand. Simultaneously, the infiltrated water weakens the electrostatic repulsion between montmorillonite crystals in laponite, causing the diffused double layer of laponite to thin. As a result, this physicochemical interaction weakens the expansion potential of the compacted laponite. Rao and Shivananda [50] explained these mechanisms in the case of the expansion of compacted bentonite caused by the infiltration of salt solution.

The measured curve for the evolution of the vertical swelling strain with time can be classified into three stages: (i) initial swell stage, (ii) primary swell stage, and (iii) secondary swell stage according to Sridharan and Gurtug [51], and Rao and Thyagaraj [52], which has been later supported by other scholars [53-55]. The findings of this study show that the swell strain of completed laponite started with a brief initial swell phase, between 10 to 20 min, in which the strain sharply rose due to the rapid growth of matric suction dissipation [54] (see **Figure *5-8***). Afterwards, the primary swell phase began and continued for approximately 180 hours in which the swelling strain increased linearly or semi-linearly during the test. Compared to the primary swell, the secondary swell process developed slowly and took a longer period to complete (≤480 hr), presumably because it was governed by the adsorption-desorption reactions [54,56]. For bentonite, the saturation process with the distilled water required about 180 days to stabilize [26]. As seen in **Figure *5-8***, the swelling strain in laponite tests were nearly identical. The test was stopped after the swelling strain versus time had plateaued, i.e., reached equilibrium. As a result, the entire swelling process took almost 4 weeks to complete and the process was similar to the

swelling strain behaviour of bentonite [26]. For all three tests, the graphs achieved equilibrium at approximately 630 hours. The final swelling strains for test 1, 2, and 3 were 1.07, 1.12, and 1.00 mm/mm, respectively. In these three tests, the amount of laponite was equal; nevertheless, there was small difference among the produced graphs. The reasons for the variance are explained as follows:

- *First*: The graphs illustrate a difference in the primary and secondary swell stages. The reason behind the difference can be consolidation. As all the tests were conducted using a similar type of Oedometer cells, there is a fraction of variations in the weight of the parts of the cells (≈0.1-0.3 g). This may cause difference in the compaction of dry fresh laponite powder, which eventually gives a little variety in the primary and secondary swell stages.
- *Second*: The plots of the three tests show visible variation at equilibrium position of the secondary swell stage. Note that this stage takes around a month to complete. After the experiments were stopped, a tiny amount of laponite gel was found outside of the cutter ring of the cells. The amount was pretty small, which can only feel while cleaning the apparatus. Little laponite gel somehow manages to escape the cutter ring during the month-long test. However, the water level is kept constant throughout the testing period, and porous stones are used at both the bottom and top of the sample.

5.4.1.3.2 Swelling tests of sand-laponite specimens

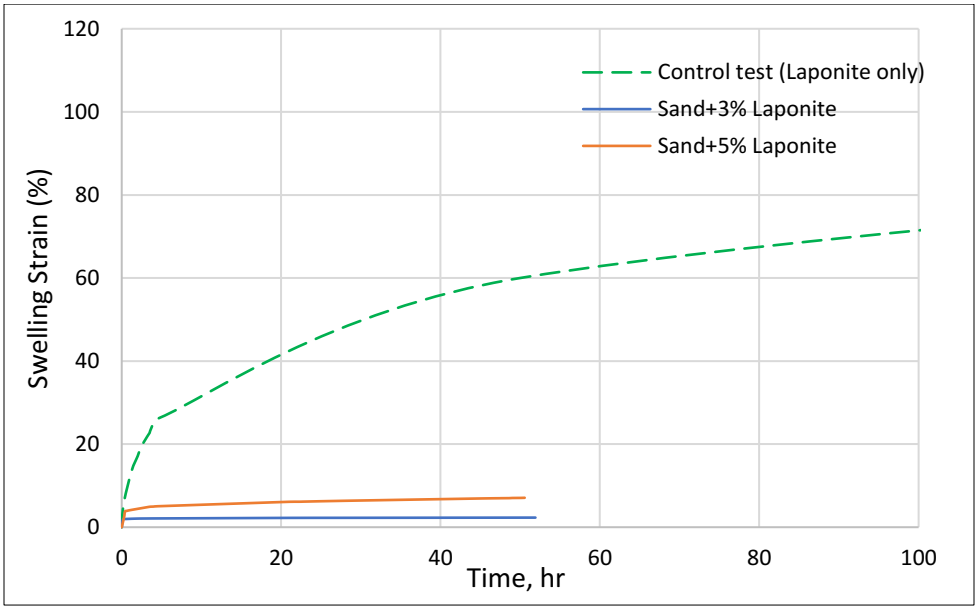

Figure 5-9: Swelling strain of sand+3% laponite and sand+5% laponite specimens.

Figure *5-9* shows the swelling strain of compacted sand-laponite mixtures with 3% and 5% laponite specimens. As shown in the figure, the swelling strain at 5% laponite is more than double the strain at 3% laponite. The swelling height of sand+3% laponite specimen reaches equilibrium within 40 hours, while in case of sand+5% laponite specimen does not reach the equilibrium state even after 50 hours. This suggests that as the concentration of laponite increases, the swelling height, as well as the time to attain the equilibrium state also increases. The osmotic pressure is generated in the clay by the concentration difference between the free pore water and the water close to clay particles [18]. In compared to **Figure *5-8***, the initial swell stage of sand specimens treated with 3% and 5% of laponite in **Figure *5-9*** is quicker (within fraction of seconds). Both the initial and primary swell states of sand+laponite samples are steeper and faster than those of the fresh laponite swelling plots. Therefore, the time to attain the equilibrium state is rather short in **Figure *5-9***. In compare to laponite hydrogel, sand has less of a tendency to swell, as well as the amount of laponite used to treat the sand is very small amount. However, these treated sand specimens show some swelling strain in this study.

5.4.2 Reswelling tests

Figure 5-10: Laponite hydrogel after dried up at 100˚C for 24 hours in a temperature-controlled oven

The ability of hydrogel to swell repeatedly is crucial for its practical applications as the sand-laponite mixture is subjected to wetting-drying cycles throughout the year. After completing the swelling test, the Oedometer equipment was dismantled. To avoid sample loss, laponite was kept in the sample ring and the ring was dried up in the oven (after discharging water from the ring). The samples were dried for 24 hours at 100°C in a temperature-controlled oven to remove moisture. A similar procedure was followed by Chen et al. [57] to investigate the reswelling ability of PAA-based nanocomposite hydrogel. Four separate tests were run in parallel to double-check

the results. Each sample was weighed to an accuracy of 0.01 g at varying intervals. The weight of the sample remains nearly constant after drying. In the case of laponite, the dried-up samples weigh between 7.85 g and 7.90 g after 24 hours, which is almost the same weight as the fresh fine power of laponite (≈8 g) utilised at the beginning of swelling tests stated earlier. Hence, no additional moisture is trapped in the sample after drying for 24 hours at 100°C. **Figure *5-10*** shows what the dried-up laponite sample looks like after completing the first swelling test. It is obvious that the dried laponite resembles irregular crystal shapes rather than a fine powder. This crystal-shaped laponite breaks down into smaller pieces when moderate pressure is given by hand, but not as finely as it was at initial state.

The reswelling behaviour of laponite hydrogel is shown in **Figure *5-11***(a). It is stated evidently that laponite reaches an equilibrium state in all reswelling experiments in less than 60 hours. On the other hand, the fresh laponite powder achieves equilibrium after 660 hours (see **Figure *5-8***), as discussed earlier. Furthermore, when the wetting and drying phases of the sample increase, the final swelling height decreases. In the reswelling tests 1, 2, 3, and 4, the final swelling strains of the identical sample are 1.13, 0.84, 0.58, and 0.40 mm/mm, respectively, representing a decrease between 16% and 60% as compared with the initial swelling strain. The outstanding reswelling capacity of the laponite hydrogel is likely due to its robust cross-linked skeleton structure, which is similar to that of PPA-based nano-composite hydrogel [58]. As with other clay minerals, laponite is composed of two basic blocks: silicon-oxygen tetrahedron and aluminum octahedron. Individual tetrahedrons share three out of four oxygens and are arranged in a hexagonal arrangement with the basal oxygens connected and the apical oxygens pointing up/down in the tetrahedral sheets. Octahedral sheets are made of individual octahedrons that share edges made up of oxygens and hydroxyl anion bases, with Al^{3+}, Mg^{2+}, and Fe^{2+} serving as the coordinating cations. These octahedrons are organised in a hexagonal pattern [59]. The cross-linked structure of the hydrogel is broken down as a result of repeated wetting and drying processes. This can be explained as a charge shielding effect of excess cations causing an osmotic pressure difference, resulting in increased water absorption performance [57]. The consequence is primarily due to the continually swelling-induced breakdown of the cross-linked structure. Hence, the graphs of reswelling tests 1 and 2 show the higher swelling height compared to the swelling height of the fresh laponite hydrogel. In the case of reswelling tests 3 and 4, laponite hydrogel has reduced swelling height and the shape of the graphs look similar to the fresh laponite.

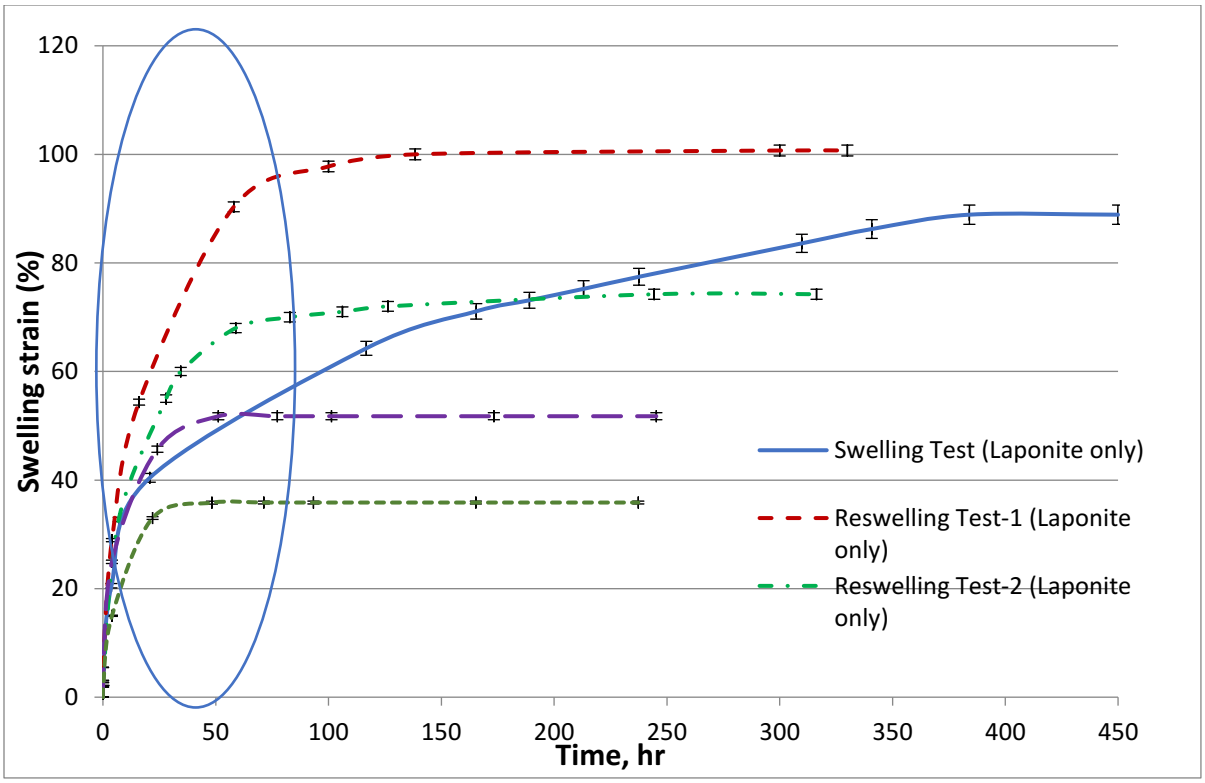

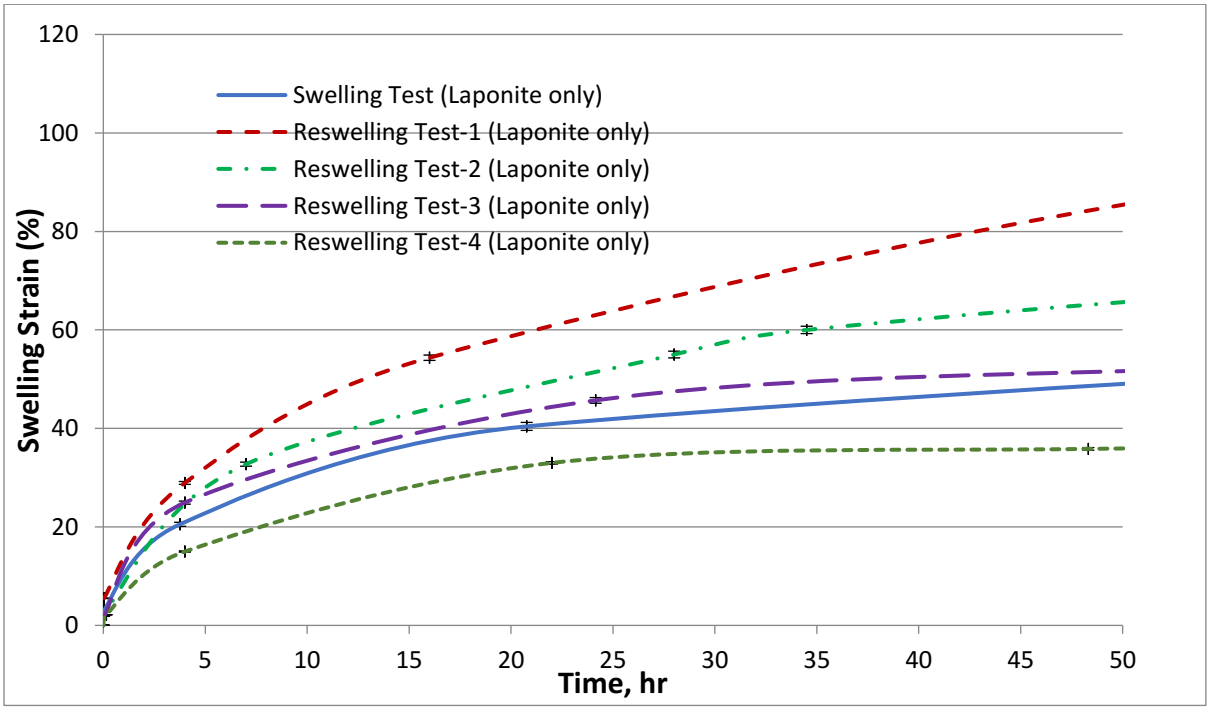

Figure 5-11: (a) Swelling strain of compacted laponite hydrogel from the swelling and reswelling tests, (b) close-up of the swelling strain of the compacted laponite hydrogel from the swelling and reswelling tests for the initial 50 hours.

Figure *5-11*(b) displays the close-up view of the pattern of the reswelling graphs of the initial and primary swell states for the initial 50 hours. The reswelling plots exhibit extremely tiny initial swell states, as can be observed. The primary swelling phases of the reswelling plots are steeper and faster than those of the fresh laponite swelling plots. Because of its great repeated swelling performance, laponite can limit the migration of contaminants, permeability of water bodies as well as formulate high-performance water-based drilling fluids [14]. As a result, it may save more money in its applications, indicating a wide range of applications in the biomaterial industry.

5.4.2.1 **Water Retention Ratio**

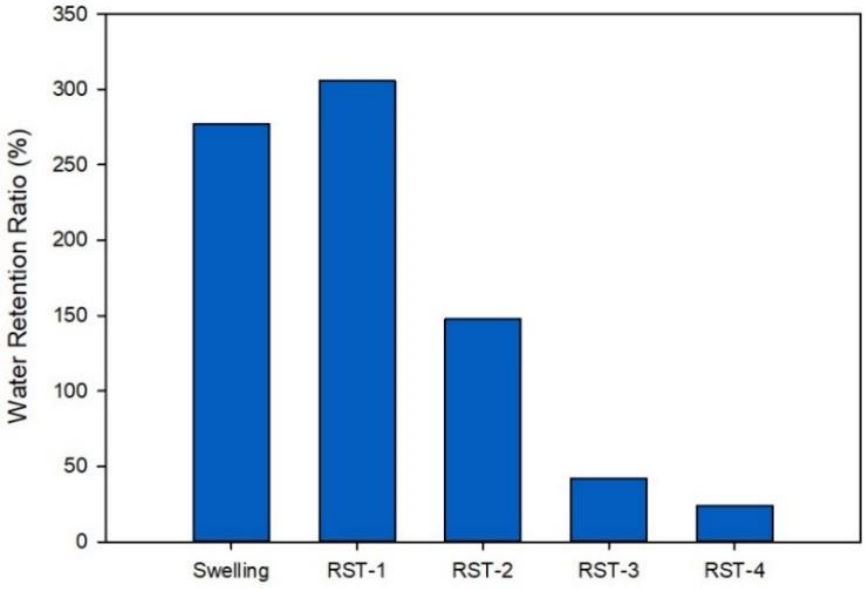

Figure 5-12: Water Retention Ratio (%) of the swollen laponite hydrogel during the reswelling tests at room temperature (23°C)

The ability of the soil to retain water is a crucial factor in determining the soil's practical use in the civil engineering applications. Changes in the water retention ratio due to seasonal weather variations or other artificial factors, can modify the mechanical properties of soils, especially on clay soils. This may ultimately change the soil's volume, causing flooding, slope displacement, rock falls, landslides, and damage to foundations. Thus, the water retention ability of laponite hydrogel was studied after each drying and wetting process during the tests. **Figure *5-12*** demonstrates that the water retention ratio of the swollen laponite hydrogel gradually decreases as the drying and wetting process increases, which is compatible with the results of **Figure *5-11***(a). This water retention property is related to its cross-linked structure and a mass of -*OH* groups. The

van der Waals force and *H*-bonding between the water molecules and polymer determine the water retention performance [27]. The pore morphology of hydrogels can be related to the water uptake capacity [38]. The cross-linked structure of the hydrogel is broken down due to repeated wetting and drying processes, resulting in forming the hydrogels with a denser and tighter structure with a smaller pore size. As a result of the tighter structure, hydrogels become more rigid and require an additional compressive force to be deformed. According to Mulhbacher et al. [60], the tighter structure would reduce the water uptake capacity by impeding the mobility of the polymer chains. The degree of swelling reduced due to the formation of a more tightly cross-linked structure.

5.4.3 Bentonite Swelling

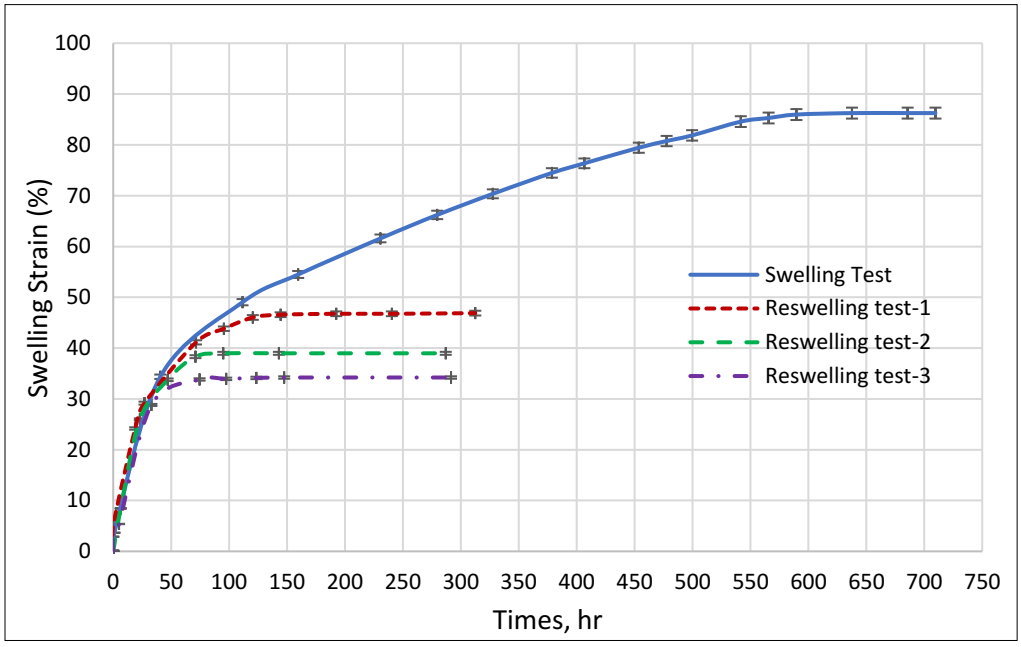

Figure 5-13: Swelling strain of the compacted bentonite from the swelling and reswelling tests

A series of experiments were carried out in a comparable laboratory setting to investigate the repeated swelling properties of laponite and bentonite (i.e., montmorillonite). Similar to laponite, 8 g of dry bentonite was used for the swelling tests. In the primally sample preparations, it was observed that the fresh bentonite has a lower swelling height than laponite. **Figure *5-13*** shows the results of the swelling and reswelling tests of bentonite. The swelling ratio of bentonite decreased as swelling time increased, supporting the findings of Chen et al. [57]. The pattern of bentonite swelling ratio is different from that of laponite, as seen in **Figure *5-11***(a, b). As seen in **Figure *5-8***

and **Figure *5-11***(a, b), laponite has a higher swelling capacity than bentonite. This is likely due to its smaller particle size of laponite as compared with bentonite.

5.4.4 Study of Hydrogel

Figure 5-14: (a) Laponite hydrogel after the initial swelling test, (b) after the reswelling test-1 (laponite only), and (c) after the reswelling test-2 (laponite only)

The hydrogels were thoroughly examined after the swelling and reswelling tests. In addition to the water absorption capacity, the colour changing pattern of hydrogels is also important. Colour is an important feature of many materials, particularly hydrogels. Incorporating a stimulus-responsive moiety into the hydrogel backbone is one of the most efficient ways to make hydrogels with colour-changing properties [58]. According to Klajn [61], colourless spiropyran (photochromic dyes) and colour merocyanine have different physicochemical properties and have particular attention in the development of colour-changing hydrogels due to their high fatigue resistance and multi-stimuli responsive properties. The spiropyran moiety is introduced into the hydrogel network by copolymerizing water-insoluble derivatives with water soluble monomer in aqueous/organic mixed solution [62,63]. **Figure *5-14*** illustrates the colours of the hydrogels from identical laponite sample following the initial swelling test, reswelling tests 1, and 2. The colour becomes darker as the number of experiments increases with the same sample. The colour of hydrogel following the swelling test with fresh laponite powder is described as practically colourless and transparent. Stimulatingly, the colour of hydrogel brightens and whitens after the reswelling test 1, but darkens and loses its glossiness after the reswelling test 2. Several parameters, including the quantity and kinds of ions, solution *pH*, ionic strength, and temperature, might affect water absorption capacity and colour changing effects [64]. In this study, temperature, deaired distilled water, and all other parameters were identical for all the swelling and reswelling tests.

Hence, the wetting and drying procedures can cause the breakdown of the cross-linked structural skeleton of laponite, resulting in colour variance. Aside from the colour and glossiness, there is a lubricating effect to consider. It has been seen that as the testing progressed, the lubrication of hydrogels decreased and became harder in comparison to the fresh hydrogel. In the other words, the hydrogel loses its lubricating properties and becomes stiffer as the number of tests increases. This study can not present any lubrication index/data due to the lack of laboratory facilities. The loss of lubrication of laponite hydrogel may be attributed to the changing of its viscosity due to the repeated swelling tests.

5.4.5 Uneven Swelling Surface

After the initial swelling test with fresh laponite power, the upper surface of the hydrogel is not consistently flat but rather sloped. This indicates that the swelling of laponite powder is not homogeneous throughout. It was challenging to capture that photograph to show in this study. Surprisingly, the uneven swelling surface of hydrogel is only observed in the initial swelling tests; none of the reswelling tests show anything like that. The following are some probable explanations:

- *First*: The dry fresh laponite powder is put on the porous stone in the bottom of the oedometer cell and gently shake it to spread it evenly. The non-uniform distribution of laponite powder into the cell could be one of the causes of the uneven swelling surface.
- *Second*: Another possible reason may be related to consolidation. Before starting the swelling tests, dry laponite samples were put under massive loads for consolidation. The load pad at the top of the cell cap was used to place this load. There is a possibility of non-uniform alignment of the load pad, which eventually developed inconsistent consolidation in the samples.
- *Third*: There is a gauge on top of the load pad attached to the oedometer cell cap. The load pad was positioned in the centre of the cap and every option was tried to keep it steady throughout the testing time. However, the cell cap became inclined within a couple of days of the swelling tests. Hence, the load pad of the cell may not be positioned in a centroidal location most likely.
- *Fourth*: Another reason may be related to laponite swollen pattern. Laponite powder itself may not be uniformly swollen at each point. There is no published evidence regarding this issue. More research should be conducted in detail on this matter.

In the case of reswelling tests, the swollen surface of the hydrogel is flat, not slopy. The most likely reason is that laponite samples are no longer fine powder but crystal-shaped type, which swell very quickly by absorbing water within 72 hours. The initial and primary swell states of the reswelling tests are quicker/faster than that of the initial swelling test.

5.4.6 Swelling Pressure of Laponite

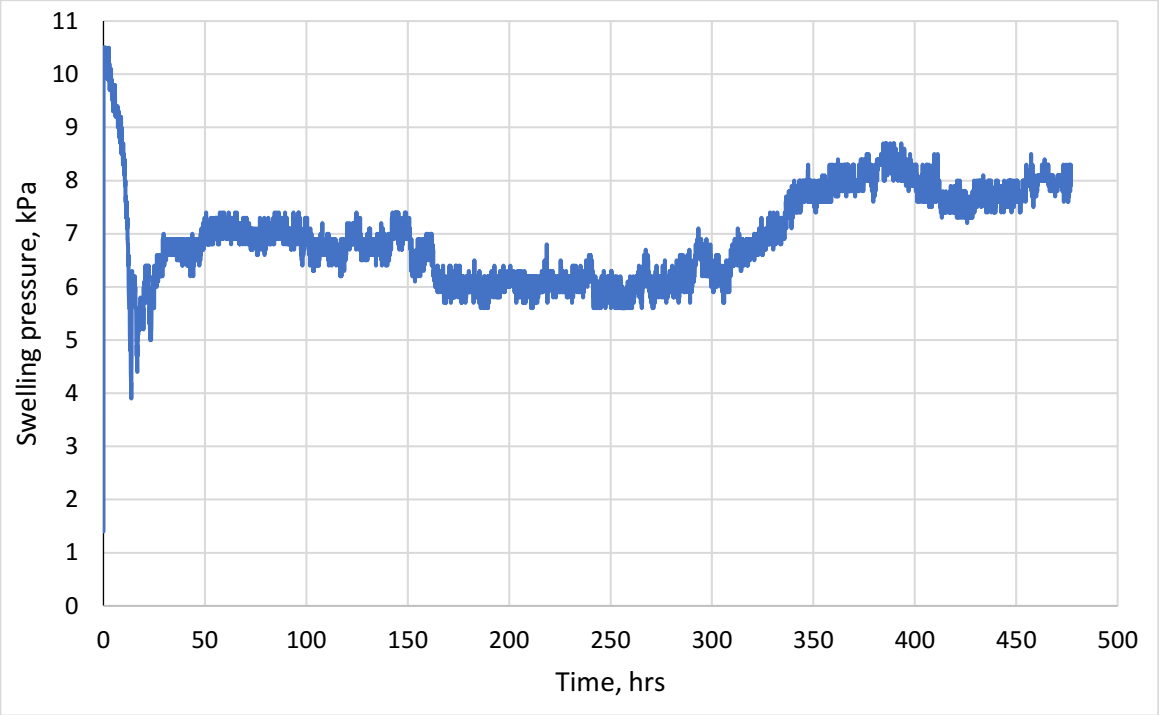

Figure 5-15: Swelling pressure of the compacted laponite hydrated with water

Several trials were undertaken to identify the correct mass of laponite sample suitable for the swelling pressure tests. The early trials used 8 g laponite samples to maintain consistency with the swelling deformation testing, although the findings were inconclusive. After that, the amount of sample was gradually increased and finally 60 g laponite sample was used at fully saturated condition. The most key feature of this test was keeping the volume consistent. Only data relevant for discussion is presented here, given that the entire presentation of test data would be too lengthy to include here. **Figure *5-15*** depicts the evolution of the swelling pressure measured by Pore Pressure Transducer (PPT). The dry compacted laponite became entirely hydrated within the initial 3.5 hours, while the swelling pressure was at a peak (about >10 kPa). Nano-clay absorbs water and expands into interlayers, occupying the void in laponite during water uptake. As a result, the volume of montmorillonite increases, resulting in swelling pressure [20]. The swelling pressure

rises quickly as the volume remains constant in this stage. After that, the pore pressure drops to 3.9 kPa at 13.7 hours and then starts rising again. Finally, there is no void to absorb water intake; hence the volume of montmorillonite cannot increase any further. At this point, the swelling pressure of the compacted laponite is measured, which varies in a range from 5.6 to 8.6 kPa throughout the experiment. The interlayer and double-layer forces are responsible for the swelling behaviour of laponite.

5.5 Conclusions

This study investigated the swelling height, reswelling behaviour, and swelling pressure of laponite hydrogel. It is speculated that the swelling process could affect the soil-nanoparticle structure.

- The swelling height of laponite has been investigated by three different methods. (a) The tea bag test, which is the most common method for assessing the hydrogel swelling, was ineffective in the case of laponite. (b) According to the visual tube test, laponite swells 2%-3.7% after 72 hours. (c) According to the Oedometer cell test, laponite took around 4 weeks to attain equilibrium. Due to the rapid expansion of matric suction dissipation, graph of the initial swell stage rose sharply. Compared to the initial swell stage, the secondary swell progressed slowly and took a long time to complete, owing to the adsorption-desorption reaction.
- The scanning electron microscope images revealed that the structures of swollen laponite are continuous sheet-like irregular structures with non-porous pore size. The network of hydrogel seems denser, resulting in a shrunken condition. The pore structure inside laponite hydrogel is made up of polymer tough branches; it can act as a storage space for water molecules. When the hydrogel absorbs water, the stress is adequately distributed by these polymer branches, ensuring the stability of the network structure.
- The results of this study show that the swelling height increases with the increase of laponite in the soil mixture. The swelling height of sand-laponite mixture with 3% laponite reached equilibrium after 40 hours, whereas the swelling height of sand-laponite with 5% laponite specimen did not reach equilibrium even after 50 hours. As the concentration of laponite rose, so did the swelling height and time to reach equilibrium.
- In the reswelling tests, laponite reached equilibrium within 60 hours. When the wetting and drying processes of the sample increase, the final swelling height shortens. The result is mostly

due to the repeatedly swelling-induced breakdown of the cross-linked structure. The reswelling plots have steeper and faster primary swelling phases than the fresh laponite swelling plots.

- As the number of drying and wetting processes rises, the water retention ratio of the swollen laponite hydrogel steadily decreases, which is entirely consistent with the swelling test results. Because of the creation of a more firmly cross-linked structure, the degree of swelling was reduced.
- As the number of experiments with the same sample increases, the colour of hydrogel becomes darker.
- Moreover, the laponite hydrogel loses its lubricating characteristics and gets stiffer as the number of tests increases.
- The upper surface of hydrogel is not consistently flat after the initial swelling test with fresh laponite power but rather slopy. Surprisingly, the uneven hydrogel swelling surface is only seen during the initial swelling test; none of the reswelling tests reveal anything similar.
- In addition, the swelling pressure of compacted laponite is found between 5.6 and 8.6 kPa throughout the experiment, which is caused by the interlayer and double-layer stresses.

5.6 References

[1] Berrill J, Christensen S, Keenan R, Okada W, Pettinga J (2001) Case Studies of Lateral Spreading Forces on a Piled Foundation. *Geotechnique* 51(6):501–517.

[2] Dodry R, Abdoun T (2001) Recent studies on seismic centrifuge modelling of liquefaction and its effect on deep foundation. *Proceedings of the 4th International Conference on Recent Advance. Geotechnical Earthquake Engineering and Soil Dynamics and Symposium* in Honour of Professor W. D. Liam Finn, San Diego, California.

[3] Madabhushi S, Patel D, Haigh S (2001) Draft version of "EEFIT report on observations of the 26th Jan 2001 Bhuj earthquake in India. Institution of Structural Engineers, UK.

[4] Bhattacharya S, Bolton M, Madabhushi S (2005) A reconsideration of the safety of the piled bridge foundations in liquefiable soils. *Soils and Foundations* 45(4):13–26.

[5] Bhattacharya S, Madabhushi S, Bolton M (2004) An alternative mechanism of pile failure in liquefiable deposits during earthquakes. *Geotechnique* 54(3):203–213.

[6] Joshi YM, Reddy GR, Kulkarni A, Kumar N, Chhabra R (2008) Rheological behaviour of aqueous suspensions of laponite: new insights into the ageing phenomena. *Proceedings of the Royal Society*, 464: 469-489.
[7] Mourchid A, Delville A, Lambard J, Lecolier E, Levitz P (1995) Phase diagram of colloidal dispersions of anisotropic charged particles; equilibrium properties, structure and rheology of laponite suspensions. *Langmuir* 13: 1942-1950.
[8] Mourchid A, Lecolier E, Van Damme H, Levitz P (1998) On viscoelastic, birefringent, and swelling properties of Laponite clay suspensions: revisited phase diagram. *Langmuir*, 14(1y), 4718-4723.
[9] Agapoulaki G, Papadimitriou A (2018) Rheological Properties of Colloidal Silica Grout for Passive Stabilization Against Liquefaction. *J of Materials in Civil Eng* 30(10): 04018251.
[10] Ochoa-Cornejo F (2015) Cyclic behaviour of sands with superplastic fines. A dissertation submitted for the degree of Doctor of Philosophy, Purdue University, West Lafayette, IN, United States.
[11] Ochoa-Cornejo F (2017) Dynamic Behavior of Sand with NanoParticles. Proceedings of the 19th International Conference. *Soil Mechanics and Geotech Eng*, Seoul.
[12] Ochoa-Cornejo F, Bobet A, Johnston C, Santagata M, Sinfield J (2016) Cyclic behavior and pore pressure generation in sands with laponite, a super-plastic nanoparticle. *Soil Dyn Earthquake Eng* 88:265–279.
[13] Huang Y, Wang L (2016) Laboratory investigation of liquefaction mitigation in silty sand using nanoparticles. *Eng Geology* 204:23–32.
[14] Huang XB, Sun JS, Huang Y, Yan BC, Dong XD, Liu F, Wang R (2021) Laponite: A promising nanomaterial to formulate high-performance water-based drilling fluids. *Pet Science* 18:579-590.
[15] Omar M, Shanableh A, Al Zaylaie M (2016) Modification of the swelling characteristics and phosphorus retention of bentonite clay using alum. *Soils and Foundations* 56(5):861–868.
[16] Bertrand T, Peixinho J, Mukhopadhyay S, MacMinn C (2016) Dynamics of swelling and drying in spherical gel. *Physical Review Appl* 6(064010).
[17] Fernandez-Nieves A, Wyss H, Mattsson J, Weitz D (2011) Microgel Suspensions: Fundamentals and Applications. John Wiley & Sons, Inc., New York.

[18] Barbour S, Fredlund D (1989) Mechanisms of osmotic flow and volume change in clay soils. *Canadian Geotech J* 26(4):551–562.
[19] Madsen F, Muller-Vonmoos M (1989) The swelling behaviour of clay. *Applied Clay Science* 4:143–156.
[20] Gonzalez S (2013) The swelling pressure of bentonite and sand mixtures. Master thesis in Chemical Engineering, KTH Chemical Science and Engineering.
[21] Liu L (2012) Hydraulic properties of unsaturated bentonite. Department of Chemical Engineering and Technology, Royal Institute of Technology.
[22] Liu L, Neretnieks I (2010) Interaction between colloidal particles: Literature Review (SKB-TR--10-26; INIS 41(37)). School of Chemical Science and Eng, Royal Inst of Technology.
[23] Mokni N, Olivella S, Valcke E, Marien A, Smets S, Li X (2011) Deformation and flow driven by osmotic processes in porous materials; application to bituminised waste materials. *Transp Porous Med* 86:635-662.
[24] Yong R (1999) Overview of modeling of clay microstructure and interactions for prediction of waste isolation barrier performance. *Eng Geology* 54:83–91.
[25] Kramer S (1996) Geotechnical Earthquake Engineering. Pearson Education India.
[26] He Y, Ye W, Chen Y, Zhang K, Wu D (2020) Effect of NaCl solution on the swelling and shrinkage behaviour of compacted bentonite under one-dimensional conditions. *Engineering Geology and the Environment* 79:399–410.
[27] Chen YG, Sun Z, Cui YJ, Ye WM, Liu QH (2019) Effect of cement solutions on the swelling pressure of compacted GMZ bentonite at different temperature. *Const Build Mat* 229:116872.
[28] Alonso E, Romero E, Hoffemann C, Garcia-Escudero E (2005) Expansive bentonite/sand mixtures in cyclic controlled suction drying and wetting. *Eng Geol* 81:213–226.
[29] Romero E (1999) Characterisation and thermo-hydro-mechanical behaviour of unsaturated Boom clay: An experimental study. Doctoral thesis, Universitat Politècnica de Catalunya. Departament d'Enginyeria del Terreny, Cartogràfica i Geofísica.
http://hdl.handle.net/2117/93536
[30] Mollins L, Stewart D, Cousens I (1996) Predicting the properties of bentonite-sand mixtures. *Clay Minerals* 31:243–252.

[31] Sun D, Cui H, Sun W (2009) Swelling of compacted sand-bentonite mixtures. *Applied Clay Science* 43:485–492.
[32] Xiang G, Ye W (2020) Swelling of bentonite-sand mixtures after long-term dissolution in alkaline solution. *Clays and Clay Minerals* 68(5):491–498.
[33] Valencia GA, Djabourov M, Carn F, Sobral PJA (2018) Novel insights on swelling and dehydration of laponite. *Colloid and Interface Science Communications* 23: 1-5.
[34] BYK (2014) Technical Information B-RI 21: Laponite performance. a member of Altana, Germany. https://docplayer.net/23462772-Technical-information-b-ri-21-laponite-performance-additives.html
[35] Kroon M, Vos G, Wegdem G (1998) Structure and formation of a gel of colloidal disks. *Physical Review E* 57:1962–1970.
[36] Tawari S, Koch A, Cohen C (2001) Electrical double-layer effects on the Brownian diffusivity and aggregation rate of Laponite clay particles. *J of Colloid and Interface Science* 240:54–66.
[37] Siddique S, Khatiwada J, Shrestha S, Chio C, Chen X, Mohamedelhassan E, Deng J, Qin W (2022) Effect of Laponite Nanoparticles on Growth Characteristics and Chlorophyll Content of *Chlorella* sp. *Water Air Soil Pollut* 233:308.
[38] Yacob N, Hashim K (2014) Morphological effect on swelling behaviour of hydrogel. Advancing Nuclear Research and Energy Development. *AIP Conf Proc* 1584:153–159.
[39] Nesse W (2000) Introduction to mineralogy. New York: Oxford University Press.
[40] Sutherland W (2014) Wyoming Bentonite. Wyoming State Geological Sur. Retrieved 12 Jan 2021.
[41] Jackson J (1997) Bentonite. Glossary of geology (4th Ed.). American Geological Institute.
[42] ASTM-D6913 (2017) Standard Test Methods for Particle-Size Distribution (Gradation) of Soils Using Sieve Analysis. ASTM International.
[43] ASTM-D2216-19 (2019) Standard Test Methods for Laboratory Determination of Water (Moisture) Content of Soil and Rock by Mass. ASTM International.
[44] ASTM-C128-15 (2015) Standard Test Method for Relative Density (Specific Gravity) and Absorption of Fine Aggregate. ASTM International.
[45] Komine H, Ogata N (1999) Experimental study on swelling characteristics of sand-bentonite mixture for nuclear waste disposal. *Soil Found* 39:83–97.

[46] Karnland O, Muurinen A, Karlsson F (2005) Bentonite swelling pressure in NaCl Solutions-Experimentally determined data and model calculations. In Advances in Understanding Engineered Clay Barriers (pp. 241–256). Taylor and Francis Group.
[47] Wang Q, Tang A, Cui YJ, Delage P, Gatmiri B (2012) Experimental study on the swelling behaviour of bentonite/claystone mixture. *Eng Geol* 124:59–66.
[48] ASTM-D5890-11 (2021) Standard Test Method for Swell Index of Clay Mineral Component of Geosynthetic Clay Liners. ASTM International.
[49] El Mohtar C, Bobet A, Santagata MC and Drnevich VP (2013) Liquefaction mitigation using bentonite suspensions. ASCE *J Geotech Geoenviron Eng*, 139(8):1369–1380.
[50] Rao S, Shivananda P (2005) Role of osmotic suction in swelling of salt amended clays. *Can Geotech J* 42:307–315.
[51] Sridharan A, Gurtug Y (2004) Swelling behaviour of compacted fine-grained soils. *Eng Geol* 72(1):9–18.
[52] Rao S, Thyagaraj T (2007) Swell-compression behaviour of compacted clays under chemical gradients. *Can Geotech J* 44:520–532.
[53] He Y, Chen Y, Ye W, Cui YJ (2016) Influence of salt concentration on volume shrinkage and water retention characteristics of compacted GMZ bentonite. *Environ Earth Sci* 75(6):535.
[54] Rao S, Thyagaraj T, Thomas H (2006) Swelling of compacted clay under osmotic gradients. *Geotechnique* 56(10):707–713.
[55] Ye W, Zhang F, Chen B, Chen Y, Wang Q, Cui YJ (2014) Effects of salt solutions on the hydro-mechanical behaviour of compacted GMZ01 bentonite. *Environ Earth Sci* 72(2):2621–2630.
[56] Shackelford C, Daniel D (1991) Diffusion in saturated soil: Back-ground. *J Geotech Geoenviorn* 117(3):467–484.
[57] Chen M, Shen Y, Xu L, Xiang G, Ni Z (2020) Synthesis of a super-absorbent nanocomposite hydrogel based on vinyl hybrid silica nanospheres and its properties. *Royal Society of Chemistry Advances* 10:41022–41031.
[58] Jia Z, Sukker I, Muller M, Schonherr H (2018) Selective discrimination of key enzymes of pathogenic and nonpathogenic bacteria on autonomously reporting shape-encoded hydrogel patterns. ACS *Appli Mater Interfaces* 10(6):5175–5184.

[59] Guggenheim S, Martin R (1995) Definition of clay and clay mineral; joint report of AIPEA nomenclature and CMS nomenclature committees. *Clay Clay Miner*. 43:255–256.
[60] Mulhbacher J, Ispas-Szabo P, Mateescu M (2004) Cross-linked high amylose starch derivatives for drug release II. Swelling properties and mechanistic study. *Int J of Pharmaceutics* 278:231–238.
[61] Klajn R (2014) Spiropyran-based dynamic materials- review article. *Chem Soc Rev* 43:148–184.
[62] Schiphorst ter J, Coleman S, Stumpel J, Azouz A, Diamond D, Schenning A (2015) Molecular design of light-responsive hydrogels, for in situ generation of fast and reversible valves for microfluidic applications. *Chem Mater* 27(17):5925–5931.
[63] Wang B, Xiao X, Zhang Y, Liao L (2019) High strength dual-crosslinked hydrogels with photo-switchable colour changing behaviour. *European Polymer J* 116:545–553.
[64] Adeyemo A, Adeoye I, Bello O (2017) Adsorption of dyes using different types of clay; a review. *Appl Water Sci* 7: 543–568.

CHAPTER 6 Experimental Investigation of Damping Ratio of Sand-Laponite Mixtures Using One-dimensional Bender Elements

Abstract

Damping ratio and dynamic shear modulus are fundamental parameters that are used to assess the seismic response of geotechnical structures such as retaining walls, dams, tunnels, foundations, landfill covers, and embankments. Numerous sources of seismic waves, which are generated by a variety of sources, can impact the stability and integrity of geotechnical structures, as well as having a big influence on the design decisions and the application of alternate solutions. In this study, the damping ratio of sand mixed with small quantities of laponite has been determined by an experimental set-up using bender elements which was meticulously constructed for this study. Similar experiments were conducted with pure sand (i.e., control test) and sand mixed with bentonite and compared with the results of the sand-laponite mixtures. This study reveals that the damping ratio (ξ) of pure sand is around 7.48% which is in general compatible with values reported in the literature, taking into account the variations of sand, and errors associated with laboratory equipment and/or electronic devices. After continuous shaking, the damping ratio of pure sand gradually drops until it reaches equilibrium (ξ=0.99%) on Day 3–4, which is relatively small in comparison to the damping ratio at the starting of the test. The findings reveal that the highest damping ratio of sand+1% laponite, sand+2% laponite, and sand+3% laponite samples are approximately 59%, 69.7%, and 98.6%, respectively. After reaching the peak, the damping ratio starts to decline gradually and reaches equilibrium at 11%, 16%, and 19.4% for sand +1%, +2%, and +3% laponite, respectively. The higher damping values for the sand-laponite specimens reflect a viscous damping contribution from the presence of laponite at sand grain contacts: the greater the amount of laponite trapped at the contacts, the greater the increase in damping. The current study also found that the peak damping ratio of sand-bentonite samples is about 21.9%, 42.7%, and 67.9% in the case of sand+1% bentonite, sand+2% bentonite, and sand+3% bentonite, respectively.

Keywords: Piezoceramics, bender element, damping ratio, half-power bandwidth method, frequency, amplitude

**A version of this chapter has been submitted for publication (under review)*

6.1 Introduction

The damping ratio is an important parameter of the dynamic characteristics of soils and is essential for analyzing the seismic response of soil and foundation as well as seismic zoning (Xie 2011). Understanding the dynamic behavior of soils at small strains is crucial for predicting ground movement and performance of earth structures. Shear modulus is correlated to shear wave velocity and bulk density, whereas the damping ratio reflects the energy dissipation of soil under dynamic or cyclic loading (Ishihara, 1996, Mog and Anbazhagan 2022). It is important to study the dynamic characteristics of soil in order to assess the potential for catastrophes under seismic events and severe dynamic loadings. Several damping (i.e., energy dissipation) parameters are used by engineers and scientists while the damping ratio is commonly used in geotechnical engineering.

If a cycle of loading is repeated for numerous cycles, the stress-strain relationship becomes a closed, hysteretic loop. Two parameters can be used to describe this loop: (a) the slope of the line connecting the loop's endpoints, and (b) the area enclosed by the loop. The shear modulus is defined by the slope of the line whereas the enclosed loop area is correlated to damping (Figure 6-1). Damping describes the quantification of the energy dissipation during cyclic loading of an inelastic medium. In other words, damping is the dissipation of energy at the grain-to-grain contact level due to friction interactions (Ram and Mohanty, 2023; Ham et al., 2012; Delfosse-Ribay et al., 2004). Therefore, to accurately describe soil response to cyclic loading, the damping needs to be accounted for in more accurate and realistic models (Park, 1998). The two general categories of damping are internal damping and external damping. Internal damping is an inherent material property that is often referred to as 'material damping'. It describes the dissipation of energy within the material due to microstructural factors such as inter-particle sliding and friction, structural rearrangement, and pore fluid. In contrast, external damping refers to the energy losses within a structure due to factors other than internal friction. Thus, external damping is termed 'system damping' because it is not an inherent element of the martial (Ashmawy et al., 1995).

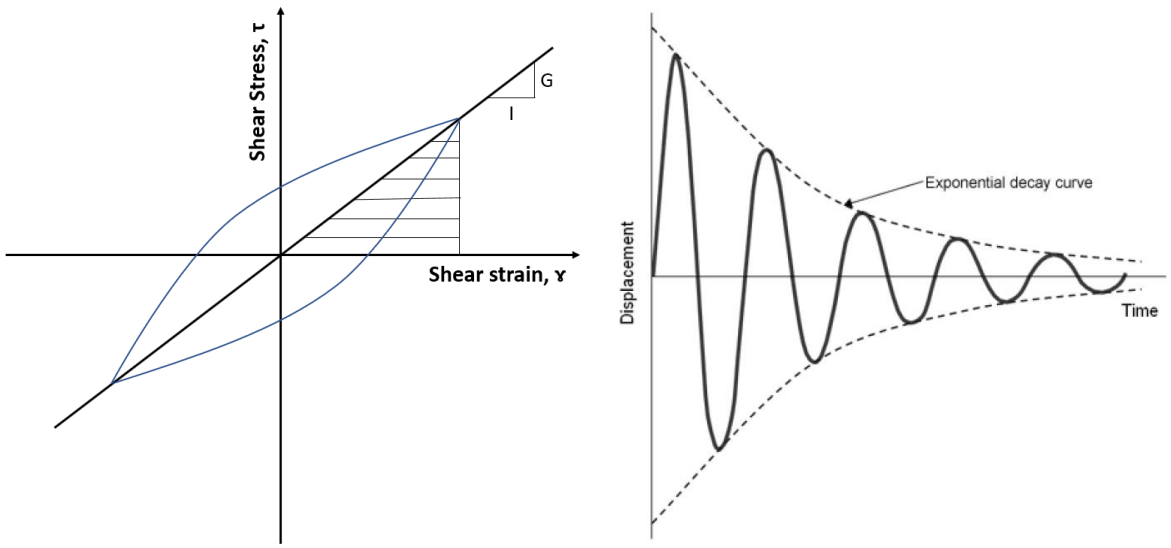

(a) (b)

Figure 6-1: (a) Hysteretic loop, shear modulus, and damping, after Park (1998), and (b) Effect of damping in a single degree of freedom system, after Moreira (2015)

In internal damping, inelastic friction loss occurs at particle interactions when soil is subjected to cyclic loading, resulting in inelastic, irreversible relative displacement between particles (Moreira, 2015; Ferreira, 2008; White, 1983; Stoll, 1989). This friction loss is difficult to estimate as it is a function of normal force at the particle's interface and the friction of contacting surfaces. The relative displacement may not even create interparticle friction at very small strains (Santamarina et al, 2001). The frequency of vibration has little effect on the inelastic friction loss (Spang and Wesley, 1995; Park, 1998). The fluid flow loss in internal damping is related to the energy dissipation that occurs by fluid flow drag because of the relative movement of water and soil grains, resulting in shear forces at the water-soil interface. This loss is proportional to velocity as well as the frequency of vibration (Park, 1998). When compared to conventional soil dynamics problems, which involve low frequencies, the frequency at which this phenomenon contributes to damping is relatively high (Moreira, 2015; Ferreira, 2008; White, 1983). There are two types of testing methodologies for determining the dynamic soil parameters: (i) low strain which can be classified as elastic, and (ii) high strain which is influenced by plasticity (Karl, 2005). Low-strain laboratory tests include both bender element and resonant column tests whereas low-strain field tests utilize the propagation of seismic waves by creating vibrations in soil and monitoring them using sensors. Seismic reflection testing and borehole procedures are examples of field tests.

Traditional static testing, such as seismic penetrometer, pressure meter, and dilatometer tests, are included in high-strain tests. High-strain tests comprehend the conventional static tests, such as simply/cyclic shear tests and cyclic triaxial tests. Either time-domain or frequency-domain study can be used to determine the damping ratio. A frequency-domain analysis entails converting data into frequency with respect to time. In other words, a frequency-domain graph depicts how much of the signal has a specific frequency. A time-domain graph depicts how amplitude changes over time. A transform function must be applied to convert data from the time domain to the frequency domain and vice versa. The Fourier transform, which is based on the Fourier's analysis theory, is the most often used transform function. According to the Fourier (1822)'s theory, complex functions, such as seismic waves, can be broken down into a sum of simpler sinusoidal functions with their frequency component. The Fast Fourier Transform (FFT) is a fast computation approach for the Discrete Fourier Transform (DFT) which is used in this study. The FFT or DFT converts an array of N-real values of sample data, with intervals according to the sampling interval (inverse of sampling frequency) into N-complex values of transformed, dimensionless sample data, with equally spaced intervals that do not correspond to time or frequency. The sampling frequency is utilized to establish a relationship between the dimensionless data (also known as bins) and their corresponding frequency range. The magnitude and phase of the signal are represented by these complex numbers, which are related to the real and imaginary parts of the processed data, respectively. The FFT-calculated spectrum is symmetric; therefore, the second half of the data is redundant. Choosing the number of degrees of freedom to allocate to the test subject is one of the grey areas in this sort of modal testing (Inmann, 2001). This single degree of freedom method is the simplest approach to utilize on this type of data.

Bender element testing has been successfully used to determine the damping ratio in triaxial cells (Ferreira, 2003; Moreira, 2015). The bender element equipment is reasonably easy to set up, the test is short, and no additional special equipment is needed to obtain the test results. Therefore, using bender elements to acquire the damping as well as other dynamic soil parameters, is a competitive method. Increasing the amount of montmorillonite in soil has been shown to increase cyclic strength, which in turn increases resistance to soil liquefaction (Lin et al., 2020; Beroya et al., 2009; Gratchev et al., 2007; Tiwari and Ajmera, 2011). During the primary consolidation, the dynamic shear modulus of remolded kaolinite and Ca-montmorillonite increased by 10% and 40%, respectively (Marcuson and Wahls, 1972). However, the impact of clay mineralogy on the damping

ratio remains unclear. Due to the rapid advancement of nanotechnology, it has been suggested that laponite be integrated with sand to reduce the risk of liquefaction during the ground vibrations (Huang and Wang 2016; Ochoa-Cornejo et al., 2016; Getchell et al., 2022). It has been reported in Ochoa-Cornejo (2015) that higher damping values for sand-laponite specimens reflect a viscous damping contribution from the presence of laponite at sand grain contacts. However, the damping ratio (ξ) of the treated sand is not thoroughly examined.

The objective of this study is to investigate the damping ratio of sand specimens mixed with laponite using a one-dimensional bender elements setup. Similar experiments were conducted with pure sand (i.e., control test) and sand mixed with bentonite to compare the findings. In this study, the bender elements set-up was meticulously built from ground, step-by-step. The experimental materials are introduced in Section 6.2, and the experimental methodologies and procedures including the setup of the bender elements are presented in Section 6.3. In Section 6.4, the experiment findings were compared and discussed. Section 6.5 concludes the paper.

6.2 Experimental Materials

6.2.1 Sand

Sand provided by Pioneer Construction, Thunder Bay, Ontario, Canada, was used in this Study. The grain size distribution analysis was performed according to ASTM D6913 (2017). The median diameter, $i.e., d_{50}$, of sand is 0.62 mm and the fines are <5% of the total mass. The uniformity and curvature coefficients of sand were found to be 4.40 and 0.74, respectively. According to the Unified Soil Classification System, the group symbol of sand is SP and the group name is poorly graded sand. The natural moisture content and specific gravity of sand, obtained in accordance with ASTM D2216-19 (2019) and ASTM C128-15 (2015), were 9.5% and 2.6.

6.2.2 Nanoparticles

6.2.2.1 **Laponite**

Laponite is a synthetic multilayer silicate made from inorganic mineral elements found in nature. As a hectorite clay, laponite is composed of disk-shaped nanoparticles with two silica tetrahedral layers and one magnesium octahedral layer layered structure (BYK, 2014). In a dry state, laponite is a fine white power with a diameter of around 25 nm, a thickness of 1 nm, and a specific gravity of 2.57 (Kroon, 1998). Estimates of the face and edge charges of laponite synthesized in deionized water using pH and conductivity measurements showed that the positive charge on the crystal

edges (4-5 mmol/100 g) is approximately 10% of the overall negative charge on the crystal faces (50-55 mmol/100 g) (BYK, 2014; Tawari et al., 2001). When dispersed in water, laponite hydrates, swells and produces a colorless, transparent monodisperse suspension that resembles a highly thixotropic gel. A physically cross-linked gel is produced when ionic strength is high because it compresses the electric double layer on particle surfaces, shortens the distance between particles, and decreases the electrostatic contact distance. (Tanaka et al., 2004). BYK (2014) Additives and Instruments produces and trades a variety of grades of laponite. Laponite-RD (rheology additive) has a wide range of applications and is particularly effective in water-based systems, surface coating rheology management, household products, and other general and industrial domains. In a recent research by the authors (Siddique et al., 2022), laponite is shown to be environment-friendly and biologically inert.

6.2.2.2 **Bentonite**

Bentonite is an absorbent aluminium phyllosilicate clay which is either Na-montmorillonite or Ca-montmorillonite. The swelling capacity of Na-montmorillonite is significantly higher than that of Ca-montmorillonite. Bentonite is usually created when volcanic ash is exposed to seawater weathering, which changes the volcanic glass contained in the ash into clay minerals (Nesse, 2000; Sutherland, 2014). Bentonite particles have a fundamental thickness of 1 nm, but the diameter is substantially larger than laponite (200-1000 nm). Fresh exposures of bentonite beds are white, pale blue, or green. As the exposure is weathered further, it changes to a cream hue, then to yellow, red, or brown (Jackson, 1997). In this study, Na-montmorillonite has been used.

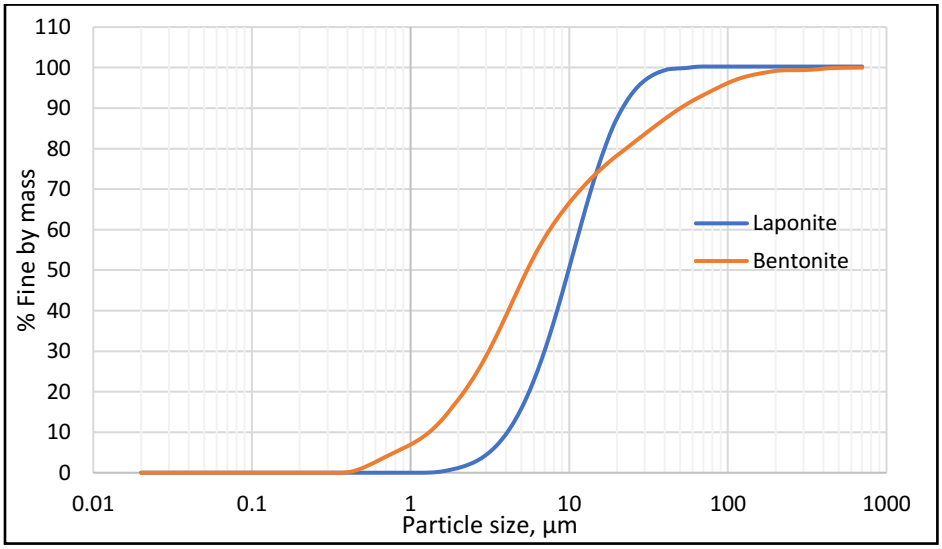

Figure 6-2: Particle Size Distribution (PSD) of laponite and bentonite.

Table 6-1: Characteristics of laponite and bentonite by the X-ray Fluorescence Method (XFM)

Properties	**Laponite**		**Bentonite**	
Mineral Name	Montmorillonite		Montmorillonite	
Cation Exchange Capacity, meq/100g	55.4		56.3	
Chemical Formula	$Na^{+0.7}[Si_8Mg_{5.5}Li_{0.3}H_4O_{24}]^{-0.7}$		$Na_{0.3}(Al,Mg)_2Si_4O_{10}(OH)_2.nH_2O$	
Compound Name	Sodium, Lithium, Magnesium, Silicate, Hydroxide		Sodium, Aluminum, Magnesium, Silicate, Hydroxide, Hydrate	
Chemical Composition	Compound Name	%	Compound Name	%
	SiO_2	60.82	SiO_2	58.05
	MgO	30.10	MgO	1.79
	Na_2O	3.20	Na_2O	2.35
	Li_2O	0.72	Al_2O_3	1.99
	H-bond	5.05	H-O	34.90

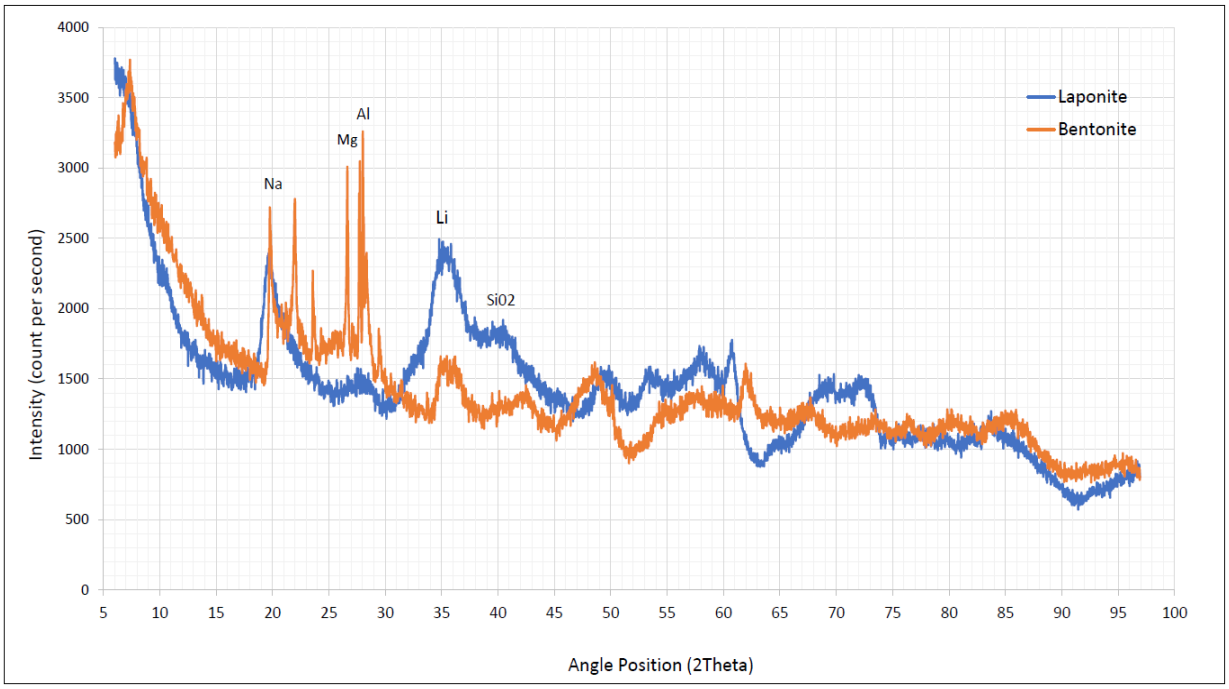

Figure 6-3: Chemical composition of laponite and bentonite using the X-ray Diffraction Method (XDM)

Figure 6-2 presents the particle size distribution of laponite and bentonite conducted by Malvern Mastersizer 2000E in Lakehead University Instrumental Laboratory, Thunder Bay, Canada. As seen in the figure, in general laponite has a larger particle size with d_{50}=10.63 µm and d_{90}=21.45 µm, as compared with bentonite which has d_{50}=5.32 µm and d_{90}=48.40 µm. The Cation Exchange Capacity (CEC) of laponite and bentonite has been determined at *ALS* Environmental- Saskatoon branch, Saskatchewan, Canada. The CEC of laponite and bentonite is 55.4 and 56.3 meq/100g, respectively.

The chemical compounds of both nanoparticles have been examined at the Activation Laboratories Ltd. (Actlabs), Hamilton, Ontario, Canada by the X-ray Fluorescence Method (XFM). The available chemical compounds of laponite and bentonite are slightly different as shown in the following table (Table 6-1). Both laponite and bentonite have SiO_2, MgO, and Na_2O compounds, however, the percentage of each compound is higher in laponite than that of bentonite. Laponite has 0.72% of Li_2O, while bentonite has 1.99% of Al_2O_3. The X-ray Diffraction Method (XDM) was conducted to find out the chemical composition/formula of both nanoparticles at Lakehead University Instrumental Laboratory, Ontario, Canada (Figure 6-3). The repulsive or attractive forces regulate the structure and behavior of nanoparticle's dispersion depending on the experimental parameters (such as clay content, *pH*, and ionic strength) (Mongondry et al., 2005; Ruzicka and Zaccarelli, 2011; Tanaka et al., 2004).

6.3 Experimental Set-up

6.3.1 Bender Elements

The damping ratio and shear modulus are determined by the field and laboratory tests using a variety of approaches with advantages and disadvantages. Low-strain laboratory tests such as bender element and resonant column tests are commonly used for studying liquefaction behavior induced by earthquakes (Karl, 2005). Although it is good practice to use a technique that can replicate the initial stress circumstances and the anticipated cyclic loading conditions as closely as possible, inaccuracies in measuring the aforementioned variables are unavoidable (Ferreira, 2008). Common sources of inaccuracy include soil variability, anisotropy, sampling disturbance, testing errors, interpretation mistakes, and equipment limitations. However, the parametric studies are conceivable in the laboratory testing contrary to the field tests. To determine the damping, the seismic wave data is analyzed after acquisition. Numerous techniques that rely on a time-domain or a frequency-domain are used for the analysis. A time-domain analysis is simpler since it involves

the evaluation of amplitude variation of the seismic wave signal with time. The seismic wave signal is evaluated in terms of frequency via the frequency-domain analysis, which provides relevant information that is not available through a time domain analysis.

Piezoceramics are primarily used to generate and transmit compression waves to dynamically analyze soil during the early stages. The piezoceramics have been coupled in various forms to generate and receive the shear waves. One of these forms, known as piezoceramic bender elements, induces bending motion in the piezoceramic elements (Karl, 2005).

A bender element, an electromechanical transducer that can convert electrical energy into mechanical energy and vice versa, is mainly advantageous over a piezoceramic element because it has a high deformation capability at low electrical voltages (Ferreira, 2009). According to Shirley and Hampton (1978), the characteristic impedance of these elements is very similar to that of soil, resulting in a closer relationship between movement and applied force for both the piezoceramic element and propagation medium. The bender element consists of two thin piezoceramic plates that are securely connected and have conducting faces on the inside and outside. It is similar to a cantilever beam, which usually vibrates along its weak axis. When a driving voltage is provided, the polarization of these ceramic materials in each plate causes one plate to elongate while the other shortens, resulting in a bending motion. Conversely, when a bender element is forced to bend, one layer becomes tensioned and the other becomes compressed, resulting in an electrical signal (Dyvik and Madshus, 1985). The use of the bender elements to determine the shear wave is an easy and low-cost method of assessing the stiffness of soil in low-strain situations. The bender elements are a double piezoceramic transducer, which is made up of two thin piezoceramic plates rigidly attached to a central metallic sheet and electrodes on its outside surfaces (Figure 6-4). Since the piezoceramic plates are extremely delicate, reinforcement is provided by the metallic sheet. The assembly was coated with epoxy resin to prevent direct contact with the soil and water to ensure accurate flexural movement, the electrical connection to the plates is formed about the polarization directions of two plates: (a) series-connection: plates polarised in the opposite directions, and (b) parallel-connection: plates polarised in the same direction. The performance of these transducers is also related to their ability to sense the shear waves. For the receiver element, a series connection is preferable because a higher output is attained for the identical movement which is twice the energy of a parallel connection. On the other hand, a parallel connection is better

for the transmitter element because the distortional movement of the transducer is greater for a given input, resulting in twice the efficiency of the series-connected bender elements used as transmitters (Dyvik and Madshus, 1985; Berignoli et al. 1996).

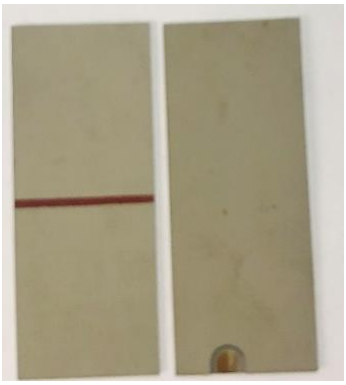

Figure 6-4: Bender Elements manufactured by Piezo.com, Division of Mide Technology, Woburn, MA, United States.

6.3.1.1 **Bender Element Wiring**

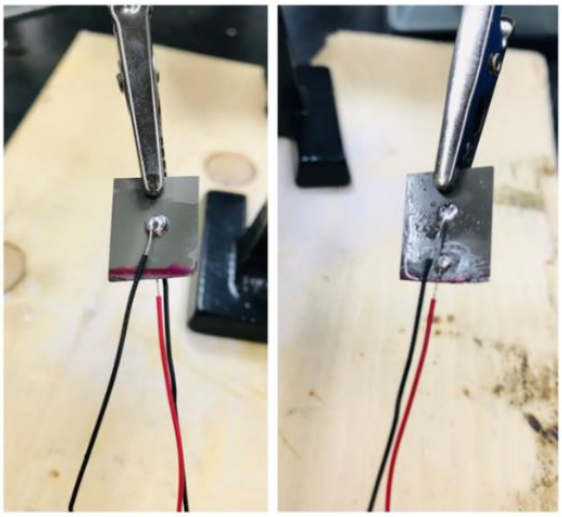

Figure 6-5: (a) Parallel-connected and (b) Series-connected wired bender elements

The bender elements used in this study are made of ceramic and electrically polarized at high temperatures and voltage. These bender elements were manufactured by Piezo.com, Division of Mide Technology, Woburn, MA, United States. The high-strength units were purchased as the more robust nature was more appealing considering they would be buried. The sender and receiver part numbers are *LOT-5A-075-2SSX-1250-0500* and *LOT-5A-075-2SSY-1250-0500-C* respectively.

Dimensions of the piezo bender elements are 1.25-inch x 0.50-inch x 0.02-inch. Each of the elements is cut into half of its length. The primary difference in the bender elements is the wiring configuration. These elements can be connected in two ways: series-connected and parallel-connected (Figure 6-5). The polarization of the ceramic material is oriented in opposing directions for each plate in a series connection, and the polarization is in the same direction for both plates in a parallel connection. For both the transmitter and receiver elements, any of these connection arrangements can be applied. For the same voltage, a series connection provides twice the energy as a parallel connection, when employed as a transmitter, a parallel-connected element is twice as effective as a series-connected element (Dyvik and Olsen 1989). As a result, the transmitter/sender is a parallel-connected element, while the receiver is a series-connected element. To prevent depolarization of the piezoceramic material, the maximum input energy must be limited. Ferreira (2003) recommended a voltage of 20 V for this effect. In practice, keeping the bender elements of equal dimensions is the simplest option because it assures that they will have similar bandwidths and frequency response characteristics, which is critical for the frequency domain analysis. To achieve 100% shear wave transmission efficiency, the bender elements must be perfectly aligned (Lee and Santamarina, 2005, Hunter et al., 2021).

6.3.1.2 **Bender Element Set-up**

6.3.1.2.1 Housing and Connections

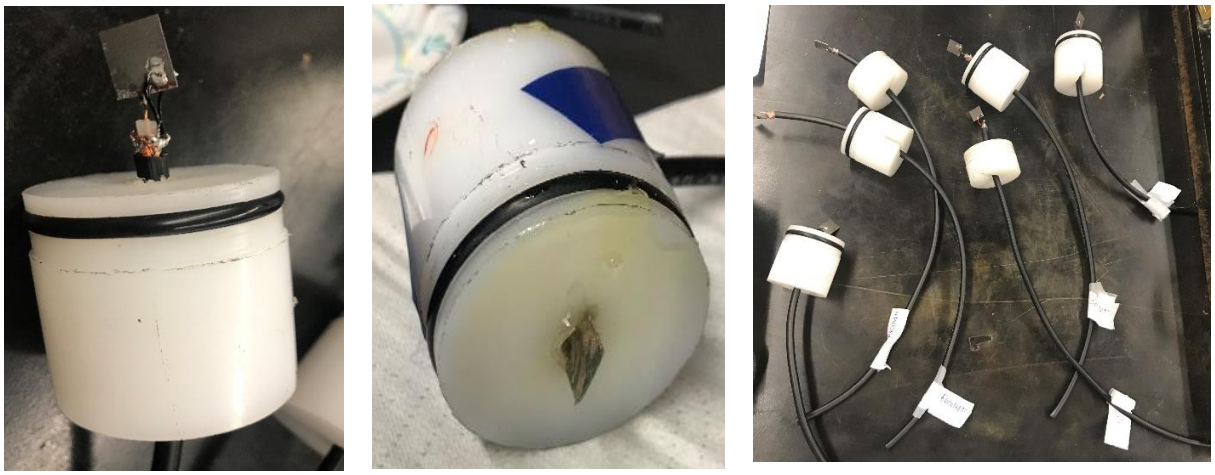

Figure 6-6: Bender elements housing set-up

The bender element housing was designed to hold the bender elements firmly, provide a robust framework to protect the electrical connections from moisture and soil intrusion, and allow the

paired elements to be aligned and accurately spaced apart. The housing for the bender elements was created from a 2-inch diameter of High-density polyethylene (HDPE) plastic purchased from Surecraft Plastics, Thunder Bay, Ontario, Canada. As the system being developed is a two-part system (e.g., sender and receiver) that is transmitting the shear waves, the two bender elements must be relatively well aligned and be oriented correctly to be in phase. To accommodate this, the cylinder of HDPE was cut into 1.5-inch segments, and slots were milled into the faces to house the bender elements. The coax cable used in the experiment was *RG-59* and had an impedance of 75 ohms. The bender elements were trimmed in half from the actual length to fit into the bender housing and fix the wiring firmly to prevent wire movement (Hunter et al., 2021). The 32-gauge wires were soldered onto the respective faces of the shorter segments in a third hand. To appropriately prepare the surface for soldering, generic lead-free solder was used. This was accomplished by using the solder and flux kit for Nichel Electrodes (*P/N: KIT-003-NI*), made by Piezo.Com. The surfaces were electrically attached to the coax cable with an electrical multimeter to make sure that the center shim did not have continuity to the piezo-ceramic coating. Waterproof and chemical-resistant silicone conformal coating from M.G. Chemicals Ltd. and water-based silver-coated copper conductive paint was applied to the surface. The coaxial cable was put through the housing once the bender elements were properly protected and shielded, and it was afterward covered in epoxy to make it waterproof and secure in its housing (Figure 6-6). The other ends of the coaxial wire are terminated with BNC connectors. The sender bender element was driven by a signal created by function generators, which were positioned at the bottom end of each sample. The generator and an oscilloscope were immediately linked to the sender bender element, while the signal analyzer was directly attached to the receiving bender element. To improve the signal readability, a signal amplifier was also used. The direction of polarisation was tested when the bender elements were fully assembled and found to function properly. For this, an oscilloscope was used to connect the sender and receiver, and the bender elements were pushed back and forth while watching the oscilloscope. When both the sender and receiver elements are pushed in the same direction, they should generate either a positive or negative voltage, not the polar opposites. Finally, the coaxial cable for the bender elements was linked to the in-house-built data acquisition system.

6.3.2 Sample Preparation

Laponite was kept in an airtight container in a dry room at room temperature to avoid moisture absorption. The sand-laponite samples were prepared by dry pluviation. In an airtight container, the desired dry amount of laponite was combined with dry sand and manually shaken for 20 minutes. The sand-laponite mixtures were prepared with laponite concentrations of 1%, 2%, and 3% (dry mass of laponite/ dry mass of sand) to determine the damping ratio of the mixtures. Deaired distilled water was added to the dry sand-laponite mixture to represent a fully saturated condition. The sample was then placed into the clear Polycarbonate Tube 2-in (50.8 mm) in diameter and 4.1-in (104 mm) long in three layers while tamping with a steel rod to prevent the formation of air bubbles. After, the sample was kept in a fully saturated condition for 24 hours before the experiment began. The same procedure was followed to prepare the pure sand (i.e., control test) and sand-bentonite (1%, 2%, and 3% of dry mass of sand) samples.

6.3.3 Sample Set-up

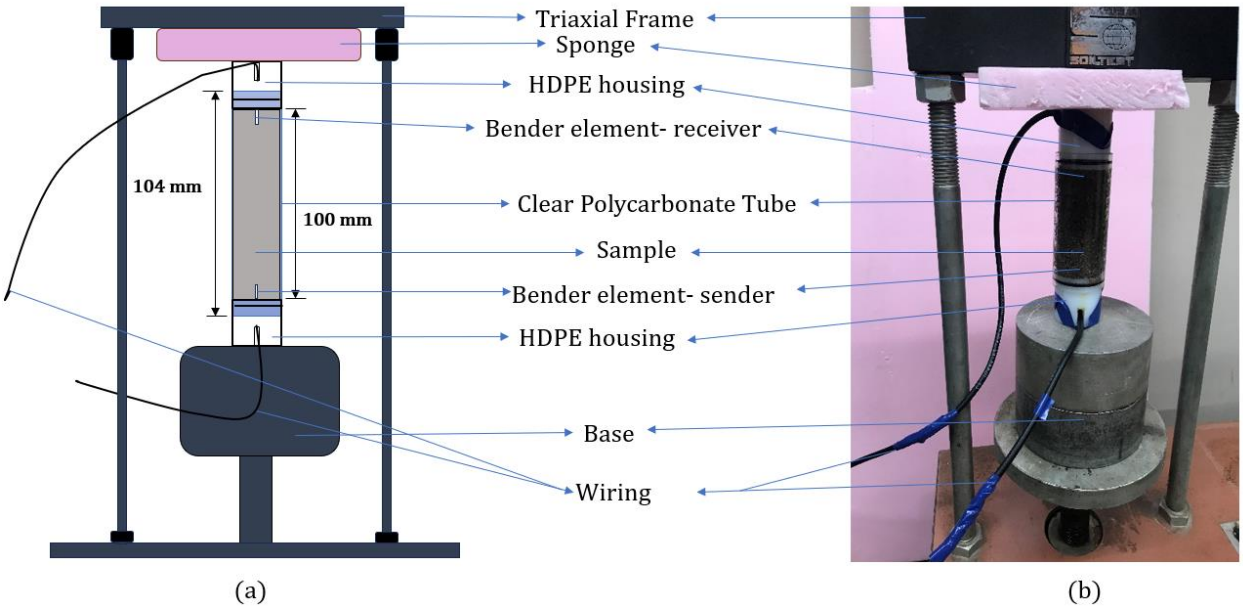

Figure 6-7: (a) Schematic diagram of experimental setup using bender elements, (b) Photo of the experimental setup

Figure 6-7 shows the assembly of the sand mixture sample with bender elements in a triaxial frame during the test. The bender element was mounted at the top and bottom and the signal to drive the transmitter bender element was generated by the function generators. While the clear

Polycarbonate tube was 104 mm in length, the sample was kept at 100 mm as from both ends, one of the HDPE housings was inserted up to 2 mm. This installation was carefully completed to minimize disturbing the initial circumstances near the bending parts and to prevent damage to them. Under standard testing conditions, a flexible impermeable substance, such as silicone rubber is typically used to fill the space between the sample and bender elements (Rio, 2006). Due to the lack of such a substance, a sponge has been used in this study. The sponge on top of the sample tube ensured that the bending elements would remain fixed to the sample. Finally, the top arm of the frame was used to maintain the sample tube in place, as depicted in Figure 6-7. To secure the grounding and wiring in place and limit background and electrical noise, the frame used to hold the bender elements in place proved helpful. Because this test was a bench test, it was revealed that the background noise was highly significant when other laboratory equipment was running. The bending elements testing has been carefully isolated to minimize noise.

6.3.4 Signal

Biot's theory (1956 a, b) describes wave propagation in a porous medium, i.e., a medium made of a solid matrix that is composed of pore structures, which are typically fluid-filled. The research found that numerous parameters influence the control of wave velocity by frequency. The term 'characteristic frequency' refers to the frequency that all fluid-saturated porous material shows and is used to normalize data. The optimum size of the bender elements is determined by the distance between elements and the estimated shear wave velocity of soil. Because the bender elements must oscillate in the first mode of vibration to convey maximum force, constructing the bender to have a natural frequency above the expected frequency needed is the finest practice. If the resonance frequency of the bender elements is lower than the desired operating frequency, the amplitude of traveling shear waves is considerably reduced, and issues due to a lack of signal amplitude at the receiver may develop. The natural vibrating frequency of a shorter element is more dependent on the qualities of the bender mounting plate apparatus than on the surrounding soil stiffness, whereas the natural vibrational frequency of a longer element is more dependent on the soil stiffness properties (Lee and Santamarina, 2005). This is especially important in studies when the soil stiffness is projected to rise during the treatment, altering the response characteristics of the system and necessitating a short cantilever length. In other words, the bender element's bandwidth must match the bandwidth of the soil.

6.3.4.1 **Electronic Devices**

Figure 6-8: Electronic Devices

The following section presents the electrical devices and equipment used in this study, along with a brief description (Figure 6-8).

- *Function generator:* FG2C function generator, manufactured by Meterman is used in this study. It is a programmable function generator with a frequency range of 0.3 Hz to 3.0 MHz. It can generate and save a variety of signal configurations of waveform outputs, including Sine, Square, Triangle, TTL, CMOS, and VCF.
- *Oscilloscopes*: Hewlett Packard's 54645D MegaZoom Mixed Signal Oscilloscope is capable of producing a 100-MHz Bandwidth Mixed Signal scope with 200 MSa/s. It has 1 MB of memory per scope channel, 16 logic timing channels with 400 MSa/s on 8 channels, and 200 MSa/s on 16 channels with 2 MB of memory per logic channel. The device supports a variety of acquisition modes, including whole sample, average sample, and peak detection.
- *Power Supplier:* The smartAmp Power Amplifier (gain), series 2100E21, of The Modal Shop Inc. is designed for use with vibration shaker systems. It operates at 92% efficiency and silent operation provides for a noise-free test environment. It supplies 400 W output power at 4 Ω load impedance, front panel, continuous gain adjustment up to 26 dB, and flat frequency response to 40 kHz.
- *Data Acquisition Unit*: An in-built multifunctional data acquisition system of mechanical engineering research lab at Lakehead University, Ontario, Canada is used. Matlab code was used to create a series of commands to control the data acquisition system as well as process

and store data. The shear wave velocity is determined by the correlation between the distance of the sender and receiver and the signal wavelength.

6.3.4.2 **Signal Analyses Technique**

Frequency Domain Technique: The FG2C function generator and Hewlett Packard's 54645D Mega-Zoom Mixed-Signal Oscilloscope were utilized in this study to acquire data to implement in both the Half-Power Bandwidth and circle-fit approaches. These devices can produce a higher sampling frequency, which is essential for frequency-domain methods that require numerous data points to accurately represent the frequency spectrum (Brocanelli and Rinaldi, 1998). In this study, the sine sweep signal was selected as the input wave, a method that has been effectively used in various published studies (Greening and Nash, 2004; Ferreira, 2008). By varying the frequency of the input signal, it is possible to gather information about the sample's resonance modes within a given frequency range. A sine-signal input ranging from 100 Hz to 20 kHz is suitable for natural soil testing (Ferreira, 2008). This non-harmonic sinusoidal continuous signal enables the acquisition of a continuous phase angle versus frequency relationship (Greening et al., 2003; Greening and Nash, 2004). The coherence of input and output (i.e., signal and received wave) versus input frequency indicates how closely these signals are coupled. This coherence function expresses the extent to which the energy in the output signal is produced by the input signal (Hoffman et al, 2006). The phase angle versus frequency can be represented as either wrapped or unwound, starting at zero and growing continuously, or varying between $[-\pi;+\pi]$. It explains the phase difference between the input and output signals. This method is particularly relevant for computing travel time, as the phase difference is obtained directly from the slope of the best-fit straight line in the unwrapped phase plot (Ferreira, 2008). In this study, the input wave frequency is set to 200 Hz, and the voltage difference between the input and output scales is 2 V. Since loose sand is being used in this study, a lower frequency (200 Hz) was selected for detailed experimentation after several trials.

6.3.5 Damping Determination

The dissipation of energy by wave propagation in a medium, also known as radiation, dispersion, or geometric damping, is a type of damping. Damping determination can be attained by either a time-domain or frequency-domain analysis. A frequency-domain analysis illustrates the transformation of data concerning time into frequency, while a time-domain graph demonstrates

how amplitude changes with time. To transform time-domain data into frequency-domain data and vice versa, a transform function must be applied to the data. Fourier transform, which follows Fourier's analysis theory, is the commonly used transform function. This study uses the FFT, which is a fast computation algorithm for the DFT. The logarithmic decrement method, circle-fit method, and half-power bandwidth method are the well-known methods to determine the damping of a system. The Half-Power Bandwidth Method (HPBM) is one of the most common methods to determine the damping using an experimental setup, which has been used in this study.

6.3.5.1 **Half-Power Bandwidth Method**

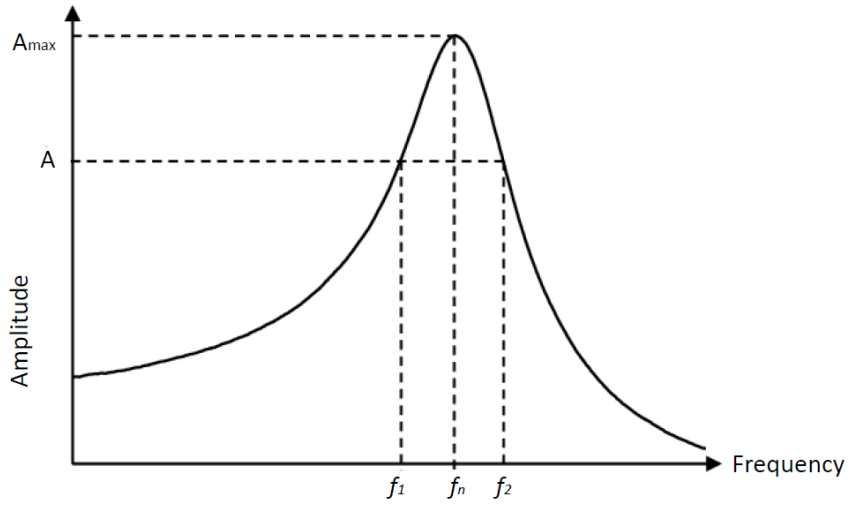

Figure 6-9: Resonant curve for the half-power bandwidth method, after Moreira, (2015)

HPBM uses the relative width of the response spectrum and resonant frequency. This method requires a large number of data points to accurately characterize the resonant curve or spectrum to calculate the damping coefficient. (Brocanelli and Rinaldi, 1998). According to Richart *et al* (1970), the logarithmic decrement (δ) can be calculated as follows:

$$\delta = \frac{\pi\left({f_2}^2 - {f_1}^2\right)}{2{f_n}^2}\sqrt{\frac{A^2}{{A_{max}}^2 - A^2}}\frac{\sqrt{1-2\xi^2}}{1-\xi^2} \qquad (1)$$

where f_n is the peak resonant frequency, and f_1 and f_2 are the frequencies at each side of f_n, for amplitude, A_{max} is the maximum amplitude, $A = A_{max}/\sqrt{2}$, and ξ is the damping ratio/coefficient (**Figure *6-9***). This equation is simplified by Brocanelli and Rinaldi (1998) for low damping ratios. Karl (2005) proposed the following form of the equation:

$$\xi = \frac{{f_2}^2 - {f_1}^2}{4{f_n}^2} \qquad (2)$$

6.3.6 Matlab Scripts

The commands to control the data acquisition system, as well as to process and store the collected data, were written in Matlab. The data-collecting devices were continuously monitored throughout the test period. Preliminary test data were used to determine the preferable data acquisition methods and to develop a treatment procedure using a Matlab script, which was then compared to results from the literature. The script was developed using a Matlab algorithm capability to analyze and represent data in a flexible and controlled manner. The signal averaging technique was used to improve test quality, as it was suggested to be more effective compared to other available filters in Matlab (Moreira, 2015). The signal averaging technique was sufficient to provide smoother signals and frequency spectra, enabling the implementation of the HPBM. To determine the damping ratio of pure sand and treated sand samples, another script was created to import the test data and calculate the damping ratio using the HPBM (Appendix B). Manual calculations were performed in Excel to cross-check the results from the Matlab code.

6.4 Results and Discussions

The sine sweep signal, which has been successfully used in numerous published research (e.g., Greening and Nash, 2004; Ferreira, 2008), was chosen as the input wave in this study. By varying the frequency of the input signal, it is possible to learn more about the sample's resonance modes for a specific frequency range. The large strain deformation behavior in soil is assessed by the fabric alterations and rearrangement, whereas the particle deformation controls the small strain deformation behavior. The particle deformation occurs mainly at contacts because the area of particle contact is relatively small and the related stresses are high (Santamarina et al., 2001). The multiphase nature of soils also influences their load-deformation performance and, consequently, affects the propagation of waves in their medium. The co-existence of soil and fluid phases creates additional complexity and phenomena such as seepage, time-dependent pressure diffusion, and effective skeletal stress. According to Palmer and Traviolia (1980), viscous damping is brought on by the relative movement of water menisci.

The sine-signal with 200 Hz was chosen in this study to conduct the experiments on all sand specimens with various laponite and bentonite concentrations. Hall and Bodare (2000) stated that amplitude decay is particularly challenging to obtain, as the signals are often corrupted by the inhomogeneous effects in soils through which ground motions travel. Moreover, factors such as sample geometry and phenomena related to bender elements—including spatial and boundary conditions, bender element alignment, wave reflections, coupling, near-field effects, and overshooting at high frequencies—significantly influence the performance of the bender elements (Rio, 2006; Ferreira, 2009). In this study, a single experiment took approximately three to four weeks to complete. A series of experiments were conducted with pure sand, sand-laponite, and sand-bentonite samples at room temperature (23°C). All the samples were kept in sealed containers for a minimum of 24 hours in fully saturated conditions before the tests were conducted.

6.4.1 Damping of Pure Sand

Table 6-2: Damping ratio (ξ) of different types of undisturbed and untreated soil samples from the published articles

Sample height, mm	ξ_a (%)	ξ_b (%)	ξ_c (%)	Soil type
50	13.20	13.14	13.26	Residual soil (silty sand) from Porto granite (undisturbed, untreated)
100	11.40	11.31	11.38	Silica sand (no soil properties mentioned)
150	9.40	9.39	9.35	Mol sand (tertiary deposit) is nearly pure quartz sand with a typical composition of 96% quartz mineral and 4% mica and traces of other minerals
20	ξ_d (%) = 15.64 - 24.53			Remolded soil, Plastic silt (Specific gravity=2.65-2.7, Liquid limit= 35.6-49.2, Plastic limit=25.2-34.5, and Plasticity index=9.6-14.5)

a) Moreira, 2015
b) Brocanelli and Rinaldi, 1998
c) Karl, 2003; 2005
d) Takele et al., 2017

Initially, the pure sand samples (i.e., control test) were examined using a one-dimensional bender elements set-up to determine the damping ratio with a function generator. The tested sand sample had a moisture content of 9.50% and a specific gravity of 2.60. Bender element testing is not yet standardized, and no available data exists for the residual soil used in this study tested by the bender elements. While in-situ testing is increasingly being used to measure various soil parameters, relatively limited research has been published on in-situ measurement of soil damping. To assess the accuracy and applicability of the methods tested, the damping ratios from undisturbed and untreated sands in published articles were presented in **Table *6-2***.

In this study, the average damping ratio of pure sand at the beginning of the test (after resting of 24 hours) was ξ=7.84% with a sample height of 100 mm. The damping ratios (ξ) obtained by Moreira (2015), Brocanelli and Rinaldi (1998), Karl (2003;2005), and Takele et al. (2017) were 11.40%, 11.31%, 11.38%, 15.64%, 24.53%, respectively (**Table *6-2***). Although the damping ratio of the current study is less than those from the previous studies, the differences in two cases are minimal (0.09%, 0.02%). Several factors may explain the variation in the damping ratios observed in this study compared to previous research:

First: The sand specimen of this study is loose and disturbed, whereas undisturbed samples were used in the other studies. Sample disturbance is primarily caused by the stress path associated with the sampling process, resulting in a change in the structure or fabric of sand (Ashmawy et al., 1995). In general, the damping capability of disturbed sand samples is unquestionably lower than that of undisturbed samples.

Second: The soil samples in this study differ from those in earlier studies due to the residual soil present in the analyzed samples. The soil anisotropy and soil variability could contribute to discrepancies in the results.

Third: Since smaller soil specimens tend to exhibit higher damping ratio, boundary reflections could play a significant role, altering the shape of the received wave.

Despite these factors, the estimated damping ratio from the current study is generally comparable to values reported by others researchers (e.g., Moreira, 2015; Brocanelli and Rinaldi, 1998; Karl, 2003; 2005; Takele et al., 2017), especially when considering the differences in soil samples, laboratory equipment, and potential errors related to electronic devices. Therefore, the bender elements setup described here is deemed appropriate for further investigation with the sand-

laponite and sand-bentonite specimens. It is worth noting that the damping ratio of pure sand gradually decreases until it achieves equilibrium at Day 3-4 (See **Figure *6-10***). The equilibrium damping ratio (ξ) is 0.991%, which is significantly lower compared to the damping ratio of Day 2. As the pure sand sample is subjected to continuous shaking for about 6-8 hours each day, the change in the structure or fabric in the sand occur, reducing its damping capacity over time.

6.4.2 Damping of Sand-laponite Samples

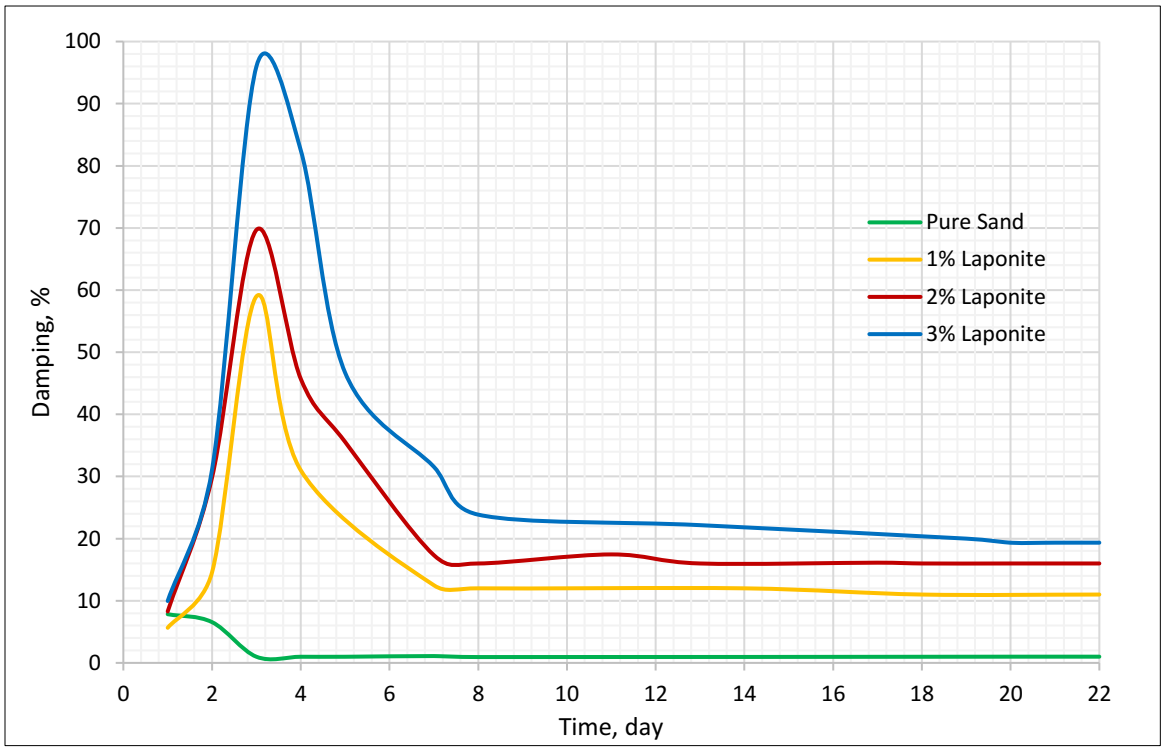

Figure 6-10: Comparisons of damping ratio (%) of pure sand and sand treated with laponite at different concentrations

Since soil is non-linear, the resonant frequency depends on the amplitude of vibration. In the frequency response plot, the locus of resonant peak for a natural clay is not described by a vertical straight line. Theoretically, if the shear stress-shear strain relationship is hyperbolic, the locus of the resonant peaks should follow the path of 'skewed' type. Due to soil non-linearity, the curve is skewed and the magnification factor at some frequencies is not unique. This is characterized during testing by a sudden jump in the observed response at some frequencies. As a result, the HPBM often yields inaccurate values because of the skewness of the frequency response curve for highly non-linear soils (Ashmawy et al., 1995). However, in this study, the maximum concentration of

natural clay (i.e., laponite, bentonite) is only 3% of dry mass of sand. It can therefore be stated that the HPBM is suitable for the current work. There is no published research relevant to the estimation of damping ratio of sand-laponite samples. Somewhat related research was published by Ochoa-Cornejo et al. (2020) where they studied the impact of a range of initial damping ratios (between 0.2% and 1.4%) on the effective confinement of sand-laponite (1% and 3% of dry mass of sand) samples. Figure 6-10 illustrates the comparison of the damping ratio of pure sand and sand sample treated with laponite at three different concentrations (1%, 2%, and 3% of dry mass of laponite/dry mass of sand) with the HPBM. All of the samples were kept in the resting time of 24 hours at fully saturated condition after preparation (all graphs start from Day 1, not Day 0).

Figure 6-10 demonstrates that sand samples mixed with laponite have a higher damping ratio than that of pure (untreated) sand, with the damping ratio increasing as laponite percentage increases. The differences between the data sets are significant and consistent. The graphs of sand+laponite samples gradually increase from Day 2 and reach the peak at Day 3. The highest damping ratio of sand+1% laponite, sand+2% laponite, and sand+3% laponite samples is 59%, 69.7%, and 98.6%, respectively. According to the rheological tests, laponite hydrogel requires minimum 48 hours to complete the gelation process (Huang and Wang, 2016). Hence, it can be said that the damping ratio, which relates to the frictional energy dissipating due to the relative motion of particles, of sand-laponite samples reaches peak values after 48 hours. After reaching the peak on Day 3, the damping ratio starts to decline and gradually achieves the equilibrium state. Sand+1% laponite sample reaches the equilibrium at Day 17 with a damping ratio of about 11%. Similarly, sand+2% laponite and sand+3% laponite samples reach the equilibrium state on Day 18 with ξ=16% and Day 20 with ξ=19.4%, respectively. It is hypothesized that, while in all cases laponite interferes with the contacts between sand particles, the amount of laponite trapped at the contacts controls the effect on the small-strain shear modulus. The higher damping values for sand-laponite specimens reflect a viscous damping contribution from the presence of laponite at sand grain contacts: the greater the amount of laponite trapped at the contacts, the greater the increase in damping (Ochoa-Cornejo et al., 2020). Majedi et al. (2013, 2019) determined the damping ratios of clay nanocomposites with latex polymer with a computer-based and multi-channel analysis system and pulse vibration measurement system. Majedi et al. (2019) found that the increasing percentage of the damping ratio for clay nanocomposite samples at optimum moisture content was 39%, 47%, 58%, and 67% for 5%, 10%, 15%, and 20% of latex percentage, respectively.

Additionally, the increased percentage of the damping ratio for dry clay nanocomposite samples were 80%, 92%, 100%, and 106% for 5%, 10%, 15%, and 20% of latex percentage, respectively (Majedi et al., 2013). More water molecules are absorbed by the bonding water layer created by the attraction force between montmorillonite particles as the montmorillonite content increases. Additional energy is used during dynamic shearing to break the bounding water away from the electrical influence zone of clay particles (Vucetic et al., 1998). This clarified why clays with higher montmorillonite concentrations have a larger damping ratio.

6.4.3 Damping of Sand-Bentonite Samples

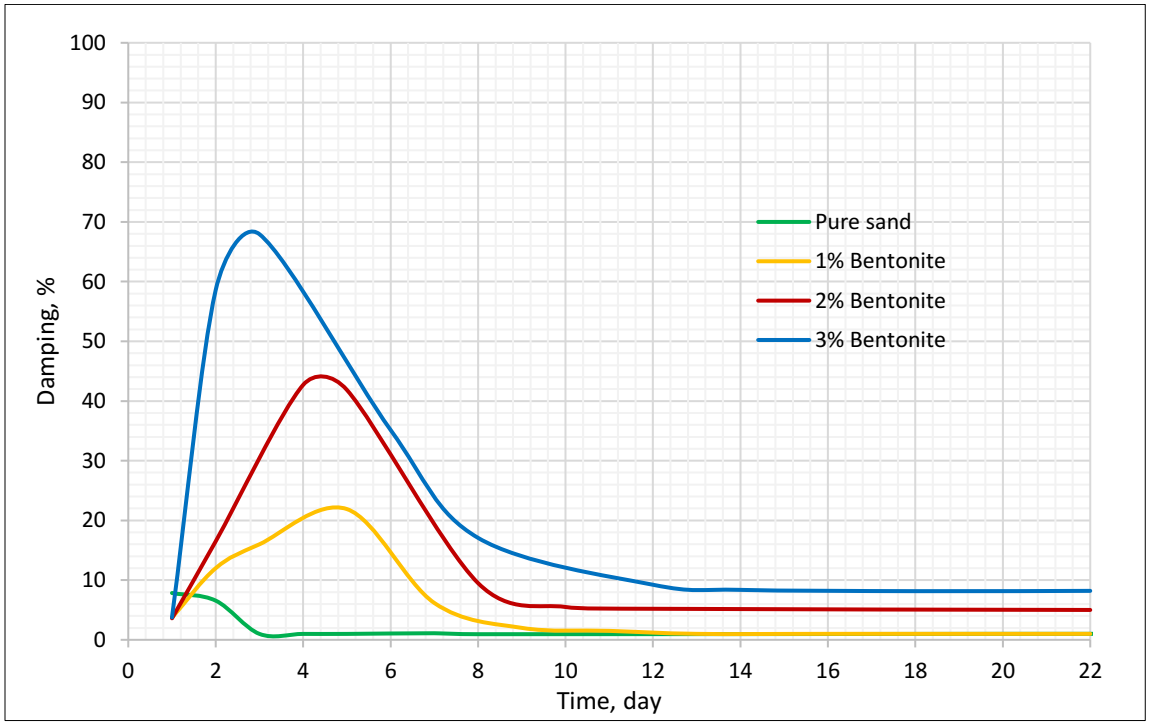

Figure 6-11: Comparisons of damping ratio (%) of pure sand and sand+bentonite at different concentrations

The damping ratio of sand mixed with another well-known nanoparticle, bentonite, has been evaluated to compare the findings of laponite in this study as there are no published data on the damping ratio of sand+laponite utilizing the bender elements or any other experimental setup. Figure 6-11 illustrates the comparisons of the damping ratio of sand samples mixed with bentonite at three different concentrations (1%, 2%, and 3% of dry mass of bentonite/dry mass of sand) with the HPBM. Similar to sand-laponite samples, the results show that the damping ratio of sand-

bentonite specimens is larger than that of pure sand. As the quantity of bentonite in the samples is increased, the damping ratio of sand-bentonite samples also steadily rises. The current study found that the peak damping ratio of sand-bentonite samples is about 21.9%, 42.7%, and 67.9% in the case of sand+1% bentonite, sand+2% bentonite, and sand+3% bentonite, respectively. In the case of sand-laponite samples, all the samples attain the peak damping ratio of the same day (i.e., Day 4). On the other hand, all sand-bentonite samples do not reach the highest damping ratio on the same day, but rather on various days. The sample with more bentonite concentration reached the peak earlier. Sand+3% bentonite sample attains the peak on Day 3, whereas sand+2% bentonite and sand+1% bentonite samples reach the peak on Day 4 and Day 5, respectively. It can be explained that in all cases bentonite gelation process affects the contacts between sand particles, however, bentonite can complete its gelation process quickly as the content of bentonite in sand sample increases. As a result, the higher concentrated bentonite samples attain the peak damping earlier compared to the lower concentrated bentonite samples. In cases of laponite samples, laponite interferes with the contacts between sand particles is still appears, but not that significant. After reaching the peak, the damping ratio of bentonite-sand samples starts to decline and progressively attains an equilibrium state similar to those of sand-laponite samples. Sand+1% bentonite sample reaches the equilibrium earlier than the other sand-bentonite samples similar to the sand+1% laponite sample. On Day 11, the sand+1% bentonite attends to an equilibrium state with a damping ratio of around 1%. The sand+2% bentonite and sand+3% laponite samples reached the equilibrium state on Day 13 with ξ=5% and Day 16 with ξ=8.2%, respectively. All of the sand-bentonite samples achieve the equilibrium damping earlier than sand-laponite samples in the same experimental set-up.

6.4.4 Samples After Releasing from the Set-Up

Figure 6-12 shows the images of the samples that were taken out of the transparent Polycarbonate Tube after the experiment was finished. Even after 22 days of constant vibration for 6–8 hours each day, sand+3% laponite sample was stiffened and compacted in both wet and dry conditions (Figure 6-12 (a, b)). Figure 6-12(c) depicts the samples of sand-laponite mixtures at 1%, 2%, and 3% laponite concentrations (by dry mass of sand). The three samples maintained their shape even after completely dried up. This may explain why sand-laponite samples were strong enough to tolerate the vibration provided by the electronic equipment for 22 days. Both sand+1% bentonite and sand+2% bentonite samples break during release from the tube after experiments (Figure

6-12(d)). Even sand+3% bentonite sample is a bit bulky at the bottom compared to sand+3% laponite sample in Figure 6-12(e). It can be stated that the bonding of sand-bentonite is significantly disturbed due to the constant vibration (6-8 hours per day) for more than 3 weeks (≈22 days). Another possible reason can be that the amount of bentonite used in the samples may be not enough to create a compacted bonding into the particles of sand-bentonite samples like laponite.

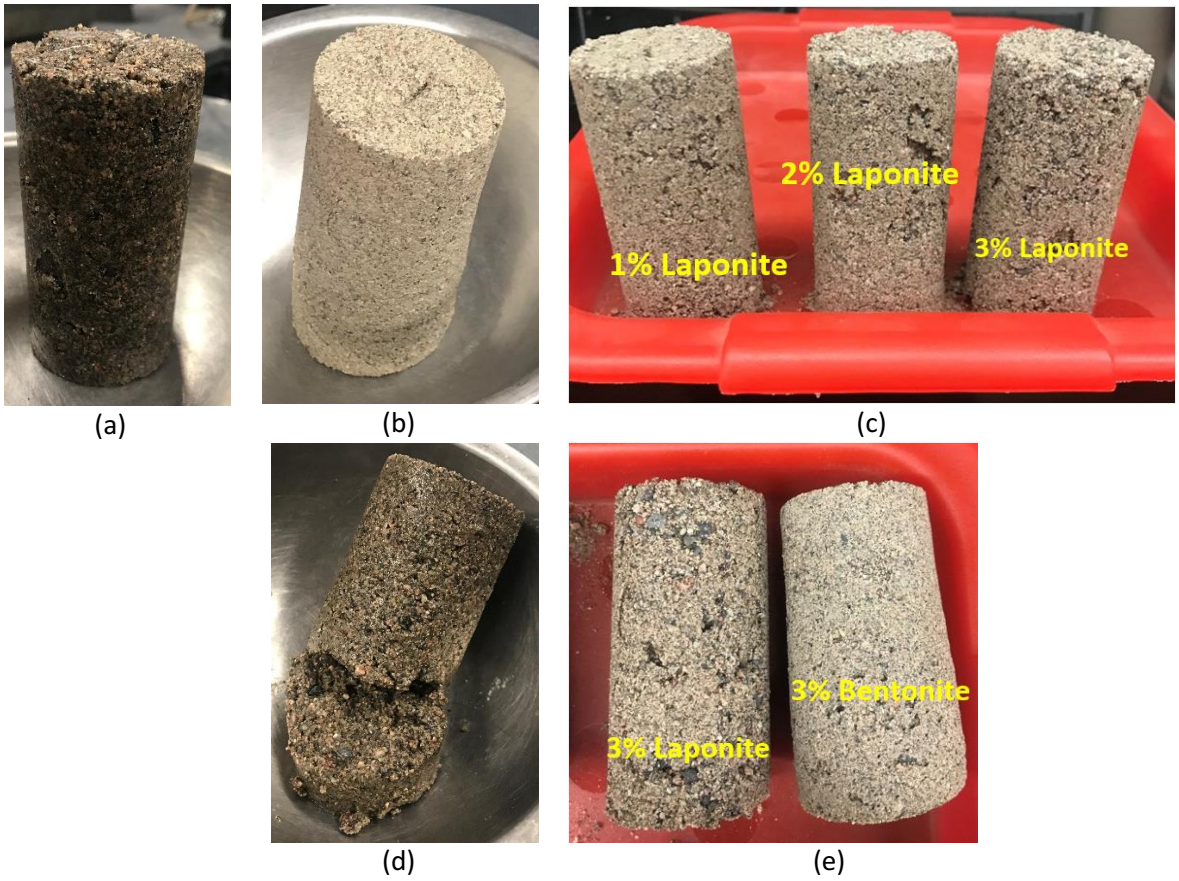

Figure 6-12: (a) Sand+3% laponite sample immediately after releasing from the experimental set-up, (b) Sand+3% laponite sample after drying, (c) Sand+1% laponite, sand+2% laponite, and sand-3% laponite samples after drying, (d) Sand+2% bentonite sample, and (e) Sand+3% laponite and sand+3% bentonite samples after drying.

6.5 Conclusions

Dynamic properties of soils such as damping ratio and shear modulus are important parameters to study ground motion, performance of machine foundation, response of soil deposits under cyclic loading, and soil-structure interaction. A significant contributor to structural damage during

earthquakes is soil liquefaction, which is brought on by a sudden increase in excess pore water pressure. Due to the inherent rheological property of transparent gels, nanoparticles such as laponite can enhance the liquefaction resistance of soil. Although it has been noted in the literature that sand treated with laponite has a higher damping ratio, there hasn't been much research done on the damping ratio of sand-laponite specimens. In this current study, an experimental set-up with bender elements has been entirely built step-by-step to determine the damping ratio of sand-laponite mixtures at three different concentrations using the half-power bandwidth method (HPBM).

- One of the most popular techniques for figuring out the damping with an experimental setup is the HPBM which uses the resonance frequency and the relative width of response spectrum. An electromechanical transducer, the bending element transforms electrical energy into mechanical energy and vice versa. It usually vibrates along its weak axis. The polarization of these ceramic materials in each plate enables one plate to lengthen while the other shortens when a driving voltage is applied, resulting in a bending motion. The sine sweep signal, which has been successfully applied in numerous published research, was chosen as the input wave in the current work. By varying the frequency of the input signal, it is possible to learn more about the sample's resonance modes for a specific frequency range. The sine-signal with 200 Hz was chosen in this study to conduct the experiments.
- Similar tests were carried out with the pure sand (i.e., control test), sand treated with laponite, and sand treated with bentonite specimens.
- This study reveals that the damping ratio of pure sand is about 7.48% which is consistent with values reported in the literature, considering the variances of soil samples, variances in laboratory equipment, and errors related to electronic devices.
- The results show that the highest damping ratio of sand+1% laponite, sand+2% laponite, and sand+3% laponite samples is approximately 59%, 69.7%, and 98.6%, respectively. The damping ratio begins to reduce after reaching its peak and eventually reaches equilibrium. The higher damping values for sand-laponite specimens reflect a viscous damping contribution from the presence of laponite at sand grain contacts: the greater the amount of laponite trapped at contacts, the greater the increase in damping.

- The study also found that the peak damping ratio of sand-bentonite samples is around 21.9%, 42.7%, and 67.9% in the case of sand+1% bentonite, sand+2% bentonite, and sand+3% bentonite, respectively.
- The images of samples after being released from the clear Polycarbonate Tube after implementation of the experiments demonstrate the compacted bonding of sand-laponite samples and loose bonding of sand-bentonite samples.

6.6 References

- American Society for Testing and Materials D6913 (2017). Standard Test Methods for Particle-Size Distribution (Gradation) of Soils Using Sieve Analysis, ASTM International, West Conshohocken, PA, United States.
- American Society for Testing and Materials D2216-19 (2019). Standard Test Methods for Laboratory Determination of Water (Moisture) Content of Soil and Rock by Mass, ASTM International, West Conshohocken, PA.
- American Society for Testing and Materials C128-15 (2015). Standard Test Method for Relative Density (Specific Gravity) and Absorption of Fine Aggregate, *ASTM International*, West Conshohocken, PA.
- American Society for Testing and Materials D5890-11 (2021). Standard Test Method for Swell Index of Clay Mineral Component of Geosynthetic Clay Liners, *ASTM International*, American National Standards Institute, 2021.
- APC International Ltd (2011). Piezoelectric Ceramics: Principles and Applications, 2nd Edition, Ian R. Henderson, President, APC.
- Ashmawy AK, Salgado R, Guha S, Drnevich VP. Soil damping and its use in dynamic analyses. Proceedings: Third International Conference on recent advances in Geotechnical Earthquake Eng. and Soil Dynamics 1995; April 2-7, vol. 1, St. Louis, Missouri.
- Beroya MAA, Aydin A, Katzenbach R. Insight into the effects of clay mineralogy on the cyclic behavior of silt-clay mixtures. Eng Geol 2009;106(3):154-162.
- Biot M. Theory of propagation of elastic waves in a fluid-saturated porous solid. I. low-frequency range. The J of the Acoustical Society of America 1956a;28(2):168-178.
- Biot M. Theory of propagation of elastic waves in a fluid-saturated porous solid. II. Higher frequency range, The J of the Acoustical Society of America 1956b;28(2):179-191.

- Brignoli E, Gotti M, Stokoe K. Measurement of shear waves in laboratory specimens by means of piezoelectric transducers, Geotechnical Testing J 1996;19(4):384-397.
- Brocanelli D, Rinaldi V. Measurement of low-strain material damping and wave velocity with bender elements in the frequency domain. Canadian Geotech. J 1998;35(6):1032-1040.
- BYK. Technical Information BRI-21: Laponite performance Additives, BYK Additives, and Instruments; 2014, a member of Altana, Germany.
- Cai Y, Dong Q, Wang Y, Gu C, Xu C. Measurement of small strain shear modulus of clean and natural sands in saturated condition using bender element test, Soil Dynamics and Earthquake Eng 2015;76:100-110.
- Delfosse-Ribey E, Djeran-Maigre I, Cabrillac R, Gouvenot D. Shear modulus and damping ratio of grouted sand. Soil Dynamics and Earthquake Eng 2004;24(6): 461-471.
- Dyvik R, Madshus C. Lab Measurements of G_{max} Using Bender Elements, ASCE 1985.
- El Howayek A. Characterization, Rheology and Microstructure of laponite suspensions, MSc thesis; 2011, School of Civil Engineering, Purdue University, West Lafayette, IN 47900, USA.
- Ferreira CMdF. The use of seismic wave velocities in the measurement of stiffness of a residual soil, Ph.D. dissertation; 2008, Faculty of Engineering, University of Porto, Portugal.
- Getchell A, Ochoa-Cornejo F, Santagata M. Behavior of Dry-mixed and permeated Laponite-treated sand: from small strains to critical state. *Geotech Geol Eng* 2022:40:5307-5331.
- Gratchev IB, Sassa K, Osipov VI, Fukuoka H, Wang G. Undrained cyclic behaviour of bentonite-sand mixtures and factor affecting it. *Geotech Geol Eng* 2007;25(3): 349-367.
- Greening PD, Nash DFT (2004). Frequency Domain Determination of G~0 Using Bender Elements. Geotechnical Testing J 2004;27(3):288-294.
- Greening PD, Nash DFT, Benahmed N, Ferreira C, Viana da Fonseca A. Comparison of shear wave velocity measurements in different materials using time and frequency domain techniques. Deformation Characteristics of Geomaterials, Di Benedetto et al. (eds.), Swets & Zeitlinger, Lisse, 2003; ISBN 90 5809 604 1.
- Hall L, Bodare A. Analysis of the cross-hole method for determining shear wave velocities and damping ratios. Soil Dynamic and Earthquake Eng 2000;20(1-4):167-175.

- Ham A, Wang J, Stammer JG. Relationships between particle shape characteristics and Macroscopic damping in dry sands. J of Geotech. and Geoenvironmental Eng *2012;*138(8):1002-1011.
- Hoffman K, Varuso R, Fratta D. The Use of Low-Cost MEMS Accelerometers in Near-Surface Travel-Time Tomography. GeoCongress 2006 Conference, Atlanta, GA.
- Huang Y, Wang L. Laboratory investigation of liquefaction mitigation in silty sand using nanoparticles. Eng Geology 2016;204:23-32.
- Hunter C, Mohamedelhassan E, and Sadhu A. Monitoring the strength properties of electrokinetically treated soil by bender elements to determine the treatment period. Soils and Foundations 2021;61:675-691.
- Ishihara K. Soil behaviour in earthquake geotechnics, Clarendon Press 1996, Oxford University, Oxfordshire.
- *Jackson, Julia A., ed. Bentonite. Glossary of geology (Fourth ed.). Alexandria, Viriginia: American Geological Institute 1997.* ISBN 0922152349.
- *Karl L, Haegeman W, Pyl L, Degrande G. Measurement of material damping with bender elements in triaxial cell. Deformation Characteristics of Geomaterials/Comportment Des Sols Et Des Roches Tendres 2003; p. 3 0415889200.*
- Karl L. Dynamic soil properties of SCPT and bender element tests with emphasis on material damping, Doctoral dissertation 2005, Department of Civil Engineering, Ghent University, Belgium.
- Karnland O, Muurinen A, Karlsson F. Bentonite swelling pressure in NaCl Solutions-Experimentally determined data and model calculations, Alonso E, Ledesma A (eds.), Advances in Understanding Engineered Clay Barriers, Taylor and Francis Group 2005, London, 241-256.
- Komine H, Ogata N. Experimental study on swelling characteristics of sand-bentonite mixture for nuclear waste disposal. *Soil Found* 1999;39:83-97.
- Kroon M, Vos WL, Wegdam GH. Structure and formation of a gel of colloidal disks, *Phys Rev E 1998;* 57: 1962–1970.
- Lee JS, Santamarina JC. Bender elements: performance and signal interpretation, J of Geotechnical and Geoenvironmental Eng 2005;1063-1070.

- Lin P, Ni J-J, Garg A, Yu S-M. Effects of Clay Minerals on small-strain shear modulus and damping ratio of saturated clay. Soil Mechanics and Foundation Eng 2020;57(2): 105-109.
- Liu LC. Hydraulic properties of unsaturated bentonite, Department of Chemical Engineering and Technology, Royal Institute of Technology 2012, Stockholm, Sweden.
- Majedi P, Akbulut S, Albayrak ZNK. Some geotechnical properties and damping ratio of clay nanocomposites. J of Eng Research 2019;7(1):1-16.
- Majedi P, Kurt ZN, Akbulut S. The investigation of some geotechnical properties and damping ratios of hydrophobic clay with latex additive, 5th National Geotechnical Symposium 2013, Adana, Turkey.
- Marcuson WF, Wahls HE. Time effects on dynamic shear modulus of clays. J Soil Mech Found Div 1972;98(12):1359-1373.
- Mog K, Anbazhagan. Evaluation of the damping ratio of soils in a resonant column using different methods. Soils and Foundations 2022;62:101091.
- Moreira ARMO. Experimental determination of soil damping- application to the residual soil from Porto granite. Master in Civil Eng -Specialization in Geotechnics 2015, Department of Civil Eng, Faculdade de Engenharia da Universidade do Porto, Porto, Portugal.
- Mongondry P, Tassin JF, Nicolai T. Revised state diagram of Laponite dispersions, J of Colloid and Interface Science 2005;283(2):397-40
- Nesse WD. Introduction to mineralogy. New York: Oxford University Press 2000. p. 257. ISBN 9780195106916.
- Ochoa-cornejo F, Bobet A, Johnston C, Santagata M, Sinfield JV. Cyclic behavior and pore pressure generation in sands with laponite, a super-plastic nanoparticle, Soil Dynamics and Earthquake Engineering 2016;88:265-279.
- Ochoa-Cornejo F. Cyclic behaviour of sands with superplastic fines. Doctoral dissertation 2015. Perdue University, West Lafayette, Indiana, USA
- Ochoa-Cornejo F, Bobet A, Johnston C, Santagata M, Sinfield JV. Dynamic Properties of a sand-nanoclay composite, Geotechnique 2020;70(3):210-225.
- Palmer ID, Traviolia ML. Attenuation by squirt flow in undersaturated gas sands. Geophysics 1980;45(12):1780-1792.
- Ram AK, Mohanty S. Laboratory investigation on damping characteristics of homogeneous and stratified soil-ash system. J of Rock Mechanics and Geotech Eng 2023;15: 2757-2777.

- Ruzicka B, Zaccarelli E. A fresh look at the Laponite phase diagram. Soft Matter 2011;7(4): 1268.
- Rio JFME. Advances in laboratory geophysics using bender elements. Doctoral thesis 2006. University of London, UK.
- Santamarina JC, Klein KA, Fam MA. Soils and waves: particulate materials behavior, characterization and process monitoring. England: John Wiley and Sons Ltd 2001.
- Shirley DJ, Hampton LD. Shear-wave measurements in laboratory sediments, The J of the Acoustical Society of America 1978;63(2):607-613.
- Siddique S, Khatiwada J, Shrestha S, Chio C, Chen X, Mohamedelhassan E, Deng J, Qin W. Effect of Laponite Nanoparticles on Growth Characteristics and Chlorophyll Content of *Chlorella* sp. Water Air Soil Pollut 2022;233:308.
- Spang, Wesley A. In situ measurements of damping ratio using surface waves. Georgia Tech Theses and Dissertations 1995, School of Civil and Environ. Eng. Atlanta, GA.
- Stoll RD. Sediment Acoustics. Lecture Notes in Earth Sciences, Berlin Springer Verlag 1989, Vol. 26.
- Sutherland WM. "Wyoming Bentonite" (PDF). Wyoming State Geological Survey (Sep 2014). Retrieved 12 January 2021.
- Tanaka H, Meunier J, Bonn D. Nonergodic states of charged colloidal suspensions: repulsive and attractive glasses and gels, Phys Rev E 2004;69(3):031404.
- Takele A, Quezon E, and Abebe T. Investigation of the Damping Ratio and Shear Modulus of Soil along Light Rail Transit Route in Megenagna-Hayat Road. Int J of Scientific and Engineering Research 2017;8(1):111-122.
- Tawari S, Koch A, Cohen C. Electrical double-layer effects on the Brownian diffusivity and aggregation rate of Laponite clay particles. J Colloid Interface Sci 2001;240(1):54-66.
- Tiwari B, Ajmera B. A new correlation relating the shear strength of reconstituted soil to the proportions of clay mineral and plasticity characteristics. Appl Clay Sci 2011;53(1):48-57.
- Wang Q, Tang AM, Cui YJ, Delage P, Gatmiri B. Experimental study on the swelling behaviour of bentonite/claystone mixture, Eng. Geol. 2012;124:59-66.
- White JE. Underground sound: application of seismic waves. Elsevier Amsterdam 1983.
- Xie DY. Soil dynamics. M. Beijing: Higher Education Press 2011.

CHAPTER 7 Permeability of Sand-Laponite Mixture and Compression Properties of Laponite Hydrogel

Abstract

Nanoparticles are proposed as an innovative means to stabilize ground susceptible to liquification, addressing the limitations of traditional stabilization techniques. However, a fundamental challenge in using nanoparticles, specifically laponite, in ground improvement applications is the lack of comprehensive understanding of their hydrogeological and mechanical properties. The objective of this study is to investigate the permeability of sand-laponite mixtures (0.5%-3% of dry mass of laponite/dry mass of sand) and the compressive behaviour of laponite hydrogel. The coefficient of permeability (κ) was assessed using both the standard compacted mold permeameter and triaxial cell. The results revealed that the κ of sand specimen decreases by an order of magnitude when mixed with a small amount of laponite (only 0.5% of laponite/dry mass of sand). As the concentration of laponite increased, the κ decreased further, mitigating the generation of excess pore water pressure generation and, ultimately, reducing the risk of liquefaction. Similar experiments with sand-bentonite mixtures showed that the permeability of sand-bentonite specimens was one to two orders of magnitude higher than that of sand-laponite samples for equivalent nanoparticles percentages. Additionally, the compressive behaviour of laponite hydrogel was evaluated using a uniaxial universal tester to assess the toughness. The findings indicated that the stress-strain graph of laponite hydrogel exhibited typical viscoelastic characteristics, demonstrating its suitability for applications requiring both elasticity and resilience under load. Laponite hydrogels have a nonlinear and dissipative behaviour when subject to mechanical loading.

Keywords: Permeability, Compression, Laponite, Hydrogel, Pore Water Pressure

7.1 Introduction

Soil permeability drastically increases due to more accessible water flow paths created by liquefaction. Due to the increase in pore water pressure in saturated sandy soils under dynamic loads, soils turn from a solid state to a liquid state, and loss its bearing capacity. Liquefaction causes various soil deformation including differential settlement, tilting, and turning which results in significant damage to structures. Determining the regions where liquefaction is anticipated and taking the appropriate steps should reduce destruction that occurs under dynamic loads. With the rapid advancement of nanotechnology, nanoparticles have gained attention for soil stabilization. Nanoparticles are specifically polymers with a three-dimensional network structure, capable of absorbing large amounts of water, are being proposed to treat soil layers susceptible to liquefaction. Nanoparticles decreases the permeability of soil, which dramatically lowers the abrupt spike in pore water pressure during seismic events and reduces the likelihood of liquefaction. Nanoparticles can reinforce soil by firming soil skeleton due to good rheological property and nano-size scale (Agapoulaki and Papadimitriou, 2018; Ochoa-Cornejo, 2015, 2017). Optimizing the treatment strategy of nanoparticles is one of the primary goals for engineering applications. To avoid plugging near injection ports of fine sand, quick low-concentration, low-*pH*, and two- or three-phase injection treatments are necessary (Cheng et al., 2019; Harkes et al., 2010). Recent research underscores that introducing nanoparticles such as bentonite and laponite represents an advanced approach for stabilizing the sandy soils.

Laponite, a new synthetic nanoparticle with structure similar to montmorillonite and made from sheets of silicate nanoparticles, shows strong properties of resisting liquefaction risk in a few published studies (Huang et al., 2020; Huang and Wang, 2016; Ochoa-Cornejo et al., 2016). Ochoa-Cornejo et al. (2016) investigated the influence of 1%–5% laponite (by dry mass of sand) on the cyclic response of sand with a relative density in the 15%–25% range. The results showed the cyclic response of sand is significantly influenced by adding only 1% of laponite. Similarly, Huang and Wang (2016) recommended laponite for use with liquefiable silty sand to enhance liquefaction resistance. Their dynamic triaxial tests analyzed the cyclic behavior and liquefaction resistance of laponite-sand specimens. They emphasized two critical factors influencing liquefaction resistance: (a) laponite concentration and (b) resting/curing time. Both studies agreed that higher laponite content and longer resting times improve the liquefaction mitigation by

solidifying pore fluids, cementing soil grains, and delaying pore pressure development. Furthermore, Huang and Wang (2016) and Ochoa-Cornejo et al. (2016) reported that rheological properties of laponite enhance liquefaction resistance through a sol-gel transition, yet its effectiveness may diminish under intensified cyclic loading due to thinning behavior.

When dry laponite powder comes into contact with water, it undergoes gelation and forms a hydrogel that is characterized by a three-dimensional network of hydrophobic polymers synthesized through cross-linking water-soluble polymers. The gelation process of laponite hydrogel typically requires a minimum resting time of 48 hours at room temperature, as determined from the rheological tests (Huang and Wang, 2016; Ochoa-Cornejo et al., 2016). Various test methods have been employed to assess the toughness properties of hydrogel samples, such as tensile tests, tear testing of a specimen with a notch, and compression. Certain features of other tests may be unsuitable due to their limits. For instance, the tensile test with no notches can only assess the toughness overall. Trouser tear tests, commonly used for soft hydrogel samples, can encounter challenges related to gripping the specimen, leading to stress concentrations that may tear the grips rather than the sample itself. Furthermore, it could take a lot of sample materials to complete the tear test with the required standard geometry. In contrast, the compressive testing offers a straightforward approach using a universal tester, providing clear force-displacement curves that directly interpret the uniaxial response of hydrogel materials. This method is practical for assessing both bulk and two-dimensional forms of hydrogels (Dastgerdi et al., 2021; Wang and Hong, 2012). However, Zhang et al. (2018) have stated that the compression testing and theory face various difficult problems, including precise volume changes. There are two different procedures for conducting this compressive test (ASTM D575-91, 2001):

(a) *Test Method A- Compression Test of Specified Deflection*: a compression test in which the force required to cases a specified deflection is determined.
(b) *Test Method B- Compression Test at Specified Force*: a compression test in which the specified mass or compressive force is placed on the specimen and the resulting deflection is measured and recorded.

Compression testing commonly involves crosshead displacements ranging from 60% to 80% of the specimen height, as commonly reported. To delineate the elastic region, researchers have occasionally employed the initial 'instant fit' (tangent) of engineering stress-strain curve derived from the crosshead displacement data (Kocen et al., 2017). However, challenges such as non-ideal

surface conditions, noise from load cells, and inaccuracies in the initial data points can affect the precision of these results. According to Bauer et al. (2017), some researchers proposed a direct method for calculating the Young's modulus. This method involves performing a linear fit along the engineering stress-strain curve derived from crosshead displacements between 5% and 10% strain. This approach aims to provide a more reliable determination of the Young's modulus despite the challenges posed by initial test conditions and instrumentation noise.

Hydrogels are inherently incompressible due to their predominant composition of water (Dastgerdi et al., 2021). The test specimen must deform extensively in the lateral direction to preserve volume (Poisson's ratio ≈ 0.5) for the compressive deformations as high as 15%–30%. Ideally, this Poisson's ratio effect vanishes under frictionless conditions with test apparatus in contact. However, the side force needed to slide the specimen out disappears when the contact friction reaches zero. To prevent specimen displacement during testing, researchers enhance friction using thin paper strips (Nakamura et al., 2001). Increasing friction necessitates greater specimen deformation and localized rotation during interactions with testing machine. Additionally, taller specimens are more susceptible to bending and buckling under compressive stress. Assessing the mechanical properties of hydrogels presents several challenges compared to the conventional materials. The researcher faces significant challenges in measuring and interpreting the mechanical data related to hydrogels because of their relatively small elastic modulus values which display neither solid nor liquid behaviour. Additionally, it is not easy to grip the hydrogel samples for testing. The elastic modulus of most hydrogel is on the scale of Kilopascals (kPa), while the most mechanical testing apparatus is optimised for the range of Megapascals (MPa) to Gigapascals (GPa) (Oyen, 2014).

There are no comprehensive studies in the available literature on coefficient of permeability (κ) of fully saturated sand-laponite mixtures. Additionally, there is a lack of data on the toughness parameters of laponite hydrogel in the literature, which is crucial for understanding its behavior when used in ground treatment to mitigate liquefaction. The permeability of sand-laponite mixture and toughness properties of laponite hydrogel are one of the most important and interesting research topics. A comprehensive understanding of these phenomena is essential for enhancing ground performance in the seismic zones before introducing laponite suspension into the ground to support engineering structures. Thus, the primary objective of this study is to examine the coefficient of permeability (κ) of sand mixed with laponite at various concentrations (ranging from

0.5% to 3% of laponite), an important property that qualitatively indicates the liquefaction resistance of sand. Another objective of this research is to evaluate the toughness of laponite hydrogels through compression testing. This novel information will help to understand the results and discussions of the two published projects of the authors, Siddique et al. (2023) and Siddique et al., (2024).

7.2 Experimental Materials

7.2.1 Laponite

Laponite is utilized as a rheology modifier in various applications, including surface coatings, household cleaners, and personal care products (BYK, 2014). In a dry state, laponite is a refined white power and has a disk-like shape with a diameter of approximately 25 nm, a thickness of 1 nm (Kroon et al. 1998), and a specific gravity between 2.10 (BYK, 2014) and 2.57 (Ochoa-Cornejo et al., 2016). The chemical composition formula of laponite is $Na^{+0.7}[(Si_8Mg_{5.5}Li_{0.3})O_{20}(OH)_4]^{-0.7}$ which is a 2:1 clay formed by a magnesium octahedral sheet sandwiched between two silica tetrahedral sheets. Isomorphic substitution of magnesium by lithium atoms generates negative charges on both faces, which are counterbalanced by interlayer cations, generally sodium. The edges have weaker *pH*-dependent positive charge. Using *pH* and conductivity measurements, estimates of magnitude of the face and edge charges of laponite when prepared in deionized water revealed that the positive charge on the crystal edges (4-5 mmol/100 g) is about 10% of the total negative charge on the crystal faces (50-55 mmol/100 g) (BYK, 2014; Tawari et al., 2001). When dispersed in water, laponite hydrates, swells, and forms a colourless transparent monodisperse suspension that resembles a highly thixotropic gel. It can be used as a high-performance water-based drilling fluid (Huang et al., 2020). Laponite-RD (rheology additive) was used in this study, which has high efficiency in water-based systems and is manufactured by BYK Additives and Instruments, Germany. In a recent research study by the authors (Siddique et al., 2022), laponite is shown to be environment-friendly and biologically inert.

Microstructure of laponite: The microstructure of laponite hydrogel was analysed by the Scanning Electron Microscope (SEM). After allowing laponite to swell for 28 days, a few drops of laponite gel were placed on a carbon tap and dried completely for 24 hours using a freeze drier. The freeze-dried method is widely recognized as effective for observing the pore morphology or inter-polymer network of the hydrogel (Yacob and Hashim 2014). Prior to scanning, the dried hydrogel samples

were coated with gold to enhance image quality. Figure 7-1 shows the SEM images of laponite hydrogel morphology at magnifications of 500, 100, and 10 µm. The images revealed that the structures of swollen laponite are continuous sheet-like irregular structures with pore sizes similar as mentioned in the case of Carrageenan hydrogel, as reported in studies by Yacob and Hashim (2014).

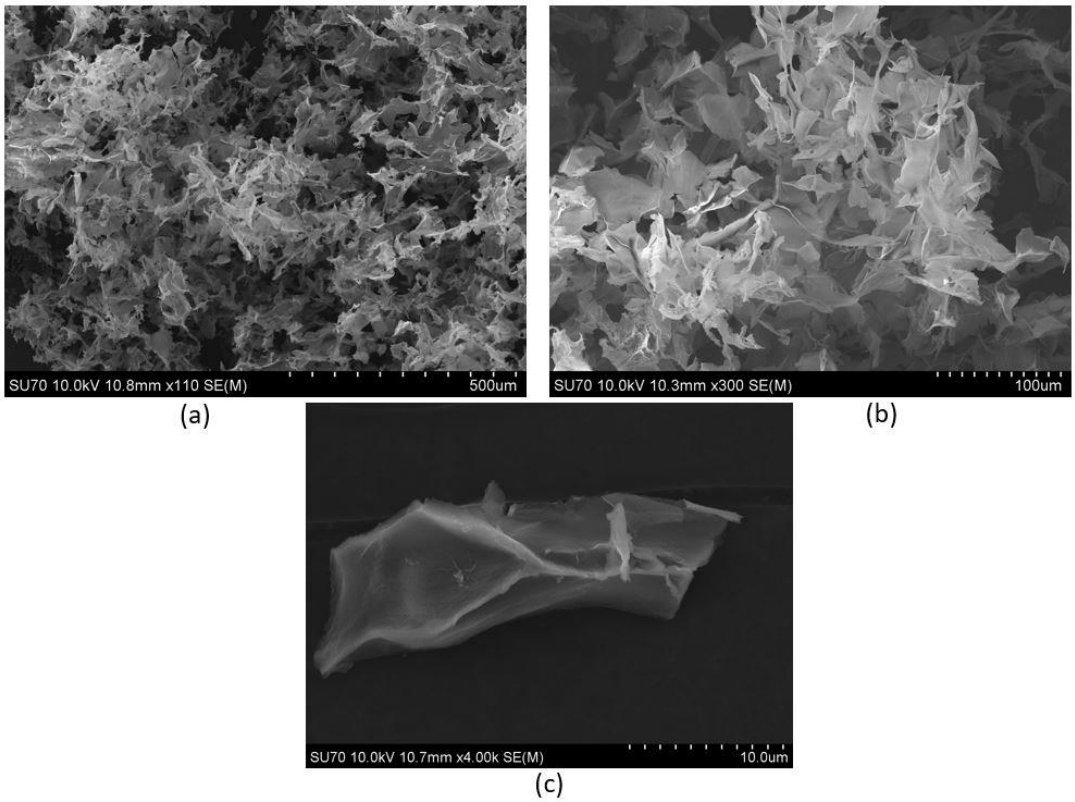

Figure 7-1: Microstructure of laponite gel, SEM images at (a) 500 µm, (b) 100 µm, and (c) 10 µm magnification

7.2.2 Bentonite

Bentonite is formed by volcanic ash being subjected to seawater weathering, which converts the volcanic glass found in the ash into clay minerals (Nesse, 2000; Sutherland, 2014). Bentonite particles also have a fundamental thickness of 1 nm, but the diameter is 200-1000 nm. Fresh exposures of bentonite beds are white, pale blue, or green. As the exposure is weathered further, it changes to a cream hue, then to yellow, red, or brown (Jackson, 1997). The Goldcorp Canada LTD supplied the bentonite used in this study.

7.2.3 Sand

The Pioneer Construction, Thunder Bay, Ontario, Canada provided sand used in this study. According to ASTM D6913 (2017), the grain size distribution analysis showed that the uniformity coefficent and the coefficient of curvature of sand were 4.40 and 0.74, respectively. According to the Unified Soil Classification System, the group symbol of sand is *SP,* the group name is poorly graded sand with d_{50}=0.62 mm, and the fine content is <5%. The moisture content was 9.5%, according to ASTM D2216-19 (2019), and the specific gravity of sand was 2.60, obtained in accordance with ASTM C128-15 (2015).

7.3 Experimental Methods

7.3.1 Specimen Preparation

Laponite specimen was stored in an airtight container in a dry room to avoid moisture absorption. For sand-laponite mixture, the specimens were prepared by dry pluviation. The desired amount of laponite was mixed with sand in an airtight container and shaken for 20 minutes. Distilled water was added to the dry sand-laponite mixture to achieve full saturation after placing the dry samples into the apparatus. To ensure homogeneity, sand-laponite mixtures were left to rest for 72 hours before testing. The same procedure was followed for preparing sand-bentonite mixtures. The compressive properties were tested using laponite hydrogel. First, laponite hydrogel was prepared by adding distilled water to fresh laponite powder and allowing it to rest for 72 hours. However, the hydrogel was too sticky to be removed from the mold for testing and was challenging to shape according to ASTM requirements. To address this, a one-dimensional oedometer consolidation cell from Humboldt Mfg. Co., USA, was used. This cell consists of a base, load pad, cutter ring, clamping ring, cap, acrylic cylinder (surrounding wall), and two porous stones. About 8 g of fresh laponite powder was lightly compacted using an initial vertical load in the cutter ring (diameter = 50.8 mm). Subsequently, a small weight (≈ 400 g) was applied through the load pad to keep the sample in place. Following that, the deaired distilled water was added to the entire cell, allowing the sample to swell only in the axial direction. Finally, the swelling strains were measured using a strain gauge with a precision of 0.01. When the vertical displacement measurement steadied, the wetting test was ended. The saturation process varied in duration based on laponite content and laboratory conditions. The water height was kept constant during the testing period to prevent evaporation and maintain consistent sample concentration. After saturation, laponite hydrogel was

removed from the sample holder ring, cut to the required height, sealed in an airtight bag, and immediately subjected to testing.

7.3.2 Experimental Procedures

7.3.2.1 **Permeability Test**

7.3.2.1.1 Using standard compacted mold permeameter

The grain structure and voids in soil particles significantly affect soil permeability. Coefficient of permeability (κ) tests have been conducted with both pure (untreated) sand and sand treated with laponite at concentrations of 0.5%, 1%, 2%, and 3% by dry mass of sand. The constant head test method was used for pure sand (cohesionless), and the falling head test was mainly performed for the sand-laponite mixtures. The same procedure was followed to determine the κ of sand treated with bentonite at various concentrations (1%, 2%, and 3% by dry mass of sand).

7.3.2.1.2 Using a triaxial cell

The triaxial cell apparatus and master panel (ELE International Tri-flex 2) were used to estimate the coefficient of permeability (κ) for each sample under three confining pressures, 69, 172, and 275 kPa. The sample was compacted in the triaxial mold, with porous stones and filter papers placed on both the top and bottom of the mold. A latex membrane was used to enclose the entire system. The cylindrical specimens were 49 mm in diameter and 48-49 mm in height. The cell pressure for all samples was set to 103 kPa. All the samples were kept in a sealed container for at least 72 hours in fully saturated condition to fully develop the rheological properties as recommended by Huang and Wang (2016) and Ochoa-Cornejo et al. (2016) before conducting the tests.

7.3.2.2 **Universal Tester**

To characterize the mechanical properties of laponite hydrogel, unconfined compression testing is conducted using a universal testing machine with the Bluehill Universal Materials Testing Software from Instron at the Green Processes Research Center, Lakehead University, Ontario, Canada. The ASTM D575-91 (2001) standard methods have been followed to conduct the tests in this study. Due to the softness of laponite hydrogel, a load cell with a maximum capacity of 5 N was used. This is typical for testing soft biological materials or biomechanical components, including hydrogels. Compression test parameters, such as displacement rate, starting point, friction, were determined through preliminary experiments, as the standard method is designed for

rubber specimens, not soft hydrogel. All tests were performed on wet hydrogels at room temperature (~23˚C) and approximately 50% humidity. The diameter and height of laponite hydrogel sample were 50.8 mm and 12.5 mm, respectively. The exact dimensions of each sample were measured with calipers before testing. In this study, the samples were compressed until reaching 80%-90% displacement of their original height (Tan et al., 2017; Ranjbardamghani et al., 2023).

For the unconfined compression testing, load-displacement (F-x) data were converted to stress-strain (σ-ε) data using simple geometrical relationships, and the Young's Modulus was reported. Because hydrogels exhibit time-dependent behaviour, the standard tests were conducted at a fixed rate until the specimen fails. However, testing at different strain rates is often necessary due to the time-dependent response of hydrogels. In addition to simple tests at a fixed rate, specimen may undergo creep (extension at fixed load or fixed stress) experiments to observe variations in response over time with constant loading. According to ASTM D575-91 (2001), the compression testing should be conducted at a head travel rate of 12±3 mm/min for rubber. However, there is no specific rate suggested for hydrogel. In this study, tests were carried out at displacement rate of 5 mm/min and 1 mm/min (Dastgerdi et al., 2021) to observe the rate dependency of the hydrogel compression. These rates were selected after extensive trials.

7.4 Results and Discussions

7.4.1 Change of Permeability

7.4.1.1 **Using Standard Compaction Mold Permeameter**

In general, an aggregate with high porosity has a low specific gravity and a high-water absorption rate, while an intact aggregate has a higher specific gravity and a lower water absorption rate (Amuda et al., 2014). Table 7-1 shows the specific gravity (G_s) and moisture content (%) of pure (untreated) sand, sand-laponite and sand-bentonite mixtures at different concentrations. According to ASTM D2216-19 (2019), the moisture content of pure sand is 9.5%, and its specific gravity, as determined by ASTM C128-15 (2015), is 2.60 in this study. When sand samples are treated with laponite and bentonite, both specific gravity and moisture content increase. As the concentration of nanoparticles (i.e., laponite, bentonite) in the specimens increases, the specific gravity gradually rises. The specific gravity largely depends on the mineral density of individual soil particles. Due to their smaller size, nanoparticles behave like clay, slightly increasing the specific gravity

compared to untreated sand. However, the specific gravity of laponite ranges between 2.10 (BYK, 2014) and 2.57 (Ochoa-Cornejo et al., 2016). According to the test specified in IS: 2720 (Part 4)-1985 (1986), the specific gravity of inorganic clays generally ranges from 2.70 to 2.80. Soils with large amounts of organic matter or porous particles, such as diatomaceous earth, have specific gravities below 2.60, with some as low as 2.00. Moisture content is another critical parameter in soil samples. In this study, untreated sand has a moisture content of 9.50%, which increases significantly when treated with nanoparticles. Al-Shayea (2001) reported that clay contains about 11.50% moisture content in its 'natural dry' state.

Table 7-1: Specific Gravity (Gs) and Moisture Content (%) of the pure (untreated) sand and sand samples treated with laponite and bentonite at various concentrations

Sample	Specific Gravity, G_S	Moisture Content (%)
Pure sand	2.60	9.50
Sand+0.5% Laponite	2.61	16.50
Sand+1% Laponite	2.63	16.36
Sand+2% Laponite	2.65	16.20
Sand+3% Laponite	2.68	15.31
Sand+1% Bentonite	2.62	17.40
Sand+2% Bentonite	2.65	16.98
Sand+3% Bentonite	2.67	15.59

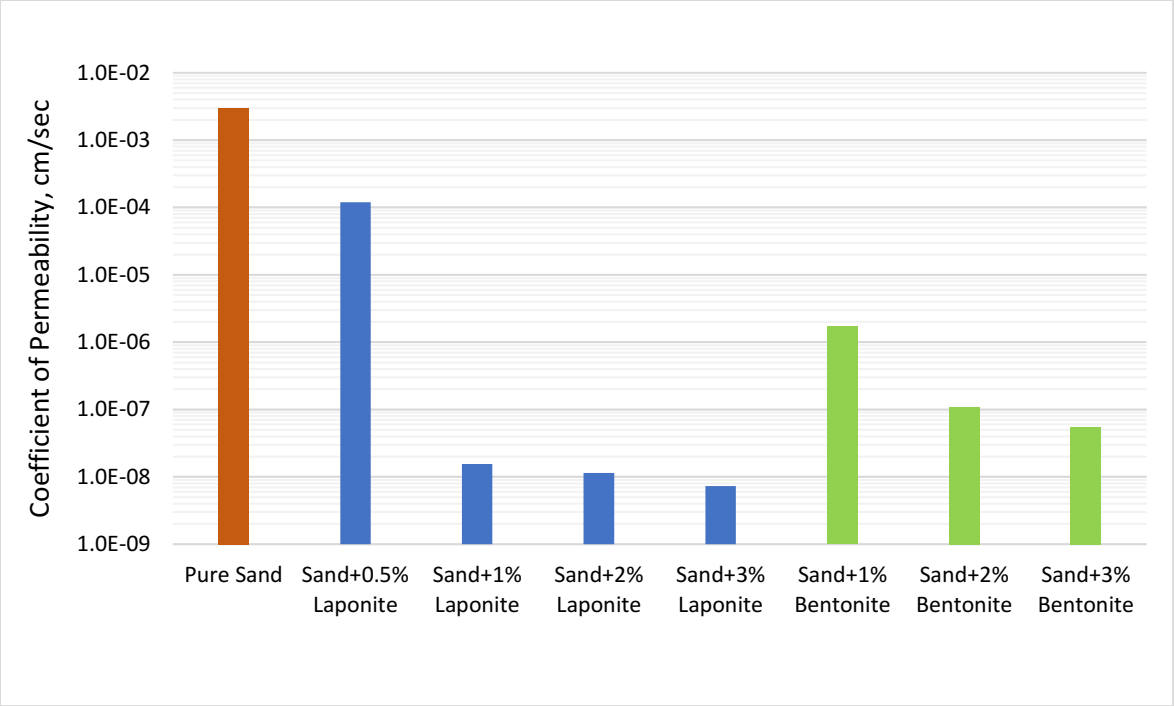

Figure 7-2: Coefficient of Permeability (κ) of untreated (pure) sand and sand treated with nanoparticles (laponite, bentonite) at various concentrations

Due to the more accessible water flow routes created by liquefaction, soil permeability increases significantly. A high coefficient of permeability (κ) allows the excess pore water pressure to dissipate quickly, leading to increased settlement during cyclic loadings. Permeability is a crucial parameter in engineering practices, and research has explored various aspects of permeability (Almisned et al., 2018; Xia et al., 2020). Figure 7-2 shows the comparisons of κ of untreated sand and sand treated at various concentrations of laponite and bentonite, which has been conducted using the falling head permeability test method. The untreated sand has a permeability (κ) of $3.0x10^{-3}$ cm/sec, whereas sand specimens treated with 0.5% laponite shows a significantly reduced κ ranging around $1.2x10^{-4}$ cm/sec. This indicates that the κ of sand reduces by an order of magnitude with even a small amount of laponite (0.5% by dry mass of sand). As the concentration of laponite increases, the κ of sand-laponite specimens decreases noticeably. The permeability of sand-laponite mixtures with 1%, 2%, and 3% of laponite (dry mass of laponite/dry mass of soil) are $1.55x10^{-8}$, $1.14x10^{-8}$, and $7.31x10^{-9}$ cm/sec, respectively. The findings clearly demonstrate that the presence of laponite reduces soil permeability, thereby mitigating the generation of excess pore water pressure and the risk of liquefaction. The κ of sand-bentonite specimens are $1.72x10^{-6}$,

$1.10x10^{-7}$, and $5.51x10^{-8}$ cm/sec for mixing the sand with 1%, 2%, and 3% bentonite (by dry mass of sand), respectively. Laponite-treated samples show a more significant reduction in permeability compared to bentonite-treated samples. In this study, as the resting time of the treated specimens increases, the κ reduces according to the conducted tests. All data in this section are collected after the specimens had rested for 72 hours under fully saturated conditions to ensure the consistency in test results.

7.4.1.2 **Using Triaxial Cell**

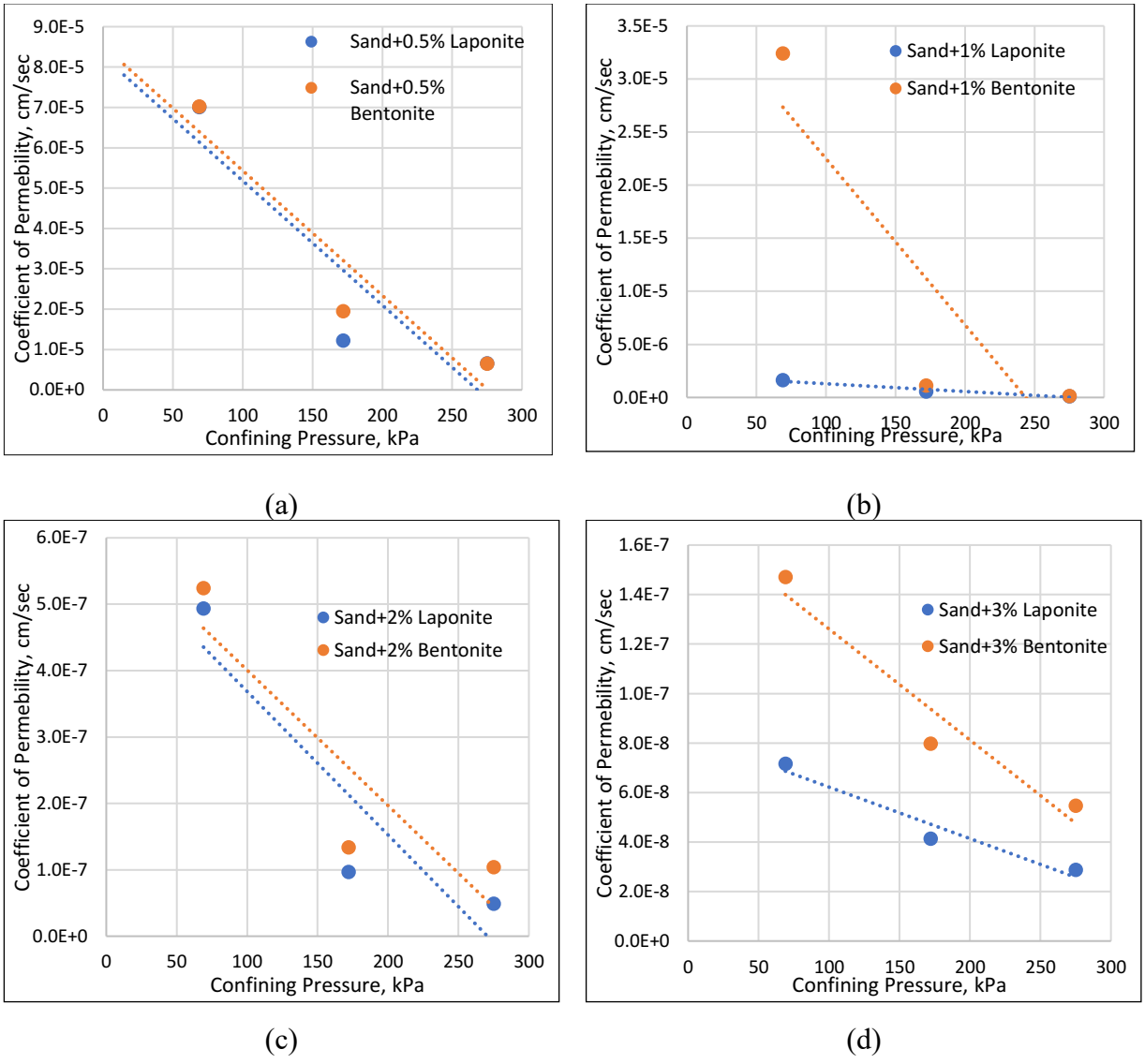

Figure 7-3: Coefficient of Permeability (κ) of sand treated with nanoparticles (laponite, bentonite) at different confining pressures (69, 172, and 275 kPa)

Figure 7-3 illustrates the coefficient of permeability (κ) of sand treated with laponite using the triaxial cell at three confining pressures (69, 172, and 275 kPa). In each case, the κ decreases gradually as the confining pressure increases from 69 kPa to 172 kPa. This trend holds true for both test methods – the falling head and triaxial cell test indicating that permeability decreases with increasing laponite concentration in the samples. Sivapullaiah et al. (2000) reported that permeability increases with a higher coarse fraction; however, clay minerals predominantly control permeability in soils with higher clay content. The confining pressure greatly affects the optimal water content, similar to compaction energy. Increasing the confining pressure increases the maximum dry density and decreases the maximum water content (Shirazi et al. 2010). The κ values varied significantly with different confining pressures. At the confining pressure of 69 kPa, the κ of sand mixed with laponite of 0.5%, 1%, 2%, and 3% are $7.00x10^{-5}$, $1.62x10^{-6}$, $4.94X10^{-7}$, and $7.16x10^{-8}$ cm/sec, respectively. As the confining pressure rises to 275 kPa, the permeability decreases to $6.61x10^{-6}$, $1.13x10^{-7}$, $4.87x10^{-8}$, and $2.87x10^{-8}$ cm/sec for sand+0.5% laponite, sand+1% laponite, sand+2% laponite, and sand+3% laponite, respectively. Shirazi et al. (2010) observed similar behaviour of permeability of sand-bentonite at different compaction rates, attributing it to structural particle rearrangement. The structural disturbance significantly impacts the permeability in fine-grained soil samples. Yoshinaka and Kazama (1973) stated that soil particles are gradually oriented as the rate of compaction increases, leading to stratified soil masses with varying permeability in parallel and perpendicular directions to stratification; permeability parallel to stratification is typically higher.

To compare the permeability of sand treated with laponite, identical experiments were conducted with the sand samples treated with bentonite (0.5%, 1%, 2%, and 3% of dry mass of bentonite/dry mass of sand). Figure 7-3 illustrates that as the percentage of bentonite increases in the samples, the κ decreases, mirroring the trend observed for laponite-treated sand samples. However, the permeability of sand-bentonite samples is consistently larger by one to two orders of magnitude compare to sand-laponite samples for an equal percentage of nanoparticles. This difference is attributed to the smaller particle size of laponite compared to bentonite. Similar to sand-laponite samples, the κ of sand-bentonite samples decreases gradually as the confining pressure increases. The κ values vary significantly with different confining pressures. For instance, at a confining pressure of 69 kPa, the permeability of sand samples mixes with bentonite of 0.5%, 1%, 2%, and 3% are $7.02x10^{-5}$, $3.24x10^{-5}$, $5.24x10^{-7}$, and $1.47x10^{-7}$ cm/sec, respectively. With an increase in the

confining pressure to 275 kPa, the κ decreases to $6.48x10^{-6}$, $1.42x10^{-7}$, $1.04x10^{-7}$, and $5.46x10^{-8}$ cm/sec for sand mixed with 0.5%, 1%, 2%, and 3% bentonite, respectively. Shirazi et al. (2010) observed similar behaviour in the permeability of sand-bentonite mixtures. Their study reported that the permeability ranged from $1x10^{-8}$ to $4x10^{-12}$ cm/sec by 50% sand containing bentonite.

The κ of sand treated with nanoparticles (laponite and bentonite) shows nearly identical when measured using both the standard compaction mold permeameter and triaxial cell (at confining pressure of 275 kPa). The slight variations in κ measured between these two apparatuses can be attributed to the variation of the specific requirements (such as the use of confining pressure and/or cell pressure), and extended duration required to complete the experiments. Notably, the results indicate that the permeability of the treated sand samples is significantly lower compared to pure sand samples.

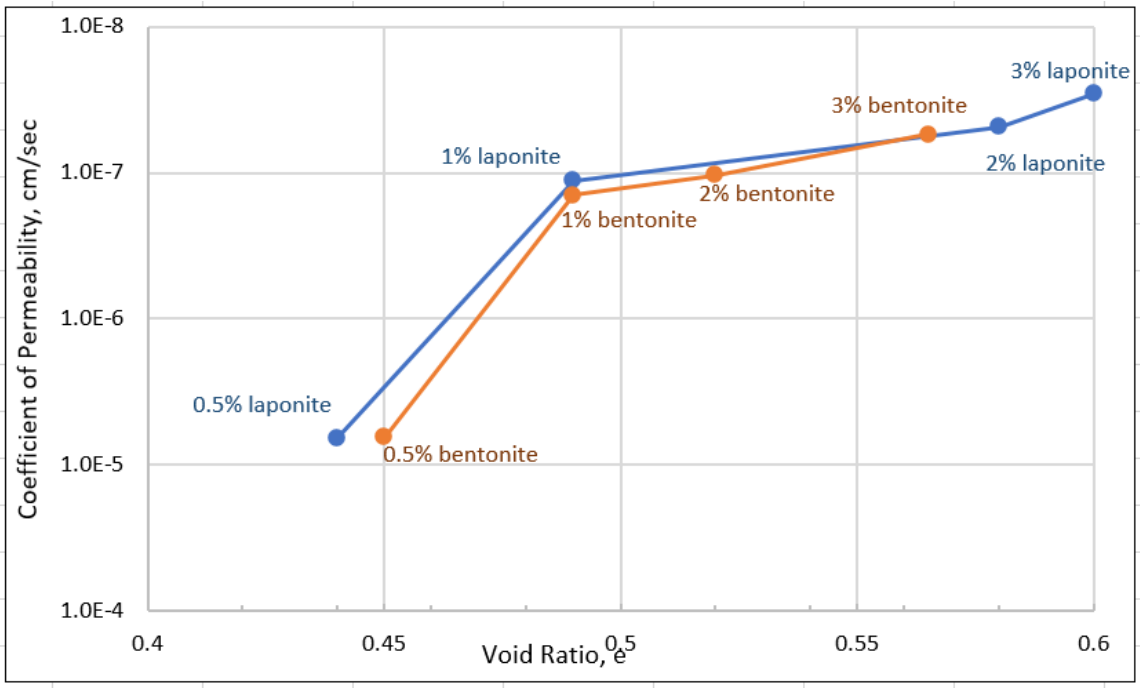

Figure 7-4: Relationship between the coefficients of permeability (κ) and void ratio (e) of sand-nanoparticle samples (0.5%, 1%, 2%, and 3% of dry mass of nanoparticle/dry mass of sand)

The relationship between the coefficients of permeability (κ) and void ratio (e) of sand treated with nanoparticles (laponite, bentonite) at various concentrations presented in Figure 7-4. It illustrated that the κ decreases due to increased laponite content in the samples, while the void ratio gradually increases. This phenomenon can be attributed to the significant specific surface area of

nanoparticles, which coat the coarser sand particles, thereby preventing direct contact between grains. The coarser particles essentially float within a matrix provided by laponite particles. Earlier studies (Pandian and Nagaraj, 1990; Murthy et al., 1987) reported that the coarser particles proportionately dilute the physicochemical potential of a soil. Soil possesses physicochemical potential due to inherent interparticle forces and the associated clay fabric. Changes in the permeability of sand-laponite mixtures can be explained by changes in the flocculation state of clay. In the flocculated state, clay particles tend to adopt an open structural arrangement with relatively high permeability. When distributed, clay minerals may be transported and deposited in narrow pore openings, causing a clogging effect. Sample compaction can influence alterations in the flocculation state (Shirazi et al., 2010). Samples treated with various concentrations of bentonite also exhibit similar behaviour in this study. Shirazi et al (2010) also reported the relationship between the void ratio and permeability at various bentonite contents in their study, which closely aligns with the findings of this study. It was illustrated that permeability decreased with an increase in bentonite at the same void ratio (Shirazi et al., 2010).

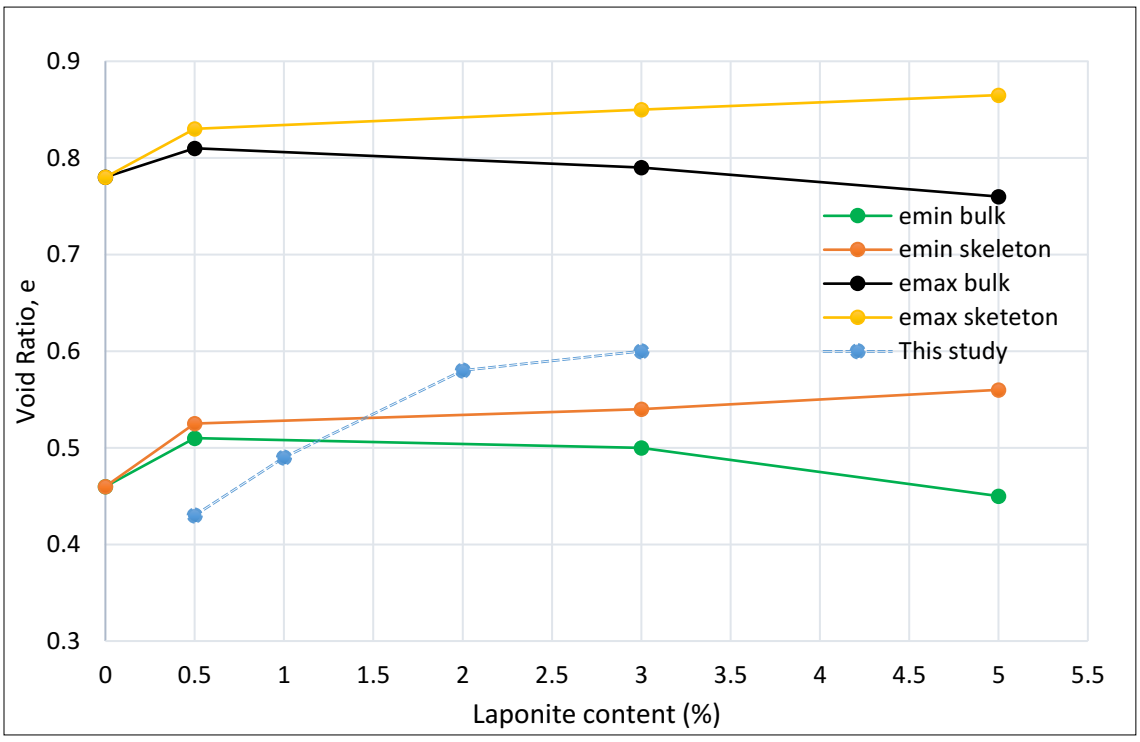

Figure 7-5: Variation of Skeleton and bulk (e_{min} and e_{max}) with laponite at different concentrations, after, Ochoa-Cornejo (2015)

Bulk void ratio represents the fraction of voids, indicating the difference between the total volume of a solid and the volume filled by solids. On the other hand, the skeleton void ratio corresponds to the void ratio of grains constituting the stress-bearing skeleton. According to Pan et al. (2023), it is necessary to consider the space occupied by fine particles that do not act the role of skeleton as pores, and than calculate a void ratio that can truly reflect the soil density, called the skeleton void ratio ($e_{skeleton}$). This parameter appears to exhibit a clear relationship between the skeleton void ratios which incorporate the influencing of gradation and density, and the strength deformation characterises (Yang et al., 2015; Pan et al., 2023). The skeleton void ratio ($e_{skeleton}$) can be written as:

$$e_{skeleton} = \frac{e + (1 - B)f_c}{1 - (1 - B)f_c}$$

Where, e is the overall void ratio, f_c is the percentage of the mass of particles smaller than 5 mm in the total particle mass and can be also expressed as $P_{<5}$. B is the percentage of the mass of the fine particles that serve as skeletons to the mass of all fine particles. The higher the fine particle content, the greater the proportion of fine grain content involved in undertaking the skeleton, that is, the larger the value of B. Value of 0 for B means that the fine particles are all filled in the pores between the coarse particles and do not act as a skeleton.

Ochoa-Cornejo (2015) presented a graph (Figure 7-5), demonstrating bulk and skeleton void ratios (e_{min} and e_{max}) attained for untreated (pure) sand (0%), 1%, 3%, and 5% laponite by dry mass of sand. The sand used in Ochoa-Cornejo's study was Ottawa Sand (specific gravity=2.65, d_{50}=0.33 mm, with less than 1% of fines). It is reported that both $e_{min\ bulk}$ and $e_{max\ bulk}$ exhibit a similar trend with increasing laponite content. Both $e_{min\ bulk}$ and $e_{max\ bulk}$ rise when 1% of laponite is added. According to Thevanayagam et al. (2002), at least some of this small quantity of laponite added positions itself at the sand-grain contacts, playing an active role of ***separator***. Conversely, the skeletal void ratios ($e_{min\ skeleton}$ and $e_{max\ skeleton}$) are higher than the reference values estimated for untreated sand. When laponite concentration is increased to 3%, both bulk void ratios decrease but remain more significant than those of untreated sand. As laponite concentration increases, both $e_{min\ bulk}$ and $e_{max\ bulk}$ gradually decrease; however, the $e_{min\ skeleton}$ and $e_{max\ skeleton}$ also increase (**Figure *7-5***). Therefore, adding laponite to sand samples has dual effects: laponite separates grains further (reflected in the rise of $e_{min\ skeleton}$ and $e_{max\ skeleton}$) but also starts to fill void spaces. More than 3%

of laponite is required for the second effect to drive a reduction in $e_{min\ bulk}$ and $e_{max\ bulk}$ (Ochoa-Cornejo, 2015). Extensive data available for sand-silt mixtures indicate that adding up to 15% silt can decrease both $e_{min\ bulk}$ and $e_{max\ bulk}$ (e.g. Carraro et al. 2009; Thevanayagan et al., 2002). Since there is no attraction between sand and silt grains, the finer grains are primarily confined in the pore space. However, further addition of silt grains can reverse this trend, eventually causing $e_{min\ bulk}$ and $e_{max\ bulk}$ to exceed the values measured for untreated sand. The void ratios of the sand-laponite samples calculated in this study indicate that sand samples containing 2% and 3 % of laponite fall within the limits of e_{min} and e_{max} (both bulk and skeleton) as reported by Ochoa-Cornejo (2015) (Figure 7-5). For lower concentrations (sand+0.5% laponite, sand+1% laponite), the void ratios of this study are slightly below the e_{min} reported by Ochoa-Cornejo (2015), although the difference is marginal.

7.4.2 Compressive Strength of Laponite Hydrogel

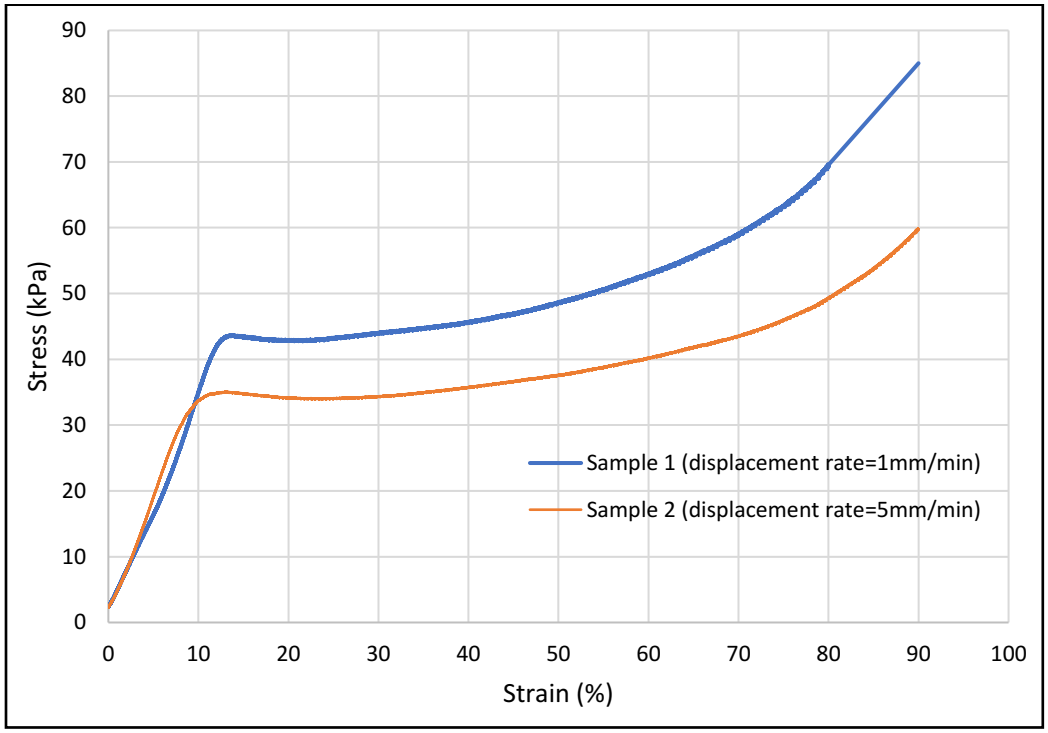

Figure 7-6: The stress-strain curves of laponite hydrogel at two different displacement rates.

The simplest way to evaluate the general toughness of a hydrogel is through compression test. This method also provides measurements of the elastic (Young's) modulus and shear modulus of the hydrogel (Xiao et al., 2013). Compression to failure is highly influenced by artifacts within the

hydrogel (Tan et al., 2017; Xiao et al., 2013). Given the nonlinear stress-strain relationship, variations in fracture strain cause substantial differences in fracture strength and even greater differences in toughness, leading to relatively high variability. This variability in inherent to the method, especially given where the extreme limit of 100% strain, and a high degree of variability in materials that fracture at 80%-90% strain under compression (Tan et al., 2017). The behaviour of laponite hydrogel in compression is illustrated in Figure 7-6. The displacement rate-dependent stress-strain behaviour of laponite hydrogel can be clearly observed in this graph. Researchers have reported a non-linear region (toe region) at the beginning of the stress-strain curve of hydrogels (Koivusalo et al., 2018; Karvinen et al., 2017). In all tested cases, hydrogels initially exhibit resistance to applied loads and subsequent deformation under increased loads at specific strains. Dastgerdi et al. (2021) proposed to characterise the stress-strain behaviour of hydrogels with an exponential toe region that transitions seamlessly into a linear elastic region, which can be fitted according to the hydrogel composition. According to Figure 7-6, the stress-strain graph of the laponite hydrogel exhibited typical viscoelastic characteristics, demonstrating its suitability for applications that demand both elasticity and resilience under load. When subject to mechanical loading, laponite hydrogels have a nonlinear and dissipative behaviour similar to other hydrogel in the literature (Dasgerdi et al., 2021; Tan et al., 2017). It is stated that laponite hydrogel samples begin to show cracks at the early stage (within 12%-15% strain). However, they withstand the entire experiment and, surprisingly, do not fail even after reaching 90% strain under compression.

In this study, the estimated Young's Modulus of laponite hydrogels range from 410 kPa to 480 kPa. This range is consistent with values reported by Tan et al. (2017) who found the compressive strength of laponite hydrogels to vary between 117 kPa to 1774 kPa depending on laponite concentration. High laponite content not only enhanced the mechanical strength, but also increases the strength gaps in different locations within the hydrogel. This feature is particularly beneficial for mimicking the extracellular matrix in 3D cell culture applications. The mechanical strength of laponite hydrogels increased by 38% compared to isotropic nanocomposite hydrogel. Moreover, laponite hydrogel exhibited 'soft-to-hard' mechanical properties due to the gradient distribution of laponite and polymers. The gradient distribution of laponite aids in the stress dissipate, thereby improving the mechanical property of hydrogel. The gradient bamboo-like structure of hydrogel further contributes to its mechanical strength, making it advantageous for use as scaffold or cell culture matrices. Tan et al. (2017) referred to laponite hydrogel as gradient laponite-crosslinked

nanocomposite hydrogel. At a low displacement rate, the stress state relaxes during the test, resulting in a higher peak stress level. In case of the higher displacement rate, the peak of stress is lower. Hence, it can be stated that displacement rate affects the stress-strain curves of laponite hydrogel. Dastgerdi et al. (2021) also reported displacement rate-dependent stress-strain behaviour of the hydrogel samples. They found that near the compression plates, the strain field is strongly uneven, primarily due to the interface between the rigid compression plate and the deforming specimen surfaces. The variation in the cross-sectional area of the specimen is significant. It is essential to check whether different boundary conditions could cause this behaviour as an artifact or as an actual material response. Thus, various experimental measurement methodologies should be explored to understand the early deformation phase. In principle, a frictionless boundary would be ideal for the compression testing (Zhang et al., 2018). The barrelling effect, which is the sideway changes in the specimen form, is significant due to friction at the interface between the specimen and the compression plate.

Thus, hydrogels are multi-phase materials composed of a porous solid and a liquid (water) solvent phase, understanding their mechanical response requires more complex analysis than what is used for solid polymers. Simple treatments established for the solid polymers are insufficient for hydrogels. Researchers aiming to develop more mechanically robust hydrogel materials need to address these complexities which will be thoroughly examined.

7.5 Conclusions

This study illustrates the results of experimental studies on the permeability of sand-laponite mixtures and the compressive behaviour of laponite hydrogel. The result showed that:

- The permeability of untreated (pure) sand is 3.00×10^{-3} cm/sec.
- The permeability of sand-laponite mixtures decreases significantly upon the addition of small quantities of laponite with sand. This reduction in permeability becomes more pronounced as the concentration of laponite increases.
- Reducing the permeability of sand can mitigate the development of excess pore water pressure and the risk of liquefaction.
- As confining pressure increases from 69 kPa to 275 kPa, the permeability (κ) of sand-laponite samples gradually decreases. The summary of the data is as follow:
  Permeability (κ) at 69 kPa:

- Sand+ 0.5% laponite: 7.00×10^{-5} cm/sec
- Sand+ 1% laponite: 1.62×10^{-6} cm/sec
- Sand+ 2% laponite: 4.94×10^{-7} cm/sec
- Sand+ 3% laponite: 7.16×10^{-8} cm/sec

Permeability (κ) at 275 kPa:

- Sand+ 0.5% laponite: 6.61×10^{-6} cm/sec
- Sand+ 1% laponite: 1.13×10^{-7} cm/sec
- Sand +2% laponite: 4.87×10^{-8} cm/sec
- Sand+ 3% laponite: 2.87×10^{-8} cm/sec

- Laponite particles coat coarser sand particles, affecting the direct grain contact and increasing void ratio.
- Changes in the flocculation state of clay minerals influence the permeability of sand-laponite mixtures. Flocculated clay particles have higher permeability due to their open structural arrangement, while dispersed clay can cause pore clogging. Sample compaction alters the flocculation state of clay minerals, thereby affecting permeability changes in sand-laponite mixtures.
- The κ of sand-bentonite mixtures also decreases with the higher bentonite concentrations similar to sand-laponite samples.

  Permeability (κ) at 69 kPa:

  - Sand+ 0.5% bentonite: 7.02×10^{-5} cm/sec
  - Sand+ 1% bentonite: 3.24×10^{-5} cm/sec
  - Sand+ 2% bentonite: 5.24×10^{-7} cm/sec
  - Sand+ 3% bentonite: 1.47×10^{-7} cm/sec

  Permeability (κ) at 275 kPa:

  - Sand+ 0.5% bentonite: 6.48×10^{-6} cm/sec
  - Sand+ 1% bentonite: 1.42×10^{-7} cm/sec
  - Sand+ 2% bentonite: 1.04×10^{-7} cm/sec
  - Sand+ 3% bentonite: 5.46×10^{-8} cm/sec
- Laponite hydrogels exhibit the nonlinear stress-strain relationships which represents typical viscoelastic characteristics.

- Laponite hydrogel is suitable for applications that require resilience and elasticity under mechanical stress.

7.6 References

Almisned OA, Aliquraishi AA, Al-Otaibi KA (2018) A simple apparatus to study the effect of lithology, permeability, and wettability on spontaneous imbibition. *Arab J Geosci* 11:235.

ASTM D575-91 (2001). Standard test methods for rubber properties in compression. These test methods are under the jurisdiction of ASTM Committee D11 on Rubber and are the direct responsibility of subcommittee D11.10 on Physical Testing.

ASTM-D5890-11 (2021) standard test method for swell index of clay mineral component of geosynthetic clay liners. ASTM international

ASTM-D6913 (2017) Standard test methods for particle-size distribution (gradation) of soils using sieve analysis. ASTM international

Bauer A, Gu L, Kwee B, Li WA, Dellacherie M, Celiz AD, Mooney DJ (2017). Hydrogel substrate stress-relaxation regulates the spreading and proliferation of mouse myoblasts, *Acta Biomater*. 62:82–90

BYK (2014) Technical information B-RI 21: Laponite Performance. A member of Altana, Germany. https://docplayer.net/23462 772-Technical- information-b-ri-21-laponite-performance-additives.html

Carraro J, Prezzi M, Salgado R (2009). "Shear strength and stiffness of sands containing plastic or nonplastic fines." *J of Geotechnical and Geoenvironmental Engineering*, 135(9):1167–1178. Thevanayagam S, Shenthan T, Mohan S, Liang J (2002). "Undrained fragility of clean sands, silty sands, and sandy silts." *J of Geotech and Geoenvironmental Engineering*, 128(10):849–859.

Cheng L., Shahin, M.A., and Chu, J. (2019). Soil bio-cementation using a new one-phase low-pH injection method. *Acta Geotechnica*, 14(3): 615–626

Dastgerdi JN, Koivisto JT, Orell O, Rava P, Jokinen J, Kanerva M, and Kellomaki M (2021). Comprehensive characterisation of the compressive behaviour of hydrogels using a new modelling procedure and redefining compression testing, *Material Today Communications* 28(21): 102518.

Harkes MP, Van Paassen LA, Booster JL, Whiffin VS, Van Loosdrecht MCM (2010). Fixation and distribution of bacterial activity in sand to induce carbonate precipitation for ground reinforcement. *Ecological Eng*, 36(2): 112–117.

Huang Y, Wang L (2016) Laboratory investigation of liquefaction mitigation in silty sand using nanoparticles. *Eng Geol* 204:23–32

Karvinen J, Koivisto JT, Jonkkari I, Kellomaki M (2017). The production of injectable hydrozone cross-linked gellan gum-hyaluronan-hydrogels with tunable mechanical and physical properties, *J Mech Behav Biomed Mater* 71: 383-391.

Kocen R, Gasik M, Gantar A, Novak SS (2017). Viscoelastic behavior of hydrogel-based composites for tissue engineering under mechanical load, *Biomed. Mater*. 12:25004

Koivusalo L, Karvinen J, Sorsa E, Jonkkari I, Valiaho J, Kallio P, Ilmarinen T, Mietinen S, Shottman H, Kellomaki M (2018). Hydrazone cross-linked hyaluronan-based hydrogels for therapeutic delivery of adipose stem cells to treat corneal defects, *Mater Sci Eng C* 85:68-78.

Murthy S, Nagaraj BR, Bindumadhava TS (1987). Influence of coarse particles on compressibility of soils, Proceedings, International symposium on prediction and performance in geotechnical engineering, Calgary, Canada, Balkema, Rotterdam, pp. 17-19

Nakamura K, Shinoda E, Tokita M (2001). The influence of compression velocity on strength and structure for gellan gels, *Food Hydrocoll*. 15: 247–252

Ochoa-Cornejo F, Bobet A, Johnston C, Santagata M, Sinfield J (2016) Cyclic behavior and pore pressure generation in sands with laponite, a super-plastic nanoparticle. *Soil Dyn Earthq Eng* 88:265–279

Pandian NS, Nagaraj TS (1990). Critical reappraisal of colloidal activity of clays. *J Geotechnical Eng. ASCE*, 116(GT2): 285-296

Ranjbardamghani F, Eslahi N and Jahanmardi R (2023). An injectable chitosan/laponite hydrogel synthesized via hybrid cross-linking system: A smart platform for cartilage regeneration, *Polymers Advanced Technologies* 34: 2298-2311.

Shirazi SM, Kazama H, Salman FA, Othman F and Akib S (2010) Permeability and swelling characteristics of bentonite, *Int J of The Physical Sciences* 5(11): 1647-1659.

Siddique SN, Deng J and Mohamedelhassan (2023). Improving the Strength Properties of Sand Using Laponite, a Promising Nanoparticle, *Int J of Civil Engineering* 21:679-693.

Siddique SN, Deng J and Mohamedelhassan (2024). Swelling Behaviour of Super-absorbent Laponite Hydrogel under One-dimensional Loading, *Geotech Geol Eng*, https://doi.org/10.1007/s10706-024-02796-3

Sivapullaiah PV, Sridharan A, Stalin VK (2000). Hydraulic conductivity of bentonite-sand mixtures, *Canadian Geotechn. J.*, 37: 406-413

Tan Y, Xu S, Wu R, Du J, Sang J and Wang J (2017). A gradient laponite-crosslinked nanocomposite hydrogel with anisotropic stress md thermos-response, *Applied Clay Science* 148: 77-82.

Yoshinaka R, Kazama H (1973). Mico-structure of compacted kaolin clay, Soils and Foundations, Japanese society of *Soil Mechanics and Foundation Engineering*, 13(2): 19-33

Wang X, Hong W (2012). A visco-poroelastic theory for polymeric gels, *Proc. Math. Phys. Eng. Sci.* 468: 3824–3841

Xia P, Zeng F, Song X, Sun B, Yan T, Li W, Meng Y (2020). Permeability dynamic variation of coal under various confining pressure using LFNMR relaxation method. *Arab J Geosci* 13:220.

Xia Y, Friis E, Gehrke SH, Detamore MS (2013). Mechncial testing of hydrogels in Cartilage Tissue Engineering: Beyond the Compressive Modulus, *Tissue Engineering* 19(5): 403-410.

Zhang YR, Xu KJ, Bai YL, Tang LQ, Jiang ZY, Liu YP, Liu ZJ, Zhou LC, Zhou XF (2018). Features of the volume change and a new constitutive equation of hydrogels under uniaxial compression, *J Mech Behav Biomed Mater* 85:181-187.

CHAPTER 8 Conclusions and Recommendations

8.1 Introduction

This dissertation aimed to investigate the influence of small quantities of laponite on the properties of sand. Laponite, a highly plastic synthetic clay with mineralogical similarities to natural hectorite, was the focus of this investigation. For the entirety of the study, laponite-RD, supplied by BYK Additives and Instruments Inc., Germany, was exclusively utilized. Laponite-RD is a rheology additive based on synthetic phyllosilicate designed for aqueous systems, enhancing rheological properties particularly at low shear rates. Laponite is a white powder consisting of nano-sized disc-shaped particles (approximately 1 nm in thickness and 25-50 nm in diameter). In hydrogel form, laponite primarily aggregates into silt-sized stacks. When combined with organic thickeners, laponite-RD exhibits a synergistic effect, facilitating the production of stable water-based electrode slurries and improving the adhesion and mechanical strength of electrode coatings. Moreover, the cycle stability can be significantly increased by using laponite. Based on the research of this dissertation, laponite, a highly promising nanoparticle, effectively mitigates the generation of pore water pressure and presents a viable alternative for ground improvement and treatment applications.

The experimental program encompassed triaxial tests, shear box tests, Oedometer tests, and an in-house experimental setup using bender elements. All experiments were conducted on pure sand (as control tests), sand treated with laponite, and in some cases, sand treated with bentonite. The tests with pure sand not only provided the base line behaviour against which the effects of the addition of laponite could be evaluated, but also were used to assess and guarantee the repeatability of procedure and results. In addition to mechanical tests, observations were made using scanning electron microscopy (SEM) on sand grains, laponite powder, and sand-laponite mixtures. These studies, along with complementary experiments such as particle size distribution analysis of dry laponite powder, viscosity analysis of laponite hydrogel, Cation Exchange Capacity (CEC), X-ray Diffraction (XRD), X-ray Fluorescence (XRF), microscopic cell count by compound microscope, and coefficient of permeability (κ) measurements on sand-laponite samples, provided insights into the structure formed in sand-laponite specimens and the underlying mechanisms governing their behavior.

There are two more sections in this chapter. A summary of the findings, outlines the major conclusions from the comprehensive study and the implications of this research are presented in Section 8.2. Future research recommendations are given in Section 8.3 which is divided into seven subsections corresponding to potential avenues for the further investigation.

8.2 Specific Conclusions

This dissertation concludes each chapter with a summary. The main conclusions are outlined in this section.

8.2.1 Laponite is Environment-Friendly

A lower concentration of laponite has been observed to positively influence microalgae growth in the growth medium, contrasting with the inhibitory effects seen at higher concentrations of laponite. Specifically, in the 0.1% treatment group, the total chlorophyll content increased by 33% compared to the control group. SEM images revealed significant microalgae aggregation at this lower laponite concentration. In contrast, at higher laponite concentrations (0.4% and 0.5% treatments), algal cells were found embedded in laponite gel, accompanied by physical impairments. Laponite particles adhering to the surface of microalgae can be absorbed, coating them in surface caveolae. At lower concentrations, laponite may integrate within microalgae. However, as laponite concentration increases, its physical impairments and inhibitory effects reduce the microalgae's ability to aggregate. The concentration of laponite used in the growth medium directly influences its effects on microalgae aggregation. Therefore, in lower quantities, laponite appears to be safe for the aquatic ecosystem.

8.2.2 Laponite Improves Shear Strength of Sand

A small amount of laponite can significantly reduce the generation of pore water pressure due to its excellent rheological properties, forming a robust transparent gel. Sand-laponite specimens exhibit approximately twice the modulus of elasticity compared to pure sand. For an equivalent amount of strain, the required stress of sand-laponite specimens is around four times higher than that of pure sand. Moreover, the gel-like laponite demonstrates robust plastic behavior after sufficient resting time. The intriguing gelation behavior of laponite is evidenced by its viscosity changes over time at different concentrations in solution. The addition of only 1% laponite dramatically reduces the friction angle due to its strong binding effect on sand particles at room temperature. Temperature plays a crucial role, affecting both mechanical responses and the thickness of the double layer in electrostatically stabilized systems. Elevated temperatures

accelerate the gelation process even with minimal laponite, whereas lower temperatures noticeably slow it down. This study provides novel insights into enhancing and modifying sand strength properties in the presence of laponite under static loading conditions.

8.2.3 Laponite Hydrogel Swells Significantly

Over time and with increasing concentrations of laponite in the samples, the swelling strain of compacted laponite also increased. Laponite took nearly four weeks to achieve equilibrium during the initial swelling, whereas in reswelling tests, equilibrium was reached within 60 hours. SEM images revealed continuous, sheet-like irregular structures of swollen laponite with non-porous pore sizes. The hydrogel network appeared denser, resulting in a shrunken state. The pore structure inside laponite hydrogel is made up of polymer rigid branches; it can act as a storage space for water molecules. As the hydrogel absorbs water, stress is effectively distributed by these polymer branches, ensuring the stability of the network structure. Interestingly, the reswelling height of laponite was higher than its initial swelling, indicating distinct reswelling behavior compared to other clay minerals. Additionally, the swelling pressure of compacted laponite ranged between 5.6 kPa and 8.6 kPa throughout the experiment, attributed to interlayer and double-layer stresses.

8.2.4 Laponite Enhances Damping Ratio

The damping ratio (ξ) of pure sand is typically around 7.48%, consistent with values found in the literature, accounting for variations in sand types and potential errors in laboratory equipment or electronic devices. Upon continuous shaking, the ξ of pure sand gradually decreases until it stabilizes at around 0.99% by Day 3–4, significantly lower than its initial value. In contrast, the ξ of treated samples (sand+laponite) is higher than that of untreated sand. Initially, the damping ratio increases and then decreases until reaching equilibrium in the case of sand + laponite samples. The higher damping values in sand-laponite specimens indicate viscous damping due to laponite presence at the contacts between sand grains: greater laponite content at these interfaces correlates with higher damping values. Images of the samples released from the clear Polycarbonate Tube after the experiments illustrate the compact bonding observed in sand-laponite samples.

8.2.5 Laponite Reduces Permeability and Compressive Strength of Hydrogel

Treating sand samples with a relatively small amount of laponite (0.5% of dry mass laponite/dry mass of sand) results in a tenfold decrease in sample permeability compared to untreated samples. As concentration of laponite increases, the permeability of samples decreases significantly, thereby reducing the generation of excess pore water pressure and ultimately lowering liquefaction risk.

Laponite hydrogels exhibit nonlinear stress-strain relationships which represent typical viscoelastic characteristics. Laponite hydrogel is suitable for applications that require resilience and elasticity under mechanical stress.

8.3 Major Contributions

Based on the findings from this research, several practical and industrial contributions can be identified, particularly in the areas of environmental sustainability, construction materials, and soil mechanics:

8.3.1 Environmentally Friendly Additive

The research demonstrates that low concentrations of laponite promote the growth of microalgae, making it a potentially eco-friendly additive in soft soil in marine area and underground water.

8.3.2 Improvement of Soil Shear Strength and Stability

The significant increase in the modulus of elasticity and shear strength when laponite is mixed with sand indicates its potential as an effective soil stabilizer. In geotechnical and civil engineering applications, this could improve the stability and strength of foundational soils in construction projects.

8.3.3 Swelling Behavior in Hydrogel Applications

The research reveals that laponite hydrogel exhibits unique swelling and reswelling characteristics, which could be beneficial in the design of hydrophilic structures or water-retaining systems. Its ability to maintain structural integrity while absorbing and holding water positions it as a potential material in sectors like agriculture (for soil moisture retention), pharmaceuticals (controlled drug delivery systems), and environmental engineering (waste containment liners).

8.3.4 Damping Properties for Vibration Control

Laponite's ability to enhance the damping ratio of sand presents opportunities in infrastructure that require improved energy absorption and vibration control. This could be particularly useful in seismic design, where the reduction of vibrations is critical for the protection of buildings and other infrastructure.

8.3.5 Potential in Soft Ground Improvement

The non-linear stress-strain behavior of laponite hydrogel suggests its application in areas requiring materials that can withstand high levels of mechanical stress while maintaining

flexibility. Its viscoelastic properties can be leveraged in projects like tunnel linings, embankments, or road construction in soft ground conditions, where traditional materials might fail under prolonged or cyclic loads.

In summary, the research provides valuable insights into the use of laponite in soil stabilization, environmental protection, infrastructure resilience, and vibration control, offering promising opportunities for its adoption across various industrial sectors.

8.4 Limitations

Although this research investigates the soil strength properties that controls the liquefaction behaviour of sand under seismic events, a physical liquefaction test was not carried out due to time constraints, and equipment availability. This study primarily focused on the fundamental properties of sand in the presence of laponite. Given the limited timeframe, the research was unable to perform long-term monitoring of certain properties, such as the aging effects of laponite in soil mixtures or the long-term performance of laponite hydrogels under various environmental conditions.

Extended testing could have provided a better understanding of how these materials behave over time, particularly under changing environmental conditions, such as prolonged mechanical stress. While the laboratory tests provided valuable insights, large-scale validation in real-world geotechnical projects was beyond the scope of this research. Field testing and in-situ measurements would be necessary to confirm the scalability of the findings and assess their effectiveness under real-world conditions, particularly in large infrastructure projects or when dealing with varying soil compositions and load conditions.

8.5 Recommendations for Future Research

8.5.1 Field-Scale Testing

The focus of this dissertation has primarily been on laboratory-scale testing. To transition towards practical applications, a comprehensive evaluation at a larger scale is essential. Future studies should consider conducting centrifuge or shaking table tests to assess how sand responds to laponite under field-scale conditions.

8.5.2 Passive Site Stabilization Technique

The viscosity of laponite suspension increases as concentration of laponite and resting time increases. Hence, it may become more difficult to introduce laponite suspension into ground unless adequate pressure is provided. However, excessive pressure, such as pumping the suspension into soil layer, could potentially induce fracturing, rendering it an unsuitable treatment method. An alternative approach could involve temporarily reducing the permeability of laponite suspensions through chemical modifications. This adjustment could facilitate the permeation of laponite suspensions into soil layers without the need for excessive pressure. Future research should thoroughly investigate and develop this technique.

8.5.3 Laboratory Testing to Find Optimal Concentration of Laponite

One of the commonly employed passive techniques is permeation grouting, which involves drilling a bore followed by injecting a probe to permeate grouting material while maintaining soil fabric nearly undisturbed. Laboratory testing should be conducted to assess the feasibility of mobilizing laponite hydrogel in aquifers. This would provide evidence on whether laponite particles can be effectively delivered into liquefiable sand layers with sufficient concentrations to stabilize soil. There have been no published studies on the mobility of laponite in liquefiable sand layers and aquifers. Column tests and box model tests are recommended to study the transportability of laponite in liquefiable sand. Therefore, it is crucial to investigate the optimal concentration of laponite for field applications. Specifically, determining the ideal concentration of laponite suspension to inject into injection wells at the upgradient edge of site is essential for delivering it to the desired location effectively.

8.5.4 Strengthening the Structure of Laponite Suspensions

In future research, it is highly recommended to conduct a detailed investigation into how various chemical additives, such as electrolytes, acids, surface-active agents, and polymers, interact with laponite particles and alter their rheological properties. Understanding these interactions will provide valuable insights into enhancing and modifying the rheological characteristics of laponite suspensions.

8.5.5 Weaken the Structure of Laponite Suspension

Adding specific compounds like condensed phosphates and polymers can weaken the original structure of laponite suspension, leading to a reduction in its aggregation rate. The literature highlights Sodium Pyrophosphate (SPP), Tetrasodium Pyrophosphate (TSPP), and polymers as

common additives used to modify the microstructure of laponite suspensions. The in-details understanding on the method of weaken the laponite structure in presence of various compounds is highly suggested.

8.5.6 Micromechanical Investigations and Studies of the Microstructure

To gain initial insights into particle-level interactions between sand grains and laponite particles within sand-laponite mixtures at varying laponite concentrations, this research involved basic micro-mechanical tests and utilized SEM images. It is recommended that this line of investigation be further pursued to fully understand the dynamics of this geomaterial. Key areas for the future study could include:

- Investigating the hydration properties of laponite during swelling.
- Exploring the hydration properties of laponite after initial swelling and subsequent re-swelling.
- Assessing the tensile characteristics of laponite hydrogels.
- Examining the adhesion or bonding mechanisms between sand grains and laponite particles.
- Evaluating the strength of bonding between sand grains in the presence of laponite at both low and high concentrations.
- Analyzing the friction generated at sand contacts when laponite is present.

These areas of investigation will provide comprehensive insights into the behavior and interactions within sand-laponite mixtures, contributing to a deeper understanding of their mechanical properties and potential applications.

8.5.7 Numerical Analyses

A more profound comprehension of the interactions between particles at nano, micro, and macro sizes has been made possible by using numerical techniques. The study conducted in this dissertation can progress incorporating available numerical techniques. Future endeavours could go in one of the following directions:

- *Finite Element Method (FEM):* FEM starts with a variational statement of problem and introduces piecewise definitions of the functions defined by a set of mesh point values. In other words, the FEM is a computational method that subdivides a CAD model into very small but finite-sized elements of geometrically simple shapes. The collection of all these simple shapes constitutes the so-called finite-element mesh. This analysis can describe the behaviour of sand-laponite considering different boundary conditions and geological conditions.

- *Finite Difference Method (FDM):* FDM is the most direct approach to discretizing partial differential equations. This method typically uses explicit or implicit schemes to march the solution forward in time, and it can handle both steady-state and time-dependent problems. The FDM starts with a differential statement of problem and replaces the derivatives with their discrete analogs. This method can analysis the behavior of sand-laponite interaction considering time lapse.
- *Discrete Element Method (DEM):* DEM (Distinct Element Method) is becoming widely accepted as an effective method of addressing engineering problems in granular and discontinuous materials, especially in granular flows, powder mechanics, ice, and rock mechanics. This numerical technique is usually used to compute the motion and effect of many small particles. However, the DEM is very closely related to molecular dynamics, which is generally distinguished by its inclusion of rotational degree-of-freedom, stateful contact, particle deformation, and often complicated geometries. This method can analysis the interaction of sand-laponite particles as a function of the rheology of the pore water.
- *Molecular Dynamics (MD)*: MD simulation is a computational method that employs Newton's laws to evaluate the physical movements of water, ions, small molecules, and macromolecules or more complex systems. The atoms and molecules are allowed to interact for a fixed period, giving a view of the dynamic evolution of the system. This computer simulation method can predict the interaction of laponite on the surface of sand grains.

APPENDICES

APPENDIX A

A.1. Comparison of Laponite Concentrations in Microalgae and Sand Experiments

To provide a comprehensive analysis of the effects of laponite on sand, it is crucial to understand the concentration ranges used in different experimental contexts. In Chapter 3, the investigation into the effects of laponite on microalgae growth involved concentrations from 0.1% to 0.5% added to the control (BG-11) medium. In contrast, other chapters focused on the impact of laponite on sand, employing a broader range of concentrations from 0.5% to 5% relative to the moisture content of sand. This introduction explores the differences in laponite concentrations used across these experiments and highlights the implications for comparing the results. By examining these varying concentrations, we aim to assess how the higher ratios of laponite in sand experiments provide a safe estimation for evaluating the effects and ensure a good comparison with the findings from microalgae studies.

In Chapter 3, to investigate the effects of laponite on microalgae growth, laponite concentrations ranging from 0.1% to 0.5% were added to the control medium. Microalgae were cultivated in 500 ml Erlenmeyer glass flasks, with a working volume of 300 ml, and subjected to a 16-hour light and 8-hour dark day-night cycle under white fluorescent lights. The flasks were placed in a constant orbital shaker set at 125 rpm. Laponite concentrations, therefore, corresponded to 0.1% to 0.5% of the 300 ml working volume, which equates to a laponite addition of 0.3 to 1.5 ml.

Assume the amount of soil is 500 gm
Amount of moisture= 500 x 9.5% = 47.5 gm = 47.5 ml water
0.5% to 5% of 47.5 ml water = 47.5*0.25% = 0.24 to 2.38 ml of laponite

In other chapters, the laponite was added to sand at concentrations ranging from 0.5% to 5% of the dry mass of sand, with the sand having a moisture content of 9.5%. For a soil sample weighing 500 grams, the moisture content is calculated as 500 x 9.5%, resulting in 47.5 grams (or 47.5 ml) of water. The laponite concentrations in this case range from 0.5% to 5% of the 47.5 ml water, which equals 0.24 ml to 2.38 ml of laponite. This comparison highlights the varying concentrations of laponite used in the microalgae and sand experiments, providing a basis for understanding the impact of laponite on different mediums in this research.

The chosen ratio of laponite in the other chapters, ranging from 0.5% to 5% relative to the moisture content in sand, is notably smaller than the ratio used in Chapter 3. This indicates that the amount of laponite introduced in sand tests is lesser than in the microalgae growth study. Given that the lower laponite concentrations in Chapter 3 already showed noticeable positive effects on microalgae, the ratios in sand experiments provide a safe estimation for comparing the results. The less substantial presence of laponite in sand suggests that any observed impact on the mechanical properties of sand would likely be more pronounced, allowing for reliable comparisons and conclusions to be drawn between the different chapters of this research.

A.2. Effects of Nanoparticles on Microalgae growth

In previous research, various types of nanoparticles have been demonstrated to have distinct and sometimes contrasting impacts on different microalgae species. For instance, Saxena and Harish (2019) found that nano-form of zinc oxide (ZnO) was notably more toxic than its bulk form to freshwater algae. The toxicity of ZnO nanoparticles, with concentrations ranging from 0.06 to 100 mg/L, has been extensively documented, revealing significant adverse effects on algal growth and viability (Ma et al., 2013; Bhuvaneshwari et al., 2018; Franklin et al., 2007; Li et al., 2017; Miao et al., 2010). This finding highlights the importance of particle size and form in determining the extent of nanoparticle toxicity. In contrast, research by Kadar et al. (2012) showed that a 100 mg/L dosage of nanoscale zero-valent iron (nZVI) led to an 18.75% increase in biomass concentration and a 3.57% increase in lipid accumulation in Isochrysis galbana. However, the same dosage resulted in approximately a 40% reduction in biomass but a 41.90% increase in lipid accumulation in *Tetraselmis suecica*. This illustrates the varied responses of different microalgae species to nZVI and emphasizes the need for species-specific assessments of nanoparticle impacts.

Furthermore, Demir et al. (2015) found that alpha-iron-oxide (α-Fe_2O_3) and gamma-iron-oxide (γ-Fe_2O_3) nanoparticles exhibited different levels of toxicity on *Nannochloropsis* sp. and *Isochrysis* sp., with α-Fe_2O_3 generally showing lower toxicity compared to other iron-based nanoparticles like nZVI and Fe_2O_3. This variation underscores the importance of evaluating the specific effects of each nanoparticle type on algal health and growth. Additionally, research by Zhang et al. (2017) reported that carbon nanotubes, iron-oxide nanoparticles, and magnesium oxide (MgO) nanoparticles caused cell growth inhibition in *Scenedesmus obliquus* at concentrations of 10, 40, and 0.8 mg/L, respectively. Notably, lower doses ($\leq$5 mg/L) of carbon nanotubes and iron-oxide

nanoparticles resulted in a significant increase in lipid accumulation, whereas higher dosages led to a decline in lipid productivity. This dose-dependent response illustrates the complexity of nanoparticle interactions with microalgae, where low concentrations may enhance certain metabolic processes, while higher concentrations can be detrimental.

Although research on the effects of bentonite and colloidal silica on microalgae growth is still emerging, some studies provide insights into their potential impacts.

Bentonite: Bentonite, a clay primarily composed of montmorillonite, has been shown to influence microbial activity in various settings, including soil and water. While studies directly linking bentonite to microalgae growth are scarce, its interaction with microorganisms in aquatic systems suggests that it could affect microalgal communities as well (Wang et al., 2010). Its high surface area and ion exchange properties may influence nutrient availability and subsequently, algal growth.

Colloidal Silica: Colloidal Silica has been studied more extensively in environmental and industrial applications. Though not focused primarily on algae, some studies suggest that its gel-like properties and role in forming stable suspensions in water may interfere with the nutrient uptake mechanisms of microorganisms, potentially impacting microalgae growth (Naveed et al., 2018).

These studies emphasize the critical need to assess nanoparticle toxicity based on their effects on microalgae growth and metabolic functions. Understanding these interactions is essential for evaluating the environmental impact of nanoparticles and optimizing their applications in biotechnological and environmental processes. The varying levels of toxicity and their effects on microalgae growth highlights the importance of carefully considering nanoparticle properties and concentrations in both research and practical applications. Additionally, emerging research on the influence of bentonite and colloidal silica on microbial activity presents further opportunities for exploration, particularly in understanding how these materials may impact microalgal growth and productivity.

A.3. References

Ma, H., Williams, P., & Diamond, S. (2013). Ecotoxicity of manufactured ZnO nanoparticles-a review. *Env. Pollut. 172*, 76–85.

Kadar, E., Rooks, P., Lakey, C., & White, D. (2012). The effect of engineered iron nanoparticles on growth and metabolic status of marine microalgae cultures. *Sci. Total. Env. 439*, 8–17.

Saxena, P., & Harish (2019). Toxicity assessment of ZnO nanoparticles to freshwater microalgae *Coelastrella terrestris*. *Env. Sci. Pollut. Res. 26*, 26991–27001.

Bhuvaneshwari, M., Iswarya, V., Vishnu, S., Chandrasekaran, N., & Mukherjee, A. (2018). Dietary transfer of zinc oxide particles from algae (*Scenedesmus obliquus*) to daphnia (*Ceriodaphnia dubia*). *Env. Res. 164*, 395–404.

Franklin, N., Rogers, N., Apte, S., Batley, G., Gadd, G., & Casey, P. (2007). Comparative toxicity of nanoparticulate ZnO, bulk ZnO, and ZnCl2 to a freshwater microalga (*Pseudokirchneriella subcapitata*): the importance of particle solubility. *Env. Sci Technol. 41*, 8484–8490.

Li, J., Schiavo, S., Rametta, G., Miglietta, M., La Ferrara, V., Wu, C., & Manzo, S. (2017). Comparative toxicity of nano ZnO and bulk ZnO towards marine algae T*etraselmis suecica* and *Phaeodactylum tricornutum*. *Env. Sci Pollut. Res.* 24, 6543–6553.

Miao, A., Zhang, X., Luo, Z., Chen, C., Chin, W., Santschi, P., & Quigg, A. (2010). Zinc oxide-engineered nanoparticles: dissolution and toxicity to marine phytoplankton. *Env. Toxicol Chem. 29*, 2814–2822.

Demir, V., Ates, M., Arslan, Z., Camas, M., Celik, F., Bogatu, C., & Can, S. (2015). Influence of Alpha and Gamma-Iron Oxide Nanoparticles on Marine Microalgae Species. *Bull. Env. Contam. Toxic. 95*, 752–757.

He, M., Yan, Y., Pei, F., Wu, M., Gebreluel, T., Zou, S., & Wang, C. (2017). Improvement on lipid production by *Senedesmus obliquus* triggered by low dose exposure to nanoparticles. *Sci. Rep. 7*, 15526.

Wang, D., Li, H., Wang, L., Xu, Y. (2010). Effects of chitosan-RE^{3+}-bentonite on growth of Chlorella vulgaris. *J of Rare Earths 28(1), 149-153*.

Naveed, S., Dong, B., Zhang, C., Ge, Y. (2018). Microalgae and their effects on metal bioavailability in paddy fields. *J of Soils and Sediments 18:936-945*.

APPENDIX B

Matlab Scripts

A.1.2. HALF-POWER BANDWIDTH METHOD

```
%1) Data import from Excel.
%Note that all the sweep's data was in a single file, each sweep in a
%different sheet with a normalized format.
filename='1% Laponite.xlsx'
time=xlsread(filename,'Sweep1','B1:B3600');
signal=xlsread(filename,'Sweep1','C1:C3600');
receptor1=xlsread(filename,'Sweep1','G1:F3600');
receptor2=xlsread(filename,'Sweep2', 'G1:F3600');
receptor3=xlsread(filename,'Sweep3', 'G1:F3600');
receptor_m=(receptor1+receptor2+receptor3)/3;
fs=1/xlsread(filename,'Sweep1','B7'); %Sampling frequency as the inverse
%of the cell value corresponding to
%the second time acquisition (the
%first corresponds to t=0).
NrUniqPts=ceil((length(receptor_m)+1)/2); %auxiliary variable corresponding
%to the number of points of the
%first half of the spectrum, in
%order to eliminate mirror
%redundancy.
freq=(0:NrUniqPts-1)*fs/length(receptor_m); %Frequency vector
  %determination.
figure(1)
subplot(2,2,1);
plotyy(time, signal, time, receptor1);
title('1st sweep');
xlabel('Time (ms)');
ylabel('Voltage [mV]');
legend('Signal wave','Receiver wave');
subplot(2,2,2);
plotyy(time, signal, time, receptor2);
title('2nd sweep');
xlabel('Time (ms)');
ylabel('Voltage [mV]');
legend('Signal wave','Receiver wave');
subplot(2,2,3);
plotyy(time, signal, time, receptor3);
title('3rd sweep');
xlabel('Time (ms)');
ylabel('Voltage [mV]');
legend('Signal wave','Receiver wave');
subplot(2,2,4);
figure(2)
plotyy(time,signal,time,receptor_m);
title('Sample P3 (50mm) averaged receiver wave');
```

```
xlabel('Time (ms)');
ylabel('Voltage [mV]');
legend('Signal wave','Receiver wave');
%2) FFT and magnitude.
%It's not required to create a new variable to save the
%magnitude values, as abs(fft( ... )) does the same. The script is
%presented this way for easier comprehension.
FFT_receptor_m=fft(receptor_m);
mag=abs(FFT_receptor_m);
%3) Damping determination by half-power bandwidth method.
%Explanation and variable nomenclature as stated before.
```

`aux=5; %Auxiliary variable used to ignore the first` `%spectrum, associated to test noise.`	`(five) points of the`

```
figure(3)
plot(freq,mag(1:NrUniqPts))
title('Sample P3 (50mm) frequency spectrum')
xlabel('Frequency [kHz]')
ylabel('Magnitude')
Am=max(mag(aux:NrUniqPts));
Anot=Am/2^0.5; %Notable value of A for determination of f1 and f2, with
%the relation already stated.
indexm=find(mag(aux:NrUniqPts)==Am)+aux-1
fm=freq(indexm)
clear aux
%3.1) 1st truncation interpolation
aux2=indexm-10 %Auxiliary variable to determine the range of data
%points (10 data points in this case) at the left of fm
%for interpolation
[c index1]=min(abs(mag(aux2:indexm)-Anot))
clear c;
index1=index1+aux2-1;
closestvalue1=mag(index1)
if closestvalue1>Anot
index1t1=index1-1
index2t1=index1
else
index1t1=index1
index2t1=index1+1
end
clear aux2
f1=freq(index1t1)+(((Anot-mag(index1t1))/(mag(index2t1)-
mag(index1t1)))*(freq(index2t1)-freq(index1t1)))%Interpolation to calculate
  %the value of f1
%3.2) 2nd truncation interpolation
aux3=indexm+10; %Same as aux2.
[c index2]=min(abs(mag(indexm:aux3)-Anot))
clear c;
index2=index2+indexm-1
closestvalue2=mag(index2)
if closestvalue2>Anot
```

```
index1t2=index2
index2t2=index2+1
else
index1t2=index2-1
index2t2=index2
end
clear aux3
f2=freq(index1t2)+(((Anot-mag(index1t2))/(mag(index2t2)-
mag(index1t2)))*(freq(index2t2)-freq(index1t2)))
%4) Damping determination
D_BR=Anot*((f2^2-f1^2)/(Anot^2*f2^4-
2*Anot^2*f2^2*f1^2+Anot^2*f1^4+16*fm^4*(Am^2-Anot^2))^0.5)*100
%Damping according to Brocanelli and Rinaldi (1998)
D_LK=(f2^2-f1^2)/(4*fm^2)*100
%Damping according to Lutz Karl (2005)
```

APPENDIX C

Copyright Release Forms

Appendix C contains copyright release forms for previously published papers, which constitutes Chapters 2, 3, 4, and 5

SPRINGER NATURE LICENSE
TERMS AND CONDITIONS

May 29, 2024

This Agreement between Lakehead University -- Shumsun Siddique ("You") and Springer Nature ("Springer Nature") consists of your license details and the terms and conditions provided by Springer Nature and Copyright Clearance Center.

License Number	5798301181902
License date	May 29, 2024
Licensed Content Publisher	Springer Nature
Licensed Content Publication	Soil Mechanics and Foundation Engineering
Licensed Content Title	The Application of Laponite Nanoparticle to Lessen the Risks of Liquefaction: An Emerging Technique for Sand Improvement (A Review)
Licensed Content Author	S. N. Siddique et al
Licensed Content Date	Jun 21, 2023
Type of Use	Thesis/Dissertation
Requestor type	academic/university or research institute
Format	print and electronic
Portion	full article/chapter

Will you be translating?	yes, including original language
Number of languages	1
Circulation/distribution	1 - 29
Author of this Springer Nature content	yes
Title of new work	Ground Improvement of Non-cohesive Soil Using Nanoparticle, Specifically, Laponite
Institution name	Lakehead University
Expected presentation date	Sep 2024
Specific Languages	English
Requestor Location	Lakehead University 955 Oliver Road Thunder Bay, ON P7B 5E1 Canada Attn: Lakehead University
Total	0.00 USD

Terms and Conditions

Springer Nature Customer Service Centre GmbH Terms and Conditions

The following terms and conditions ("Terms and Conditions") together with the terms specified in your [RightsLink] constitute the License ("License") between you as Licensee and Springer Nature Customer Service Centre GmbH as Licensor. By clicking 'accept' and completing the transaction for your use of the material ("Licensed Material"), you confirm your acceptance of and obligation to be bound by these Terms and Conditions.

1. Grant and Scope of License

1. 1. The Licensor grants you a personal, non-exclusive, non-transferable, non-sublicensable, revocable, world-wide License to reproduce, distribute, communicate to the public, make available, broadcast, electronically transmit or create derivative works using the Licensed Material for the purpose(s) specified in your RightsLink Licence Details only. Licenses are granted for the specific use requested in the order and for no other use, subject to these Terms and Conditions. You acknowledge and agree that the rights granted to you under this License do not include the right to modify, edit, translate, include in collective works, or create derivative works of the Licensed Material in whole or in part unless expressly stated in your RightsLink Licence Details. You may use the Licensed Material only as permitted under this Agreement and will not reproduce, distribute, display, perform, or otherwise use or exploit any Licensed Material in any way, in whole or in part, except as expressly permitted by this License.

1. 2. You may only use the Licensed Content in the manner and to the extent permitted by these Terms and Conditions, by your RightsLink Licence Details and by any applicable laws.

1. 3. A separate license may be required for any additional use of the Licensed Material, e.g. where a license has been purchased for print use only, separate permission must be obtained for electronic re-use. Similarly, a License is only valid in the language selected and does not apply for editions in other languages unless additional translation rights have been granted separately in the License.

1. 4. Any content within the Licensed Material that is owned by third parties is expressly excluded from the License.

1. 5. Rights for additional reuses such as custom editions, computer/mobile applications, film or TV reuses and/or any other derivative rights requests require additional permission and may be subject to an additional fee. Please apply to journalpermissions@springernature.com or bookpermissions@springernature.com for these rights.

2. Reservation of Rights

Licensor reserves all rights not expressly granted to you under this License. You acknowledge and agree that nothing in this License limits or restricts Licensor's rights in or use of the Licensed Material in any way. Neither this License, nor any act, omission, or statement by Licensor or you, conveys any ownership right to you in any Licensed Material, or to any element or portion thereof. As between Licensor and you, Licensor owns and retains all right, title, and interest in and to the Licensed Material subject to the license granted in Section 1.1. Your permission to use the Licensed Material is expressly conditioned on you not impairing Licensor's or the applicable copyright owner's rights in the Licensed Material in any way.

3. Restrictions on use

3. 1. Minor editing privileges are allowed for adaptations for stylistic purposes or

formatting purposes provided such alterations do not alter the original meaning or intention of the Licensed Material and the new figure(s) are still accurate and representative of the Licensed Material. Any other changes including but not limited to, cropping, adapting, and/or omitting material that affect the meaning, intention or moral rights of the author(s) are strictly prohibited.

3. 2. You must not use any Licensed Material as part of any design or trademark.

3. 3. Licensed Material may be used in Open Access Publications (OAP), but any such reuse must include a clear acknowledgment of this permission visible at the same time as the figures/tables/illustration or abstract and which must indicate that the Licensed Material is not part of the governing OA license but has been reproduced with permission. This may be indicated according to any standard referencing system but must include at a minimum 'Book/Journal title, Author, Journal Name (if applicable), Volume (if applicable), Publisher, Year, reproduced with permission from SNCSC'.

4. STM Permission Guidelines

4. 1. An alternative scope of license may apply to signatories of the STM Permissions Guidelines ("STM PG") as amended from time to time and made available at https://www.stm-assoc.org/intellectual-property/permissions/permissions-guidelines/.

4. 2. For content reuse requests that qualify for permission under the STM PG, and which may be updated from time to time, the STM PG supersede the terms and conditions contained in this License.

4. 3. If a License has been granted under the STM PG, but the STM PG no longer apply at the time of publication, further permission must be sought from the Rightsholder. Contact journalpermissions@springernature.com or bookpermissions@springernature.com for these rights.

5. Duration of License

5. 1. Unless otherwise indicated on your License, a License is valid from the date of purchase ("License Date") until the end of the relevant period in the below table:

Reuse in a medical communications project	Reuse up to distribution or time period indicated in License
Reuse in a dissertation/ thesis	Lifetime of thesis
Reuse in a journal/ magazine	Lifetime of journal/magazine
Reuse in a book/ textbook	Lifetime of edition
Reuse on a website	1 year unless otherwise specified in the License
Reuse in a presentation/ slide kit/poster	Lifetime of presentation/slide kit/poster. Note: publication whether electronic or in print of presentation/slide kit/poster may require further

	permission.
Reuse in conference proceedings	Lifetime of conference proceedings
Reuse in an annual report	Lifetime of annual report
Reuse in training/CME materials	Reuse up to distribution or time period indicated in License
Reuse in newsmedia	Lifetime of newsmedia
Reuse in coursepack/ classroom materials	Reuse up to distribution and/or time period indicated in license

6. Acknowledgement

6. 1. The Licensor's permission must be acknowledged next to the Licensed Material in print. In electronic form, this acknowledgement must be visible at the same time as the figures/tables/illustrations or abstract and must be hyperlinked to the journal/book's homepage.

6. 2. Acknowledgement may be provided according to any standard referencing system and at a minimum should include "Author, Article/Book Title, Journal name/Book imprint, volume, page number, year, Springer Nature".

7. Reuse in a dissertation or thesis

7. 1. Where 'reuse in a dissertation/thesis' has been selected, the following terms apply: Print rights of the Version of Record are provided for; electronic rights for use only on institutional repository as defined by the Sherpa guideline (www.sherpa.ac.uk/romeo/) and only up to what is required by the awarding institution.

7. 2. For theses published under an ISBN or ISSN, separate permission is required. Please contact journalpermissions@springernature.com or bookpermissions@springernature.com for these rights.

7. 3. Authors must properly cite the published manuscript in their thesis according to current citation standards and include the following acknowledgement: '*Reproduced with permission from Springer Nature*'.

8. License Fee

You must pay the fee set forth in the License Agreement (the "License Fees"). All amounts payable by you under this License are exclusive of any sales, use, withholding, value added or similar taxes, government fees or levies or other assessments. Collection and/or remittance of such taxes to the relevant tax authority shall be the responsibility of the party who has the legal obligation to do so.

9. Warranty

9. 1. The Licensor warrants that it has, to the best of its knowledge, the rights to license reuse of the Licensed Material. **You are solely responsible for ensuring**

that the material you wish to license is original to the Licensor and does not carry the copyright of another entity or third party (as credited in the published version). If the credit line on any part of the Licensed Material indicates that it was reprinted or adapted with permission from another source, then you should seek additional permission from that source to reuse the material.

9. 2. EXCEPT FOR THE EXPRESS WARRANTY STATED HEREIN AND TO THE EXTENT PERMITTED BY APPLICABLE LAW, LICENSOR PROVIDES THE LICENSED MATERIAL "AS IS" AND MAKES NO OTHER REPRESENTATION OR WARRANTY. LICENSOR EXPRESSLY DISCLAIMS ANY LIABILITY FOR ANY CLAIM ARISING FROM OR OUT OF THE CONTENT, INCLUDING BUT NOT LIMITED TO ANY ERRORS, INACCURACIES, OMISSIONS, OR DEFECTS CONTAINED THEREIN, AND ANY IMPLIED OR EXPRESS WARRANTY AS TO MERCHANTABILITY OR FITNESS FOR A PARTICULAR PURPOSE. IN NO EVENT SHALL LICENSOR BE LIABLE TO YOU OR ANY OTHER PARTY OR ANY OTHER PERSON OR FOR ANY SPECIAL, CONSEQUENTIAL, INCIDENTAL, INDIRECT, PUNITIVE, OR EXEMPLARY DAMAGES, HOWEVER CAUSED, ARISING OUT OF OR IN CONNECTION WITH THE DOWNLOADING, VIEWING OR USE OF THE LICENSED MATERIAL REGARDLESS OF THE FORM OF ACTION, WHETHER FOR BREACH OF CONTRACT, BREACH OF WARRANTY, TORT, NEGLIGENCE, INFRINGEMENT OR OTHERWISE (INCLUDING, WITHOUT LIMITATION, DAMAGES BASED ON LOSS OF PROFITS, DATA, FILES, USE, BUSINESS OPPORTUNITY OR CLAIMS OF THIRD PARTIES), AND WHETHER OR NOT THE PARTY HAS BEEN ADVISED OF THE POSSIBILITY OF SUCH DAMAGES. THIS LIMITATION APPLIES NOTWITHSTANDING ANY FAILURE OF ESSENTIAL PURPOSE OF ANY LIMITED REMEDY PROVIDED HEREIN.

10. Termination and Cancellation

10. 1. The License and all rights granted hereunder will continue until the end of the applicable period shown in Clause 5.1 above. Thereafter, this license will be terminated and all rights granted hereunder will cease.

10. 2. Licensor reserves the right to terminate the License in the event that payment is not received in full or if you breach the terms of this License.

11. General

11. 1. The License and the rights and obligations of the parties hereto shall be construed, interpreted and determined in accordance with the laws of the Federal Republic of Germany without reference to the stipulations of the CISG (United Nations Convention on Contracts for the International Sale of Goods) or to Germany´s choice-of-law principle.

11. 2. The parties acknowledge and agree that any controversies and disputes arising out of this License shall be decided exclusively by the courts of or having jurisdiction for Heidelberg, Germany, as far as legally permissible.

11. 3. This License is solely for Licensor's and Licensee's benefit. It is not for the

benefit of any other person or entity.

Questions? For questions on Copyright Clearance Center accounts or website issues please contact springernaturesupport@copyright.com or +1-855-239-3415 (toll free in the US) or +1-978-646-2777. For questions on Springer Nature licensing please visit https://www.springernature.com/gp/partners/rights-permissions-third-party-distribution

Other Conditions:

Version 1.4 - Dec 2022

Questions? customercare@copyright.com.

SPRINGER NATURE LICENSE
TERMS AND CONDITIONS

May 29, 2024

This Agreement between Lakehead University -- Shumsun Siddique ("You") and Springer Nature ("Springer Nature") consists of your license details and the terms and conditions provided by Springer Nature and Copyright Clearance Center.

License Number	5798301304080
License date	May 29, 2024
Licensed Content Publisher	Springer Nature
Licensed Content Publication	Soil Mechanics and Foundation Engineering
Licensed Content Title	Review on the Application of Nanoparticles to Mitigate Liquefaction Risks
Licensed Content Author	S. N. Siddique et al
Licensed Content Date	Aug 11, 2023
Type of Use	Thesis/Dissertation
Requestor type	academic/university or research institute
Format	print and electronic
Portion	full article/chapter
Will you be translating?	yes, including original language

Number of languages	1
Circulation/distribution	1 - 29
Author of this Springer Nature content	yes
Title of new work	Ground Improvement of Non-cohesive Soil Using Nanoparticle, Specifically, Laponite
Institution name	Lakehead University
Expected presentation date	Sep 2024
Specific Languages	English
Requestor Location	Lakehead University 955 Oliver Road Thunder Bay, ON P7B 5E1 Canada Attn: Lakehead University
Total	0.00 USD

Terms and Conditions

Springer Nature Customer Service Centre GmbH Terms and Conditions

The following terms and conditions ("Terms and Conditions") together with the terms specified in your [RightsLink] constitute the License ("License") between you as Licensee and Springer Nature Customer Service Centre GmbH as Licensor. By clicking 'accept' and completing the transaction for your use of the material ("Licensed Material"), you confirm your acceptance of and obligation to be bound by these Terms and Conditions.

1. Grant and Scope of License

1. 1. The Licensor grants you a personal, non-exclusive, non-transferable, non-sublicensable, revocable, world-wide License to reproduce, distribute, communicate

to the public, make available, broadcast, electronically transmit or create derivative works using the Licensed Material for the purpose(s) specified in your RightsLink Licence Details only. Licenses are granted for the specific use requested in the order and for no other use, subject to these Terms and Conditions. You acknowledge and agree that the rights granted to you under this License do not include the right to modify, edit, translate, include in collective works, or create derivative works of the Licensed Material in whole or in part unless expressly stated in your RightsLink Licence Details. You may use the Licensed Material only as permitted under this Agreement and will not reproduce, distribute, display, perform, or otherwise use or exploit any Licensed Material in any way, in whole or in part, except as expressly permitted by this License.

1. 2. You may only use the Licensed Content in the manner and to the extent permitted by these Terms and Conditions, by your RightsLink Licence Details and by any applicable laws.

1. 3. A separate license may be required for any additional use of the Licensed Material, e.g. where a license has been purchased for print use only, separate permission must be obtained for electronic re-use. Similarly, a License is only valid in the language selected and does not apply for editions in other languages unless additional translation rights have been granted separately in the License.

1. 4. Any content within the Licensed Material that is owned by third parties is expressly excluded from the License.

1. 5. Rights for additional reuses such as custom editions, computer/mobile applications, film or TV reuses and/or any other derivative rights requests require additional permission and may be subject to an additional fee. Please apply to journalpermissions@springernature.com or bookpermissions@springernature.com for these rights.

2. Reservation of Rights

Licensor reserves all rights not expressly granted to you under this License. You acknowledge and agree that nothing in this License limits or restricts Licensor's rights in or use of the Licensed Material in any way. Neither this License, nor any act, omission, or statement by Licensor or you, conveys any ownership right to you in any Licensed Material, or to any element or portion thereof. As between Licensor and you, Licensor owns and retains all right, title, and interest in and to the Licensed Material subject to the license granted in Section 1.1. Your permission to use the Licensed Material is expressly conditioned on you not impairing Licensor's or the applicable copyright owner's rights in the Licensed Material in any way.

3. Restrictions on use

3. 1. Minor editing privileges are allowed for adaptations for stylistic purposes or formatting purposes provided such alterations do not alter the original meaning or intention of the Licensed Material and the new figure(s) are still accurate and representative of the Licensed Material. Any other changes including but not limited to, cropping, adapting, and/or omitting material that affect the meaning, intention or moral rights of the author(s) are strictly prohibited.

3. 2. You must not use any Licensed Material as part of any design or trademark.

3. 3. Licensed Material may be used in Open Access Publications (OAP), but any such reuse must include a clear acknowledgment of this permission visible at the same time as the figures/tables/illustration or abstract and which must indicate that the Licensed Material is not part of the governing OA license but has been reproduced with permission. This may be indicated according to any standard referencing system but must include at a minimum 'Book/Journal title, Author, Journal Name (if applicable), Volume (if applicable), Publisher, Year, reproduced with permission from SNCSC'.

4. STM Permission Guidelines

4. 1. An alternative scope of license may apply to signatories of the STM Permissions Guidelines ("STM PG") as amended from time to time and made available at https://www.stm-assoc.org/intellectual-property/permissions/permissions-guidelines/.

4. 2. For content reuse requests that qualify for permission under the STM PG, and which may be updated from time to time, the STM PG supersede the terms and conditions contained in this License.

4. 3. If a License has been granted under the STM PG, but the STM PG no longer apply at the time of publication, further permission must be sought from the Rightsholder. Contact journalpermissions@springernature.com or bookpermissions@springernature.com for these rights.

5. Duration of License

5. 1. Unless otherwise indicated on your License, a License is valid from the date of purchase ("License Date") until the end of the relevant period in the below table:

Reuse in a medical communications project	Reuse up to distribution or time period indicated in License
Reuse in a dissertation/ thesis	Lifetime of thesis
Reuse in a journal/ magazine	Lifetime of journal/magazine
Reuse in a book/ textbook	Lifetime of edition
Reuse on a website	1 year unless otherwise specified in the License
Reuse in a presentation/ slide kit/poster	Lifetime of presentation/slide kit/poster. Note: publication whether electronic or in print of presentation/slide kit/poster may require further permission.
Reuse in conference proceedings	Lifetime of conference proceedings
Reuse in an annual report	Lifetime of annual report

Reuse in training/CME materials	Reuse up to distribution or time period indicated in License
Reuse in newsmedia	Lifetime of newsmedia
Reuse in coursepack/ classroom materials	Reuse up to distribution and/or time period indicated in license

6. Acknowledgement

6. 1. The Licensor's permission must be acknowledged next to the Licensed Material in print. In electronic form, this acknowledgement must be visible at the same time as the figures/tables/illustrations or abstract and must be hyperlinked to the journal/book's homepage.

6. 2. Acknowledgement may be provided according to any standard referencing system and at a minimum should include "Author, Article/Book Title, Journal name/Book imprint, volume, page number, year, Springer Nature".

7. Reuse in a dissertation or thesis

7. 1. Where 'reuse in a dissertation/thesis' has been selected, the following terms apply: Print rights of the Version of Record are provided for; electronic rights for use only on institutional repository as defined by the Sherpa guideline (www.sherpa.ac.uk/romeo/) and only up to what is required by the awarding institution.

7. 2. For theses published under an ISBN or ISSN, separate permission is required. Please contact journalpermissions@springernature.com or bookpermissions@springernature.com for these rights.

7. 3. Authors must properly cite the published manuscript in their thesis according to current citation standards and include the following acknowledgement: '*Reproduced with permission from Springer Nature*'.

8. License Fee

You must pay the fee set forth in the License Agreement (the "License Fees"). All amounts payable by you under this License are exclusive of any sales, use, withholding, value added or similar taxes, government fees or levies or other assessments. Collection and/or remittance of such taxes to the relevant tax authority shall be the responsibility of the party who has the legal obligation to do so.

9. Warranty

9. 1. The Licensor warrants that it has, to the best of its knowledge, the rights to license reuse of the Licensed Material. **You are solely responsible for ensuring that the material you wish to license is original to the Licensor and does not carry the copyright of another entity or third party (as credited in the published version).** If the credit line on any part of the Licensed Material indicates that it was reprinted or adapted with permission from another source, then you should seek additional permission from that source to reuse the material.

9. 2. EXCEPT FOR THE EXPRESS WARRANTY STATED HEREIN AND TO THE EXTENT PERMITTED BY APPLICABLE LAW, LICENSOR PROVIDES THE LICENSED MATERIAL "AS IS" AND MAKES NO OTHER REPRESENTATION OR WARRANTY. LICENSOR EXPRESSLY DISCLAIMS ANY LIABILITY FOR ANY CLAIM ARISING FROM OR OUT OF THE CONTENT, INCLUDING BUT NOT LIMITED TO ANY ERRORS, INACCURACIES, OMISSIONS, OR DEFECTS CONTAINED THEREIN, AND ANY IMPLIED OR EXPRESS WARRANTY AS TO MERCHANTABILITY OR FITNESS FOR A PARTICULAR PURPOSE. IN NO EVENT SHALL LICENSOR BE LIABLE TO YOU OR ANY OTHER PARTY OR ANY OTHER PERSON OR FOR ANY SPECIAL, CONSEQUENTIAL, INCIDENTAL, INDIRECT, PUNITIVE, OR EXEMPLARY DAMAGES, HOWEVER CAUSED, ARISING OUT OF OR IN CONNECTION WITH THE DOWNLOADING, VIEWING OR USE OF THE LICENSED MATERIAL REGARDLESS OF THE FORM OF ACTION, WHETHER FOR BREACH OF CONTRACT, BREACH OF WARRANTY, TORT, NEGLIGENCE, INFRINGEMENT OR OTHERWISE (INCLUDING, WITHOUT LIMITATION, DAMAGES BASED ON LOSS OF PROFITS, DATA, FILES, USE, BUSINESS OPPORTUNITY OR CLAIMS OF THIRD PARTIES), AND WHETHER OR NOT THE PARTY HAS BEEN ADVISED OF THE POSSIBILITY OF SUCH DAMAGES. THIS LIMITATION APPLIES NOTWITHSTANDING ANY FAILURE OF ESSENTIAL PURPOSE OF ANY LIMITED REMEDY PROVIDED HEREIN.

10. Termination and Cancellation

10. 1. The License and all rights granted hereunder will continue until the end of the applicable period shown in Clause 5.1 above. Thereafter, this license will be terminated and all rights granted hereunder will cease.

10. 2. Licensor reserves the right to terminate the License in the event that payment is not received in full or if you breach the terms of this License.

11. General

11. 1. The License and the rights and obligations of the parties hereto shall be construed, interpreted and determined in accordance with the laws of the Federal Republic of Germany without reference to the stipulations of the CISG (United Nations Convention on Contracts for the International Sale of Goods) or to Germany´s choice-of-law principle.

11. 2. The parties acknowledge and agree that any controversies and disputes arising out of this License shall be decided exclusively by the courts of or having jurisdiction for Heidelberg, Germany, as far as legally permissible.

11. 3. This License is solely for Licensor's and Licensee's benefit. It is not for the benefit of any other person or entity.

Questions? For questions on Copyright Clearance Center accounts or website issues please contact springernaturesupport@copyright.com or +1-855-239-3415 (toll free in the US) or +1-978-646-2777. For questions on Springer Nature licensing please visit

https://www.springernature.com/gp/partners/rights-permissions-third-party-distribution

Other Conditions:

Version 1.4 - Dec 2022

Questions? customercare@copyright.com.

SPRINGER NATURE LICENSE
TERMS AND CONDITIONS

May 29, 2024

This Agreement between Lakehead University -- Shumsun Siddique ("You") and Springer Nature ("Springer Nature") consists of your license details and the terms and conditions provided by Springer Nature and Copyright Clearance Center.

License Number	5798300947563
License date	May 29, 2024
Licensed Content Publisher	Springer Nature
Licensed Content Publication	Water, Air, and Soil Pollution
Licensed Content Title	Effect of Laponite Nanoparticles on Growth Characteristics and Chlorophyll Content of Chlorella sp.
Licensed Content Author	Shumsun Nahar Siddique et al
Licensed Content Date	Jul 25, 2022
Type of Use	Thesis/Dissertation
Requestor type	academic/university or research institute
Format	print and electronic
Portion	full article/chapter
Will you be translating?	yes, including original language

Number of languages	1
Circulation/distribution	1 - 29
Author of this Springer Nature content	yes
Title of new work	Ground Improvement of Non-cohesive Soil Using Nanoparticle, Specifically, Laponite
Institution name	Lakehead University
Expected presentation date	Sep 2024
Specific Languages	English
Requestor Location	Lakehead University 955 Oliver Road Thunder Bay, ON P7B 5E1 Canada Attn: Lakehead University
Total	0.00 CAD

Terms and Conditions

Springer Nature Customer Service Centre GmbH Terms and Conditions

The following terms and conditions ("Terms and Conditions") together with the terms specified in your [RightsLink] constitute the License ("License") between you as Licensee and Springer Nature Customer Service Centre GmbH as Licensor. By clicking 'accept' and completing the transaction for your use of the material ("Licensed Material"), you confirm your acceptance of and obligation to be bound by these Terms and Conditions.

1. Grant and Scope of License

1. 1. The Licensor grants you a personal, non-exclusive, non-transferable, non-sublicensable, revocable, world-wide License to reproduce, distribute, communicate

to the public, make available, broadcast, electronically transmit or create derivative works using the Licensed Material for the purpose(s) specified in your RightsLink Licence Details only. Licenses are granted for the specific use requested in the order and for no other use, subject to these Terms and Conditions. You acknowledge and agree that the rights granted to you under this License do not include the right to modify, edit, translate, include in collective works, or create derivative works of the Licensed Material in whole or in part unless expressly stated in your RightsLink Licence Details. You may use the Licensed Material only as permitted under this Agreement and will not reproduce, distribute, display, perform, or otherwise use or exploit any Licensed Material in any way, in whole or in part, except as expressly permitted by this License.

1. 2. You may only use the Licensed Content in the manner and to the extent permitted by these Terms and Conditions, by your RightsLink Licence Details and by any applicable laws.

1. 3. A separate license may be required for any additional use of the Licensed Material, e.g. where a license has been purchased for print use only, separate permission must be obtained for electronic re-use. Similarly, a License is only valid in the language selected and does not apply for editions in other languages unless additional translation rights have been granted separately in the License.

1. 4. Any content within the Licensed Material that is owned by third parties is expressly excluded from the License.

1. 5. Rights for additional reuses such as custom editions, computer/mobile applications, film or TV reuses and/or any other derivative rights requests require additional permission and may be subject to an additional fee. Please apply to journalpermissions@springernature.com or bookpermissions@springernature.com for these rights.

2. Reservation of Rights

Licensor reserves all rights not expressly granted to you under this License. You acknowledge and agree that nothing in this License limits or restricts Licensor's rights in or use of the Licensed Material in any way. Neither this License, nor any act, omission, or statement by Licensor or you, conveys any ownership right to you in any Licensed Material, or to any element or portion thereof. As between Licensor and you, Licensor owns and retains all right, title, and interest in and to the Licensed Material subject to the license granted in Section 1.1. Your permission to use the Licensed Material is expressly conditioned on you not impairing Licensor's or the applicable copyright owner's rights in the Licensed Material in any way.

3. Restrictions on use

3. 1. Minor editing privileges are allowed for adaptations for stylistic purposes or formatting purposes provided such alterations do not alter the original meaning or intention of the Licensed Material and the new figure(s) are still accurate and representative of the Licensed Material. Any other changes including but not limited to, cropping, adapting, and/or omitting material that affect the meaning, intention or moral rights of the author(s) are strictly prohibited.

3. 2. You must not use any Licensed Material as part of any design or trademark.

3. 3. Licensed Material may be used in Open Access Publications (OAP), but any such reuse must include a clear acknowledgment of this permission visible at the same time as the figures/tables/illustration or abstract and which must indicate that the Licensed Material is not part of the governing OA license but has been reproduced with permission. This may be indicated according to any standard referencing system but must include at a minimum 'Book/Journal title, Author, Journal Name (if applicable), Volume (if applicable), Publisher, Year, reproduced with permission from SNCSC'.

4. STM Permission Guidelines

4. 1. An alternative scope of license may apply to signatories of the STM Permissions Guidelines ("STM PG") as amended from time to time and made available at https://www.stm-assoc.org/intellectual-property/permissions/permissions-guidelines/.

4. 2. For content reuse requests that qualify for permission under the STM PG, and which may be updated from time to time, the STM PG supersede the terms and conditions contained in this License.

4. 3. If a License has been granted under the STM PG, but the STM PG no longer apply at the time of publication, further permission must be sought from the Rightsholder. Contact journalpermissions@springernature.com or bookpermissions@springernature.com for these rights.

5. Duration of License

5. 1. Unless otherwise indicated on your License, a License is valid from the date of purchase ("License Date") until the end of the relevant period in the below table:

Reuse in a medical communications project	Reuse up to distribution or time period indicated in License
Reuse in a dissertation/ thesis	Lifetime of thesis
Reuse in a journal/ magazine	Lifetime of journal/magazine
Reuse in a book/ textbook	Lifetime of edition
Reuse on a website	1 year unless otherwise specified in the License
Reuse in a presentation/ slide kit/poster	Lifetime of presentation/slide kit/poster. Note: publication whether electronic or in print of presentation/slide kit/poster may require further permission.
Reuse in conference proceedings	Lifetime of conference proceedings
Reuse in an annual report	Lifetime of annual report

Reuse in training/CME materials	Reuse up to distribution or time period indicated in License
Reuse in newsmedia	Lifetime of newsmedia
Reuse in coursepack/ classroom materials	Reuse up to distribution and/or time period indicated in license

6. Acknowledgement

6. 1. The Licensor's permission must be acknowledged next to the Licensed Material in print. In electronic form, this acknowledgement must be visible at the same time as the figures/tables/illustrations or abstract and must be hyperlinked to the journal/book's homepage.

6. 2. Acknowledgement may be provided according to any standard referencing system and at a minimum should include "Author, Article/Book Title, Journal name/Book imprint, volume, page number, year, Springer Nature".

7. Reuse in a dissertation or thesis

7. 1. Where 'reuse in a dissertation/thesis' has been selected, the following terms apply: Print rights of the Version of Record are provided for; electronic rights for use only on institutional repository as defined by the Sherpa guideline (www.sherpa.ac.uk/romeo/) and only up to what is required by the awarding institution.

7. 2. For theses published under an ISBN or ISSN, separate permission is required. Please contact journalpermissions@springernature.com or bookpermissions@springernature.com for these rights.

7. 3. Authors must properly cite the published manuscript in their thesis according to current citation standards and include the following acknowledgement: '*Reproduced with permission from Springer Nature*'.

8. License Fee

You must pay the fee set forth in the License Agreement (the "License Fees"). All amounts payable by you under this License are exclusive of any sales, use, withholding, value added or similar taxes, government fees or levies or other assessments. Collection and/or remittance of such taxes to the relevant tax authority shall be the responsibility of the party who has the legal obligation to do so.

9. Warranty

9. 1. The Licensor warrants that it has, to the best of its knowledge, the rights to license reuse of the Licensed Material. **You are solely responsible for ensuring that the material you wish to license is original to the Licensor and does not carry the copyright of another entity or third party (as credited in the published version).** If the credit line on any part of the Licensed Material indicates that it was reprinted or adapted with permission from another source, then you should seek additional permission from that source to reuse the material.

9. 2. EXCEPT FOR THE EXPRESS WARRANTY STATED HEREIN AND TO THE EXTENT PERMITTED BY APPLICABLE LAW, LICENSOR PROVIDES THE LICENSED MATERIAL "AS IS" AND MAKES NO OTHER REPRESENTATION OR WARRANTY. LICENSOR EXPRESSLY DISCLAIMS ANY LIABILITY FOR ANY CLAIM ARISING FROM OR OUT OF THE CONTENT, INCLUDING BUT NOT LIMITED TO ANY ERRORS, INACCURACIES, OMISSIONS, OR DEFECTS CONTAINED THEREIN, AND ANY IMPLIED OR EXPRESS WARRANTY AS TO MERCHANTABILITY OR FITNESS FOR A PARTICULAR PURPOSE. IN NO EVENT SHALL LICENSOR BE LIABLE TO YOU OR ANY OTHER PARTY OR ANY OTHER PERSON OR FOR ANY SPECIAL, CONSEQUENTIAL, INCIDENTAL, INDIRECT, PUNITIVE, OR EXEMPLARY DAMAGES, HOWEVER CAUSED, ARISING OUT OF OR IN CONNECTION WITH THE DOWNLOADING, VIEWING OR USE OF THE LICENSED MATERIAL REGARDLESS OF THE FORM OF ACTION, WHETHER FOR BREACH OF CONTRACT, BREACH OF WARRANTY, TORT, NEGLIGENCE, INFRINGEMENT OR OTHERWISE (INCLUDING, WITHOUT LIMITATION, DAMAGES BASED ON LOSS OF PROFITS, DATA, FILES, USE, BUSINESS OPPORTUNITY OR CLAIMS OF THIRD PARTIES), AND WHETHER OR NOT THE PARTY HAS BEEN ADVISED OF THE POSSIBILITY OF SUCH DAMAGES. THIS LIMITATION APPLIES NOTWITHSTANDING ANY FAILURE OF ESSENTIAL PURPOSE OF ANY LIMITED REMEDY PROVIDED HEREIN.

10. Termination and Cancellation

10. 1. The License and all rights granted hereunder will continue until the end of the applicable period shown in Clause 5.1 above. Thereafter, this license will be terminated and all rights granted hereunder will cease.

10. 2. Licensor reserves the right to terminate the License in the event that payment is not received in full or if you breach the terms of this License.

11. General

11. 1. The License and the rights and obligations of the parties hereto shall be construed, interpreted and determined in accordance with the laws of the Federal Republic of Germany without reference to the stipulations of the CISG (United Nations Convention on Contracts for the International Sale of Goods) or to Germany´s choice-of-law principle.

11. 2. The parties acknowledge and agree that any controversies and disputes arising out of this License shall be decided exclusively by the courts of or having jurisdiction for Heidelberg, Germany, as far as legally permissible.

11. 3. This License is solely for Licensor's and Licensee's benefit. It is not for the benefit of any other person or entity.

Questions? For questions on Copyright Clearance Center accounts or website issues please contact springernaturesupport@copyright.com or +1-855-239-3415 (toll free in the US) or +1-978-646-2777. For questions on Springer Nature licensing please visit

https://www.springernature.com/gp/partners/rights-permissions-third-party-distribution

Other Conditions:

Version 1.4 - Dec 2022

Questions? customercare@copyright.com.

SPRINGER NATURE LICENSE
TERMS AND CONDITIONS

May 29, 2024

This Agreement between Lakehead University -- Shumsun Siddique ("You") and Springer Nature ("Springer Nature") consists of your license details and the terms and conditions provided by Springer Nature and Copyright Clearance Center.

License Number	5798301454692
License date	May 29, 2024
Licensed Content Publisher	Springer Nature
Licensed Content Publication	International Journal of Civil Engineering
Licensed Content Title	Improving the Strength Properties of Sand Using Laponite, a Promising Nanoparticle
Licensed Content Author	Shumsun Nahar Siddique et al
Licensed Content Date	Dec 28, 2022
Type of Use	Thesis/Dissertation
Requestor type	academic/university or research institute
Format	print and electronic
Portion	full article/chapter
Will you be translating?	yes, including original language

Number of languages	1
Circulation/distribution	1 - 29
Author of this Springer Nature content	yes
Title of new work	Ground Improvement of Non-cohesive Soil Using Nanoparticle, Specifically, Laponite
Institution name	Lakehead University
Expected presentation date	Sep 2024
Specific Languages	English
Requestor Location	Lakehead University 955 Oliver Road Thunder Bay, ON P7B 5E1 Canada Attn: Lakehead University
Total	0.00 USD

Terms and Conditions

Springer Nature Customer Service Centre GmbH Terms and Conditions

The following terms and conditions ("Terms and Conditions") together with the terms specified in your [RightsLink] constitute the License ("License") between you as Licensee and Springer Nature Customer Service Centre GmbH as Licensor. By clicking 'accept' and completing the transaction for your use of the material ("Licensed Material"), you confirm your acceptance of and obligation to be bound by these Terms and Conditions.

1. Grant and Scope of License

1. 1. The Licensor grants you a personal, non-exclusive, non-transferable, non-sublicensable, revocable, world-wide License to reproduce, distribute, communicate

to the public, make available, broadcast, electronically transmit or create derivative works using the Licensed Material for the purpose(s) specified in your RightsLink Licence Details only. Licenses are granted for the specific use requested in the order and for no other use, subject to these Terms and Conditions. You acknowledge and agree that the rights granted to you under this License do not include the right to modify, edit, translate, include in collective works, or create derivative works of the Licensed Material in whole or in part unless expressly stated in your RightsLink Licence Details. You may use the Licensed Material only as permitted under this Agreement and will not reproduce, distribute, display, perform, or otherwise use or exploit any Licensed Material in any way, in whole or in part, except as expressly permitted by this License.

1. 2. You may only use the Licensed Content in the manner and to the extent permitted by these Terms and Conditions, by your RightsLink Licence Details and by any applicable laws.

1. 3. A separate license may be required for any additional use of the Licensed Material, e.g. where a license has been purchased for print use only, separate permission must be obtained for electronic re-use. Similarly, a License is only valid in the language selected and does not apply for editions in other languages unless additional translation rights have been granted separately in the License.

1. 4. Any content within the Licensed Material that is owned by third parties is expressly excluded from the License.

1. 5. Rights for additional reuses such as custom editions, computer/mobile applications, film or TV reuses and/or any other derivative rights requests require additional permission and may be subject to an additional fee. Please apply to journalpermissions@springernature.com or bookpermissions@springernature.com for these rights.

2. Reservation of Rights

Licensor reserves all rights not expressly granted to you under this License. You acknowledge and agree that nothing in this License limits or restricts Licensor's rights in or use of the Licensed Material in any way. Neither this License, nor any act, omission, or statement by Licensor or you, conveys any ownership right to you in any Licensed Material, or to any element or portion thereof. As between Licensor and you, Licensor owns and retains all right, title, and interest in and to the Licensed Material subject to the license granted in Section 1.1. Your permission to use the Licensed Material is expressly conditioned on you not impairing Licensor's or the applicable copyright owner's rights in the Licensed Material in any way.

3. Restrictions on use

3. 1. Minor editing privileges are allowed for adaptations for stylistic purposes or formatting purposes provided such alterations do not alter the original meaning or intention of the Licensed Material and the new figure(s) are still accurate and representative of the Licensed Material. Any other changes including but not limited to, cropping, adapting, and/or omitting material that affect the meaning, intention or moral rights of the author(s) are strictly prohibited.

3. 2. You must not use any Licensed Material as part of any design or trademark.

3. 3. Licensed Material may be used in Open Access Publications (OAP), but any such reuse must include a clear acknowledgment of this permission visible at the same time as the figures/tables/illustration or abstract and which must indicate that the Licensed Material is not part of the governing OA license but has been reproduced with permission. This may be indicated according to any standard referencing system but must include at a minimum 'Book/Journal title, Author, Journal Name (if applicable), Volume (if applicable), Publisher, Year, reproduced with permission from SNCSC'.

4. STM Permission Guidelines

4. 1. An alternative scope of license may apply to signatories of the STM Permissions Guidelines ("STM PG") as amended from time to time and made available at https://www.stm-assoc.org/intellectual-property/permissions/permissions-guidelines/.

4. 2. For content reuse requests that qualify for permission under the STM PG, and which may be updated from time to time, the STM PG supersede the terms and conditions contained in this License.

4. 3. If a License has been granted under the STM PG, but the STM PG no longer apply at the time of publication, further permission must be sought from the Rightsholder. Contact journalpermissions@springernature.com or bookpermissions@springernature.com for these rights.

5. Duration of License

5. 1. Unless otherwise indicated on your License, a License is valid from the date of purchase ("License Date") until the end of the relevant period in the below table:

Reuse in a medical communications project	Reuse up to distribution or time period indicated in License
Reuse in a dissertation/ thesis	Lifetime of thesis
Reuse in a journal/ magazine	Lifetime of journal/magazine
Reuse in a book/ textbook	Lifetime of edition
Reuse on a website	1 year unless otherwise specified in the License
Reuse in a presentation/ slide kit/poster	Lifetime of presentation/slide kit/poster. Note: publication whether electronic or in print of presentation/slide kit/poster may require further permission.
Reuse in conference proceedings	Lifetime of conference proceedings
Reuse in an annual report	Lifetime of annual report

Reuse in training/CME materials	Reuse up to distribution or time period indicated in License
Reuse in newsmedia	Lifetime of newsmedia
Reuse in coursepack/ classroom materials	Reuse up to distribution and/or time period indicated in license

6. Acknowledgement

6. 1. The Licensor's permission must be acknowledged next to the Licensed Material in print. In electronic form, this acknowledgement must be visible at the same time as the figures/tables/illustrations or abstract and must be hyperlinked to the journal/book's homepage.

6. 2. Acknowledgement may be provided according to any standard referencing system and at a minimum should include "Author, Article/Book Title, Journal name/Book imprint, volume, page number, year, Springer Nature".

7. Reuse in a dissertation or thesis

7. 1. Where 'reuse in a dissertation/thesis' has been selected, the following terms apply: Print rights of the Version of Record are provided for; electronic rights for use only on institutional repository as defined by the Sherpa guideline (www.sherpa.ac.uk/romeo/) and only up to what is required by the awarding institution.

7. 2. For theses published under an ISBN or ISSN, separate permission is required. Please contact journalpermissions@springernature.com or bookpermissions@springernature.com for these rights.

7. 3. Authors must properly cite the published manuscript in their thesis according to current citation standards and include the following acknowledgement: '*Reproduced with permission from Springer Nature*'.

8. License Fee

You must pay the fee set forth in the License Agreement (the "License Fees"). All amounts payable by you under this License are exclusive of any sales, use, withholding, value added or similar taxes, government fees or levies or other assessments. Collection and/or remittance of such taxes to the relevant tax authority shall be the responsibility of the party who has the legal obligation to do so.

9. Warranty

9. 1. The Licensor warrants that it has, to the best of its knowledge, the rights to license reuse of the Licensed Material. **You are solely responsible for ensuring that the material you wish to license is original to the Licensor and does not carry the copyright of another entity or third party (as credited in the published version).** If the credit line on any part of the Licensed Material indicates that it was reprinted or adapted with permission from another source, then you should seek additional permission from that source to reuse the material.

9. 2. EXCEPT FOR THE EXPRESS WARRANTY STATED HEREIN AND TO THE EXTENT PERMITTED BY APPLICABLE LAW, LICENSOR PROVIDES THE LICENSED MATERIAL "AS IS" AND MAKES NO OTHER REPRESENTATION OR WARRANTY. LICENSOR EXPRESSLY DISCLAIMS ANY LIABILITY FOR ANY CLAIM ARISING FROM OR OUT OF THE CONTENT, INCLUDING BUT NOT LIMITED TO ANY ERRORS, INACCURACIES, OMISSIONS, OR DEFECTS CONTAINED THEREIN, AND ANY IMPLIED OR EXPRESS WARRANTY AS TO MERCHANTABILITY OR FITNESS FOR A PARTICULAR PURPOSE. IN NO EVENT SHALL LICENSOR BE LIABLE TO YOU OR ANY OTHER PARTY OR ANY OTHER PERSON OR FOR ANY SPECIAL, CONSEQUENTIAL, INCIDENTAL, INDIRECT, PUNITIVE, OR EXEMPLARY DAMAGES, HOWEVER CAUSED, ARISING OUT OF OR IN CONNECTION WITH THE DOWNLOADING, VIEWING OR USE OF THE LICENSED MATERIAL REGARDLESS OF THE FORM OF ACTION, WHETHER FOR BREACH OF CONTRACT, BREACH OF WARRANTY, TORT, NEGLIGENCE, INFRINGEMENT OR OTHERWISE (INCLUDING, WITHOUT LIMITATION, DAMAGES BASED ON LOSS OF PROFITS, DATA, FILES, USE, BUSINESS OPPORTUNITY OR CLAIMS OF THIRD PARTIES), AND WHETHER OR NOT THE PARTY HAS BEEN ADVISED OF THE POSSIBILITY OF SUCH DAMAGES. THIS LIMITATION APPLIES NOTWITHSTANDING ANY FAILURE OF ESSENTIAL PURPOSE OF ANY LIMITED REMEDY PROVIDED HEREIN.

10. Termination and Cancellation

10. 1. The License and all rights granted hereunder will continue until the end of the applicable period shown in Clause 5.1 above. Thereafter, this license will be terminated and all rights granted hereunder will cease.

10. 2. Licensor reserves the right to terminate the License in the event that payment is not received in full or if you breach the terms of this License.

11. General

11. 1. The License and the rights and obligations of the parties hereto shall be construed, interpreted and determined in accordance with the laws of the Federal Republic of Germany without reference to the stipulations of the CISG (United Nations Convention on Contracts for the International Sale of Goods) or to Germany´s choice-of-law principle.

11. 2. The parties acknowledge and agree that any controversies and disputes arising out of this License shall be decided exclusively by the courts of or having jurisdiction for Heidelberg, Germany, as far as legally permissible.

11. 3. This License is solely for Licensor's and Licensee's benefit. It is not for the benefit of any other person or entity.

Questions? For questions on Copyright Clearance Center accounts or website issues please contact springernaturesupport@copyright.com or +1-855-239-3415 (toll free in the US) or +1-978-646-2777. For questions on Springer Nature licensing please visit

https://www.springernature.com/gp/partners/rights-permissions-third-party-distribution

Other Conditions:

Version 1.4 - Dec 2022

Questions? customercare@copyright.com.

SPRINGER NATURE LICENSE
TERMS AND CONDITIONS

May 29, 2024

This Agreement between Lakehead University -- Shumsun Siddique ("You") and Springer Nature ("Springer Nature") consists of your license details and the terms and conditions provided by Springer Nature and Copyright Clearance Center.

License Number	5798310110630
License date	May 29, 2024
Licensed Content Publisher	Springer Nature
Licensed Content Publication	Geotechnical and Geological Engineering
Licensed Content Title	Swelling Behaviour of Super-absorbent Laponite Hydrogel under One-dimensional Loading
Licensed Content Author	Shumsun Nahar Siddique et al
Licensed Content Date	Apr 29, 2024
Type of Use	Thesis/Dissertation
Requestor type	academic/university or research institute
Format	print and electronic
Portion	full article/chapter
Will you be translating?	yes, including original language

Number of languages	1
Circulation/distribution	1 - 29
Author of this Springer Nature content	yes
Title of new work	Ground Improvement of Non-cohesive Soil Using Nanoparticle, Specifically, Laponite
Institution name	Lakehead University
Expected presentation date	Sep 2024
Specific Languages	English
Requestor Location	Lakehead University 955 Oliver Road Thunder Bay, ON P7B 5E1 Canada Attn: Lakehead University
Total	0.00 USD

Terms and Conditions

Springer Nature Customer Service Centre GmbH Terms and Conditions

The following terms and conditions ("Terms and Conditions") together with the terms specified in your [RightsLink] constitute the License ("License") between you as Licensee and Springer Nature Customer Service Centre GmbH as Licensor. By clicking 'accept' and completing the transaction for your use of the material ("Licensed Material"), you confirm your acceptance of and obligation to be bound by these Terms and Conditions.

1. Grant and Scope of License

1. 1. The Licensor grants you a personal, non-exclusive, non-transferable, non-sublicensable, revocable, world-wide License to reproduce, distribute, communicate

to the public, make available, broadcast, electronically transmit or create derivative works using the Licensed Material for the purpose(s) specified in your RightsLink Licence Details only. Licenses are granted for the specific use requested in the order and for no other use, subject to these Terms and Conditions. You acknowledge and agree that the rights granted to you under this License do not include the right to modify, edit, translate, include in collective works, or create derivative works of the Licensed Material in whole or in part unless expressly stated in your RightsLink Licence Details. You may use the Licensed Material only as permitted under this Agreement and will not reproduce, distribute, display, perform, or otherwise use or exploit any Licensed Material in any way, in whole or in part, except as expressly permitted by this License.

1. 2. You may only use the Licensed Content in the manner and to the extent permitted by these Terms and Conditions, by your RightsLink Licence Details and by any applicable laws.

1. 3. A separate license may be required for any additional use of the Licensed Material, e.g. where a license has been purchased for print use only, separate permission must be obtained for electronic re-use. Similarly, a License is only valid in the language selected and does not apply for editions in other languages unless additional translation rights have been granted separately in the License.

1. 4. Any content within the Licensed Material that is owned by third parties is expressly excluded from the License.

1. 5. Rights for additional reuses such as custom editions, computer/mobile applications, film or TV reuses and/or any other derivative rights requests require additional permission and may be subject to an additional fee. Please apply to journalpermissions@springernature.com or bookpermissions@springernature.com for these rights.

2. Reservation of Rights

Licensor reserves all rights not expressly granted to you under this License. You acknowledge and agree that nothing in this License limits or restricts Licensor's rights in or use of the Licensed Material in any way. Neither this License, nor any act, omission, or statement by Licensor or you, conveys any ownership right to you in any Licensed Material, or to any element or portion thereof. As between Licensor and you, Licensor owns and retains all right, title, and interest in and to the Licensed Material subject to the license granted in Section 1.1. Your permission to use the Licensed Material is expressly conditioned on you not impairing Licensor's or the applicable copyright owner's rights in the Licensed Material in any way.

3. Restrictions on use

3. 1. Minor editing privileges are allowed for adaptations for stylistic purposes or formatting purposes provided such alterations do not alter the original meaning or intention of the Licensed Material and the new figure(s) are still accurate and representative of the Licensed Material. Any other changes including but not limited to, cropping, adapting, and/or omitting material that affect the meaning, intention or moral rights of the author(s) are strictly prohibited.

3. 2. You must not use any Licensed Material as part of any design or trademark.

3. 3. Licensed Material may be used in Open Access Publications (OAP), but any such reuse must include a clear acknowledgment of this permission visible at the same time as the figures/tables/illustration or abstract and which must indicate that the Licensed Material is not part of the governing OA license but has been reproduced with permission. This may be indicated according to any standard referencing system but must include at a minimum 'Book/Journal title, Author, Journal Name (if applicable), Volume (if applicable), Publisher, Year, reproduced with permission from SNCSC'.

4. STM Permission Guidelines

4. 1. An alternative scope of license may apply to signatories of the STM Permissions Guidelines ("STM PG") as amended from time to time and made available at https://www.stm-assoc.org/intellectual-property/permissions/permissions-guidelines/.

4. 2. For content reuse requests that qualify for permission under the STM PG, and which may be updated from time to time, the STM PG supersede the terms and conditions contained in this License.

4. 3. If a License has been granted under the STM PG, but the STM PG no longer apply at the time of publication, further permission must be sought from the Rightsholder. Contact journalpermissions@springernature.com or bookpermissions@springernature.com for these rights.

5. Duration of License

5. 1. Unless otherwise indicated on your License, a License is valid from the date of purchase ("License Date") until the end of the relevant period in the below table:

Reuse in a medical communications project	Reuse up to distribution or time period indicated in License
Reuse in a dissertation/ thesis	Lifetime of thesis
Reuse in a journal/ magazine	Lifetime of journal/magazine
Reuse in a book/ textbook	Lifetime of edition
Reuse on a website	1 year unless otherwise specified in the License
Reuse in a presentation/ slide kit/poster	Lifetime of presentation/slide kit/poster. Note: publication whether electronic or in print of presentation/slide kit/poster may require further permission.
Reuse in conference proceedings	Lifetime of conference proceedings
Reuse in an annual report	Lifetime of annual report

Reuse in training/CME materials	Reuse up to distribution or time period indicated in License
Reuse in newsmedia	Lifetime of newsmedia
Reuse in coursepack/ classroom materials	Reuse up to distribution and/or time period indicated in license

6. Acknowledgement

6. 1. The Licensor's permission must be acknowledged next to the Licensed Material in print. In electronic form, this acknowledgement must be visible at the same time as the figures/tables/illustrations or abstract and must be hyperlinked to the journal/book's homepage.

6. 2. Acknowledgement may be provided according to any standard referencing system and at a minimum should include "Author, Article/Book Title, Journal name/Book imprint, volume, page number, year, Springer Nature".

7. Reuse in a dissertation or thesis

7. 1. Where 'reuse in a dissertation/thesis' has been selected, the following terms apply: Print rights of the Version of Record are provided for; electronic rights for use only on institutional repository as defined by the Sherpa guideline (www.sherpa.ac.uk/romeo/) and only up to what is required by the awarding institution.

7. 2. For theses published under an ISBN or ISSN, separate permission is required. Please contact journalpermissions@springernature.com or bookpermissions@springernature.com for these rights.

7. 3. Authors must properly cite the published manuscript in their thesis according to current citation standards and include the following acknowledgement: '*Reproduced with permission from Springer Nature*'.

8. License Fee

You must pay the fee set forth in the License Agreement (the "License Fees"). All amounts payable by you under this License are exclusive of any sales, use, withholding, value added or similar taxes, government fees or levies or other assessments. Collection and/or remittance of such taxes to the relevant tax authority shall be the responsibility of the party who has the legal obligation to do so.

9. Warranty

9. 1. The Licensor warrants that it has, to the best of its knowledge, the rights to license reuse of the Licensed Material. **You are solely responsible for ensuring that the material you wish to license is original to the Licensor and does not carry the copyright of another entity or third party (as credited in the published version).** If the credit line on any part of the Licensed Material indicates that it was reprinted or adapted with permission from another source, then you should seek additional permission from that source to reuse the material.

9. 2. EXCEPT FOR THE EXPRESS WARRANTY STATED HEREIN AND TO THE EXTENT PERMITTED BY APPLICABLE LAW, LICENSOR PROVIDES THE LICENSED MATERIAL "AS IS" AND MAKES NO OTHER REPRESENTATION OR WARRANTY. LICENSOR EXPRESSLY DISCLAIMS ANY LIABILITY FOR ANY CLAIM ARISING FROM OR OUT OF THE CONTENT, INCLUDING BUT NOT LIMITED TO ANY ERRORS, INACCURACIES, OMISSIONS, OR DEFECTS CONTAINED THEREIN, AND ANY IMPLIED OR EXPRESS WARRANTY AS TO MERCHANTABILITY OR FITNESS FOR A PARTICULAR PURPOSE. IN NO EVENT SHALL LICENSOR BE LIABLE TO YOU OR ANY OTHER PARTY OR ANY OTHER PERSON OR FOR ANY SPECIAL, CONSEQUENTIAL, INCIDENTAL, INDIRECT, PUNITIVE, OR EXEMPLARY DAMAGES, HOWEVER CAUSED, ARISING OUT OF OR IN CONNECTION WITH THE DOWNLOADING, VIEWING OR USE OF THE LICENSED MATERIAL REGARDLESS OF THE FORM OF ACTION, WHETHER FOR BREACH OF CONTRACT, BREACH OF WARRANTY, TORT, NEGLIGENCE, INFRINGEMENT OR OTHERWISE (INCLUDING, WITHOUT LIMITATION, DAMAGES BASED ON LOSS OF PROFITS, DATA, FILES, USE, BUSINESS OPPORTUNITY OR CLAIMS OF THIRD PARTIES), AND WHETHER OR NOT THE PARTY HAS BEEN ADVISED OF THE POSSIBILITY OF SUCH DAMAGES. THIS LIMITATION APPLIES NOTWITHSTANDING ANY FAILURE OF ESSENTIAL PURPOSE OF ANY LIMITED REMEDY PROVIDED HEREIN.

10. Termination and Cancellation

10. 1. The License and all rights granted hereunder will continue until the end of the applicable period shown in Clause 5.1 above. Thereafter, this license will be terminated and all rights granted hereunder will cease.

10. 2. Licensor reserves the right to terminate the License in the event that payment is not received in full or if you breach the terms of this License.

11. General

11. 1. The License and the rights and obligations of the parties hereto shall be construed, interpreted and determined in accordance with the laws of the Federal Republic of Germany without reference to the stipulations of the CISG (United Nations Convention on Contracts for the International Sale of Goods) or to Germany´s choice-of-law principle.

11. 2. The parties acknowledge and agree that any controversies and disputes arising out of this License shall be decided exclusively by the courts of or having jurisdiction for Heidelberg, Germany, as far as legally permissible.

11. 3. This License is solely for Licensor's and Licensee's benefit. It is not for the benefit of any other person or entity.

Questions? For questions on Copyright Clearance Center accounts or website issues please contact springernaturesupport@copyright.com or +1-855-239-3415 (toll free in the US) or +1-978-646-2777. For questions on Springer Nature licensing please visit

https://www.springernature.com/gp/partners/rights-permissions-third-party-distribution

Other Conditions:

Version 1.4 - Dec 2022

Questions? customercare@copyright.com.
